The role of Colony Stimulating Factor 1 Receptor in microglial phenotype and function *in vitro* and *in vivo*

By

Sadia Islam

Thesis submitted for the degree of Doctor of Philosophy
at the University of Dublin, Trinity College

Supervised by: Professors James T. Murray and Colm Cunningham,
School of Biochemistry and Immunology, Trinity College Dublin

Submitted 7th January 2022

Declaration

I declare that this thesis has not been submitted as an exercise for a degree at this or any other university and it is entirely my own work except elements of section 5.6.1 which were produced in collaboration with Dr. Dáire Healy and section 5.6.9 where microglial isolation was performed with Dr. Arshed Nazmi. This thesis has not been previously submitted as an exercise for a degree at this or any other University.

I agree to deposit this thesis in the University's open access institutional repository or allow the library to do so on my behalf, subject to Irish Copyright Legislation and Trinity College Library conditions of use and acknowledgement.

I consent to the examiner retaining a copy of the thesis beyond the examining period, should they so wish (EU GDPR May 2018).

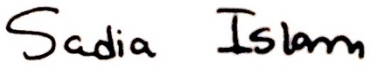

Sadia Islam

Acknowledgements

Completion of this thesis would not have been possible without the support of many people, to whom I owe a great deal of gratitude. In particular, I would like to thank:

Dr. Colm Cunningham and Dr. James Murray, my supervisors for taking me on with this project and for supervising me throughout the years. Your practical advice, sound judgement, expert guidance and encouragement was invaluable to me for completing the project and this research would not be produced at such standard without their help. Both of you have gone above and beyond to support me and for that I will always be grateful.

To all members of the Cunningham and Murray lab who have taught and advised me. Arshed Nazmi, Dáire Healy, Carol Murray, Ana-Belen Lopez-Rodriguez, Salma Aljahdali, Ana Lopez Garza thank you all for your encouragement in getting me this far and I look forward to working alongside and hopefully collaborating with you all in the future.

My family for providing me all the necessities, care, encouragement, motivation, and everything else I needed for the duration of my time in Trinity. My brothers Sofwat for the final touches on the thesis and Safwan for his ongoing support.

To all of you, Thank You!

Table of Contents

Figures and Tables

Abstract

As the brain ages multiple cellular processes become less efficient leading to a decline in cognitive and other functions, and in many cases giving rise to chronic neurodegenerative conditions such as Alzheimer's Disease (AD). Microglial cells are brain macrophages that regulate brain development, maintain neuronal networks, and repair damage and are the key immune cell population during neuroinflammation in chronic neurodegeneration. Inflammation is a consistent feature of neurodegenerative diseases but its precise role remains unclear. However, the role of microglia in AD pathogenesis is unclear, with different studies showing either beneficial or damaging outcomes on disease progression. Understanding how microglia are regulated is essential for identifying new ways of treating AD.

A critical growth factor that controls microglial function is Colony Stimulating Factor 1 (CSF1). Neurons produce ligands that are known to activate CSF1R signalling in microglia. During neuronal injury and degeneration, these signals change, bringing about altered microglial function. However, the precise mechanisms by which the CSF1R axis elicits this phenotype remains poorly understood and required further investigation. Additional aspects of microglial function, including the ability to phagocytose protein aggregates and how this is affected by activation of CSF1R signalling may also contribute to disease progression. An unexplored aspect of microglial function is autophagy, a pathway that is often associated to phagocytic processes. In this study, the hypothesis that therapeutic modulation of CSF1R signalling may regulate phagocytic and neuroinflammatory phenotypes was addressed both in a microglial cell line and in the APP/PS1 mouse model of AD.

The findings presented in this thesis demonstrate that CSF1 modestly impairs phagocytosis in IMG cells and that inhibition of the CSF1R with GW2580 *in vitro* may restore normal phagocytosis. The mechanisms of latex bead phagocytosis in IMG cells were not dependent on LC3B-Associated Phagocytosis (LAP). Moreover, despite mTORC1 activation by CSF1R signalling, and mTORC1 inhibition by rapamycin, these treatments had no effect on microglial autophagy, indicating that autophagy is non-canonically regulated (independent of CSF1R and mTORC1 signalling) in IMG cells. *In vitro*, CSF1R inhibition in the presence or absence of

LPS, a model of acute inflammatory stimulation of toll-like receptor (TLR) signalling, influenced several aspects of microglial function including inhibition of LPS-induced CCL2 and CXCL1 and nitric oxide (NO) secretion.

In vivo, chronic inhibition of CSF1R signalling by GW2580 in the APP/PS1 mouse model of AD was effective at improving cognitive function in APP/PS1 mice. Molecular analysis of microglial populations from isolated from APP/PS1 and WT mice also provided evidence that microglia display Disease-Associated Microglia (DAM)/ Microglial Neurodegenerative Phenotype (MGnD) phenotypes that were ameliorated by GW2580 treatment of APP/PS1 mice. During the study, it was observed that female mice had more pronounced microglial proliferation. However, GW2580 was more effective in relieving DAM phenotype in male APP/PS1 mice. It was also found that controlling microglial proliferation and phenotype via CSF1R inhibition was sufficient to mitigate synaptic and cognitive signs of disease without any impact on the Aβ levels in the APP/PS1 mouse brain.

Taken together, the data presented in this thesis suggest that CSF1R can both inhibit microglial proliferation and alter microglial phenotype and that this may have beneficial outcomes in both acute and chronic neuroinflammatory settings, with possible implications for the treatment of neurodegenerative conditions such as Alzheimer's disease.

List of Abbreviations

4E-BP1/2	eIF4E-binding proteins 1 and 2
4EBP1	4E-binding Protein
5XFAD	5X Familial AD
7-AAD	7-Aminoactinomycin D
Aβ	Amyloid β
ABC	Avidin-Biotin Complex
ABCA7	ATP-binding cassette transporter A7
AD	Alzheimer's disease
AKT	Protein kinase B
AMPK	PRKAA/AMP-activated protein kinase
ApoE	Apolipoprotein E
APP	Amyloid precursor protein
APS	Ammonium persulfate
ARM	Activated Response Microglia
Atg	Autophagy related protein
ATGs	Autophagy related proteins
ATP	Adenosine triphosphate
AV	Autophagic Vacuoles
B-cells	B lymphoid cells
Baf A1	Bafilomycin A1
BBB	Blood-brain-barrier
BCA	Bicinchoninic acid
BCB	Blood-Cerebrospinal Fluid Barrier
BDNF	Brain derived neurotrophic factor
Bicine	2-(bis(2-hydroxyethyl)amino) acetic acid
Bis – Tris	1,3-bis(tris(hydroxymethyl)methylamino)propane
BSA	Bovine serum albumin
c-Kit	Tyrosine-protein kinase Kit
C-X-C	Motif chemokine Ligand 1
C1q	Complement component 1q
C3	Complement component 3
CAPE	Caffeic Acid Phenethyl Ester
CCL2	C-C motif chemokine Ligand 2

CD	Cluster of Differentiation
CHAPS	3-(3-cholamidopropyl)dimethylammonium-1-propanesulfonate
CMA	Chaperone-mediated autophagy
CNS	Central Nervous System
CR1	Complement Receptor 1
CSF	Cerebrospinal Fluid
CSF1	Colony Stimulating Factor 1
CSF1R	Colony Stimulating Factor 1 Receptor
CSF2	Colony stimulating factor 2
CSF3	Colony Stimulating Factor 3
CXCL1	CXC Motif chemokine Ligand 1
CXCL10	CXC Motif chemokine Ligand 10
D-PBS	Dulbecco's Phosphate Buffered Saline
DAM	Disease-associated microglia
DAMPs	Danger-Associated Molecular Patterns
DAP12	DNAX-activation protein 12
DC	Dendritic cells
DEPTOR	Domain-containing mTOR-interacting protein
DMEM	Dulbecco's Modified Eagle Medium
DMSO	Dimethyl sulfoxide
dsRNA	Double stranded RNA
EAE	Experimental autoimmune encephalomyelitis
EBSS	Earle's Balanced Salt Solution
ECL	Enhanced chemiluminescent
EDTA	Ethylenediaminetetraacetic acid
EGFR	Epidermal growth factor receptor
EGTA	Ethylene glycol tetraacetic acid
ELISA	Enzyme-Linked ImmunoSorbent Assay
EPHA1	Ephrin A1
ER	Endoplasmic reticulum
ERK1/2	Extracellular signal Regulated Kinases 1/2
FBS	Fetal Bovine Serum
FGFRs	Fibroblast growth factor receptor
FLT3	fms-like tyrosine kinase 3
FSC	forward scatter are

G-CSF	Granulocyte Colony Stimulating Factor
GABARAP	Gamma-aminobutyric acid receptor-associated protein
GABARAPL1/2/3	GABARAP-Like 1/2/3
GATE-16	Golgi-associated ATPase enhancer of 16 kDa
GM-CSF	Granulocyte/Macrophage Colony Stimulating Factor
GWAS	Genome-wide association studies
H2DCFDA	2',7'-dichlorodihydrofluorescein diacetate
H2O2	Hydrogen peroxide
H2SO4	Sulphuric acid
HBSS	Hanks' Balanced Salt Solution
HCl	Hydrochloric acid
HEPES	4-(2-hydroxyethyl)-1-piperazineethanesulfonic acid
HGF/SF	Hepatocyte growth factor/scatter factor
HMGB1	High mobility group box protein 1
HPRA	Health Product Regulatory Authority
HRP	horseradish peroxidase
IBD	Inflammatory Bowel Disease
IDE	Insulin-degrading enzyme
IFN-□	Interferon-gamma
IL-1β	Interleukin-1 beta
IL-6	Interleukin 6
IL-8	Interleukin 8
IMG	Immortalized microglial
iNOS	Nitric oxide synthase
iPSC	Induced pluripotent stem cells
JAK1	Janus Kinase 1
JNK	c-Jun N-terminal protein Kinase
KO	Knock Out
LAP	LC3-associated phagocytosis
LC3B	Microtubule-associated protein 1A/1B-light chain 3
LDAM	Lipid droplet accumulating microglia
LDS	Lithium dodecyl sulphate
LIR	LC3B-interacting region
LOAD	Late-onset AD
LPS	Lipopolysaccharide

LRP	Lipoprotein receptor-related protein
M-CSF	Macrophage Colony Stimulating Factor
M2-polarisation	Alternatively activated macrophages
MACS	Magnetic-activated cell sorting
MAPK	Mitogen-activated protein kinase
MBL	Mannose-binding lectin
MBP	Mannose-binding protein
MCP1	Monocyte chemoattractant protein 1
MEF	Embryonic Fibroblast
MGnD	Microglia neurodegenerative phenotype
MHC	Major histocompatibility complex
mLST8	Mammalian lethal with SEC13 protein 8
MOPS	3-morpholino propane-1-sulfonic acid
MPTP	1-Methyl-4-phenyl-1,2,3,6-tetrahydropyridine
MRI	Magnetic Resonance Imaging
mRNA	Messenger ribonucleic acid
MS	Multiple Sclerosis
mTORC1	Mammalian/mechanistic target of rapamycin complex 1
MWM	Morris Water Maze
MyD88	Myeloid differentiation primary response 88
NaCl	Sodium Chloride
NADPH	Nicotinamide Adenine Dinucleotide Phosphate
NDRG1	N-myc downstream-regulated gene 1
NFκB	Nuclear Factor Kappa B
NFTs	Neurofibrillary tangles
NK-cells	Natural Killer cells
NLRP3	(NOD)-like receptor protein 3
NO	Nitric oxide
NSAIDs	Non-steroidal anti-inflammatory drugs
p-38	p-38 mitogen-activated protein kinase
PAMPS	Pathogen-associated molecular patterns
PBS	Phosphate-buffered saline
PD	Parkinson’s disease
PDGF	Platelet-derived growth factor
PDGFRs	Platelet-derived growth factor receptors

PDK1	3-Phosphoinositide-Dependent protein Kinase-1
PE	Phosphatidylethanolamine
PET	Positron Emission
PGE_2	Prostaglandin E2
PHOX	Phagocytic oxidase that generates oxygen radicals
PI3K	Phosphoinositide 3-kinase
PIK3C3	Phosphatidylinositol 3-kinase catalytic subunit type 3
PLX	Plexxikon
PM	Plasma membrane
PNS	Peripheral nervous system
PRKAA/AMP	Protein kinase AMP-activated catalytic subunit alpha
PRR	Pattern Recognition Receptors
PS1	g-secretase Presenilin 1
PtdIns3,4,5	Phosphatidylinositol (3,4,5)-trisphosphate
PTP-□□	Protein Tyrosine Phosphatase zeta
PVDF	Polyvinylidene difluoride transfer
RACE	Receptor for Advanced Glycation End-products
RNA	Ribonucleic acid
ROS	Reactive oxygen species
RPMI	Roswell Park Memorial Institute
RT-PCR	Real-Time Polymerase Chain Reaction
RTK	Receptor Tyrosine Kinase
S6K1	S6 kinase 1
SDS	Sodium dodecyl-sulphate
PAGE	Polyacrylamide gel electrophoresis
SH2	Src Homology 2
shRNA	Short hairpin RNA
SNARE	Soluble N-ethylmaleimide-sensitive factor-attachment protein receptors
SNPs	Single-nucleotide polymorphisms
SQSTM1/p62	Sequestosome 1
SREBP	Sterol-responsive element binding protein
SSC	Side scatter area
STAT1	Signal transducer and activator of transcription 1
STAT3	Signal transducer and activator of transcription 3

T-cells	T lymphoid cells
TBS	Tris-buffered saline solution
TBS-T	Tris-buffered saline -Tween solution
TEM	Transmission Electron Microscope
TEMED	Tetramethylethylenediamine
TGF-β	Transforming growth factor beta
TLRs	Toll-Like receptor
TMB	3,3′,5,5′-Tetramethylbenzidine
TMEM119	Transmembrane protein 119
TNFα	Tumour necrosis factor alpha
TREM2	Triggering receptor expressed on myeloid cells 2
Trk A/B	Tropomyosin related kinases A and B
TSC1/2	Tuberous sclerosis 1/2
ULK1	Unc51-Like Kinase 1
Vps34	Vacuolar protein sorting 34

Chapter 1: Introduction

1.1 Colony stimulating factor 1 (CSF1)

CSF1 (also known as Macrophage Colony Stimulating Factor (M-CSF)) is a growth factor that stimulates survival, proliferation and differentiation of haematopoietic cells of the monocyte-macrophage myeloid lineage and is key in the maintenance and proliferation of macrophages resident in multiple tissues throughout the body (Figure 1.1.1). CSF1 is a disulphide-linked homodimeric glycoprotein, produced by a number of cell types, mainly by monocytes and macrophages, but also fibroblasts, epithelial and endothelial cells, osteoblasts, activated B- and T-cells and also a number of tumour cell lines (Sherr *et al.*, 1985; Sherr, 1988). In the 'CSF network', there are two other CSFs: Granulocyte/Macrophage Colony Stimulating Factor (GM-CSF) or CSF2 and Granulocyte Colony Stimulating Factor (G-CSF) or CSF3, which are able to generate colonies of mature myeloid cells from bone-marrow precursor cells following the proliferation and differentiation of these cells. GM-CSF generates both granulocyte and macrophage colonies, macrophages are generated from CSF1 (M-CSF) and granulocytes are generated from G-CSF (Burgess and Metcalf, 1980).

There are three alternatively spliced forms of CSF1: a secreted glycoprotein, a cell surface protein and a proteoglycan (Dai *et al.*, 2004). Each form of CSF1 shares an N-terminal region containing an active 149-amino acid fragment that forms a 4-helix bundle (Chitu & Stanley 2006). CSF1 is found in the circulation at steady state detectable levels, primarily in the proteoglycan form, at biologically active concentrations of approximately 10 ng mL^{-1}. However, this increases in different pathologies including chronic inflammatory diseases (Hume & MacDonald 2012).

The function of CSF1 in the brain is the focus of the thesis. To understand more about the context in which CSF1 and its receptor may contribute to brain homeostasis and pathology, it is necessary to introduce the innate immune system, macrophages, microglia, neuroinflammation and Alzheimer's disease (AD).

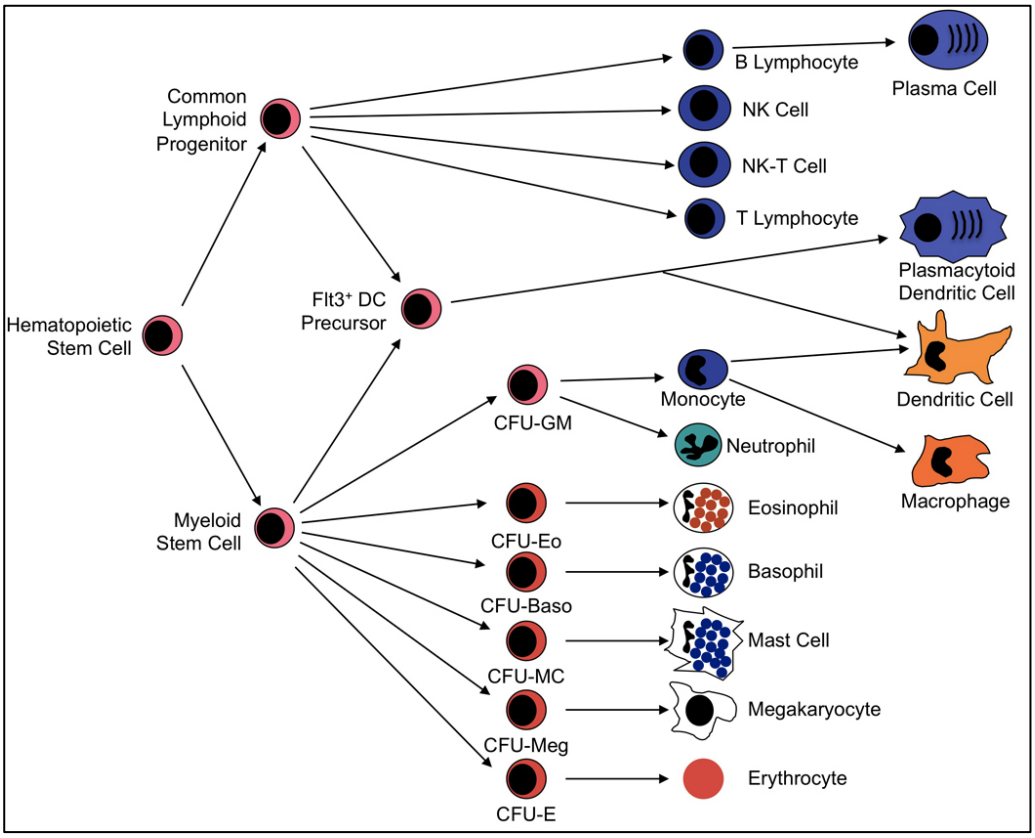

Figure 1.1.1: Cells of the immune system. Both lymphoid and myeloid progenitor cells are produced in the bone marrow from the hematopoietic stem cells. Lymphoid progenitors give rise to B-, NK (Natural Killer)- and T-lymphoid cells. Myeloid progenitor cells produce neutrophils, monocytes, eosinophils, basophils, mast cells, megakaryocytes, and erythrocytes. Further differentiation of monocytes produces macrophages and dendritic cells (Figure adapted from Chaplin, 2010).

1.2 The innate immune system & tissue macrophages

The immune system is a defence mechanism that protects against germs and foreign particles on the skin, in body tissues and bodily fluids, including blood. There are two separate branches of the immune system: the innate (general) and the adaptive (specialised) immune systems that work together and are highly inter-dependent. The innate immune system is the first line of defence, characterised by a non-specific response to pathogens and foreign particles. The innate immune system is comprised of physical barriers such as epithelial cell layers with tight cell-cell contacts, mucosal layers overlaying the epithelium, epithelial cilia. Innate immunity also relies on the constitutive presence of soluble proteins or bioactive small molecules such as complement proteins and defensins, and also includes proteins which are released from cells as they are activated such as cytokines and chemokines (Gallo and Nakatsuji, 2011). As the innate immune system provides an acute response to challenge, the innate immune response also recruits the adaptive immune system to provide a longer term and highly specific targeted response (Bonilla and Oettgen, 2010). Cells of adaptive immunity include B-cells and T-cells and Natural Killer (NK) cells, derived from the lymphoid lineage (Figure 1.1.1).

1.2.1 Cells of the immune system

The cells of the innate immune system include neutrophils, basophils, eosinophils and antigen presenting phagocytic cells such as dendritic cells and macrophages. When confronted with foreign particles, pathogens or injuries, immune cells become activated as a natural protective response known as inflammation to remove the cause and instigate tissue repair (Bennett *et al.*, 2018). Activation of Pattern Recognition Rps1eceptors (PRR) on immune cells by recognition of evolutionarily conserved pathogen-associated molecular patterns (PAMPS) on pathogens leads to the activation of complement cascades, phagocytosis and induction of apoptosis, stimulating the release of various cytokines, chemokines, toxic molecules such as nitric oxide (NO) and reactive oxygen species (ROS) (For review, see Li and Wu, 2021).

1.2.2 The Complement system

In innate immunity, the complement system plays a crucial role in host protection and inflammation. The complement system is composed of 30 proteins that typically circulate as inactive precursors in blood (For review see Mathern and Heeger,

2015). Confrontation by an immune stimulus activates the system through one of three different pathways: (1) a classical pathway triggered by antibody or direct binding of Complement component 1q (C1q) to the pathogen surface, (2) binding of Mannose-binding lectin (MBL) or Mannose-binding protein (MBP) to the surface of the encapsulated pathogen triggering the MBL pathway, and (3) the alternative pathway activated directly on pathogen surfaces through the spontaneous hydrolysis of complement C3 (For review see Mayilyan *et al.*, 2008). Activation of the Complement system leads to opsonization of pathogens, recruitment of inflammatory cells to the site of activation, thereby facilitating removal of pathogens by phagocytosis.

1.2.3 Cytokines and chemokines

Cytokines are small proteins that modulate inflammation via a complex signalling network of interactions between pro- and anti-inflammatory molecules. Pro-inflammatory cytokines such as interleukin (IL)-1β, tumour necrosis factor α (TNFα) and IL-6 are regarded as essential mediators of systemic inflammation and signal transduction in the Central Nervous System (CNS) (Kennedy and Silver, 2015). Chemokines are a family of small, secreted proteins that are also known as chemotactic cytokines. Their function is to initiate signalling cascades to regulate chemotactic leukocyte migration between blood and tissue via the establishment of chemotactic concentration gradients (Hughes and Nibbs, 2018). Examples of chemokines include C-C motif chemokine Ligand 2 (CCL2) or Monocyte chemoattractant protein 1 (MCP1), C-X-C Motif chemokine Ligand 1 (CXCL)1 and CXCL10 (Mohammadi and Kariminik, 2021).

1.2.4 Monocytes and macrophages

Both monocytes and macrophages are members of the mononuclear phagocytic system and play crucial roles in the immune response. Monocytes are derived from the bone marrow express a wide range of receptors to monitor and detect environmental changes. Monocytes are characterised by their ability to phagocytose foreign material, present antigens, produce ROS and cytokines, and secrete chemokines (For review see Serbina *et al.*, 2008). Monocytes present in the blood and spleen upon detection of tissue damage or infection, migrate to the site of inflammation, where they infiltrate and differentiate into dendritic cells (DC) or macrophages (Yang *et al.*, 2014).

Like monocytes, macrophages are circulating or tissue-resident mononuclear cells capable of phagocytosis. Macrophages primarily originate from infiltrating monocytic precursors, but can also derive directly from bone marrow under certain conditions (Ajami *et al.*, 2007). Recent studies performed on murine models reveal that some tissue-resident macrophages are capable of self-renewal, such as the Kuppfer cells in the liver, red pulp macrophages in the spleen, cardiac-resident macrophages and alveolar macrophages in the lungs (Hashimoto *et al.*, 2013). CSF1 is a crucial regulator of macrophage differentiation, proliferation and survival, and the level of CSF1 expression in macrophages is positively correlated with key periods of organogenesis (Roth and Richard Stanley, 1996), while lack of CSF1 expression results in developmental abnormalities (Wiktor-Jedrzejczak *et al.*, 1990). Intriguingly, CSF1 has been shown to induce M2-polarisation state of macrophages and will be discussed in detail later in this chapter (Svensson *et al.*, 2011).

1.3 Microglia

Microglia are the resident macrophage population of the CNS and constitute 5-12 % of the glial cell population, depending upon the region (Lawson *et al.*, 1990). They originate from the uncommitted c-Kit^{+} stem cells found in the embryonic yolk sac (Kierdorf *et al.*, 2013) and migrate into the brain around embryonic day 10.5 in the mouse, after which they propagate, spread throughout the brain parenchyma and their processes become ramified (Ginhoux *et al.*, 2013). In the CNS, microglia form an autonomous population, as under physiological conditions, infiltration of peripheral monocytes or macrophages is blocked by the blood-brain-barrier (BBB) (Ginhoux *et al.*, 2013).

Microglia functions as the resident phagocyte that continuously surveys the CNS microenvironment for the elimination of dead cells, microbes, protein aggregates, redundant synapses and other particulate and soluble antigens that may endanger the CNS. Efficient microglial phagocytosis contribute to the maintenance of CNS homeostasis (Figure 1.3.1).

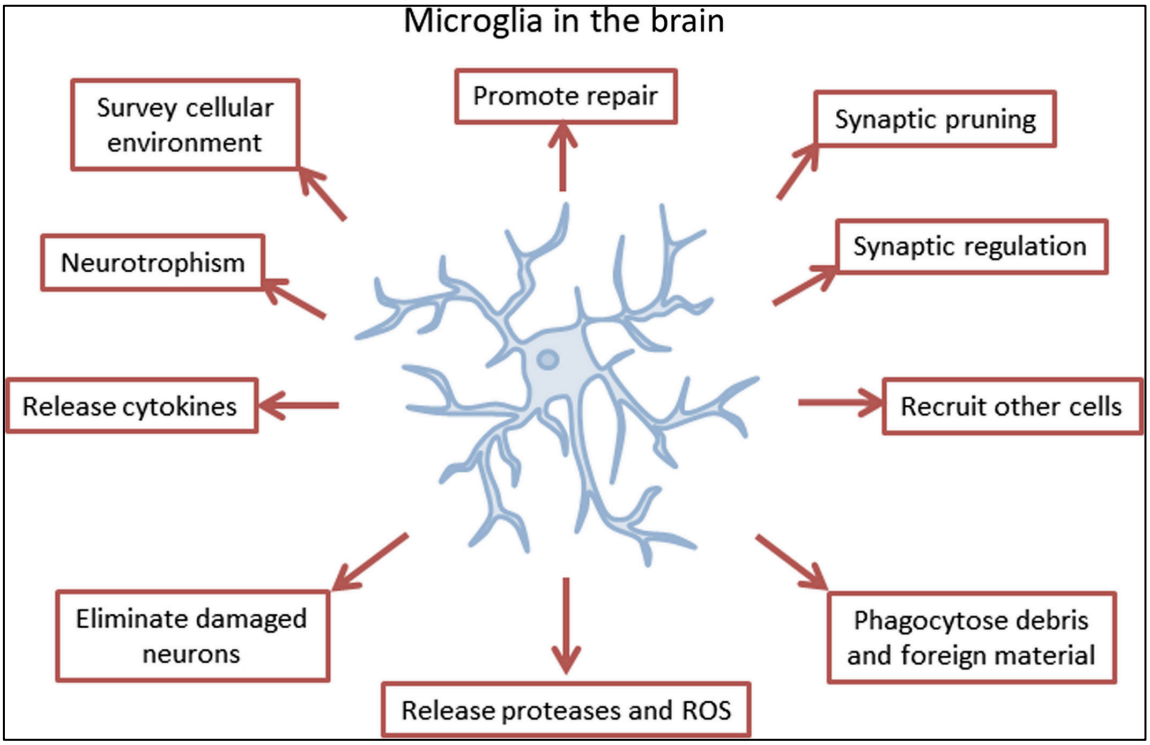

Figure 1.3.1: Functions of microglia in the brain. Microglia play various supportive roles in the brain including damage sensing, intercellular communication, promotion of inflammation, degradation, and repair in physiological conditions. (Figure adapted from Angelova and Brown, 2019).

This process is elicited by exposure of ‘eat-me’ signals and/or loss of ‘don’t-eat-me’ signals by viable cells resulting in self destruction (Figure 1.3.2) (Brown and Neher, 2012). Microglial phagocytosis relies on specific receptors expressed on the surface of cells and particles ready to be phagocytosed. Ligand-receptor interaction initiates downstream signalling pathways necessary for recognising and engulfment of dangerous particles. For example, Toll-Like Receptors (TLRs) on microglia allow the recognition of PAMPs and Danger-Associated Molecular Patterns (DAMPs), including lipopolysaccharide (LPS), viral nucleic acids and deposited Amyloid β (Aβ) (Fu et al. 2014). Triggering receptor expressed on myeloid cells 2 (TREM2) on microglia binds with DNAX-activation protein 12 (DAP12), an adaptor protein, to clear away apoptotic neurons by triggering the reorganisation of F-actin and phosphorylation of Extracellular signal Regulated Kinases (Erk)1/2 (Takahashi, Rochford and Neumann, 2005). Fc-receptor-mediated phagocytosis and Complement activation by microglia play an important role in removal of plaques from the AD brain (Koenigsknecht-Talboo, 2005). Besides phagocytosis, microglia also participate in the developmental sculpting of neural circuits through microglia-neuronal interactions (Kettenmann, Kirchhoff and Verkhratsky, 2013). Microglia are also pivotal mediators of neuroinflammation, regulating the production of proinflammatory cytokines and chemokines such as IL-1β, IL-6, IL-8 and TNF-α (Wang *et al.*, 2015). Altered microglial function is implicated in aging and neurodegeneration as they can induce or modulate a broad spectrum of detrimental cellular responses (Colonna and Butovsky, 2017).

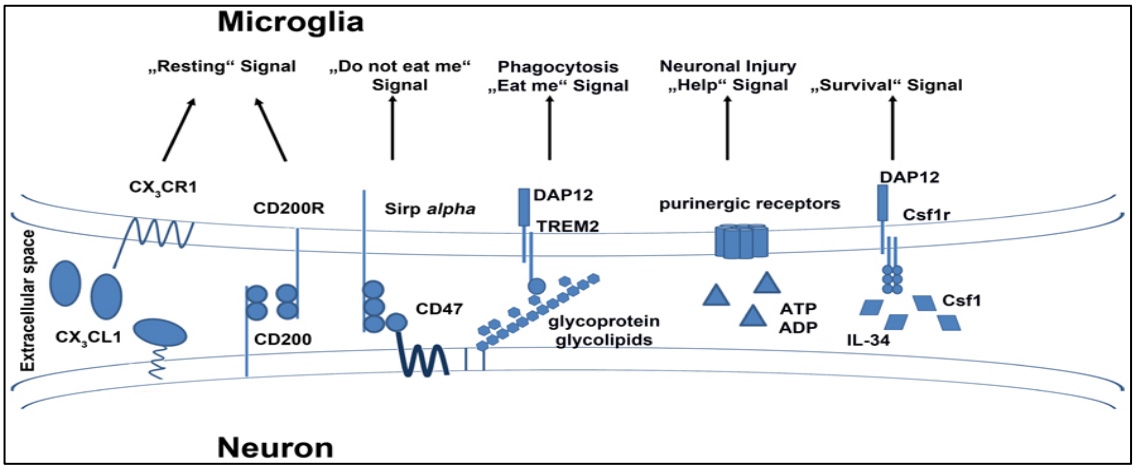

Figure 1.3.2: Receptors expressed on microglia and their exogenous ligands. Microglia have surface receptors that stimulate signals under ‘resting’ conditions. (Figure adapted from Kierdorf and Prinz, 2013).

1.4 Neuroinflammation

Inflammation occurring in the brain is described by the term neuroinflammation. Inflammation was described by Aulus Cornelius Celsus in AD30 as heat, pain, redness and swelling, which are generally beneficial to the defence against microorganism. The brain has its own immune system consisting of resident microglia and astrocytes, since the BBB and the Blood-Cerebrospinal Fluid (CSF) Barrier (BCB) separate external immune cells such as T-cells and neutrophils. However, these cells can infiltrate the brain in response to injury or acute or chronic neurodegenerative stimulus (Brendecke and Prinz, 2015).

It has been a topic of much debate whether neuroinflammation, inflammation of the brain and spinal cord, is a driver of pathology or a consequence of brain pathology and disease progression in various degenerative states (Kielian, 2014). It is now believed to play both roles during AD. One early indication that inflammation may play a significant role in the pathophysiology of AD stemmed from research showing that prolonged use of non-steroidal anti-inflammatory drugs (NSAIDs) reduces the risk of AD by approximately 50 % (in 't Veld *et al.*, 2001). In the Amyloid precursor protein (APP) / γ-secretase Presenilin 1 (PS1) mouse model of AD, inhibiting neuronal cyclooxygenase 1/2 (COX1/2) enzymes by NSAIDs prevented early memory deficits through the reduction of the levels of prostaglandins, prostacyclin, and thromboxanes, which are associated with AD pathogenesis (Woodling *et al.*, 2016). However, clinical trials using NSAIDs in AD patients have, to date, been disappointing (Wyss-Coray, 2006). Alternatively, the clinical trials may have failed because NSAIDs are only beneficial in healthy brain before any deposition of Aβ proteins, and once excessive deposition of Aβ has started, NSAIDs may no longer be effective (Imbimbo, 2009). In addition, NSAIDs may even be harmful to AD brains due to their proposed inhibitory effect on activated microglia, which are involved in both Aβ protein clearance and in triggering compensatory hippocampal neurogenesis (Imbimbo, 2009).

1.5 Alzheimer's disease

A gradual decline in some aspects of cognitive abilities such as speed, attention, visuospatial abilities and memory occurs with aging. These age-related cognitive changes are correlated with structural and functional alterations in the brain,

including a loss of grey and white matter volume and a decrease in synapses (Murman, 2015). However the rate of cognitive decline occurs earlier and much more rapidly with neurodegenerative conditions such as AD.

AD, first described by Alois Alzheimer's in 1906, is the most common form of dementia. It is a chronic neurodegenerative disorder, accounting for 60-80% of all dementia cases. In 2021, there were 44 million people worldwide living with AD and other forms of dementia. In Ireland, there are 64,000 people affected with AD or another dementia (Alzheimer's Society, Ireland). In the USA, more than 6 million people are living with AD in 2021 and this number is projected to rise to 13 million by 2050, while currently 1 in 3 seniors die in the USA with AD or another dementia. Where statistics are available, the economic cost of dealing with AD in the USA is $355 billion in 2021 alone, and this is expected to rise to $1.1 trillion by 2050 (Alzheimer's Association, USA).

AD is thought to begin 20 years or more before an individual experiences noticeable symptoms and these are preceded by pathological changes such as the sequential build-up of Aβ, phosphorylated Tau in the CSF, changes in glucose utilisation (imaged using Positron Emission Tomography (PET)) and brain structure (imaged by Magnetic Resonance Imaging (MRI)), all of which occur long before cognitive symptoms appear (Jack *et al.*, 2013). Characteristic symptoms of AD include memory loss and difficulty with language, thinking and problem solving skills, affecting the quality of the life of the suffering individual. Build-up of extracellular neuritic deposition of Aβ and intracellular accumulation of hyperphosphorylated microtubule- associated tau proteins, known as neurofibrillary tangles (NFTs) are still regarded as the major neuropathological hallmarks of the disease, however individuals affected by AD also suffer from a loss of synapses and neurons, predominantly in the temporal and frontal cortices and hippocampi, and these are strong correlates of the cognitive impairment observed (Davies *et al.*, 1987).

The Amyloid Cascade Hypothesis suggests that β-amyloidosis results from an imbalance in the production vs clearance of Aβ that occurs in early stages of AD and is considered the initiating factor of this disease (Villemagne *et al.*, 2013). Genetic mutations in APP or in its processing enzyme (PS1 or PS2) results in increased β-site cleavage of APP or a favoured production of longer, aggregation-

prone variants of Aβ peptides (Selkoe and Hardy, 2016). However, the Amyloid Cascade Hypothesis cannot completely explain the deterioration observed in AD pathogenesis. Firstly, there have been studies showing that specific therapies against Aβ accumulation are successful in removing Aβ fragments in animal models and also in humans, but this did not stop the progression of AD (Holmes *et al.*, 2008). Secondly, Aβ is detectable in healthy human brain tissue and in mammalian cell cultures, while, 20-30 % of individuals with normal cognition show significant burden of Aβ in the brain have normal cognition and never develop dementia (Aizenstein *et al.*, 2008). The presence of Aβ and Tau pathology in individuals with no signs of dementia, gives rise to a third key marker of AD; synaptic loss and cortical atrophy. Cortical atrophy signifies neuronal loss in the brain and adds to a more accurate diagnosis of AD, while synaptic loss is the best correlate of cognitive decline (Terry *et al.*, 1991).

1.5.1 Genetic risk factors of AD

There are two main types of AD: the rare early onset familial AD (5 %) that is diagnosed when people are in their fourth and fifth decades of life, and the most common form of dementia, late-onset AD (LOAD) that develops after the age of sixty (Selkoe and Hardy, 2016). Mutations in genes such as, APP, PS1 and PS2 cause familial AD (autosomal dominant) (Bertram, Lill and Tanzi, 2010) while risk factors for sporadic AD include a mix of genetic, epigenetic and environmental factors, including aging. Genome-wide association studies (GWAS), have identified over 20 genetic loci that are highly associated with AD development and progression. Although no single gene has been identified yet as causal for LOAD, a small number of such predisposing genetic risk factor does increase an individual's risk of developing the disease. Interestingly, the majority of the sporadic risk genes, are expressed either selectively or preferentially in microglia, the resident macrophage population of the CNS compared to other cell types in the CNS (Hansen, Hanson and Sheng, 2018). Multiple variants in genes related to immune functions, including Apolipoprotein E (ApoE; ε4 allele of ApoE), TREM2, Cluster of Differentiation (CD)33, Complement Receptor (CR)1, Ephrin A1 (EPHA1) and ATP-binding cassette transporter A7 (ABCA7) are also associated with LOAD (Hollingworth *et al.*, 2011). For instance, ApoE plays an important role in the lipoprotein transport system and is present at the Aβ plaques (Namba *et al.*, 1991) and contributes to both the clearance and deposition of Aβ peptide (Bien-Ly *et al.*,

2012). The precise mechanism(s) by which ApoE confers increased AD risk are not well understood. TREM2, a macrophage gene involved in phagocytosis and suppression of pro-inflammatory phenotype on microglia, increases the risk of developing AD by 2- to 3-fold (Ulrich *et al.*, 2017). Some variants of TREM2, including p.Arg47His (R47H), p.Arg62His (R62H), p.Asp87Asn (D87N) and p.His157Tyr (H157Y) have been associated with significant increased risk for AD (Jin *et al.*, 2014; Jiang *et al.*, 2016). Polymorphisms in cytokine genes and genes controlling cytokine expression may predispose for risk of AD, and this may be a mechanism for emergent neuroinflammation in certain subsets of AD (Hensley 2010). For instance, polymorphisms in TNFα, transforming growth factor (TGF)-β, IL-6 and CCL2 genes are associated with increasing risk for AD (Flex *et al.*, 2014). These indicate that genetic predisposition is a major contributing factor towards the onset of AD.

1.5.2 Microglia in inflammation and AD

Microglia showing enhanced proliferation and activation play key roles in neuroinflammation, thereby interfering with normal microglia-neuron interactions. Cerebral neuroinflammation is mediated by microglial activation following deposition of Aβ peptides around neurons. As part of the inflammatory reaction, microglia putatively bind to Aβ via one or more receptors, including class A scavenger receptor A1, CD36, CD14, CD47 and TLRs (TLR2, TLR4, TLR6 and TLR9) in order to produce proinflammatory cytokines and chemokines. Genetic deletion of CD36, TLR4, TLR6 reduces *in vitro* Aβ-induced cytokine production (Stewart *et al.*, 2010). Following receptor activation, microglia phagocytose deposited Aβ, but insufficient clearance increases cytokine production and sustained neuroinflammation, which can exacerbate AD pathogenesis. Aβ itself has redox properties to promote metal-catalysed redox cycling reactions and ROS production in certain circumstances that could also contribute to neuroinflammatory cycles (Kamat *et al.*, 2008).

The exact role microglia play in AD is not completely understood. For instance, microglia may be neurotoxic and contribute to a chronic neuroinflammatory environment in neurodegeneration. In support of this idea, Aβ can induce the production of proinflammatory cytokines in microglia, such as IL-1β and TNF-α, after being primed with either LPS or Interferon-gamma (IFN-γ), and parallel production

of ROS and NO, leading to neuronal cell injury *in vitro* (Von Bernhardi, Tichauer and Eugenín, 2010). Conversely, microglia may play a positive role in neurodegenerative diseases such as AD, by providing protection to neurons. Microglia might prevent neuronal dystrophy by clustering around plaques in both AD mouse models and in AD patients, thereby, creating a protective layer between Aβ and neurons (Condello *et al.*, 2015). Imaging of rat brain slices for uptake of Aβ that fluoresces when sequestered within acidic organelles revealed that microglia did more phagocytosis than astrocytes (Prakash *et al.*, 2021). In a very recent study it has been proposed that microglia and astrocytes play a synergistic role in processing Aβ aggerates in AD and PD, as the phagocytosis of intercellular Aβ deposits is greater in glial co-cultures, compared to monocultures of human or mouse induced pluripotent stem cells (iPSC)-derived microglia or astrocytes (Rostami *et al.*, 2021).

1.6 The Colony Stimulating Factor 1 receptor (CSF1R) in microglia

The cell surface receptor for CSF1, is the protein product of the c-*fms* proto-oncogene and is expressed in blood, spleen, liver, bone marrow of adult animals and in the brain, reflecting the distribution of monocytes and macrophages (Rettenmier, Roussel and Sherr, 1988). During development, CSF1 expression is detected in the embryonic brain, except in the hippocampus and striatum (day 16), while transcripts for CSF1R are detectable in microglia and in cells of the hippocampus, striatum, cerebellum and cortex (day 16) (Pollard, 1997). The production and consumption of CSF1 is balanced by tissue macrophages, through receptor-mediated endocytosis followed by intracellular degradation of the growth factor (Bartocci *et al.*, 1987). Microglial homeostasis, survival and proliferation is maintained by several factors including CSF1R signalling. Treatment of WT mice with a CSF1R inhibitor, PLX3397 (290 mg kg^{-1}), depleted 50 % of microglia by 3 days and by 21 days, the whole mouse brain was microglia depleted proving the dependence of microglial survival on CSF1R signalling. The same group also showed that within 48-72 hrs of removal of the CSF1R inhibitor microglia started to repopulate the brain from $nestin^{+}$ progenitor cells (Elmore *et al.*, 2014). Communication between microglia and neurons is vital for the survival and proliferation of microglia. Neurons, and possibly astrocytes, release factors such as CSF1 and IL-34, which both can bind to microglial CSF1R to induce cell survival and proliferation (Easley-Neal *et al.*, 2019).

1.6.1 CSF1R is a Receptor Tyrosine Kinase (RTK)

The CSF1R, is a type III RTK composed of an extracellular ligand-binding domain, a transmembrane region and a cytoplasmic split kinase domain that possesses an intrinsic tyrosine kinase activity (Figure 1.6.1.1) (Sherr *et al.*, 1985). RTKs facilitate interactions with the external environment to regulate cell proliferation and differentiation, cell survival, locomotion and cellular metabolism (Hubbard, Mohammadi and Schlessinger, 1998). Humans have 58 known RTKs, which fall into 20 subfamilies based on their architecture and ligand binding specificity (Lemmon and Schlessinger, 2010). The RTK family includes, among others, epidermal growth factor receptor (EGFR), platelet-derived growth factor receptors (PDGFRs), fibroblast growth factor receptor (FGFRs), Met (hepatocyte growth factor/scatter factor [HGF/SF] receptor) and the insulin receptor.

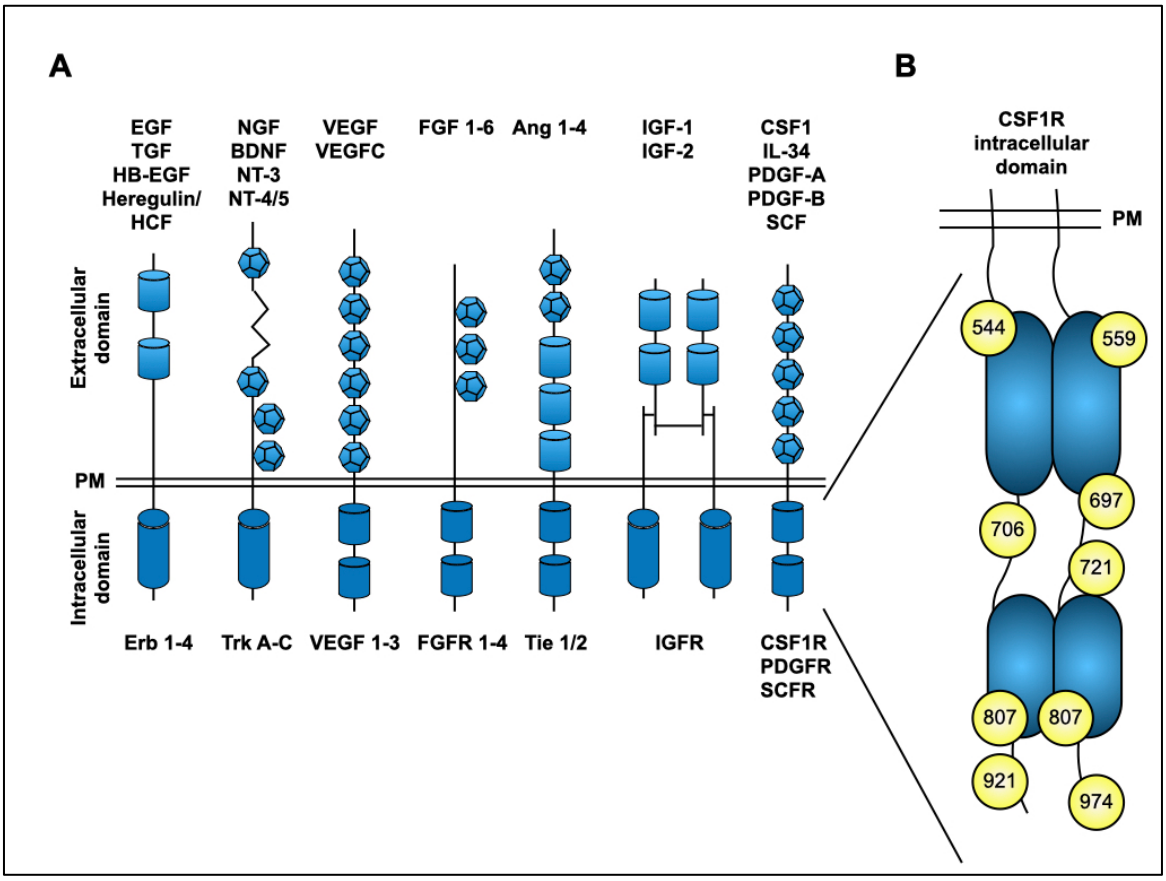

Figure 1.6.1.1: Topology of example receptor tyrosine kinases. *Subfamilies of RTKs with different intracellular and extracellular domain structure.* Binding of CSF1 to CSF1R leads to auto-phosphorylation on numerous tyrosine residues as shown in the diagram.

The CSF1R regulates the differentiation of myeloid progenitors into heterogeneous populations of monocytes, macrophages, DC and bone-resorbing osteoclasts (Douglass *et al.*, 2008). Moreover, this receptor regulates the survival, proliferation, differentiation and chemotaxis of differentiated macrophages. Binding of CSF1 to CSF1R leads to auto-phosphorylation on numerous tyrosine residues including Tyr-559 and Tyr-544 in the juxtamembrane domain, Tyr-697, Tyr-706, Tyr-721 in the kinase insert domain and Tyr-807, Tyr-921, Tyr-974 in the carboxy-terminal tail (Figure 1.6.1.1) (Stanley and Chitu, 2014a). Phosphorylation of CSF1R tyrosine residues creates various docking sites for several signalling molecules that lead to activation of downstream signalling pathways. In order to avoid dysfunctionality in the signalling pathway, an early and important step in controlling receptor activity is attenuation of signalling. Under varying conditions, both clathrin-mediated and clathrin-independent endocytosis play an important role in ligand-stimulated endocytosis, or micropinocytosis of occupied receptors and subsequent intracellular degradation of both ligand and receptor molecules (Murray, Wilson and Kellie, 2000; Sorkin and Goh, 2009). Thus, CSF1R activity may be controlled by ligand-induced down-regulation or down-modulation that occurs by ectodomain shedding on the plasma membrane as well as ligand-induced tyrosine phosphorylation (Sbarba and Rovida, 2002). Interestingly, CSF1R signalling may also be activated in a ligand-independent manner, following transactivation by other stimuli, such as, prostaglandin E2 (PGE_2), a key mediator of immunity and inflammation, following engagement to its G-protein-coupled E-prostanoid receptors, inducing Erk1/2 phosphorylation to promote macrophage migration (Digiacomo *et al.*, 2015).

1.7 IL-34 also activates CSF1R signalling

Proteomic analysis has confirmed that IL-34 is another ligand for CSF1R that competes with CSF1 for receptor binding and, like CSF1, promotes differentiation, proliferation and survival of monocytes, macrophages (Guillonneau, Bézie and Anegon, 2017). Fold recognition studies have reported that IL-34 is a four-helix bundle cytokine belonging to the same family as CSF1, but it shares no substantial sequence similarity with any other protein (Garceau *et al.*, 2010). IL-34 forms a non-covalently linked homodimer that binds to the same general region of the CSF1R as CSF1, but by interacting with distinctly different epitopes on the receptor (Felix *et al.*, 2013). This cytokine is primarily expressed in neurons, especially neurons that differ to those where CSF1 is expressed and is released by tissues such as

keratinocytes (Guillonneau, Bézie and Anegon, 2017). Recently, the receptor type protein-tyrosine phosphatase zeta (PTP-ζ) and CD138 (Syndecan 1) have been identified as potential IL-34 receptors (Nandi *et al.*, 2013; Segaliny *et al.*, 2015). Interestingly, researchers have not been able to establish any CSF1R- independent functions of IL-34 yet, indicating the possibility that PTP-ζ or CD138 and CSF1R work together to mediate IL-34 activity. Thus CSF1 and IL-34 signal through overlapping and distinct mechanisms.

Additional differences in the signalling activity of these two cytokines have been reported, with IL-34 having a higher affinity than CSF1 for the CSF1R that also resulted in a stronger, but more transient tyrosine phosphorylation of CSF1R and downstream mediators (Chihara *et al.*, 2010). Additionally, the biological activity and signal activation in human monocytes may differ for both ligands too (Boulakirba *et al.*, 2018). Unlike CSF1, IL-34 was found not to be required for embryonic development of microglia but it was essential for microglial homeostasis in specific areas of the adult brain (Greter *et al.*, 2012). Studies suggest that IL-34 enhances neuroprotection against oligomeric Aβ through insulin-degrading enzyme (IDE, also known as Aβ degrading enzyme) activity (Leissring *et al.*, 2003). Sustained overexpression of IDE in neurons also decreased Aβ levels and prevented amyloid plaque formation in IDE/APP double transgenic mice (Leissring *et al.*, 2003).

1.8 CSF1R in microglia and AD

An imbalance in CSF1R signalling exists in AD and manipulating CSF1 signalling has shown divergent effects in models of AD. An increase in the expression of CSF1 and CSF1R messenger ribonucleic acid (mRNAs) was found in the human AD brain (Walker, Tang and Lue, 2017). CSF1 is a key regulator of inflammatory responses as inducer of microglial proliferation in the brain and brain CSF1 increases in AD (Imai and Kohsaka, 2002). Several lines of evidence also suggest that robust microglial activation is mediated by a CSF1/CSF1R autocrine loop resulting in the release of inflammatory cytokines (Hao, Dheen and Ling, 2002). CSF1 was shown to be upregulated in human AD brain compared with non-demented controls and in AD-like transgenic mice (Olmos-Alonso *et al.*, 2016). Injecting CSF1 into APP/ PS1 mice intraperitoneally on a weekly basis, prior to the appearance of cognitive impairment, prevented cognitive deterioration, while, mice with already established

Aβ pathology had their cognitive decline stabilised (Boissonneault *et al.*, 2009). Conversely, in a primary rat neuron and microglia co-culture model, CSF1 synergised with fibrillar Aβ to induce neurotoxicity (Li *et al.*, 2004). Primary microglial cells in culture are able to phagocytose Aβ (Spangenberg *et al.*, 2016). However, the overall Aβ levels or plaque load was not affected by deletion of microglia in 5XFAD mouse models of AD, suggesting that, microglial phagocytosis can be compensated for, perhaps by other glial cells such as astrocytes (Spangenberg *et al.*, 2016). Elimination of microglia by inhibition of CSF1R with PLX5622, in 5XFAD mice, for 10 weeks did not result in accumulation of Aβ plaques. The elimination of microglia also reversed the altered (upregulated or downregulated) array of 413 synaptic genes in the mouse hippocampus (Spangenberg *et al.*, 2019).

Thus, the inherent difficulty in developing appropriate models that recapitulate the *in vivo* environment has led to several conflicting outcomes that emphasise the need for a more mechanistically detailed analysis of the involvement of CSF1R signalling, in terms of microglial function.

1.9 CSF1R inhibitors

PLX3397 (Pexidartinib) is a selective tyrosine kinase inhibitor, primarily inhibiting CSF1R (IC_{50} = 0.02 μM) but also closely related family members, c-Kit (IC_{50} = 0.01 μM) and FLT3 (IC_{50} = 0.16 μM) (Patwardhan *et al.*, 2014; Chitu *et al.*, 2016).

PLX647 is a potent and selective CSF1R inhibitor (IC_{50} = 0.028 μM) and c-Kit (IC_{50} = 0.016 μM) (Bollag *et al.*, 2012). PLX647 blocked proliferation, migration, and activation of macrophages, osteoclasts, and mast cells (Zhang *et al.*, 2013).

Ki20227 is another comparably specific and potent inhibitor of CSF1R and c-Kit with IC_{50} of 0.023 μM for both kinases (Ohno *et al.*, 2006; Zhang *et al.*, 2013).

GW2580 is a competitive inhibitor of adenosine triphosphate (ATP) binding to the CSF1R with an IC_{50} of 0.03 μM that blocked receptor autophosphorylation (Figure 1.9.1) (Conway *et al.*, 2008). GW2580 was highly selective, against a panel of 186 other kinases *in vitro* and completely inhibited CSF-1-induced growth of rat monocytes, with an IC_{50} value of 0.2 μM (Conway *et al.*, 2008).

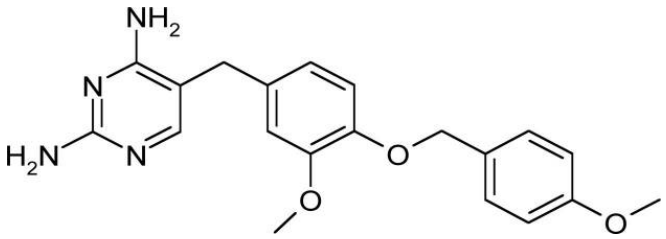

Figure 1.9.1: Chemical structure of GW2580. (adapted from Conway et al., 2005).

The CSF1R pathway is upregulated in a number of diseases such as rheumatoid arthritis, inflammatory bowel disease, glomerulonephritis, arteriosclerosis, some type of cancers and various neurodegenerative diseases including AD (Conway *et al.*, 2005). Excessive microglial proliferation driven by overactivation of CSF1R-dependent signalling is associated with disease pathology. Therefore, controlling microglial proliferation under pathological conditions is critical for handling the innate inflammatory responses which is key to the onset of neuroinflammatory diseases and their progression. Thus any drug that could attenuate CSF1R signalling would be a promising candidate for treating AD (Figure 1.9.2). GW2580 will be used in this study because most of the other CSF1R inhibitor strategies may deplete the whole microglial population. GW2580 only inhibits microglial proliferation and even at higher doses total microglial cell number is not affected (Olmos-Alonso *et al.*, 2016). As microglia has a role in the maintaining homeostasis in the brain, elimination of a beneficial microglial population is undesirable.

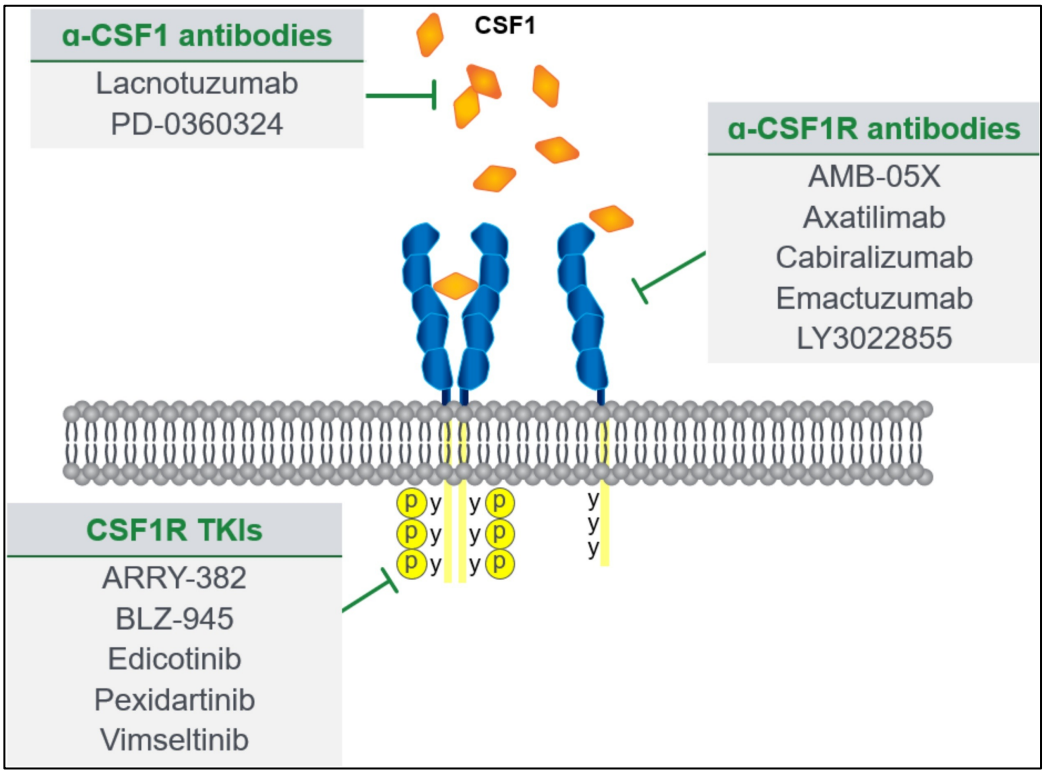

Figure 1.9.2: Clinical Approaches to inhibiting CSF1R signalling. Inhibition of the CSF1R pathway may be achieved through small molecule inhibitors or anti-CSF1R monoclonal antibodies. Monoclonal antibodies against CSF1 are currently being tested in clinical trials. (Figure adapted from Ordentlich, 2021).

1.10 CSF1R signalling activates cell growth and proliferation in macrophages

CSF1R activation leads to the stimulation of various downstream signalling pathways, including phosphoinositide 3-kinase (PI3K) signalling (Figure 1.10.1) (Stanley and Chitu, 2014b). PI3Ks are lipid kinases that are important in cell differentiation, survival, motility and intracellular trafficking (Ji *et al.*, 2011). PI3Ks are comprised of heterodimers of catalytic and adaptor subunits that are classified into three main groups based on their homology to each other and substrate specificity. PI3Ks phosphorylate phosphatidylinositol substrates at the 3' position of the inositol ring to generate lipid second messengers that activate downstream signalling and membrane trafficking responses. Members of the Class 1 PI3Ks are heterodimers of a regulatory subunit (p85) and a catalytic subunit (p110). Stimulation of RTK phosphorylation at specific tyrosine residues leads to the recruitment of Class 1 PI3K complexes via binding to the tandem Src Homology 2 (SH2) domains present in the p85 regulatory subunit (Figure 1.10.1). The CSF1R activates PI3K signalling directly through phosphorylation of Tyr-721 (Sampaio *et al.*, 2011).

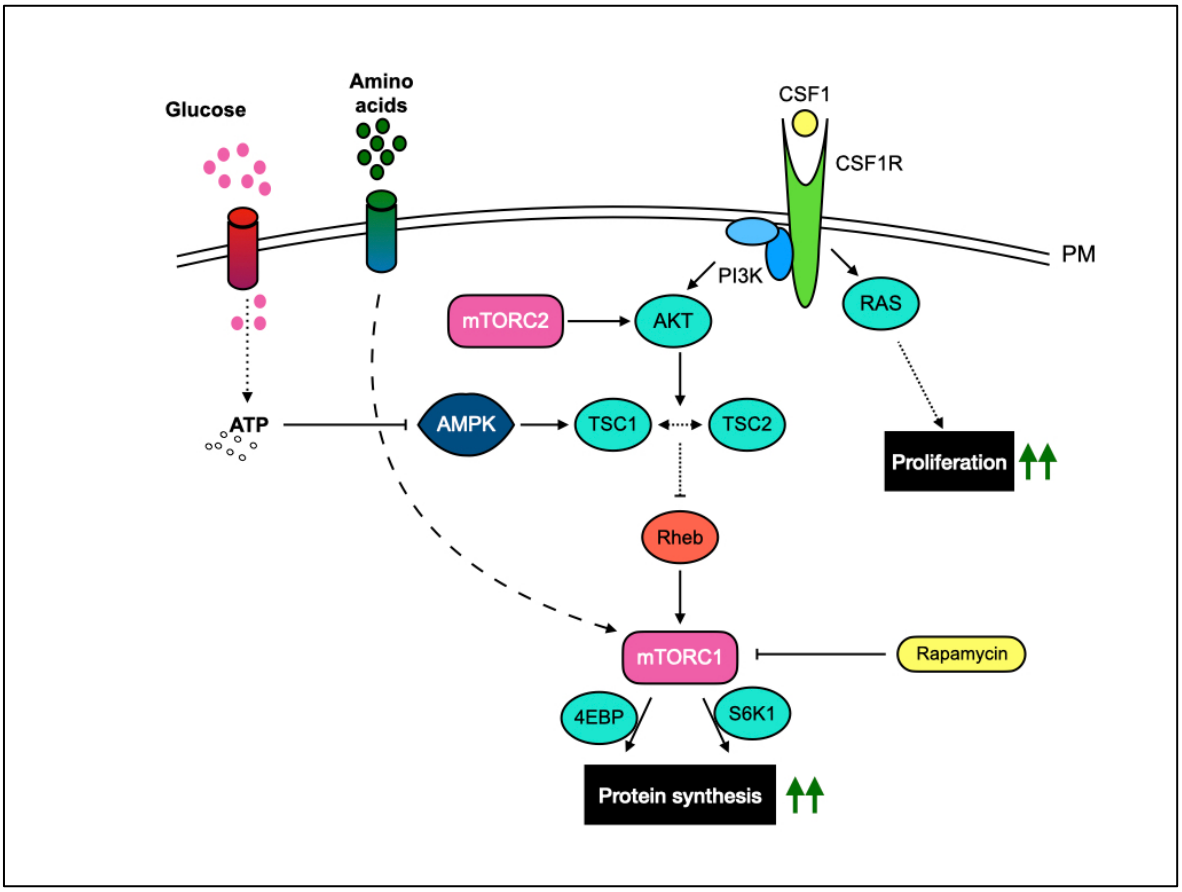

Figure 1.10.1: The putative mechanisms of mTORC1 regulation by CSF1R. By analogy with other RTK signalling, CSF1 presumably binds to the CSF1R to activate class I Phosphatidylinositol 3-kinase (PI3K) signalling that generates a Phosphatidylinositol (3,4,5)-trisphosphate (PtdIns3,4,5)P3 signal at the plasma membrane (PM) to recruit Akt (or PKB) and its upstream kinase 3-Phosphoinositide-Dependent protein Kinase-1 (PDK1). Once activated, Akt phosphorylates and causes the disassociation of the Tuberous sclerosis 1/2 (TSC1/2) complex, and in so doing, derepresses the small GTPase Ras-homologue enriched in brain (Rheb). Rheb GTPase activity then promotes activation of mammalian target of rapamycin complex 1 (mTORC1) signalling. In tandem, mTORC1 also receives signals from energy sensing and amino acid availability that together led to full mTORC1 stimulation. The mTORC1 complex then phosphorylates and activates S6 kinase 1 (S6K1) and 4E-binding Protein (4EBP1), which in turn promote protein translation and supports cell growth, proliferation, and metabolism, combined with activation of RAS pathway signalling. Activity of mTROC1 can be attenuated by pharmacological inhibition, by drugs such as rapamycin, or by removal of nutrients and/or growth factors.

PI3K subsequently phosphorylates phosphatidylinositol 4,5-bisphosphate (PtdIns 4,5 P2 or PIP2) in the plasma membrane to generate the second messenger phosphatidylinositol-3,4,5-trisphosphate (PtdIns 3,4,5 P3 or PIP3). Generation of PIP3 promotes the recruitment and activation of downstream mediators of the PI3K signalling pathway, including the Ser/Thr protein kinase, Akt also known as Protein Kinase B (PKB). Activated PIP3 recruits 3-Phosphoinositide-Dependent protein Kinase-1 (PDK1) and Akt, via their PIP3-binding Pleckstrin Homology domains (PH domains). PDK1 phosphorylates Akt isoforms; Akt1, Akt2 and Akt3, although Akt1 is the most broadly expressed in brain, and in microglial cells (Levenga *et al.*, 2021). Akt is partially activated when phosphorylated on its hydrophobic motif Ser473, but PDK1 then phosphorylates the T-loop of Akt at Thr308 to fully activate Akt. Activated Akt then phosphorylates multiple downstream signalling proteins, including Tuberous Sclerosis Complex proteins 1 and 2 (TSC1/2), leading to disassociation of this complex. As a result, the GTPase Ras-homologue enriched in brain (Rheb) is de-repressed and leads to activation of mammalian/mechanistic Target Of Rapamycin Complex 1 (mTORC1) activation (Rad, Murray and Tee, 2018). PI3K signalling is attenuated by dephosphorylation of PIP3 to PIP2 by the dual specificity Phosphatase and Tensin homolog deleted on chromosome 10 (PTEN) (Chalhoub and Baker, 2009).

1.11 mTORC1 acts as a nexus of multiple pro-growth signals

The mTOR kinase is a highly conserved serine/threonine kinase and a master regulator of cell size, growth and proliferation and is found in two different complexes: mTORC1 and mTORC2 (Figure 1.10.1) (Rad, Murray and Tee, 2018). The mTORC1 complex consists of the proteins mTOR, Raptor, GβL (mammalian lethal with SEC13 protein 8, mLST8) and domain-containing mTOR-interacting protein (DEPTOR). Much less is known about the mTORC2 pathway. This complex is composed of mTOR, Rictor, GβL, Sin1, PRR5/Protor-1 and DEPTOR, which promote cell survival through the direct activation of Akt through phosphorylation of its hydrophobic motif Ser 473 (Sarbassov *et al.*, 2005). The mTORC1, but not the mTORC2 complex is inhibited by its namesake, rapamycin, through targeting of the Raptor protein that facilitates substrate recognition (Rad, Murray and Tee, 2018). mTORC1 is activated by the small GTPase Rheb through direct interaction with mTOR (Long *et al.*, 2005). mTORC1 phosphorylates multiple downstream targets,

including eukaryotic translation initiation factor 4EBP1 and S6K1 to control protein synthesis and therefore cell growth and proliferation.

1.11.1 Role of mTORC1 in growth and proliferation

Various environmental inputs including cellular energy levels, nutrient availability and growth factor activation of RTKs are coordinated by the mTORC1 to regulate cell growth and proliferation. Aside from driving protein synthesis, mTORC1 also supports *de novo* lipid synthesis through the sterol-responsive element binding protein (SREBP) transcription factor, in order to facilitate new cell membrane formation and expansion (Porstmann *et al.*, 2008). Through SHREBP, mTORC1 also promotes the oxidative pentose phosphate pathway (PPP), which utilises carbons from glucose to generate Nicotinamide Adenine Dinucleotide Phosphate (NADPH) and other intermediary metabolites needed for proliferation and growth (Düvel *et al.*, 2010). mTORC1 also promotes the synthesis of nucleotides required for DNA replication and ribosome biogenesis in growing and proliferating cells (Valvezan *et al.*, 2017). To facilitate all this anabolic activity, mTORC1 also suppresses catabolic destruction of material by regulating the activity of the major route of cellular turnover; autophagy (Wang and Zhang, 2019).

1.12 Maintenance of cellular homeostasis requires autophagy

During periods of physiological stress, including nutrient or energetic stress, almost all eukaryotic cells initiate catabolic processes to preserve cellular homeostasis and to prevent catastrophic damage from overwhelming the cell. Physiological stresses can lead to the accumulation of damaged and unwanted organelles, misfolded proteins or irreparable DNA fragments that are degraded to maintain normal homeostatic functions. To this end, autophagy is a specialised series of mechanisms that facilitate the delivery of unwanted material to the lysosome. Autophagy is also a cytoprotective mechanism that can remove damaged organelles and facilitate cellular and organismal development, survival, differentiation and proliferation (Wolfe *et al.*, 2013).

There are three main types of autophagy: macroautophagy, microphagy and chaperone-mediated autophagy (CMA). Macroautophagy can be further classified as either selective or non-selective “bulk” autophagy. They differ in their mechanism for lysosomal delivery and also cargo specificity. Macroautophagy, the most common form of autophagy, is dependent on the specialised autophagy related proteins (ATGs) and is distinct from other cytoplasmic digestive processes,

including proteasomal degradation. This is due to its ability to capture and eliminate bulk cytoplasmic targets such as toxic protein aggregates of misfolded proteins or damaged organelles (Deretic, Saitoh and Akira, 2013). Microautophagy, involves degradation of portions of the cytoplasm, which are directly enveloped by the lysosomal membrane (Chen, Cescon and Bonaldo, 2014). Finally, CMA, only degrades individual, unfolded soluble proteins in a selective manner across the lysosomal membrane using a series of chaperone proteins (Chen, Cescon and Bonaldo, 2014). Ultimately, the process of lysosomal degradation is common to all forms of autophagy (Wolfe *et al.*, 2013). Microautophagy and CMA will not be discussed here and the term autophagy will, hereafter, refer to macroautophagy.

1.12.1 Homeostatic macroautophagy

Macroautophagy is a membrane trafficking pathway capable of sequestering cytosolic material and delivering that material to the lysosome for degradation. Under normal physiological conditions, most cells undergo autophagy at a low, basal level to maintain a balance between biosynthesis and turnover, whose activity level is upregulated upon induction of stress to the cellular environment. Deregulation of macroautophagy has been implicated in many pathologies, including neurodegenerative diseases such as AD (Nilsson *et al.*, 2013). Autophagy begins with the sequestration of certain cytoplasmic components within a nascent phagophore that then closes to form an autophagosome. Autophagosomes then traffic to, and fuse with lysosomes, exposing their contents to lysosomal hydrolases that then degrade this cargo and allow the liberation of biosynthetic building blocks, including small molecules, amino acids, lipids and ATP (Schulze, Kolter and Sandhoff, 2009).

While macroautophagy is regulated by diverse signalling mechanisms, most are integrated through mTORC1 signalling (Laplante and Sabatini, 2009). The mTORC1 complex negatively regulates autophagy during times of minimal physiological stress or nutrient replete conditions (Schmelzle and Hall, 2000). The mTORC1 complex also integrates signals from amino acids, oxygen or energy status, to control protein and lipid synthesis (Laplante & Sabatini 2012). Thus, reduced availability of these signals, or inhibition of mTORC1, induces autophagosome formation (Mizushima, 2007) and also increases efficiency of autophagosome-lysosome fusion by upregulating lysosome biogenesis (Zhou *et al.*,

2013). Therefore, when mTORC1 activity is inhibited through various different mechanisms, this results in activation of autophagy beyond basal levels (Sengupta, Peterson and Sabatini, 2010).

Autophagy is induced not only by hypoxia, energy stress and nutrient deprivation, but also upon exposure to ROS, endoplasmic reticulum (ER) stress and bacterial infection (Rubinsztein, Mariño and Kroemer, 2011). However, the most potent physiological inducer of autophagy is nutrient depletion and this will be focused on in Chapter 3. Autophagy is upregulated within minutes in most cultured mammalian cells, in response to nutrient deprivation, in order to provide the cell with essential nutrients such as amino acids and fatty acids during the starvation period (Rubinsztein, Mariño and Kroemer, 2011). Maximal levels of autophagy are observed when cells are cultured in simultaneous absence of nutrients and growth factors such as those contained in serum (Boya *et al.*, 2005). When starved for 24-48 hrs most cells in most tissues display increased numbers of autophagosomes (Mizushima, 2010).

1.13 The autophagy pathway

Autophagy activation includes (1) initiation, (2) nucleation, (3) phagophore expansion, (4) lysosomal fusion and (5) degradation of cargo (Figure 1.13.1).

During step 1, initiation of autophagy occurs in part through activation of the Unc51-Like Kinase 1 (ULK1) complex. During step 2 vesicle nucleation/autophagosome formation, 'horse-shoe-shaped' structures, known as omegasomes bud from the endoplasmic reticulum (Axe *et al.*, 2008). Omegasomes form with the aid of PtdIns3P, generated by the class III PtdIns 3-kinase, PIK3C3, also known as a vacuolar protein sorting 34 (Vps34) (Axe *et al.*, 2008). (Mizushima, Yoshimori and Ohsumi, 2011). During phagophore expansion (step 3), the Autophagy related protein 12 (Atg12) and Microtubule-associated protein 1A/1B-light chain 3 (LC3)B conjugation systems coordinate multiple aspects of autophagosome assembly, including recruitment of additional membranes for membrane expansion and recruitment of cargo receptors to complete autophagosomal formation. Finally, in steps 4 and 5 mature autophagosomes fuse with lysosomes to form auto(phago)lysosomes thereby delivering their contents to the lumen of the lysosome where hydrolytic enzymes break down cargo (Figure 1.13.1).

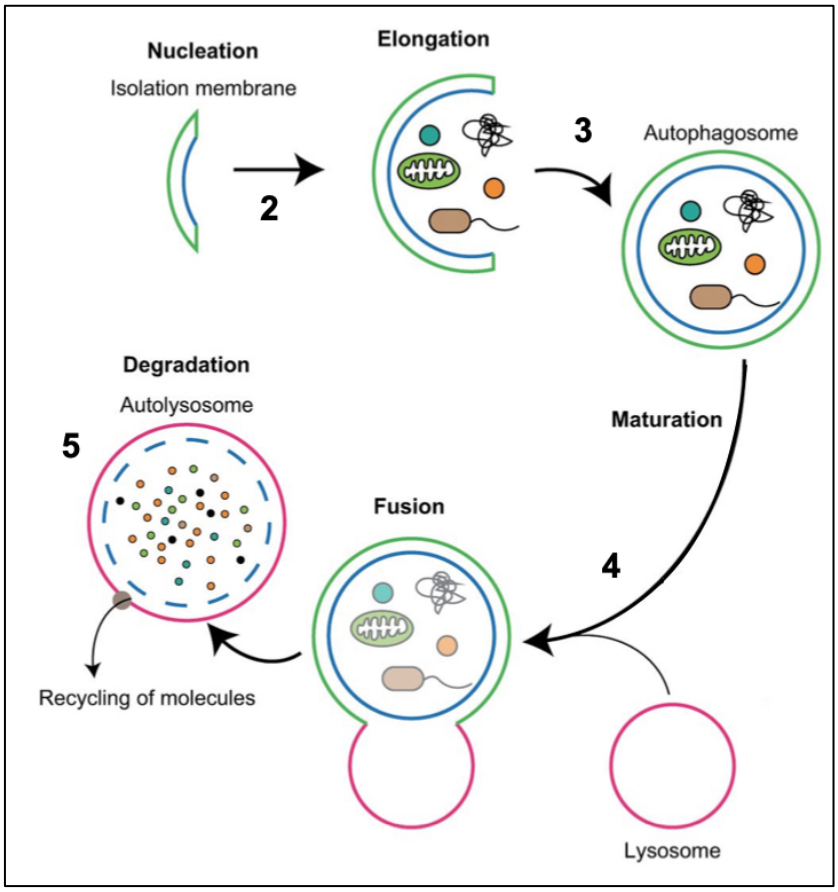

Figure 1.13.1: Steps of macroautophagy. Initiation of autophagy (not shown) forms an isolation membrane (phagophore) around cytoplasmic material that needs to be sequestered (nucleation, step 2), the isolation membrane then elongates to form a double-membraned autophagosome (elongation and autophagosome formation, step 3), autophagosome transports to a lysosome (maturation), docks and fuse with the lysosome to form an autophagolysosome (fusion, step 4), to degrade the cargo of an autophagolysosome (degradation, step 5). (Figure adapted from review Nakamura and Yoshimori, 2017).

1.13.1 Autophagy initiation and nucleation

Autophagy initiation is controlled by regulatory serine/threonine protein kinases ULK1 and/or ULK2 in the initiation complex, and by the lipid kinase activity of the class III PtdIns 3-kinase PIK3C3 complex (Figure 1.13.1.1). ULK1 phosphorylation on Ser555 by protein kinase AMP-activated catalytic subunit alpha (PRKAA/AMP)-activated protein kinase (AMPK) pathway is one of the main mechanisms leading to the induction of autophagy via phosphorylation and activation of PIK3C3 complex components (Russell *et al.*, 2013). Activated ULK1 then auto-phosphorylates at multiple sites, including Ser341 and Ser1047 (Dorsey *et al.*, 2009).

The ULK1 complex then translocates to the isolation membrane and induces autophagosome formation, thereby activating autophagy (Hosokawa *et al.*, 2009). Nutrient starvation such as amino acid withdrawal inactivates mTORC1 leading to dephosphorylation of ULK1 at Ser757 and Ser637, thereby increasing autophagy flux (Nwadike *et al.*, 2018).

Cellular compartments such as the ER, golgi apparatus, the mitochondria and plasma-membrane-derived endocytic organelles also contribute to phagophore formation (Mizushima, Yoshimori and Ohsumi, 2011).

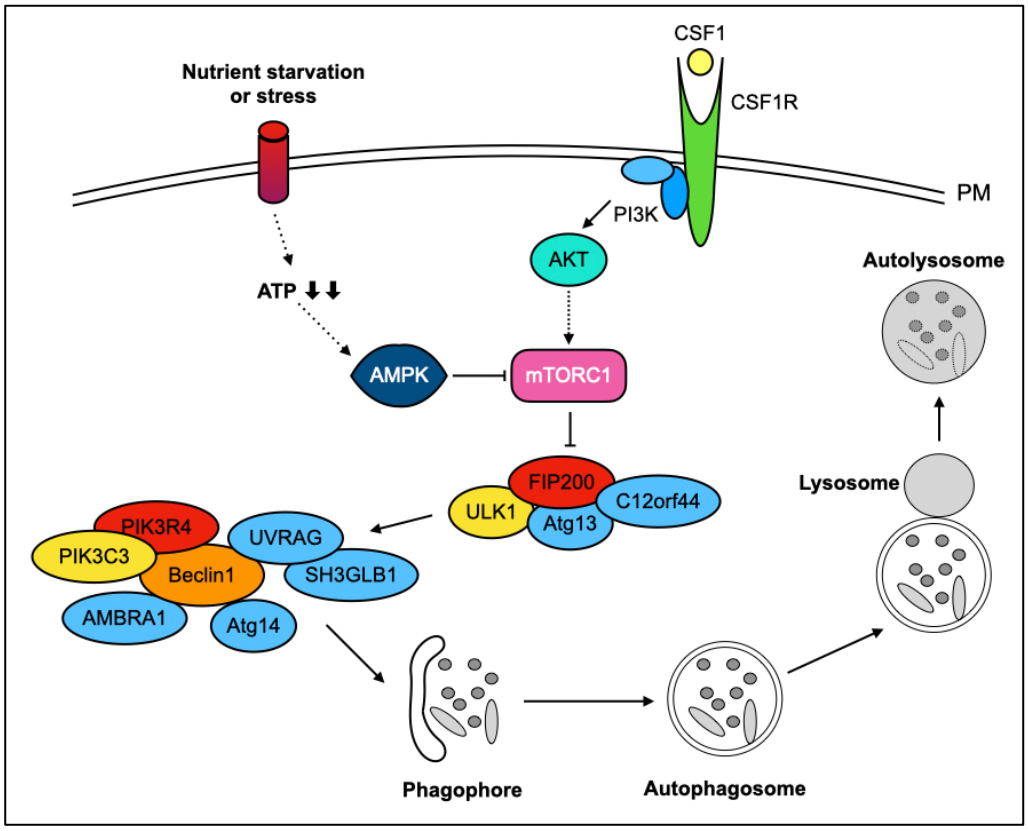

Figure 1.13.1.1: Regulation of autophagy initiation in cells. Under nutrient replete conditions, mTORC1 activity prevents activation of the ULK1 initiation complex. Following nutrient stress, mTORC1 is inactivated and ULK1 initiation complexes are activated and then promote the activity of the PIK3C3 complex to drive nucleation. Elongation of membranes that evolve into autophagosomes is then regulated by two ubiquitination-like reactions involving the ubiquitin-like molecules Atg12 and then LC3B (or related proteins Gamma-aminobutyric acid receptor-associated protein (GABARAP) and Golgi-associated ATPase enhancer of 16 kDa (GATE-16)). Atg12 is conjugated to Atg5 by Atg7 (E1-like activity) and by Atg10 (E2-like activity), then the Atg5-Atg12 complex associates with Atg16L on forming phagophores but dissociates before the autophagosome completes. Conjugation of LC3B to phosphatidylethanolamine occurs through Atg7 (E1-like activity) and Atg3 (E2-like activity), resulting in autophagosome-associated LC3B-II.

1.13.2 LC3 proteins and autophagosome formation

The ubiquitously expressed LC3B is a critical component of the autophagy pathway and a useful biomarker of the pathway itself. LC3B is expressed as a pro-form that is modified to a cytosolic form called LC3B-I. When autophagy is activated, LC3B-I is lipidated with phosphatidylethanolamine (PE), to form LC3B-II. Briefly, pro-LC3B is cleaved after the c-terminal glycine by Atg4B, a cysteine protease to form LC3B-I in the cytosol (Skytte Rasmussen *et al.*, 2017). Conjugation to PE is facilitated by Atg3/7, regulated by the Atg12 conjugation system (Fujita *et al.*, 2008). This conversion of LC3B-I to LC3B-II is reversible so that when autophagosome fusion with the lysosome is completed, any LC3B-II that is attached to the outer membrane of the autophagosome is de-lipidated by Atg4 proteases to regenerate the cytosolic form, LC3B-I thereby recycled in a semi-conservative manner that can become rate-limiting for the pathway (Kirisako *et al.*, 2000).

LC3B-II is associated with the isolation membrane, the outer and inner membrane of completed autophagosomes and some is also found in autolysosomes, therefore it is commonly used as an autophagosome/autolysosome formation marker (Kabeya *et al.*, 2004). Disappearance of LC3B-I can indicate induction of autophagy, especially when increase OR decrease of LC3B-II is also observed. However, this only demonstrates an activation of autophagy, not an ongoing process. Instead, monitoring 'flux' of autophagy over time is the standard for characterising autophagy activity. If autophagy is 'active', LC3B-II/LC3B-I ratios will at first increase as LC3B-I is converted to LC3B-II, then decrease over time as LC3B-II is then consumed. If autophagy is inhibited or no longer active, then the ratio of LC3B-II/LC3B-I will remain unchanged (Klionsky *et al.*, 2012). In mammals there is a second subfamily of related proteins containing GABARAP and GABARAPL 1/2/3 that undergoes similar modification to LC3B, but these proteins tend to only regulate phagophore maturation (Weidberg et al. 2010).

1.13.3 Autophagosome-lysosomal fusion and degradation of contents

Following elongation and closure of this phagophore, a double-membraned autophagosome is formed. This is where the phagophore-captured cytoplasmic cargo is sequestered and disposed of via fusion with the lysosome (Mizushima, Yoshimori and Ohsumi, 2011). Autophagosomes, are the principal morphological feature of autophagy, with a diameter of 0.5-1.5 μm (Mizushima et al. 2002).

This completed double-membrane autophagosome then traffics to the juxtanuclear regions where lysosomes are mainly found. Autophagosomes fuse with lysosomes, induced by the translocation of the soluble N-ethylmaleimide-sensitive factor-attachment protein receptors (SNARE) protein syntaxin 17 to the outer membrane of the completed autophagosome to mature into a single-membrane autolysosome (Itakura, Kishi-Itakura and Mizushima, 2012). After fusion, degradation of the captured cargo begins, facilitated by lysosomal hydrolases, such as peptidases, lipases and nucleases (Mizushima, Yoshimori and Ohsumi, 2011). Each step of mammalian autophagy cycle is rapid and it is estimated that autophagosome formation takes 5-10 minutes (Mizushima et al. 2001). After ending the degradation process in the lysosome, monomeric units are exported to the cytosol for reuse.

1.14 Autophagy in AD

Autophagy is an essential process with the crucial role of removing and degrading the intracytoplasmic deposition of proteins which tend to accumulate in neurodegenerative disorders, such as AD.

1.14.1 Dysfunctional autophagy in neurons

In AD, autophagy may be dysfunctional at different steps of the pathway starting from autophagosome formation through to degradation. Aberrant accumulation of immature autophagic vacuoles have been found in the hippocampal neuron long before the occurrence of any synaptic and neuronal loss occurred in 4-6 months old PS1M146L/APP751SL mouse model (Sanchez-Varo *et al.*, 2012). Autophagy is fundamental in both the generation and clearance of Aβ in AD. The Aβ production rate exceeds the clearance rate when the process of autophagic turnover of APP-rich organelles is malfunctional (Steele *et al.*, 2013). Nilsson and colleagues have shown that neurons release Aβ peptides in an autophagy-dependent manner in *Atg7* KO APP/PS1 mice (Nilsson *et al.*, 2013). An accumulation of autophagic vacuoles (AV) in neurons due to impeded maturation of autophagosomes and their retrograde transport and greater number of dystrophic neurites containing the AVs, were found in post-mortem AD brain compared to age-matched controls. (Cataldo *et al.*, 1997; Nixon, 2007). The interaction between autophagy machinery, lysosomal activity and neuroinflammation is regarded as a key event in AD advancement. For instance, deletion of cystatin B, an endogenous inhibitor of lysosomal cysteine proteases of the cathepsin family, restores lysosomal proteolytic activity (Yang *et*

al., 2011). This in turn prevents autophagy flux blockade in neurons, decreases Aβ load, and protects mice from learning and memory deficits in the TgCRND8 mouse model of AD (Yang *et al.*, 2011). Inhibition of Aβ-degrading metalloprotease enzyme, neprilysin, saw an increased level of $A\beta_{42}$ accumulation in the lysosome, especially in the lysosome of ApoE4 transgenic mice, with an accompanied death of hippocampal, entorhinal and septal neurons and a remarkable decline in cognitive ability (Belinson *et al.*, 2008).

1.14.2 Dysfunctional autophagy in microglia

Although, it remains uncertain whether dysfunctional autophagy is the cause or consequence of AD pathology, there is evidence of disrupted autophagy in microglia. Abundant autophagic vesicles has been reported in microglia from AD patients carrying TREM2 risk variants and in TREM2-deficient mice with AD-like pathology and in TREM2-deficient macrophages under growth factor limitations by Ulland and colleagues. In this study, the aberrant autophagy has been linked to impaired mTOR signalling as seen by decreased phosphorylation of 4EBP1, Akt at Ser473 and N-myc downstream-regulated gene 1 (NDRG1) in Trem2 deficient microglia isolated from $Trem2^{-/-}$ 5XFAD mice, affecting ATP level and bioenergetic pathways (Ulland *et al.*, 2017). Aβ degradation is impaired in microglia isolated from 5XFAD mice and rapamycin-induced autophagy ameliorated Aβ degradation (Daily and Amer, 2020). Microglia are found in an inflamed state in AD, while autophagy can influence microglial inflammatory response in AD: in Aβ-treated microglia *in vitro*, knockdown of autophagy-related genes *LC3B* and *Atg7* activate the (NOD)-like receptor protein 3 (NLRP3) inflammasome, a multiprotein cytosolic complexes that are assembled by the PRR following the detection of infectious and damaging stimuli to regulate the activity of inflammatory proteases of the caspase family, and this enhanced IL-1β secretion while TNF-α release was not affected (Cho *et al.*, 2014). In general. studies performed on microglial autophagy are still limited and the correlation between autophagy and microglial function during AD needs further attention.

1.14.3 Upregulation of autophagy may be beneficial in AD

Stimulation of autophagy may conversely play a positive role in the disease. For instance, elevated autophagy lowered Aβ and tau levels and prevented memory loss in TgCRND8 AD mouse model (Yang *et al.*, 2011). While retroviral-mediated

overexpression of the autophagy-regulating transcription factor Transcription Factor EB (TFEB) in 5xFAD and rTg4510 mice significantly decreased neurofibrillary tangles, abrogated behavioural and synaptic deficits, and neurodegeneration (Polito *et al.*, 2014). In the APP/PS1 mouse model of AD, depletion of Beclin1, a component of the PIK3C3 nucleation complex, resulted in accumulation of intracellular and extracellular Aβ, highlighting the importance of early autophagosome formation in limiting the disease (Pickford *et al.*, 2008). Here, results demonstrated that a decrease in Beclin1 was observed in AD patients but not in the APP/PS1 mouse model of AD, pointing to the possibility that Beclin1 reduction occurs upstream of amyloid pathology. An increase of CD68 immunoreactivity (an endosomal/lysosomal activation marker) in the microglia of *Beclin1*$^{+/-}$ AD mice has been observed, without affecting microglial number, determined by Iba1 labelling (Pickford *et al.*, 2008). In accordance with this work, it has been demonstrated that overexpression of the autophagy cargo protein Sequestosome 1 (SQSTM1/p62), by adenoviral infection of neurons, improved cognitive functions and reduces Aβ pathology in an autophagy-dependent manner in APP/PS1 mice. This finding was confirmed by both removal of the LC3B-interacting region (LIR) motif of p62, or with pharmacological inhibition of autophagy, which were both sufficient to prevent Aβ clearance (Caccamo *et al.*, 2017).

An autophagy-mediated rescue of cognitive deficits and amelioration in Aβ and tau pathology has been observed following pharmacological inhibition of mTORC1 with rapamycin, where decreased mTORC1 signalling by chronic administration of rapamycin for 60 weeks decreased Aβ levels in 3xTg-AD mice (Caccamo *et al.*, 2010). Similar data was also obtained by Spilman and colleagues, who showed long term inhibition of mTORC1, by administration of rapamycin for 13 weeks prevented AD-like cognitive deficit and decreased Aβ levels in a PDAPP transgenic mouse model of AD (Spilman *et al.*, 2010). The above studies involving microglial autophagy and modulation of the mTORC1 signalling pathway indicate that converting proliferating microglia into non-proliferating, autophagy competent microglia, could be a potential therapeutic strategy for the amelioration of AD (Figure 1.14.3.1).

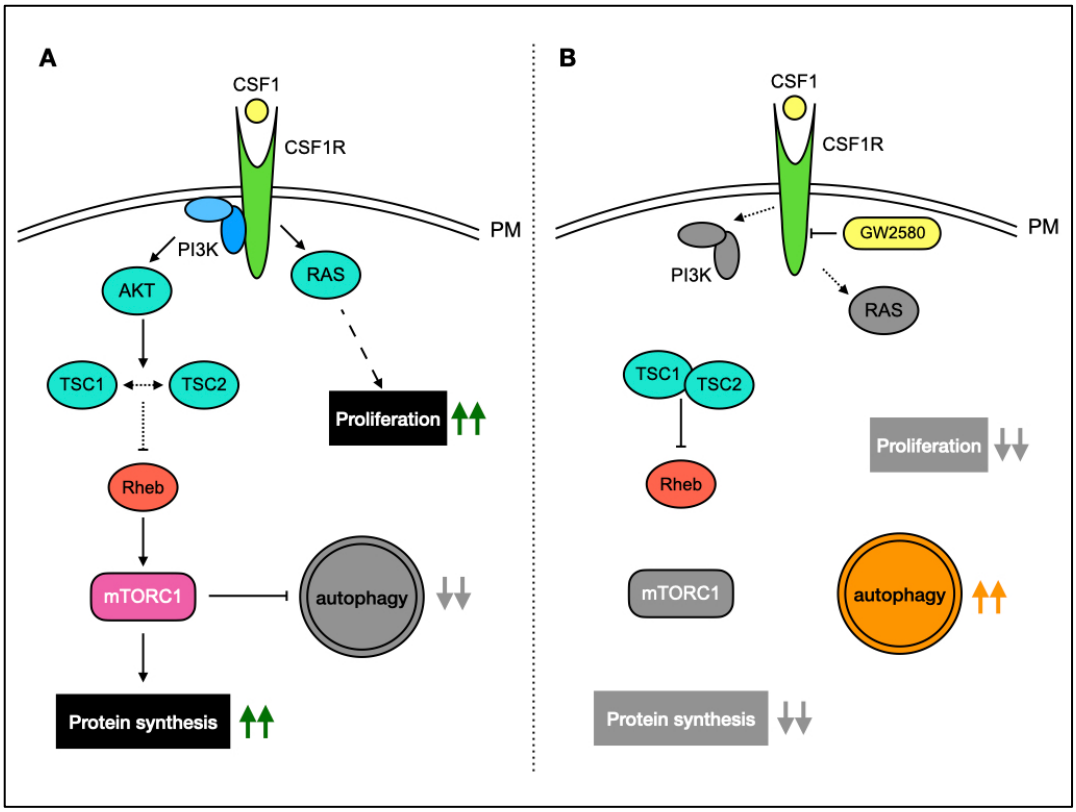

Figure 1.14.3.1: Hypothesis of thesis. Under normal signalling, microglial cells are driven to proliferate by CSF1. This occurs via activation of RAS and PI3K signalling, leading to increased protein synthesis and biomass to support cell division (panel A). Treatment of microglia with GW2580 to inhibit CSF1R signalling will attenuate microglial cell proliferation and may also drive autophagy, by inhibition of PI3K and therefore mTORC1 signalling (panel B).

1.15 Aims and objectives

The studies described in this thesis were designed to address three key questions:

1) Does CSF1R signalling control autophagy in microglia, *in vitro?*

2) What aspects of CSF1R signalling influence microglial phenotypes, *in vitro*?

3) How does CSF1R inhibition affect microglial activation, in the APP/PS1 model of AD?

Chapter 2: Materials and methods

2.1 Materials

Table 2.1.1 Tissue Culture Reagents & Products:

Dulbecco's Modified Eagle Medium with High Glucose, L- glutamine (DMEM)	Sigma Aldrich
Dulbecco's Phosphate Buffered Saline without calcium chloride and magnesium chloride (D-PBS)	Sigma Aldrich
Earle's Balanced Salt Solution (EBSS)	Sigma Aldrich
Fetal Bovine Serum (FBS)	Sigma Aldrich
L-glutamine (100x)	Sigma Aldrich
Penicillin/Streptomycin	Sigma Aldrich
Trypan blue	Sigma Aldrich

Table 2.1.2 Animals & in vivo Products:

Animal Recovery Chamber HE010	Vet Tech, UK
ANY-maze video tracking software	ANY-maze
APP/PS1 mice	Jackson Laboratories, USA
Burrowing tubes	Custom designed in TCD
C57BL/6 mice	Jackson Laboratories, USA
Heating pad	Physitemp
Laboratory mouse diet	LabDiet, USA
Morris Water Maze Tank	Ugo Basille
Non-toxic water-based paint	Reeves, UK
Open Field Box	Custom designed in TCD
T-Maze	Custom designed in TCD
Tunnel (6cm high X 9cm wide X 40cm long)	Custom designed in TCD

Table 2.1.3 Molecular Reagents & Products:

0.2 mL qPCR sterile tubes	Fisher Scientific
Ammonium persulfate	Sigma Aldrich, UK
Biometra Trio RT-PCR thermocycler	Analytick Jena
Cheemidoc MP gel imager	BioRad
Complete™ Protease Inhibitor Cocktail	Roche
Coomassie Protein Assay Reagent	Thermo Scientific Pierce)
Dimethyl sulfoxide (DMSO)	Sigma Aldrich, UK
Dried Skimmed Milk	Marvel
FastStart SYBR green PCR master mix	Roche, UK
FastStart universal ROX probe PCR master mix	Roche, UK
Fluorescent Mounting Medium	Dako
Gel loading pipette tips	Cruinn
Gel tank AE6450 ATTO	Medical Supply Company
GelRed™ nucleic acid stain	Scientific laboratory supplies
Greiner Plate sealer transparent	Greiner, USA
Griess Reagent Kit, for nitrite quantitation	Invitrogen
H2DCFDA	Invitrogen
High Capacity cDNA Reverse Transcriptase Kit	Applied Biosystems, UK
Immobilon-P Transfer Membrane	Millipore
iScript cDNA synthesis kit	BioRad
LDS (4x) Sample Buffer	Invitrogen
MicroAmp 96-well Reaction Plate	Applied Biosystems, UK
Molecular grade absolute ethanol	Sigma Aldrich, UK
Molecular grade chloroform	Sigma Aldrich, UK
Molecular grade glycogen	Thermo Fisher
Molecular grade isopropanol	Honeywell
Molecular grade water	Sigma Aldrich, UK
Mouse CCL2 DuoSet ELISA	RnD Biosystems, USA
Mouse CXCL1 DuoSet ELISA	RnD Biosystems, USA
Mouse CXCL10 DuoSet ELISA	RnD Biosystems, USA
Mouse IL-1ra DuoSet ELISA	RnD Biosystems, USA

Mouse IL-6 DuoSet ELISA	RnD Biosystems, USA
Mouse TNFα DuoSet ELISA	RnD Biosystems, USA
Nanodrop ND1000 Spectrophotometer	Thermo Fisher
Nunc™ MaxiSorp™ ELISA Plates, Uncoated	Biolegend Way, USA
Optical adhesive covers	Applied Biosystems, UK
Paraformaldehyde (PFA), 32 % (v/v) solution	Electron Microscopy Sciences
pGEM® DNA Markers	Promega
Primers custom designed oligonucleotides	Sigma Aldrich, UK
Qiashredder columns	Qiagen, UK
Ribolock Rnase Inhibitor	Thermo Fisher
RNase-free DNase I enzyme	Qiagen, UK
RNeasy Plus micro kits	Qiagen, UK
RNeasy Plus mini kits	Qiagen, UK
StepOne 96 well qPCR machine	Thermo Fisher
Substrate Reagent Pack	RnD Biosystems, USA
TEMED	Sigma Aldrich, UK
Tetramethylethylenediamine (TEMED)	Melford
TMB Liquid Substrate for ELISA	Applied Biosystems
Tris HCl	Melford
Tris(hydroxymethyl)aminomethane Base (Tris Base)	Melford
TRIzol™ Reagent	Invitrogen
Whatman 3MM Blotting and Chromatography paper	Thermo Fisher Scientific

Table 2.1.4 FACS Reagents & Products:

70 µM cell strainers	Sigma Aldrich, UK
7-AAD conjugated antibody	Miltenyi
BD FACS Aria II Cell Sorter	BioSciences, USA
CD11b FITC conjugated antibody	Miltenyi
CD45 APC conjugated antibody	Miltenyi
Collagenase	Roche
Dnase I	Thermo Fisher, USA
FBS	BioSciences, USA
GLAST ACSA-1-PE conjugated antibody	Miltenyi
HBSS	BioSciences, USA
HEPES	Merck
Lobind 1.5ml Eppendorfs	Fisher Scientific
LS positive selection columns	Miltenyi
MACS anti myelin beads	Miltenyi
MACS Buffer	Miltenyi
MACS sorting rig	Miltenyi
Purified Rat Anti-Mouse CD16/CD32 (Mouse BD Fc Block™)	BioSciences, USA
TRIzol™ LS Reagent	Invitrogen

Table 2.1.5 General Laboratory Chemicals:

1,3-bis(tris(hydroxymethyl)methylamino)propane (Bis-Tris)	Melford
2-(bis(2-hydroxyethyl)amino) acetic acid (Bicine)	Melford
3-(3-cholamidopropyl)dimethylammonium-1-propanesulfonate (CHAPS)	Melford
3-morpholino propane-1-sulfonic acid (MOPS)	Melford
Acrylamide 30 % (w/v)	BioRad
Ammonium persulfate (APS)	Sigma Aldrich, UK
Bafilomycin A1	Sigma Aldrich, UK
Bis Acrylamide	Melford
Bovine Serum Albumin (fraction V)	Sigma Aldrich, UK
Butan-1-ol	Sigma Aldrich, UK
β-Mercaptoethanol	Sigma Aldrich, UK
EDTA	Sigma Aldrich, UK
Glycerol	Sigma Aldrich, UK
Heparin (bovine)	Leo Laboratories, UK
Hydrochloric acid	VWR, USA
Hydrogen peroxide (H_2O_2)	Sigma Aldrich, UK
Methanol	Sigma Aldrich, UK
Paraformaldehyde	Sigma Aldrich, UK
Phosphate-buffered saline (PBS)	Sigma Aldrich, UK
Potassium Bicarbonate	Sigma Aldrich, UK
Sodium Bicarbonate	Sigma Aldrich, UK
Sodium Carbonate	Sigma Aldrich, UK
Sodium Chloride (NaCl)	Sigma Aldrich, UK
Sodium Hydroxide	Sigma Aldrich, UK
Sodium phosphate dibasic heptahydrate	Sigma Aldrich, UK
Sodium phosphate monobasic dihydrate	Sigma Aldrich, UK
Sulphuric acid (H_2SO_4)	VWR, USA
Tris-base	Sigma Aldrich, UK
Tris-HCl	Sigma Aldrich, UK
Triton X-100	Sigma Aldrich, UK
Tween 20	Sigma Aldrich, UK

Table 2.1.6 General Laboratory Equipment

800W compact microwave	SANY
AutoRep E automatic pipette	Ranin
Cell culture laminar flow hood	NuAire
Countess® Automated Cell Counter	Invitrogen
Cryogenic liquid nitrogen TR7 dewar 7 litre	Air Liquide
Driblock DB-2A tube heating block	Techne
Easy-Read® thermometer	Sigma Aldrich
Edge pH Probe	Hanna
Electroblot transfer tanks; Trans-blot Cell; Invitrogen, XCell II Blot Module	BioRad
Electrophoresis power supply	BioRad
FB15012 TopMix vortex	Fisher Scientific
Finn pipettes	Cruinn
Gilson pipettes	Gilson
JB Aqua Pluss Water Bath	Grant
Mag stirrer heat stir CB162	Stuart
Mammalian cell culture incubator	Sanyo
ME1002 weighing Scale	Mettler Toledo
Micro CL21R desktop centrifuge	Thermo Fisher
Microscope - Eclipse TS100	Nikon
MilliQ water dispenser	Millipore
PS-M3D orbital shaker	Grant Bio
PYREX™ glassware beakers 100, 250, 500, 2000ml	Fisher Scientific
PYREX™ media bottles 100, 250, 500, 1000ml	Fisher Scientific
S810R Eppendorf centrifuge	Merck
SDS-PAGE systems, Mini-Cell and Criterion Cell	Invitrogen and BioRad
See saw rocker SSM4	Stuart
Spectrophotometer, BioPhotometer	Eppendorf
Stainless steel liquid nitrogen dewar 2 litres	Dilvac
Technico mini-picofuge	Analytix
Ultra-Low Temperature Freezer -86℃	Haier Biomedical
Vibra Cell Sonicator with Stepped Microtip	Sonics

2.2 Buffers and Solutions:

All reagents were obtained from Sigma-Aldrich, Poole Dorset, unless otherwise stated.

LDS protein electrophoresis sample buffer (4x):

To make a final 4x stock, 900 µL of 4x LDS Sample Buffer (Invitrogen) was mixed with 100 µL of 500mM dithiothreitol.

Lysis Buffer:

50 mM Tris Base, pH 7.5, 1 mM EGTA, 1 mM EDTA, 1 mM activated sodium orthovanadate, 10 mM ß-glycerol phosphate, 50 mM sodium fluoride, 5 mM sodium pyrophosphate, 0.27 M sucrose, 0.3 % (w/v) CHAPS, 0.1 % (v/v) ß-mercaptoethanol and one Complete Protease Inhibitor Cocktail tablet (Roche) per 50 mL of lysis buffer were added just before use.

MOPS SDS PAGE protein electrophoresis buffer (20x):

1 M MOPS, pH 7.7, 1 M Tris Base, 69.3 mM SDS, 20.5 mM EDTA.

Phosphate-buffered saline solution (PBS):

137 mM sodium chloride, 2.7 mM potassium chloride, 10 mM sodium phosphate, 1.8 mM potassium phosphate monobasic, pH 7.4.

Tris-buffered saline solution (TBS):

20 mM Tris base, pH 7.5, 150 mM sodium chloride.

TBS-Tween (TBS-T):

20 mM Tris base, pH 7.5, 150 mM sodium chloride, 0.1 % (v/v) Tween 20.

Western blot transfer buffer:

500 mM Bicine, 500 mM Bis-Tris, 20.5 mM EDTA, 1 mM chlorobutanol, pH 7.2.

Western blot blocking buffer:

5 %(w/v) non-fat dried milk powder in TBS-T.

Stripping buffer (100 mL):

25 mM glycine, 0.1 % (w/v) SDS, 1 % (v/v) Tween-20 – pH 2.2.

2.3 Cell culture

2.3.1 Aseptic technique

All cell culture work was done under sterile conditions in NuAire laminar flow hood. This hood maintains a sterile environment by filtering air to prevent air-borne pathogens from entering the work area. The interior of the hood was sprayed with 70 % (v/v) ethanol solution before and after cell work to ensure sterile conditions. Any materials put into the hood was also sprayed with 70 % (v/v) ethanol solution. Disposable latex gloves were always worn and were sprayed with 70 % (v/v) ethanol solution before entering the work area.

2.3.2 Maintenance of BV2 cell line

BV2 cells were a generous gift from Prof. Marina A. Lynch, Trinity College Dublin. BV2 cells were maintained in Roswell Park Memorial Institute (RPMI) medium supplemented with 10 % (v/v) fetal bovine serum (FBS), 100 U mL^{-1} penicillin, 100 µg mL^{-1} streptomycin and 2 mM L-glutamine (complete media). Cells were cultured in 175 cm^2 flasks until they reached 80-90 % confluency and were then sub cultured 1:2, thrice a week.

2.3.3 Maintenance of IMG cell line

Immortalized microglial (IMG) cells were a kind gift from Prof. Antonio Cuadrado, Autonomous University of Madrid. IMG cells were maintained in Dulbecco's Modified Eagle's Medium (DMEM) supplemented with 10 % (v/v) fetal bovine serum (FBS), 100 U mL^{-1} penicillin, 100 µg mL^{-1} streptomycin and 2 mM L-glutamine (complete media). Cells were cultured until in 175 cm^2 flasks until they reached 80-90 % confluency and were then sub cultured 1:5 or 1:10, thrice a week.

2.3.4 Passaging and counting cell lines

Cells were maintained at 37 °C and 7.5 % CO2 in a humified incubator with cell growth and viability monitored by light microscopy (Nikon Eclipse TS100). To subculture, redundant media was aspirated out. Cells were washed twice with 10 mL PBS before adding 2 mL trypsin solution (0.025 g mL-1)/ EDTA (0.002 g mL-1) and incubating at 37 °C for 10 min to detach the cells. Dissociation was terminated by adding 8 mL of full media to the flask to obtain a 10 mL cell suspension. Cells were then centrifuged at 280 x g, for 5 min before resuspending in 10 mL of full media. Cells were passaged at a 1:2, 1:5 or 1:10 dilution as required.

When seeding cells for an experiment, an equal volume of cell suspension (10 µL) was mixed with Trypan Blue in a clean microcentrifuge tube and cells were counted and viability estimated using a Countess Automated Cell Counter (Invitrogen).

2.4 Cell proliferation and viability assay

2.4.1 Crystal Violet assay

Crystal violet is a triarylmethane dye, which binds to cellular DNA. Thus, staining of cells with crystal violet quantifies cell viability/cell proliferation. Cells were seeded at the densities indicated in the results chapters in 6-well plates and incubated overnight. The following day, cells were treated as required before washing once with 2 mL PBS then being fixed with 1 mL of 100 % methanol for 10 mins. Cells were stained with 2 mL of a 0.5 % (w/v) crystal violet solution for 10 mins on a see-saw rocker, followed by several washes in a large beaker of water until excess stain had been removed. Plates were allowed to air-dry overnight after which they were destained by the addition of 2 mL of 1 % (w/v) SDS to each well. Plates were placed on the see-saw rocker for several minutes until the crystal violet dye had been released and 0.5 mL of this solution was transferred to a cuvette containing 0.5 mL of water, mixed and the absorbance was read at 563 nm on a spectrophotometer. Dilutions of the destained samples were made using 1% (w/v) SDS when crystal violet incorporation was beyond the detection limits of the spectrophotometer and the samples were re-read.

2.4.2 Alamar Blue Viability Assay

Cells were trypsinised and counted using a Countess Automated Cell Counter, as described above. Cells were seeded in 96 well plates at the densities indicated in the results chapters. Wells were topped up with 100 µL of media without any serum and incubated overnight. The following day cells were treated as required before adding 10 µL of Alamar blue into each well**.** Plates were incubated for a further 4 hrs at 37 °C. The plates were then read on a Spectramax Pro at 544 nM excitation 590 nM emission filter set.

2.5 Functional Assays

2.5.1 Phagocytosis assay

IMG cells were seeded at the densities indicated in the results chapters in six-well plates and allowed to adhere overnight. The following day, cells were treated as required before removing old media and adding carboxylate-modified polystyrene fluorescent yellow-green latex beads diluted at 1:1,000 of 2.5 mg mL^{-1} stock per well in DMEM with or without FBS for a further 2 hrs.

2.5.2 Flow Cytometry

To remove non-internalised beads cells were washed thrice with 1 mL of ice-cold PBS. After washing, cells were incubated with 0.5 mL of trypsin/EDTA solution for 10 min at 37 °C. Trypsin was neutralized with 0.5 mL of fresh DMEM before collecting them in 15 mL tubes. Cells were centrifuged at 1,250 rpm for 5 min at room temperature and then resuspended in 0.5 mL of PBS containing 3 % (v/v) FBS. To the cell suspensions, 5 µL of 7-Aminoactinomycin D (7-AAD) was added before counting, to distinguish between live and dead cells. Flow cytometric analysis was performed on all samples using a FACS Canto II and analysed with FlowJo v7.6.5 software.

To identify single cells with internalized fluorescent latex beads, cells were gated to exclude debris, doublets and dead cells. Therein, cells were sequentially gated

according to their relative size, as specified by their forward scatter area/ width of light, and according to their relative granularity, as specified by their side scatter area/ width of light. Here, firstly, the debris was removed by gating according to their side scatter area (SSC-A) against their forward scatter area (FSC-A) refraction of light. Single cells were distinguished from the doublets by gating by their FSC-A against their forward scatter height (FSC-H). From the available single cells, live and dead cells were distinguished based on 7-AAD-positive labelling of lysed cells' DNA and plotted against FSC-A. From the living cell population, cells with beads were identified based on FITC+ staining. For graphical version of the strategy, see Chapter 4, Figure 4.5.1.1.

2.5.3 Griess Reagent Kit for Nitrite (NO^{2-}) Determination (G-7921) Assay:

Cells were trypsinised and counted using a Countess Automated Cell Counter. Cells were seeded as indicated in the results section in 96-well plates and incubated overnight. The following day, cells were treated as required. Nitrite quantification was performed following the manufacturer's protocol. In brief, equal amounts of N-(1-naphthyl)ethylenediamine and sulfanilic acid was added to prepare a reagent. A calibration curve was prepared by adding 9 mL of distilled water with 1 mL of 1 mM stock of $NaNO_2$ to prepare a 0.1 mM working solution. This working solution was serially diluted to make 7 known concentrations of nitrite solution for reference, in such a way that final volume of calibrator in each well was 150 µL. A reference standard curve was plotted using these calibrators. An equal volume of the sulfanilic acid mixture was added to the samples. In the presence of nitrite, sulfanilic acid is quantitatively converted to a diazonium salt, which then conjugates with N-(1-naphthyl)ethylenediamine to form a deep purple azo dye compound. The amount of (NO^{2-}) in samples was measured by reading the absorbance of the optical density at 540 nm.

2.5.4 Reactive Oxygen Species (ROS) Assay

Cells were trypsinised and counted using a Countess Automated Cell Counter. Cells were seeded as indicated in the results section in 96-well plates and incubated

overnight. The following day, cells were treated as required. To assay for ROS production, carboxy-H_2DCFDA was diluted to 6 µM in pre-warmed PBS. Media was removed and 200 µL of 6 µM Carboxy-H_2DCFDA was added to each well. The plate was incubated at 37 °C in 5 % CO_2 for 45 mins. At the end of 45 mins, 20 µL of 100 µM H_2O_2 (positive control) was added to control wells on the plate and incubated for further 5 mins. The plate was read immediately at 492 nm using Spectra Max Gemini. Data were graphed as percentage of control.

2.6 Western immunoblotting

2.6.1 Preparation of cell lysates

Plates or dishes containing cells had media removed by aspiration and then were placed on ice. Cells were then washed with ice-cold PBS twice and excess PBS was removed by aspiration. Cells were scraped into 100-300 µL CHAPS lysis buffer, depending on size of culture dish, and transferred to 1.5 mL microcentrifuge tubes to generate protein lysates of between 1-2 mg mL^{-1}. Cell lysates were either used immediately or snap frozen in liquid nitrogen and stored at -20 °C until required.

2.6.2 Determination of protein concentration by Bradford or BCA Protein Assay

Protein concentration from cell lysates was determined by Coomassie (Bradford) Protein Assay (Thermo Fisher Scientific, UK). Briefly, 2 µL of cell lysate was added to 500 µL Bradford Protein Assay Reagent, vortexed and incubated for 5 min at RT. The absorbance was read at 595 nm using a spectrophotometer and the protein concentration was calculated against a predetermined BSA standard curve (0.025 - 2.0 mg mL^{-1}), prepared by following the manufacturer's protocol for each lot of Coomassie Reagent obtained.

Protein concentration was determined using a BCA Protein Assay kit on lysate extracted from mouse hippocampal homogenate as per manufacturer's instruction (Fisher Scientific, UK). Briefly, a standard curve was produced by carrying out serial dilutions of BSA from a stock solution of 2 mg mL^{-1} to give a range of standards

(0.0625 - 1 mg mL^{-1}). Samples were diluted 1:50 in dH_2O and both standards and samples were added to 96-well plates, in duplicate. The BCA reagents A and B were prepared in a 50:1 ratio and 175 µL was added to each well. The plate was incubated at 37 °C for 30 min and protected from light before being read at an absorbance of 562 nm using a microplate reader. The mean of the standards was calculated, and a standard curve was constructed. Protein concentrations were determined relative to the standard curve (expressed as µg mL^{-1}).

2.6.3 Sample Preparation

Protein concentrations were equalised in lysis buffer to obtain 1 mg mL^{-1} lysate then lysates were mixed with 4x NuPAGE LDS sample buffer in the ratio 3:1. Samples were sonicated using a MicroTip probe sonicator (20 % output, for 5 seconds twice), then heated at 70 °C for 10 min to denature proteins and either used immediately or stored at -20 °C until required.

2.6.4 Sodium dodecylsulphate polyacrylamide gel electrophoresis (SDS-PAGE)

Prepared samples were resolved by either 8 % or 10 % PAGE, depending on the protein of interest to be analyzed. Gels were prepared according to the recipes in Table 2.6.4.1.

Table 2.6.4.1: Recipes for SDS-PAGE.

	Stacking	**Resolving**	
	4%	**8%**	**10%**
Water [mL]	4.00	6.13	5.19
Acrylamide:Bis (30:2%) [mL]	0.93	3.73	4.67
1.25 M Bis-Tris, pH 6.7 [mL]	2.00	4.00	4.00
10 % APS [mL]	0.05	0.10	0.10
TEMED [mL]	0.02	0.04	0.04
Total volume [mL]	7.00	14.0	14.0

The resolving gel was overlaid with a small layer of butanol saturated in 0.35 M Bis-Tris solution to ensure a smooth interface between stacking and resolving gel. The butanol overlay was rinsed off with distilled water once resolving gel had set and the 4 % stacking gel was poured on top with a comb inserted to create loading wells. Gels were mounted in a vertical electrophoresis cell (BioRad Laboratories, USA) containing 1x MOPS running buffer. Combs were removed to create wells for addition of lysates of which, 20 - 30 µg of protein extract was loaded adjacent to Precision Plus Protein All Blue Standards (BioRad) to determine progress of protein migration. Proteins were separated by applying 175 V across the unit for approximately 1 hr and until protein markers were sufficiently separated.

2.6.5 Electrotransfer

Proteins resolved by SDS-PAGE was transferred onto Immobilon-P polyvinylidene difluoride transfer (PVDF) membrane (Millipore) by wet electroblotting. In brief, PVDF membrane was activated in methanol, rinsed in water and pre-soaked in transfer buffer. A ‘sandwich’ was made with pre-soaked sponge pads and a sheet of Whatman 3MM paper at the cathode (-), followed by gel, PVDF membrane and another pre-soaked sheet of Whatman 3MM paper and finally another sponge pad at the anode (+), ensuring no bubbles were present between the layers. Proteins were electroblotted in transfer buffer for 2 hours at 40 mV and 4 °C.

2.6.6 Immunoprobing membranes for proteins

Following transfer of protein on to the PVDF membranes, non-specific antibody binding was prevented by blocking the membranes in blocking buffer for 1 hr at room temperature. Membranes were washed thrice then incubated overnight with primary antibodies diluted in blocking buffer according to Table 2.6.6.1.

After washing with TBS-T three times for 15 minutes, membranes were then incubated for 1 hr at room temperature with horseradish peroxidase (HRP)-conjugated secondary antibodies generated specifically against the primary antibody species (Table 2.6.6.3). Membranes were washed three more times for 15

minutes in TBS-T to remove any non-bound secondary antibody. Protein-antibody complexes were detected using enhanced chemiluminescent (ECL) HRP substrate detection kit (Millipore). Sufficient ECL reagent was added to cover the membrane and chemiluminescence was promptly detected using a ChemiDoc MP Imaging System with Image Lab software (BioRad). Following imaging, and if necessary, membranes were stripped using Stripping buffer, re-probed and imaged for β-actin or other proteins as required. Intensity of protein bands was quantified densitometrically using Image Lab software. Values were expressed as a ratio of phosphorylated protein to total protein or total protein of interest to β-actin.

Table 2.6.6.1: Commercial primary antibodies.

Antigen	Species	Dilution	Manufacturer
β -Actin	Mouse	1: 10,000	Sigma Aldrich
p62/ SQSTM1	Rabbit	1: 1,000	MBL
LC3B	Rabbit	1: 1,000	Cell Signaling Technology
Phospho-S6K1 (Thr389)	Rabbit	1: 1,000	Cell Signaling Technology
Total S6K1	Rabbit	1: 1,000	Cell Signaling Technology
Phospho-Akt (Ser473)	Rabbit	1: 1,000	Cell Signaling Technology
IκBα	Rabbit	1: 1,000	Cell Signaling Technology
Phospho-p-38 (Thr180/Tyr182)	Rabbit	1: 1,000	Cell Signaling Technology
Total p-38	Rabbit	1: 1,000	Cell Signaling Technology
Phospho Erk1/2 (Thr 202/Tyr204)	Mouse	1: 1,000	Cell Signaling Technology
Total Erk1/2	Rabbit	1: 1,000	Cell Signaling Technology
Phospho SAPK/JNK	Rabbit	1: 1,000	Cell Signaling Technology
Total SAPK/JNK	Rabbit	1: 1,000	Cell Signaling Technology
Synaptophysin	Rabbit	1: 1,000	Cell Signaling Technology
PSD95	Rabbit	1: 1,000	Cell Signaling Technology
6E10	Mouse	1: 1,000	Biolegend
GFAP	Rabbit	1: 1,000	Cell Signaling Technology
Iba1	Goat	1: 1,000	Abcam
Cathepsin D	Goat	1: 1,000	Santa Cruz
Cystatin F	Rabbit	1: 1,000	Cell Signaling Technology

Table 2.6.6.2: Lab made primary antibodies.

Antigen	Species	Concentration	Source
Beclin1	Sheep	0.1 μg mL^{-1}	Murray lab
Phospho Ser30 Beclin1	Rabbit	0.5 μg mL^{-1}	Murray lab
Total Akt	Sheep	0.8 μg mL^{-1}	Murray lab

Table 2.6.6.3: Horseradish peroxidase-conjugated secondary antibodies.

Antigen	Host species	Dilution	Manufacturer
Rabbit IgG	Goat	1:10,000	Thermo Pierce
Sheep IgG	Rabbit	1:10,000	Thermo Pierce
Mouse IgG	Rabbit	1:10,000	Thermo Pierce
Goat IgG	Rabbit	1:1,000	Dako

2.7. ELISA (Enzyme-Linked ImmunoSorbent Assay)

Cells were trypsinised and counted using a Countess Automated Cell Counter. Cells were seeded as indicated in the results section in 96-well plates and incubated overnight. The following day, cells were treated as required. Protein quantification was performed using the manufacturer's protocol for TNF-α, IL-6 and IL-1ra and CCL2, CXCL1 and CXCL10. ELISA MAX^{TM} Nunc (Biolegend, Thermo Scientific, USA) plates were used for the assays. The plate was coated with 100 µL primary (capture) antibody. This was sealed and incubated over night at room temperature on a rotating shaker. Next day, the plate was washed three times using 300 µL of Wash Buffer (0.05 % Tween-20 in PBS) per well. The same wash buffer was used in between each step before moving onto the next. To block any non-specific binding sites on the surface of the ELISA plate 250 µL 1 % (w/v) BSA in PBS was used. This was incubated on a rocker for 1 hr. Serial dilutions of both samples and standards were performed. Different dilutions of sample were used (1:2, 1:4 and 1:8) depending on the expected concentrations of the protein. All samples and standards were diluted using 1 % (w/v) BSA in PBS to a final volume of 100 µL. After loading the samples on the plate, it was sealed and incubated on the rocker for 2 hrs at room temperature. Following this incubation period plates were washed 3 times before addition of 100 µL of the biotinylated detection to the plate for 2 hrs. After a further 3 washes streptavidin–HRP was added to the plate to form an avidin-biotin complex (ABC) with the biotinylated detection antibody. The plate was incubated at room temperature out of direct light for 20 mins. A mixture of TMB and H_2O_2 provided with the kit were used as substrate solution, 100 µL of which was added to each well. The substrate solution turned blue as the bound HRP oxidised TMB. The plate was incubated for ~20 mins at room temperature out of direct light.

50 µL of the stop solution (2N Sulphuric acid) was added to each well. The absorbance of the plate at 450 nm with correction at 570 nm used to determine the protein quantity by using SpectramaxM3 plate reader.

Table 2.7.1 ELISA antibody concentrations

	Capture	**Detection**
TNFα	800 ng mL^{-1}	75 ng mL^{-1}
IL-6	2 µg mL^{-1}	75 ng mL^{-1}
IL-1ra	800 ng mL^{-1}	400 ng mL^{-1}
CCL2	200 ng mL^{-1}	50 ng mL^{-1}
CXCL1	2 µg mL^{-1}	50 ng mL^{-1}
CXCL10	2 µg mL^{-1}	100 ng mL^{-1}

2.8 Microscopy

2.8.1 Immunofluorescent staining of cultured cells

IMG cells were cultured on 13 mm round coverslips placed in 6-well plates at a seeding density of 1 x 10^5 cells per well. Cells were grown to reach 50-60 % density and following experimental treatments coverslips were washed twice with PBS before being fixed with 200 µL of 37% formaldehyde for 20 mins at room temperature. Cells were then permeabilized with 0.2 % (v/v Triton X-100 in PBS at room temperature for 15 mins. Coverslips were then washed three times with PBS prior to incubation in 2 % (w/v) BSA in PBS blocking buffer for 20 mins. To probe for protein localization, 100 µL of protein specific primary antibody, diluted in blocking buffer, was overlayed onto each coverslip and incubated overnight at 4 °C. Next day, coverslips were drained of antibody solution by dabbing onto tissue and washed three times in PBS. To detect bound primary antibodies, 100 µL of secondary antibody conjugated to a relevant fluorescent moiety diluted in blocking buffer was overlayed onto each coverslip and incubated in darkness at room temperature for 1 hr. Coverslips were drained of antibody solution by dabbing the coverslip edge onto tissue and then washed four times in PBS under darkness. Coverslips were then mounted on glass microscope slides with mounting medium (Hydromount) and left to dry. Digital images were captured using and Olympus

BX61WI microscope equipped with a CCD camera and filter blocks for FITC, TRITC and DAPI illumination and 40x (air), 60x (oil) lenses. Alternatively, specimens were examined with a Leica SP8 confocal microscope. Images were processed using Fiji Image.

2.8.2 Transmission Electron Microscope (TEM) assessment of latex bead uptake

IMG cells were seeded in 10 cm dishes and cells grown to 80 % confluency before adding latex beads to the dishes for 2 hrs. Cells were then washed with PBS, trypsinized and centrifuged at 1250 rpm to form a pellet. The pellet was then prepared for TEM and analysed by the TBSI TEM unit. In brief, the pellet was fixed in 3 % (v/v) glutaraldehyde in 0.05 M Potassium Phosphate buffer: pH 6.8 for 1 to 1.5 hrs at room temperature while agitating the solutions on a rotator. The samples were subsequently post-fixed in 2 % Osmium Tetroxide in 0.05 M Potassium Phosphate buffer (pH 6.8) for 30 min at room temperature. The samples were further processed by standard procedures, including dehydration, transition to resin and embedding. Ultrathin sections were post-stained and examined using a JEOL JEM1400 Transmission Electron Microscope (Hitachi, Ltd., Tokyo, Japan).

2.9 Animals

Male/female B6.Cg- Tg(APPswe,PSEN1dE9)85Dbo/Mmjax (Strain #034832; MMRRC, Jackson Laboratories, California, USA) and non-transgenic littermate controls were obtained from an in-house colony (male +/0 x female 0/0 to produce heterozygous transgenic and non-transgenic offspring only). Mice were housed in cages of up to 5 at 21 °C with a 12:12 hrs light:dark cycle. Food and water access was *ad libitum*. All animal experimentation was performed under a license granted by the Health Product Regulatory Authority (HPRA), Ireland, with approval from the Trinity College Dublin Animal Research Ethics Committee and in compliance with the Cruelty to Animals Act, 1876 and the European Community Directive, 86/609/EEC. Every effort was made to minimize suffering and stress to the animals.

2.9.1 Treatment administration

To evaluate the effect of long-term CSF1R inhibition, mice were administered GW2580 orally in diet [Modified LabDiet® PicoLab EURodent Diet 14 %, 5L0W (5LF2) with 0.1 % (w/w) (1000 ppm) GW2580 (LC Laboratories); TestDiet] for 3 months, starting at 6 months of age. Untreated control animals were fed with a diet without GW2580 (5L0W, [5LF2]). Body weight was monitored regularly during the treatment period and all behavioural experiments.

2.9.2 Behavioural tests

Y-maze reference memory task: Before the start of the treatment with GW2580, this hippocampal-dependent reference memory task was performed to ensure that treatment and control groups were balanced with respect to hippocampal-dependent cognitive status. A clear Perspex Y-shaped maze (30 x 8 x 13 cm), mounted on a white plastic base, was used to perform this task. The maze was placed in the middle of a room with prominent black and white extra-maze cues. It was filled to a depth of 2 cm water at 20-22 °C, sufficient to motivate the mice to escape the maze by ‘paddling’ (walking rather than swimming) to an exit tube at the outer end of one arm, 4 cm in diameter and 2 cm above the floor. Each animal had

a fixed location for its escape arm (to test reference memory). In order to make all the arms look identical from the centre, burrowing tubes were placed over the correct exit tube and the false exit tubes. Mice were placed in one of the two possible start arms in a pseudorandomised order for 12 trials on each of 4 consecutive days. An arm entry was defined as entry of the whole body excluding the tail. The mouse exits to a burrowing tube, and it was then hand-dried and returned to its home cage. When the mouse explored an arm which was not its escape arm, it was considered as an incorrect trial.

Reversal: On day 5, during the 'reversal testing', the exit for each mouse was switched to a different arm (also counterbalanced, with the exception that they could not start in their original escape arm on the first trial). Mice had to learn the location of the new exit over 12 trials in one day. For analysis, the 12 trials were divided into 3 blocks of 4 and correct trials per block were recorded.

Spontaneous T-maze alternation task: Discrete trial spontaneous alternation in the T-maze was performed 11 weeks into the diet to assess the effect of GW2580 on hippocampal-dependent working memory in mice. Deficits on this task may reflect the lack of memory retention of recently visited maze locations. A grey T-shaped maze, consisted of 69 cm long axis × 39 cm short axis × and depth of 20 cm, with a partition extending 14 cm into the start arm from the back of the maze (Figure 2.9.2.1), was used for the task. Mice were placed in the start arm of the maze and allowed to make a choice of entering the left or right goal arm. After the choice was made, a guillotine door was lowered to enclose the mouse in their chosen arm for 30 sec, to restrict exploration to that arm. At the end of 30 sec, mice were taken out of the maze, the guillotine door reopened, and the central partition removed. Mice were once again placed into the start arm and allowed to make a free choice of one of the goal arms. Choosing the alternative arm to the one chosen before was regarded as a spontaneous alternation and was scored 1, while a return to the original arm was scored 0. Alternation is viewed as the recognition of the novelty of the arm not yet visited, based on the memory of the original choice. The natural exploratory drive of the mouse dictates that it will most often choose the arm not yet explored. The test was performed 5 times a day over two days (a total of 10 trials over 2 days) and the alternation ratio was obtained as the mean of the 10 scores. If the mouse did not move in 30 sec it was nudged once, if still not moving after 60 sec it was nudged once more and if it did not move in 90 sec, it was

considered a failed trial. Wooden chip bedding from cages of the opposite sex was added to the floor of the maze to increase motivation for exploring. The used bedding was removed, and maze cleaned with 10 % ethanol before adding new bedding to the maze between each trial.

Open Field Test: The open field test was carried out using ANY-maze activity monitor software (Version 4.99). The open field consisted of a white plastic box (58 cm ×33 cm ×19 cm) with the floor of the box divided into a grid of equal sized squares. The mice were placed in the box for a period of 5 minutes each. Measurements of the total distance travelled (cm) in the Open and Centre Zone was taken for analysing anxiety related behaviour. Total number and time of rears (frequency and time with which the mice were on their two hind legs in the maze), as the marker for exploratory behaviour was also monitored (Figure 2.9.2.2).

Morris water maze (MWM): To study the effect of genotype and of GW2580 on spatial learning and memory of the mice, the MWM task was performed (Figure 2.9.2.3). The home cages were all moved into the behaviour room 10 min before beginning the task. The MWM consisted of a tank 150 cm in diameter, 60 cm in depth. Maze was filled to a depth of 31 cm of water. The water temperature was maintained at 21-22 °C and water opacity was achieved using non-toxic white tempura paint powder (Reeves, UK). Cues were positioned symmetrically around the maze, clearly visible to the mice from the maze. Lighting and cue positions were kept constant for all of the training and testing. The water maze was virtually divided into four quadrants, numbered 1, 2, 3 and 4. A transparent escape platform (diameter 11.5 cm; height 30 cm) was placed in one of the quadrants, submerged 1 cm below the surface of the water, for mice to escape using various visual cues on the wall. The platform position was fixed for any individual mouse but placed in different quadrants for each mouse (i.e., 1 of 4 locations, pseudo-randomised to ensure that each target quadrant is used, equally, by each experimental group). The path taken by each mouse was recorded using a ceiling-mounted video camera and analysed using ANY-maze software to track distance and time taken for the mice to find the platform. The swimming speed was also calculated.

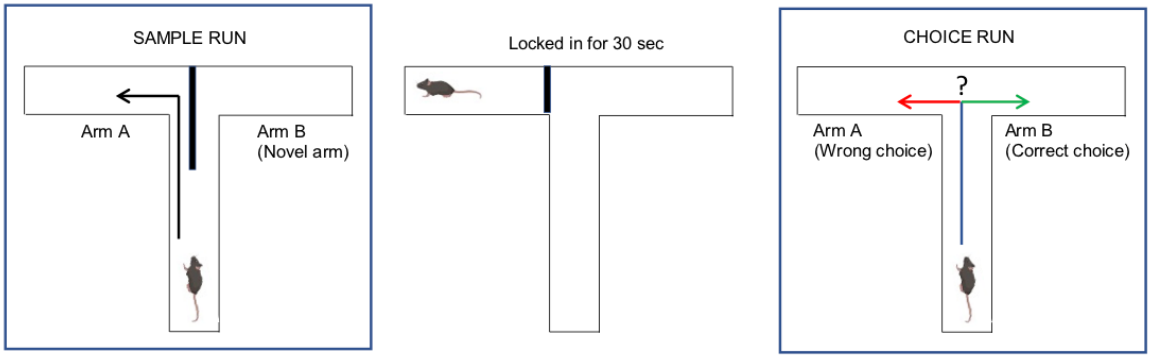

Figure 2.9.2.1: Schematic for T-maze set up.

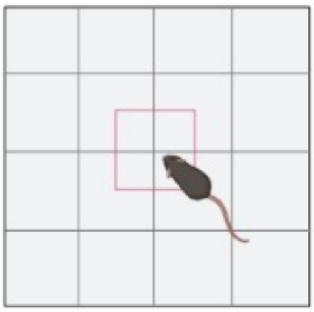

Figure 2.9.2.2: Schematic for Open field set up.

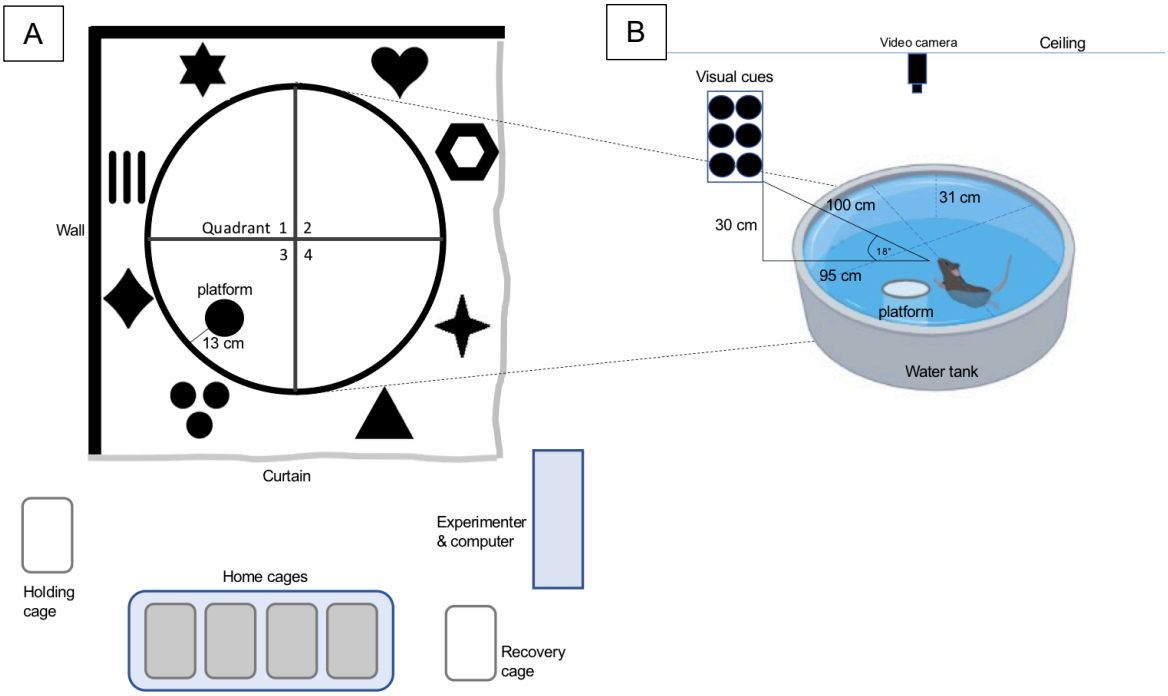

Figure 2.9.2.3: Schematic for Morris Water Maze set up. (A) Room layout for MWM behaviour task. (B) The MWM set up.

Training: At the beginning of training, mice were removed from home cage and placed in holding cage for approx. 15 sec to ensure proper arousal. On day 1, each mouse was placed on the platform in the maze and held there for 20 sec to familiarise them with the escape platform, hidden just below the surface of the water, in relation to the extra-maze cues. For each trial, the animal was gently lowered into the water facing the wall of the tank and was allowed to find the escape platform for up to 60 sec. If they could not find the platform by this time, then they were guided to the platform with the experimenter's hand and were allowed to remain on the platform for 15 sec. If it left the platform, it was guided back onto it, as before. Although the location of the platform was fixed for any given animal, the starting position was randomised from trial to trial and on successive training days. Animals each underwent 4 trials per day for 5 days (a total of 20 trials over 5 days) and trials were spaced approximately 2 hrs apart. After each trial the animals were hand dried and returned to their home cage.

Probe Test: After 5 days of training to find the platform using visuospatial cues, a probe test (a single trial) was performed on the mice to assess whether they remember the location of the platform with respect to visuospatial cues. This test involved removing the escape platform and placing the animals in the water in the opposite quadrant to their original platform quadrant during training days. The percentage of time spent in the correct quadrant was recorded for 60 sec. The time in each quadrant during the probe test was also analysed, as an indication of their memory of the original location of the hidden platform.

Flag Test: In Flag test (two trials per mouse), a black and white crossed flag (width 25 cm, height 17 cm) was attached to the platform (1 cm below water) with a shaft high enough for the mouse to see when it is placed in the maze. The location of the flag for each trial was counterbalanced between cohorts. The 1st cohort had their flag in their original exit quadrant in their first trial, while, for their second trial the flag was moved to the opposite quadrant to their original exit quadrant. For the 2nd and 3rd cohorts, the flag was placed in the quadrant opposite to the original exit quadrant for their first trial and was moved to their original exit quadrant in their second trial. The time taken for the mice to readily run to the flagged platform was noted as a measure of their intact eyesight.

2.10 Microglial cell isolation

2.10.1 Tissue preparation

Animals were terminally anaesthetised using 300 µL Sodium Pentobarbital i.p (Euthatal, Merial Animal Health, Essex, UK) and transcardially perfused with heparinised saline (0.1 % (v/v) heparin, (Leo Pharma, UK) in 0.9 % saline) using a peristaltic pump (Anachem, Luton, UK). Brains were rapidly removed. The left hippocampus and overlying cortex dissected out was used for isolation of microglia and astrocytes on the same day. The right hippocampus with the overlying cortex, hypothalamus and part of the frontal cortex was dissected out and snap frozen on liquid nitrogen and stored at -80 °C for other molecular analysis.

2.10.2 Enzymatic digestion and myelin removal

The hippocampus and overlying cortex (area of maximum pathology in APP/PS1) for cell isolation was kept in 1 mL of ice cold HBSS). This tissue was minced thoroughly and dissociated in 5 mL of enzyme mixture containing 2 mg mL^{-1} collagenase, 28 U mL^{-1} DNase I, 5 % (v/v) FBS, and 10 µM HEPES in HBSS at 35 °C for 45 min, 15-20 rounds of trituration every 15 min. The rest of the steps were performed on ice. This digested tissue was filtered using a 70 µm cell strainer (BD Falcon) to achieve a single-cell suspension. The single-cell suspension was incubated with Myelin Removal Beads II for 20 min to bind the myelin, which was then removed by passing through LS columns mounted over QuadroMACS magnet.

2.10.3 Staining and cell sorting

The myelin-depleted single-cell suspension was obtained from the above steps. The suspension was incubated for 15 min on ice with anti-mouse CD16/CD32 antibody (1:100; BD Biosciences) to block Fc receptors. It was subsequently incubated with anti-CD11b PEcy7 (1:100; Biolegend), anti-CD45 APC (1:100; Biolegend), and anti-GLAST PE (1:100; Milteny) antibodies for 30 min on ice. A final wash with FACS buffer (1 % (w/v) BSA and 2 mM EDTA in PBS) was performed and cells were resuspended in FACS buffer (200 µL) and sorted on FACSAria Fusion cell sorter (Becton Dickinson) using a 100 µm nozzle. To gate-out non-viable cells 5 µL of 7-AAD was added. Sorted cells were collected in 1.5 mL Lobind RNAse/DNAse free tubes containing 350 µL of Trizol LS (Invitrogen) for microglia

and 500 µL of Trizol LS for astrocytes. Between 40,000 to 50,000 $CD45^{low}CD11b^{+}$ microglia and 80,000 to 100,000 $GLAST^{+}CD45^{-}$ astrocytes were sorted.

After the cells are sorted, hippocampal homogenate labelled with fluorescent antibody are gated down to single cells, excluding debris or cell doublets. Then cells are sequentially gated according to their relative size, as specified by their forward scatter area/ width of light, and according to their relative granularity, as specified by their side scatter area/ width of light. Here, firstly, the debris was removed by gating according to their side scatter area (SSC-A) against their forward scatter area (FSC-A) refraction of light. Two stages of gating strategy were employed to distinguish single cells from the doublets : 1) gating by their FSC-A against their forward scatter width (FSC-W) and 2) gating by their SSC-A against side scatter width (SSC-W). Cells on the upper or right side of these plots were likely to be debris due to their size and/or granularity and were excluded. From the available single cells, live and dead cells were distinguished based on 7-AAD-positive labelling of lysed cells' DNA and plotted against FSC-A. From the living cell population, microglia were identified based on CD11b-$FITC^{+}$ and intermediate CD45-APC^{+}, while astrocytes were identified based on of high GLAST1-PE^{+} and CD45-APC^{-} staining (Figure 2.10.3.1).

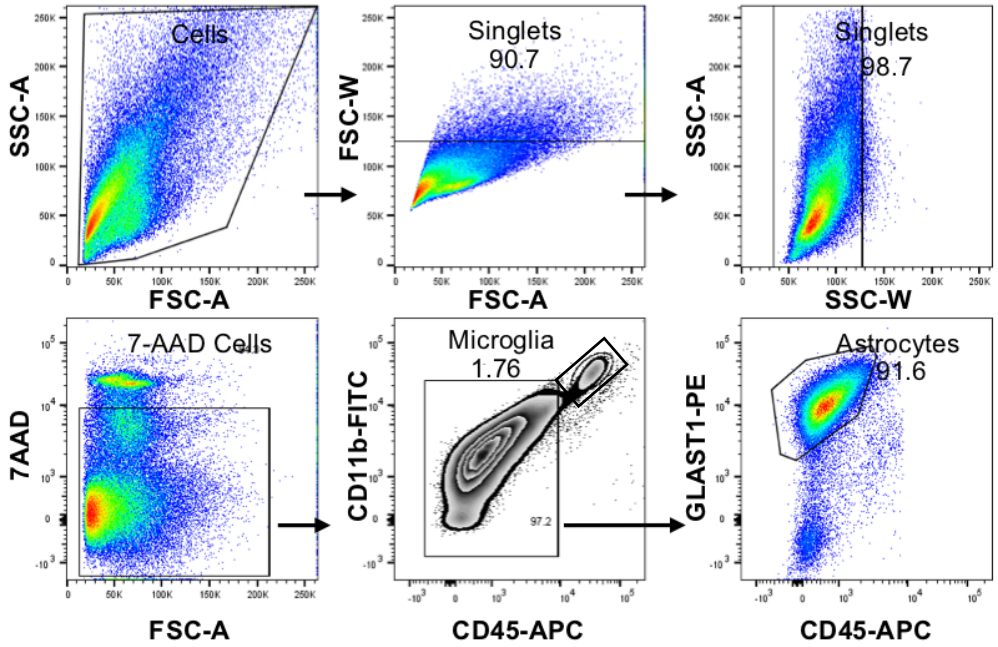

Figure 2.10.3.1: Gating strategy of fluorescence-activated cell sorted (FACS) microglia (and astrocytes) from normal and APP/PS1 mouse hippocampus. Gating strategy used for sorting of microglia and astrocytes. All cells were gated to single cells. Live and dead cells were separated using 7-AAD. Microglia were identified and isolated based off high CD11b-FITC^{+} and intermediate CD45-APC^{+} staining and Astrocytes were identified according to high GLAST1-PE^{+} staining.

2.11 Real-Time quantitative Polymerase Chain Reaction (RT-qPCR)

2.11.1 RNA extraction

Prior to starting RNA extraction, the RNA area and all equipment were wiped down with 70 % ethanol solution. Sorted cells in Trizol LS were vortexed and samples incubated with 200 µL of chloroform (Sigma Aldrich) for 3 min at room temperature. The samples were then centrifuged for 15 mins at 12,000 x g and 4 °C. The aqueous phase was placed in a new 1.5 mL Lobind RNAse/DNAse free tubes and 0.5 mL of isopropanol was added to samples for 10 min. To this, 7 µL of glycogen (Thermo Scientific) was added to help with RNA precipitation and stored at -20 °C overnight. The following day, samples were centrifuged for 10 mins at 12,000 x g and 4 °C then washed three times with 1 mL of 75 % ethanol solution. DNAse digestion was performed using RNase-free DNase I enzyme (Qiagen, UK) before the DNase was washed off with 1 mL of 75 % ethanol solution. The pellet collected was then air dried before being resuspended in 20 µL of RNAase free water with Ribolock RNAse inhibitor (1:10,000; Thermo Scientific).

2.11.2 Quantification of the extracted RNA

The Nanodrop ND1000 Spectrophotometer (Thermo Fisher Scientific) was used for quantifying the total concentration and purity of RNA in each sample. The machine was blanked using 1 µL of RNase free water, before the absorbance of 1 µL of each sample was measured at 260 nm and 280 nm. The concentration of RNA was obtained using the formula $A=\varepsilon Cl$, where A is absorbance at 260nm, ε is the RNA extinction coefficient (25 µL μg^{-1} cm^{-1}), C is RNA concentration and l is the pathlength of the spectrophotometer (0.05 mm - 0.1 mm). The purity of the RNA was determined using the A260/280 (i.e., the ratio of absorbance at 260 nm to that at 280 nm, where a ratio of 1.8 to 2.1 indicates pure RNA. The RNA was stored at -80 °C until required for cDNA synthesis.

2.11.3 Reverse transcription for cDNA synthesis

An iScript™ cDNA Synthesis Kit (BioRad) was used for cDNA synthesis. All calculations were based on a reaction using 60 ng of RNA per 20 µL. The 60 ng RNA-containing sample was then made up to 15 µL using RNase free water. The other 5 µL in the reaction was Master Mix composed of 4 µL 5X iScript Reaction Mix and 1 µL iScript Reverse Transcriptase. The 15 µL of sample and 5 µL of Master Mix were placed in sterile PCR mini tubes and centrifuged rapidly to ensure a homogenous mixture, without bubbles, in a single volume at the bottom of the tube. Samples were then placed in the thermocycler (Biometric Trio, analyticjena) at 25 °C for 5 mins, 46 °C for 20 mins and 95 °C for 1 min and left 4 °C until collection. Samples were then centrifuged and stored at 4 °C and used within 2 weeks, otherwise they were stored at -20 °C for future use.

2.11.4 Amplification of cDNA by RT-PCR

The StepOne Real-Time PCR system (Applied Biosystems, Warrington, UK) was used in 96-well format with a 25 µL reaction volume per well for quantitative (Q)-PCR. Primers and probes that were used (Table 2.11.4.1) were obtained either from previous publications or designed using the NCBI website (https://www.ncbi.nlm.nih.gov/tools/primer-blast/index.cgi) and all primers and probes were synthesized for this study. Probes were designed to cross introns so that their specificity to the cDNA was increased. Where no probe was available SYBR green, a fluorescent DNA binding probe, was used. All primer pairs were tested for specificity following standard RT-PCR using DNA gel electrophoresis to produce a discrete band of the expected amplicon size.

Table 2.11.4.1: Mouse PCR Taqman probes and primers

Target	Accession Number	Oligo-nucleotide	Sequence	Amplicon size (bp)
18S	NR_003278.3	Forward	5'-CGCCGCTAGAGGTGAAATTCT-3'	67
		Reverse	5'-CATTCTTGGCAAATGTCTTTCG-3'	
ApoE	NM_009696.4	Forward	5'-CTGACAGGATGCCTAGCCG-3'	113
		Reverse	5'-CGCAGGTAATCCCAGAAGC-3'	
LPL	NM_008509.2	Forward	5'-CGAGAGGATCCGAGTGAAAG-3'	153
		Reverse	5'-TTTGTCCAGTGTCAGCCAGA-3'	
Map1lc3b	NM_026160.5	Forward	5'-GTCCTGGACAAGACCAAGTTCC-3'	119
		Reverse	5'-CCATTCACCAGGAGGAAGAAGG-3'	
TFEB	NM_011549.3	Forward	5'-AAGGTTCGGGAGTATCTGTCTG-3'	188
		Reverse	5'-GGGTTGGAGCTGATATGTAGCA-3'	
Tyrobp	NM_011662.2	Forward	5'-CGTACAGGCCCAGAGTGAC-3'	91
		Reverse	5'-CACCAAGTCACCCAGAACAA-3'	
Cathepsin D	NM_009983.2	Forward	5'-GGCGTCTTGCTGCTCATTCT-3'	90
		Reverse	5'-CCGACGGATAGATGTGAACTTG-3'	
Sall1	NM_001371070.1	Forward	5'-CAATCTGAAGGTCCACATGGGCAC-3'	109
		Reverse	5'-TGCCTCCTAGAAATGTCATGGG-3'	
P2ry12	NM_027571.4	Forward	5'-GTTCTACGTGAAGGAGAGCA-3'	199
		Reverse	5'-CTACATTGGGGTCTCTTCGC-3'	
Itgax	NM_021334.3	Forward	5'-CTGGATAGCCTTTCTTCTGCTG-3'	115
		Reverse	5'-GCACACTGTGTCCGAACTC-3'	
C1q	NM_007572.2	Forward	5'-GCCGAGCACCCAACGGGAAGG-3'	268
		Reverse	5'-GGCCGGGGCTGGTCCCTGATA-3'	
TGF-β	AJ009862	Forward	5'-CGTGGAAATCAACGGGATCA-3'	84
		Reverse	5'-GGCCATGAGGAGCAGGAA-3'	
		Probe	5'-ACCTGGGCACCATCCATGACATGA-3'	
Trem2	NM_031254	Forward	5'-TGTGGTCAGAGGGCTGGACT-3'	68
		Reverse	5'-CTCCGGGTCCAGTGAGGA-3'	
		Probe	5'-CCAAGATGCTGGGCACCAACTTCAG-3'	
Gp91phox	NM_007807	Forward	5'-CAGGAACCTCACTTTCCATAAGATG-3'	113
		Reverse	5'-TCCCGACTCTGGCATTCAC-3'	
		Probe	5'-CACACCGCCATCCACACAATTGC-3'	
Cst7	NM_009977.3			Premade

A PCR Master Mix of 24 µL per well was made up in bulk as per Table 2.11.4.2. To this, 1 µL of the template cDNA was then added, and mixed thoroughly. The plate was then sealed using the ABI Prism Optical Adhesive Cover and centrifuged to ensure there are no bubbles in the mix.

Table 2.11.4.2: qPCR master-mix formula for 96-well format.

	Volume Per Sample (µl)	
Component	**TaqMan MasterMix**	**SYBR-Green**
2X Master Mix	12.5	12.5
Rnase- free water	9	9.5
10µM Probe	0.5	0
10µM Forward	0.5	0.5
10µM Reverse	0.5	0.5

The plate was then placed in the Applied Biosystems StepOnePlus RT-PCR instrument. The first stage of the PCR cycle was at 95 °C for 10 mins (denaturation of reverse transcriptase), the second stage was at 95 °C for 10 secs, the third stage was at 60 °C for 30 secs. Stages 2 and 3 were repeated for 50 cycles.

2.11.5 PCR Quantification

Assays were quantified using a relative standard curve. The standard was prepared using total RNA from a 25-month-old male mouse brain that had been challenged for 4 hrs with a 250 μg kg^{-1} intrahippocampal LPS injection. cDNA for the standards was made using a High-Capacity cDNA Reverse Transcription Kit (Applied Biosystems, Warrington, UK) with up to three times more RNA than used for typical samples, calculated to ensure that the samples being tested fell within the range of the standard curve. The curve was constructed using 1 in 4 serial dilutions from 1 to $1/4096^{th}$. A curve was plotted of the Ct value (cycle threshold - the cycle number at which the fluorescence of each standard crosses a threshold that is set for each individual gene) versus the log of the concentration (assigned an arbitrary value since the absolute concentration of cytokine transcripts was not known). A straight line of best fit was plotted and the efficiency of the PCR reaction across the entire concentration range was verified by confirming that the curve was a straight line using the Pearson coefficient. The equation of this line was then used to calculate the relative concentrations of the experimental samples. Since the highest standard was assigned an arbitrary value (such as 4000) it followed that the calculated concentrations of all experimental samples also had arbitrary values, but these were calculated from the equation of the line and were thus reliably quantified with respect to the values assigned to the standards. All PCR data were normalised to the expression of the housekeeping gene,18S.

2.12 Statistical Analysis

Statistical analyses were chosen based on the nature of the experimental design and on the scientific hypotheses to be tested. Where data where normally distributed, one-way ANOVA was used to compare multiple groups with treatment

as the only inter-group factor. Likewise two-way ANOVA was used where 2 independent factors determined the dependent variable (e.g., experimental stimulus and drug treatment). Three-way ANOVA was used where the dependent variable was influenced by 3 independent factors (e.g., genotype, drug treatment and sex). A 3 way ANOVA with repeated measures was used when the dependent variable was measured multiple times in the same experimental subject (e.g., 3 way ANOVA of genotype x treatment with training day as a repeated measure). Contingent on significant main effects or interactions in the primary ANOVA analysis, Bonferroni multiple comparison *post hoc* was used where appropriate. All analyses were performed using GraphPad Prism 9 and all data are expressed as mean ± SEM (except otherwise stated in the Figure legend).

Chapter 3: Mechanistic investigation of CSF1R signalling and regulation of autophagy

3.1 Introduction

CSF1R function and signal transduction has been studied comprehensively in macrophages, where it is essential for macrophage survival (Stanley and Chitu, 2014). CSF1 stimulates macrophage survival through the PI3K/Akt pathway (Murray *et al.*, 2000). CSF1 stimulation leads to consecutive rounds of phosphorylation and dephosphorylation of the receptor on Tyr723, which correlates with periodic activation of PI3K and Erk1/2 pathways in primary human monocytes (Jacquel *et al.*, 2009). Repeated waves of Akt activation with increasing amplitude and duration activates caspase-8 and 3, which via cleavage of nucleophosmin, promotes monocyte differentiation into macrophages (Jacquel *et al.*, 2009). CSF1 also increases macrophage protein synthesis in a dose-dependent manner, leading to increased proliferation (Stanley and Chitu, 2014). Stimulation of CSF1R also leads to phosphorylation of Tyr807 and activation of MEK and Akt pathways to induce receptor kinase-dependent proliferation in macrophages (Yu *et al.*, 2012). Mammalian cell growth is controlled via activation of mTORC1 signalling complexes downstream of PI3K. This occurs through Akt activation and disruption of TSC1/2 complexes that allows the GTPase Rheb to activate mTORC1. Activated mTORC1 complexes then phosphorylate downstream substrates, including 4EBP1 and S6K1, leading to increased protein synthesis (Dibble and Cantley, 2015). Since microglia are the main resident macrophages of the brain, sharing many functional and signal transduction similarities with peripheral macrophages, this chapter will explore whether microglial cell growth is also regulated through mTORC1, *in vitro*.

Upregulation of autophagy is one of the key cellular responses to nutrient withdrawal. mTORC1 and AMPK are examples of key nutrient sensing kinases (Hindupur, González and Hall, 2015). It is well known that amino acid fluctuations in cells affect autophagy status and one of the major downstream effectors of amino acid-mediated autophagy repression is the mTORC1 complex (Blommaart *et al.*, 1995). As such, the mTORC1 complex is sensitive to both nutrients and growth factors, and acts as a signalling nexus coordinating extracellular signals that promote cell growth and proliferation. mTORC1 resides on late endosomal/lysosomal membranes under amino acid replete conditions, whereas, a cytosolic translocation of mTORC1 from this compartment is observed in the absence of amino acids (Kim *et al.*, 2008). Autophagy is tightly regulated through the ULK1 signalling complex. Autophagy induction is prevented when ULK1 is

phosphorylated on Ser757 by mTORC1 (Kim *et al.*, 2011). Activated ULK1 stimulates the ATG14-containing PIK3C3 complex through phosphorylation of Ser15 and Ser30 on Beclin1 to promote omegasome formation, by PIK3C3-dependent generation of PtdIns3P resulting in autophagosome formation (Park *et al.*, 2018). Inhibition of mTORC1 signalling, either by amino acid withdrawal or treatment with rapamycin or Torin1 also activates autophagy. Additionally, the PIK3C3 complex, also positively regulates mTORC1 signalling, suggesting a tight interplay between anabolic and catabolic pathways (Byfield, Murray and Backer, 2005).

By analogy with other RTKs in macrophages, interruption of CSF1R signalling may induce autophagy in microglial cells. Autophagy flux impairment in microglia could be associated with (1) inhibition of autophagosome formation, (2) inhibition of autophagosome trafficking, or by (3) disruption of lysosomal function that prevents fusion of autophagosomes. An increase or accumulation of autophagosomes may also indicate blockade, and thus impairment of the pathway (Zhang *et al.*, 2013). SQSTM1/p62 is a cargo protein that binds ubiquitin-tagged autophagy substrates and sequesters them to autophagosomes for selective autophagy (Lamark *et al.*, 2009). SQSTM1/p62 is also a crucial moderator of amino acid signalling for the activation of S6K1 and 4EBP and the translocation of mTORC1 to the lysosome (Duran *et al.*, 2011). De novo expression of SQSTM1/p62 is suppressed with activation of autophagy, thus any decrease in SQSTM1/p62 protein expression represents autophagic turnover (Klionsky *et al.*, 2012). As well as linking various autophagic cargo to the nascent phagophore membrane, SQSTM1/p62 also binds to LC3B (Pankiv *et al.*, 2007). The lipidation of LC3B, following activation of autophagy is a commonly used biomarker for monitoring autophagic flux, as autophagosomal membrane-associated LC3B-II can be detected by microscopy and its lipidation, by Western immunoblotting (Pugsley, 2017).

A mechanistic link between CSF1R signalling and the control of autophagy in microglial cells is not as clearly delineated as in macrophages or other cell types. Therefore, the focus of this chapter was to establish how CSF1R signalling may regulate autophagy.

3.2 Aims and objectives

Autophagy is impaired in neurodegenerative diseases. Microglia play a critical role in such disorders. Their survival and proliferation is controlled by CSF1R signalling, a pathway also linked to autophagy. Therefore, the specific objectives of this chapter are to:

- Characterise CSF1 signalling in microglia and how their growth and proliferation is controlled *in vitro*.
- Investigate how microglia regulate autophagy *in vitro*.
- Analyse the role of mTORC1 in autophagy induction in immortalised microglial (IMG) cells.

It is hypothesized that inhibiting microglial CSF1R signalling, will increase microglial autophagy.

3.3 Results

3.3.1 CSF1 treatment of BV2 cells does not activate mTORC1 signalling

Activation of PI3K/mTORC1 and RAS/Erk1/2 signalling are key pathways known to play a critical role in AD pathogenesis. These pathways are activated by various growth factors. Therefore, whether these signalling pathways are activated by CSF1 in BV2 cells was examined. Cells were treated with CSF1 (50 ng mL^{-1}) for 10, 60 or 120 mins (Figure 3.3.1.1).

Increased phosphorylation of Akt on Ser473 was detectable at 10 mins but not significant, compared to serum-deprived control and remained elevated at 120 mins. Stimulation of BV2 cells with CSF1 in the absence of serum was insufficient to induce mTORC1-mediated phosphorylation of S6K1 on Thr389 following serum-deprivation. Also unexpectedly, phosphorylation of Erk1/2 was decreased following CSF1 stimulation, and had only partially recovered by 120 mins. These data indicate that CSF1 does not activate the PI3K/Akt/mTORC1 pathway.

3.3.2 Amino acid starvation induces autophagy in BV2 cells

Activated mTORC1 inhibits autophagy under nutrient replete conditions, although BV2 cells are known to signal through mTORC1, this does not seem to occur downstream of CSF1R signalling (Figure 3.3.1.1). Nonetheless, to investigate how BV2 cells regulate autophagy, cells were deprived of amino acids for the times indicated (Figure 3.3.2.1). Cells were incubated in either full RPMI media or EBSS for up to 4 hrs (Figure 3.3.2.1). Starvation of cells with EBSS induced autophagy as early as 2 hrs (p= 0.0179), determined by the degradation of p62, and decrease in LC3B-II levels by 4 hrs (p= 0.0161). Taken together, BV2 cells respond to nutrient deprivation by inducing autophagy.

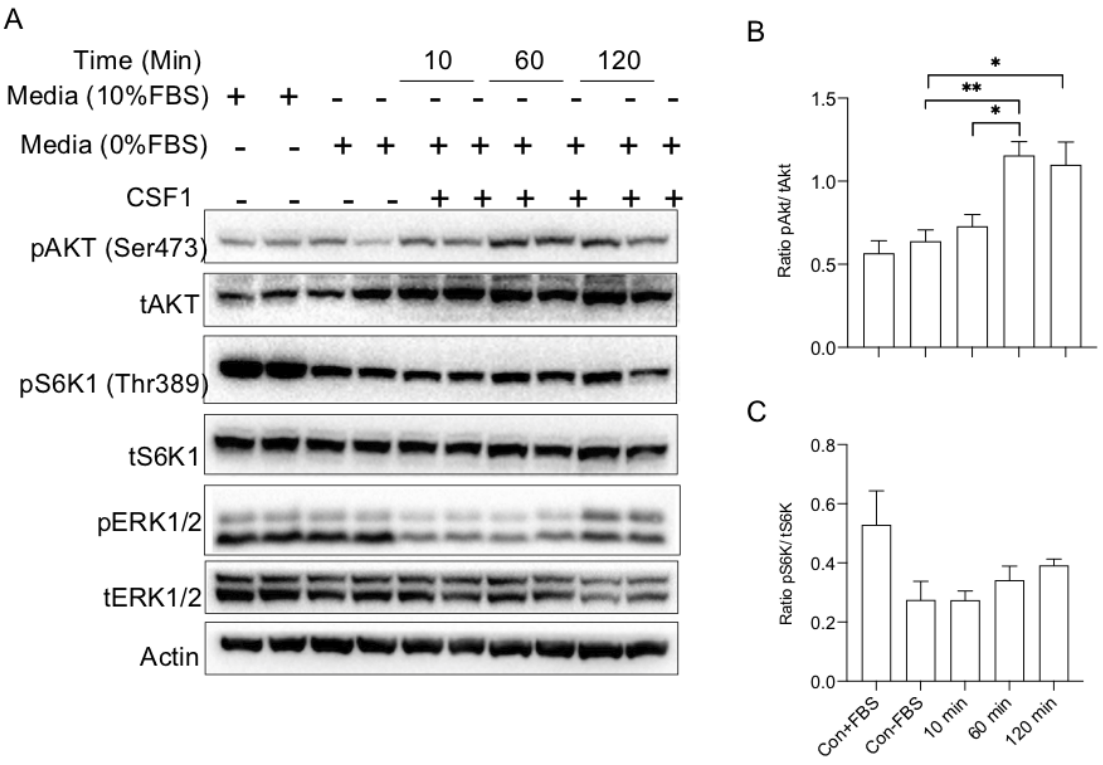

Figure 3.3.1.1: CSF1 treatment does not activate PI3K/mTORC1 or RAS/Erk1/2 signalling. BV2 cells were cultured in with or without 10 % FBS and incubated with CSF1 in the absence of FBS for the times indicated. Cell lysates were resolved by 10 % SDS-PAGE before electroblotting onto PVDF membrane. Membranes were immunoprobed with antibodies for the proteins and phosphorylated epitopes indicated. Actin was used as loading control. Ratio of pAkt/tAkt (panel B) and pS6K/tS6K (panel C) was assessed by densitometry (error bars = ± S.E.M.) Results are representative of three independent experiments. Data was analysed by one-way ANOVA and significant differences are depicted by $p < 0.05$.

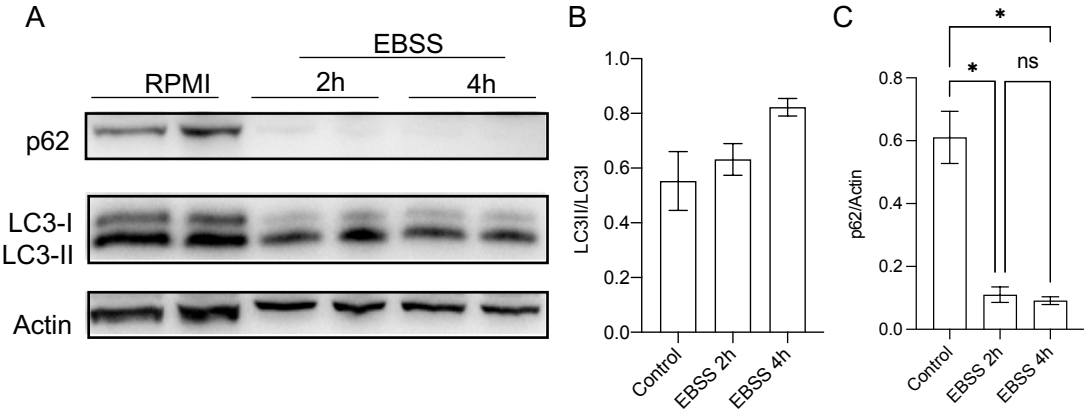

Figure 3.3.2.1: Amino acid starvation induces autophagy in BV2 cells. (A) Cells were cultured and incubated in full media or EBSS for the times indicated. Cell lysates were resolved by 10 % SDS-PAGE gel before proteins were electroblotted onto PVDF membrane. Membranes were immunoprobed with antibodies for the proteins indicated. Actin was used as loading control. Ratio of LC3B-II to LC3-I (panel B) and p62 to actin (panel C) was assessed by densitometry (error bars = ± S.E.M.). Results are representative of three independent experiments.

3.3.3 CSF1 does not induce dose-dependent proliferation in BV2 cells

CSF1 is a growth factor responsible for growth and proliferation in cells of the myelomonocytic lineage. In Figure 3.3.1.1, there was no evidence to support the notion that CSF1 stimulated either PI3K/mTORC1 or RAS/Erk1/2 signalling. Irrespective of this, to determine whether CSF1 stimulated BV2 cell proliferation, cells were incubated with various concentrations of CSF1 in 1 % FBS supplemented media and incubated for 48 hrs before measuring DNA content with a crystal violet incorporation assay (Figure 3.3.3.1).

Stimulation of BV2 cells with CSF1 did not show dose-dependent proliferation, although increased proliferation was detected with 0.1 ng mL^{-1}, increasing concentrations of CSF1 did not further increase cell proliferation. Overall, the data suggest that BV2 cells do not respond in a typical manner to CSF1 stimulation, either by showing activation of relevant signalling pathways, nor by dose dependent increases in cell proliferation.

In summary, BV2 cells do not offer a reliable or predictable model for investigating CSF1R signalling and its ability to regulate cellular autophagy.

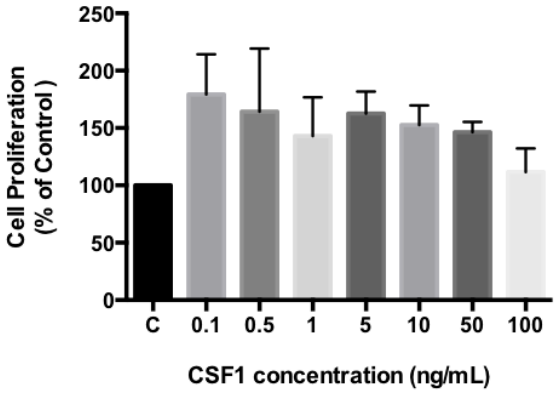

Figure 3.3.3.1: BV2 cells are only modestly stimulated to proliferate by CSF1. Cells were seeded at $1x10^6$ cells/well in 6-well plates and left to adhere overnight. Cell were then treated with various concentrations of CSF1 in 1 % serum supplemented RPMI and incubated for 48 hrs before assaying crystal violet incorporation (A570 nm). Results are representative of three independent experiments with values representing the mean ± S.E.M.

3.3.4 CSF1 increases proliferation of IMG cells in a dose-dependent manner

Instead of continuing with BV2 cells, an alternative, immortalised microglial line of murine origin was validated instead. Images of both cell types were obtained. IMG cells are similar in morphology to primary microglial cells (Figure 3.3.4.1, panels A and B) and their natural doubling time was determined by crystal violet assay (Figure 3.3.4.1, panel C). IMG cells doubled approximately every 24 hrs.

Separately, a CSF1 dose-response analysis determined the optimal dose of CSF1 for subsequent experiments. Cells were treated with CSF1 at the concentrations indicated in 1% FBS-supplemented DMEM and incubated for 48 hrs before analysis of DNA content by crystal violet incorporation assay. Treatment of IMG cells with CSF1 induced proliferation in a dose-dependent manner, with almost 4-fold increase in proliferation with 50 ng mL^{-1} (Figure 3.3.4.1, panel D). From here on, CSF1 was used at 50 ng mL^{-1} when required.

3.3.5 CSF1 treatment of IMG cells activates mTORC1 signalling

To assess whether CSF1 activated PI3K/Akt/mTORC1 and RAS/Erk1/2 signalling in IMG cells, cells were treated with 50 ng mL^{-1} of CSF1 in 0 % FBS/DMEM for the times indicated (Figure 3.3.5.1). CSF1 stimulated Akt Ser473 phosphorylation at 10 min before diminishing by 60 min, reflecting an induction of strong but transient Akt activation. S6K1 phosphorylated at Thr389 was also observed at 10 min, similar to Akt, and this gradually decreased over 120 min. Unexpectedly, phosphorylation of Erk1/2 was not stimulated by CSF1. Together, these data confirm that CSF1 activates the PI3K/mTORC1 pathway.

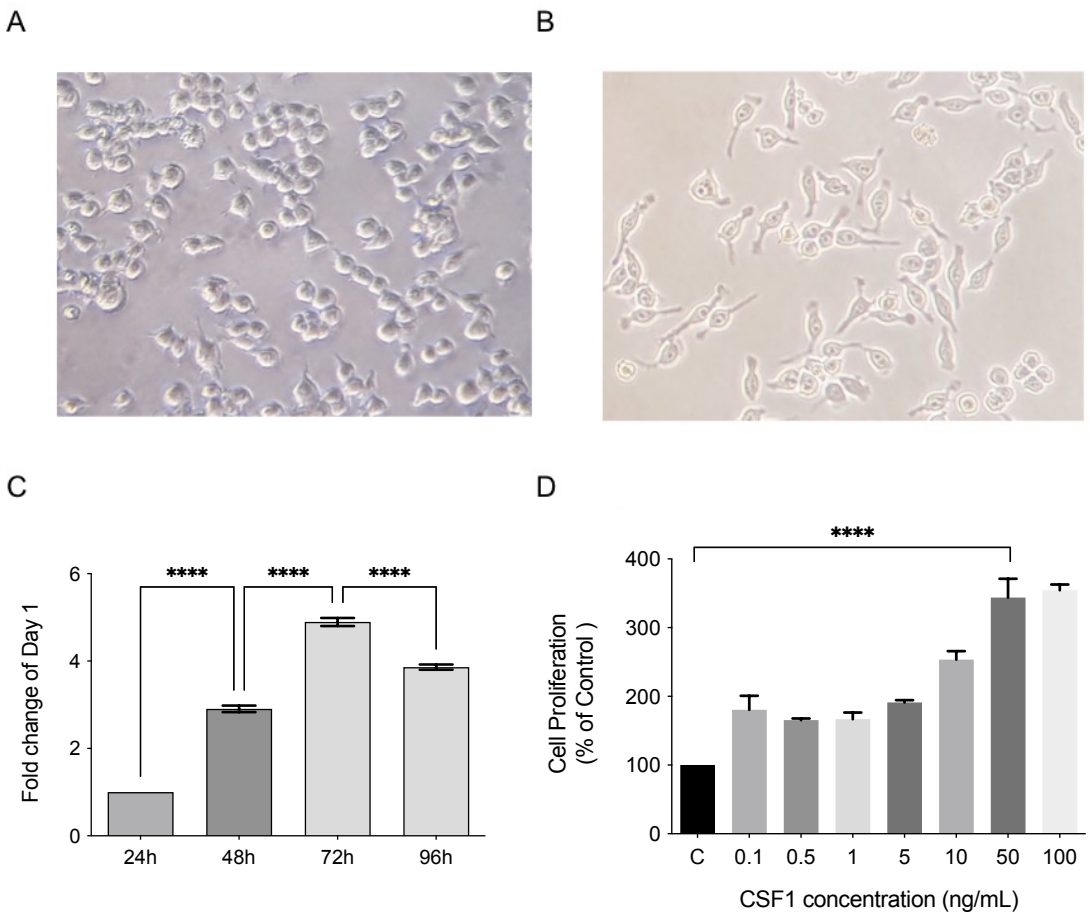

Figure 3.3.4.1: CSF1-stimulated proliferation of IMG cells in a dose-dependent manner. Cells were seeded at $1x10^6$ cells/well in 6-well plates and left to adhere overnight. Difference between BV2 (panel A) and IMG (panel B) cell morphology under 40x magnification. (C) In the absence of CSF1 cells were cultured in 10 % FBS/DMEM for the times shown (culture doubling time). (D) cells were treated with CSF1 at the indicated concentrations in 1 % FBS/DMEM and incubated for 48 hrs before analysis with crystal violet incorporation assay (A570 nm). Results are representative of three independent experiments with values representing the mean ± S.E.M. Data was analysed by one-way ANOVA and significant differences are depicted by p <0.0001.

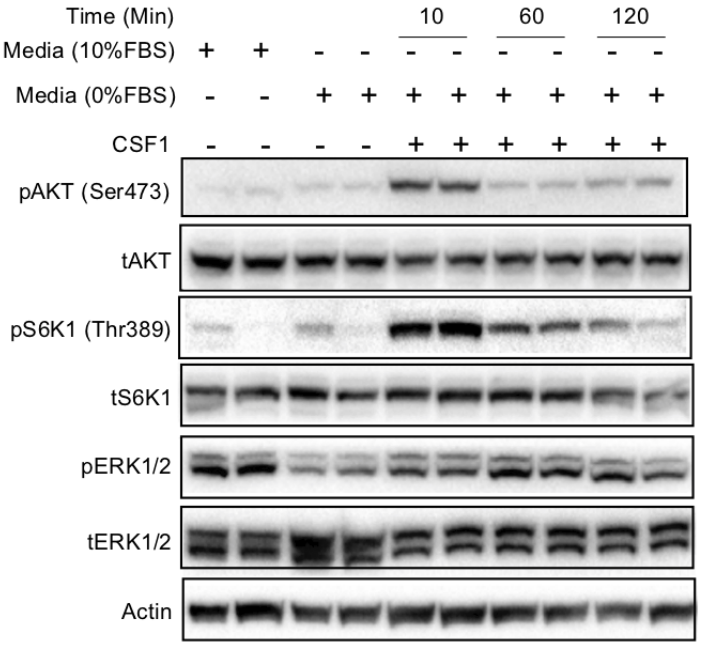

Figure 3.3.5.1: CSF1 treatment of IMG cell activates mTORC1 signalling. Cells were cultured in either 10 % FBS/DMEM or 0 % FBS/DMEM and incubated with CSF1 50 ng mL^{-1} for the times indicated. Cell lysates were resolved by 10 % SDS-PAGE gel before proteins were electroblotted onto PVDF membrane. Membranes were immunoprobed with antibodies for the proteins indicated. Actin was used as loading control. Results are representative of three independent experiments.

3.3.6 Inhibition of CSF1R signalling by the small molecule inhibitor, GW2580

Having determined that CSF1R stimulates PI3K signalling in IMG cells, the optimal dose of GW2580, a potent and selective inhibitor of CSF1R signalling was examined next (Conway *et al.*, 2005). Cells were cultured in 10 % FBS/DMEM or 0 % FBS/DMEM and pre-treated with various concentration of GW2580 for 1 hr prior to stimulation with 50 ng mL^{-1} CSF1 for 10 min (Figure 3.3.6.1).

Western immunoblot revealed that CSF1R protein expression was increased with serum deprivation. Stimulation of CSF1R with 50 ng mL^{-1} CSF1 resulted in downregulation of receptors, and stimulation of Akt and S6K1 phosphorylation. Low dose of GW2580 (0.01 and 0.05 μM) did not prevent receptor downregulation but did reduce Akt and S6K1 phosphorylation. Phosphorylation of Akt and S6K1 was markedly decreased with 0.1 μM GW2580 and abolished by 0.5 μM GW2580. Therefore, for subsequent experiments, 1 μM was the concentration chosen for treating IMG cells with GW2580 as it completely prevented receptor downregulation and activation of downstream signalling.

3.3.7 GW2580 inhibits CSF1R signalling in IMG cells

After optimisation of the dose of GW2580 that completely inhibited early receptor activation, the effect of GW2580 on CSF1-stimulated signalling was also assessed over 2 hrs. To this end, IMG cells were pre-incubated with 1 μM of GW2580 in the absence of FBS then stimulated with 50 ng mL^{-1} CSF1 for the times indicated (Figure 3.3.7.1). GW2580 inhibited Akt and S6K1 phosphorylation with no evidence of signalling pathway re-activation, even after 2 hrs.

3.3.8 IL-34 weakly stimulates proliferation of IMG cells

An alternative ligand for the CSF1R is IL-34 (Wang *et al.*, 2012), so the effect of IL-34 on IMG proliferation was examined next. Cells were seeded at $1x10^6$ cells/well in 6-well plates and left to adhere overnight. Cells were then treated with various concentrations of IL-34 in 1 % FBS/DMEM and incubated for 48 hrs before analysing DNA content by the crystal violet incorporation assay (A570 nm). Cell proliferation only increased by 30 % with 0.1 ng mL^{-1} IL-34 and did not increase further with increasing concentrations of IL-34 even at 100 ng mL^{-1}. Thus IL-34 is a poor inducer of proliferation, at least in IMG cells (Figure 3.3.8.1).

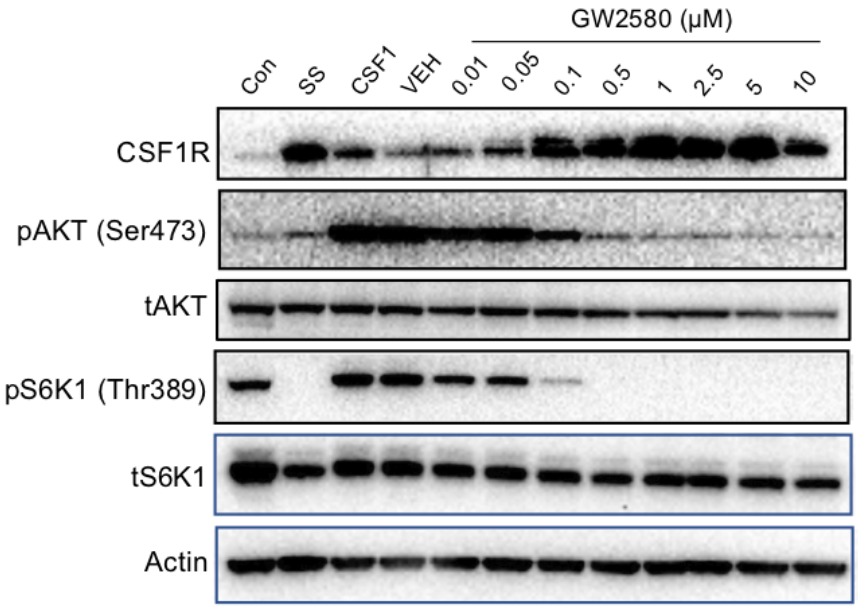

Figure 3.3.6.1: GW2580 inhibits receptor downregulation and downstream signalling in IMG cells. Cells were cultured and incubated in 10 % FBS/DMEM or 0 % FBS/DMEM, pre-treated with or without GW2580 at the concentrations indicated for 1 hr before stimulation with 50 ng mL^{-1} CSF1 for 10 min. Cell lysates were resolved by 10 % SDS-PAGE gel before proteins were electroblotted onto PVDF membrane. Membranes were immunoprobed with antibodies for the proteins indicated. Actin was used as loading control. Results are representative of three independent experiments. (SS=serum starved, VEH= vehicle).

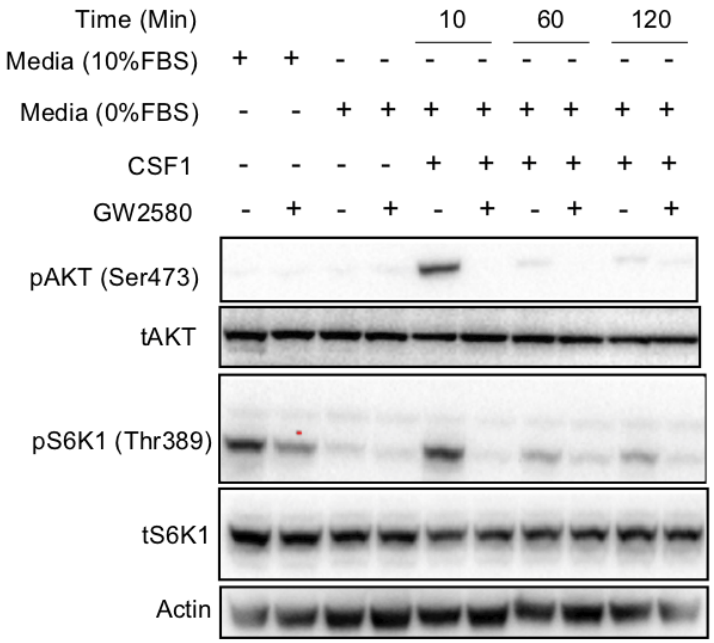

Figure 3.3.7.1: GW2580 prevents pathway reactivation following CSF1 stimulation in IMG cells. Cells were incubated in either 10 % FBS/DMEM or 0 % FBS/DMEM with or without 1 μM GW2580 and 50 ng mL^{-1} CSF1 for the times indicated. Cell lysates were resolved by 10 % SDS-PAGE gel before proteins were electroblotted onto PVDF membrane. Membranes were immunoprobed with antibodies for the proteins indicated. Actin was used as loading control. Results are representative of three independent experiments.

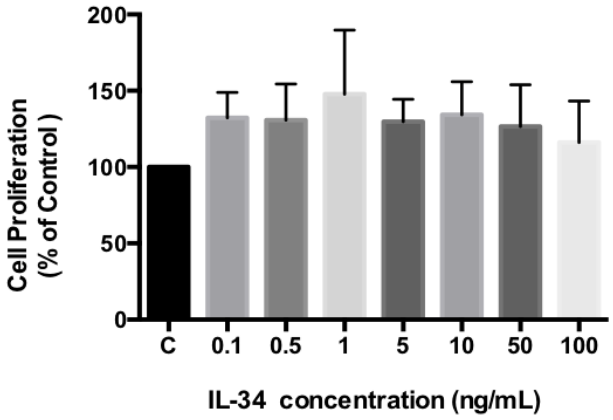

Figure 3.3.8.1: IL-34 is a poor inducer of proliferation in IMG cells. Cells were then treated with IL-34 at the indicated concentrations in 1% FBS/DMEM and incubated for 48 hrs before assessing DNA content by crystal violet assay. Results are representative of three independent experiments with values representing the mean ± S.E.M..

3.3.9 IL-34 does not activate mTORC1 signalling in IMG cells

Since IL-34 did not robustly stimulate cell proliferation, whether IL-34 could still engage CSF1R signalling and activate PI3K/mTORC1 signalling was tested. Following treatment with 50 ng mL^{-1} IL-34, IMG cells were incubated for the times indicated (Figure 3.3.9.1). No phosphorylation of Akt on Ser473 was observed with IL-34 treatment at 10 and 60 min but pAkt recovered to baseline levels by 120 min, while phosphorylation of S6K1 on Thr389 was undetectable. These data indicate IL-34 does not activate PI3K/mTORC1 pathway in IMG cells.

3.3.10 IL-34 does not activate autophagy in IMG cells

Although IL-34 did not induce cell proliferation, nor activated PI3K/mTORC1 signalling, the possibility that IL-34 could alter autophagy activity was assessed. Extracts were prepared as for Figure 3.3.9.1 and probed for LC3B (Figure 3.3.10.1). No differences in the conversion of LC3B-I to LC3B-II was detected following IL-34 treatment confirming that IMG cells do not respond to IL-34 by modulating cellular autophagy activity.

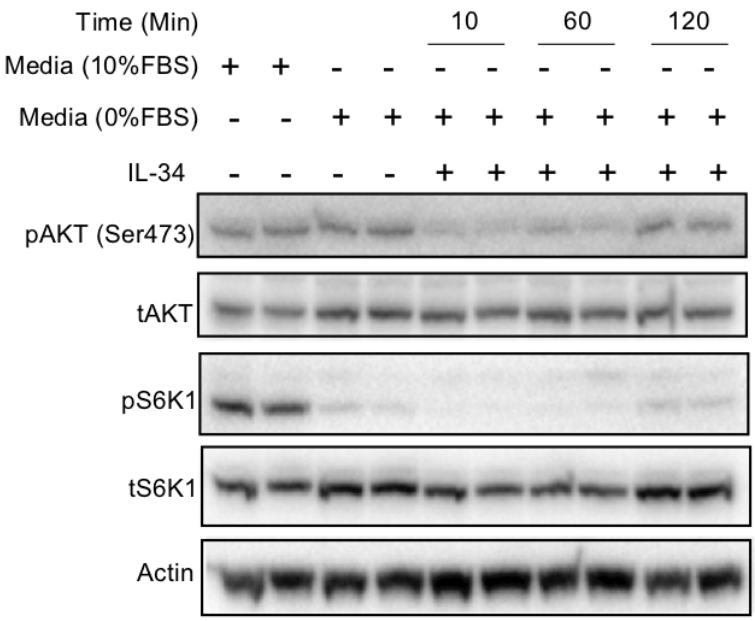

Figure 3.3.9.1: IL-34 treatment of IMG cells does not activate PI3K/mTORC1 pathway signalling. Cells were cultured in 10 % FBS/DMEM or 0 % FBS/DMEM and incubated with 50 ng mL^{-1} IL-34 for 10, 60 or 120 mins. Cell lysates were resolved by 10 % SDS-PAGE gel before proteins were electroblotted onto PVDF membrane. Membranes were immunoprobed with antibodies for the proteins indicated. Actin was used as loading control. Results are representative of three independent experiments.

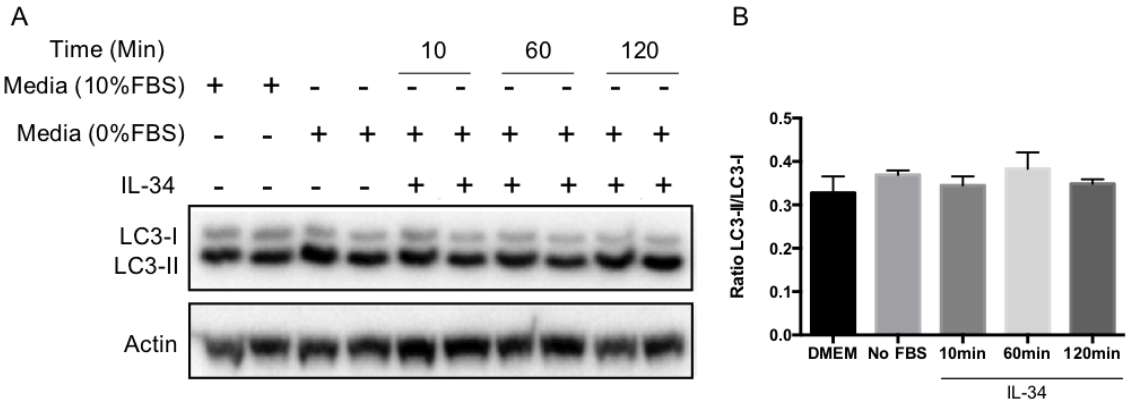

Figure 3.3.10.1: IL-34 treatment of IMG cells does not alter autophagy activity in IMG cells. Cells were cultured in 10 % FBS/DMEM or 0 % FBS/DMEM and incubated with IL-34 (50 ng/mL) for 10, 60 or 120 mins. (A) Cell lysates were resolved by 10 % SDS-PAGE gel before proteins were electroblotted onto PVDF membrane. Membranes were immunoprobed with antibodies for the proteins indicated. Actin was used as loading control. (B) Ratio of LC3B-II/LC3B-I expression, by densitometry. Results are representative of three independent experiments with values representing the mean ± S.E.M..

3.3.11 Amino acid starvation induces autophagy in IMG cells

To confirm that IMG cells can regulate autophagy following nutrient stress, the induction of autophagy with amino acid starvation was characterised next. Cells were incubated with or without EBSS for up to 24 hrs (Figure 3.3.11.1). EBSS starvation blocked mTORC1 signalling as seen by the disappearance of S6K1 phosphorylation at Thr389. SQSTM1/p62 expression was decreased after 1 hr of EBSS but rebounded by 2 hrs. This may be due to de novo synthesis of SQSTM1/p62 during autophagy (Sahani, Itakura and Mizushima, 2014). Whereas there was a clear turnover of LC3B-II at 4 and 24 hrs, that was statistically significant. Taken together, these data confirmed the induction of autophagy by nutrient stress in IMG cells.

At earlier time points, the induction of autophagy was unclear, apart from decreased SQSTM1/p62 at 1 hr of EBSS treatment. To establish that autophagy induction occurred as early as 1 hr of EBSS treatment the degradation of LC3B-II was prevented by inhibition of lysosomal fusion events using the lysosomatrophic drug, Bafilomycin A1 (Baf A1) (Mauvezin and Neufeld, 2015). Cells were, this time, incubated with or without EBSS for up to 4 hrs. Duplicate dishes were treated with 100 nM Baf A1 concurrently with the 1 hr EBSS treatment or for 2 hrs concurrently with the 2 hrs EBSS, or the last 2 hrs of the 4 hr EBSS treatment (Figure 3.3.11.2). Accumulation of LC3B-II was observed at all three time points indicating that there was an induction of autophagy following EBSS treatment. At 4 hrs, accumulation of SQSTM1/p62 was also observed.

3.3.12 Amino acid starvation promotes ULK1 dependent autophagy

EBSS starvation promoted dephosphorylation of ULK1 at Ser757, the major site of mTORC1 phosphorylation (Kim *et al.*, 2011) (Figure 3.3.12.1). This was concomitant with dephosphorylation of S6K1 at Thr389. Surprisingly, Beclin1 phosphorylation at Ser30 was also decreased by EBSS treatment, and although this is in disagreement with published studies (Park *et al.*, 2018), it is consistent with data from the laboratory (Lois Lee Dekkers, unpublished data).

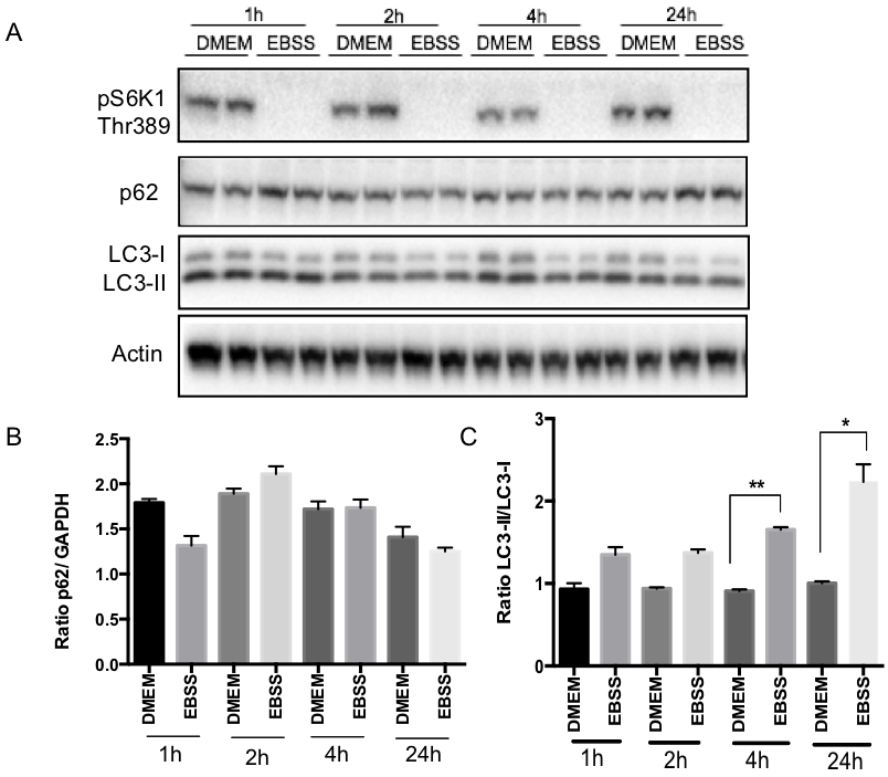

Figure 3.3.11.1: Amino acid starvation induced autophagy in IMG cells. Cells were cultured in the presence or absence of EBSS for the times indicated. (A) Cell lysates were resolved by 10 % SDS-PAGE gel before proteins were electroblotted onto PVDF membrane. Membranes were immunoprobed with antibodies for the proteins indicated. Actin was used as loading control. The ratio of SQSTM1/p62 to actin (B) or LC3B-II/LC3B-I was quantified by densitometry. Results are representative of three independent experiments with values representing the mean ± S.E.M.. Statistical analysis was performed using one-way ANOVA and Bonferroni post hoc analysis (*$p<0.05$, **$p<0.01$).

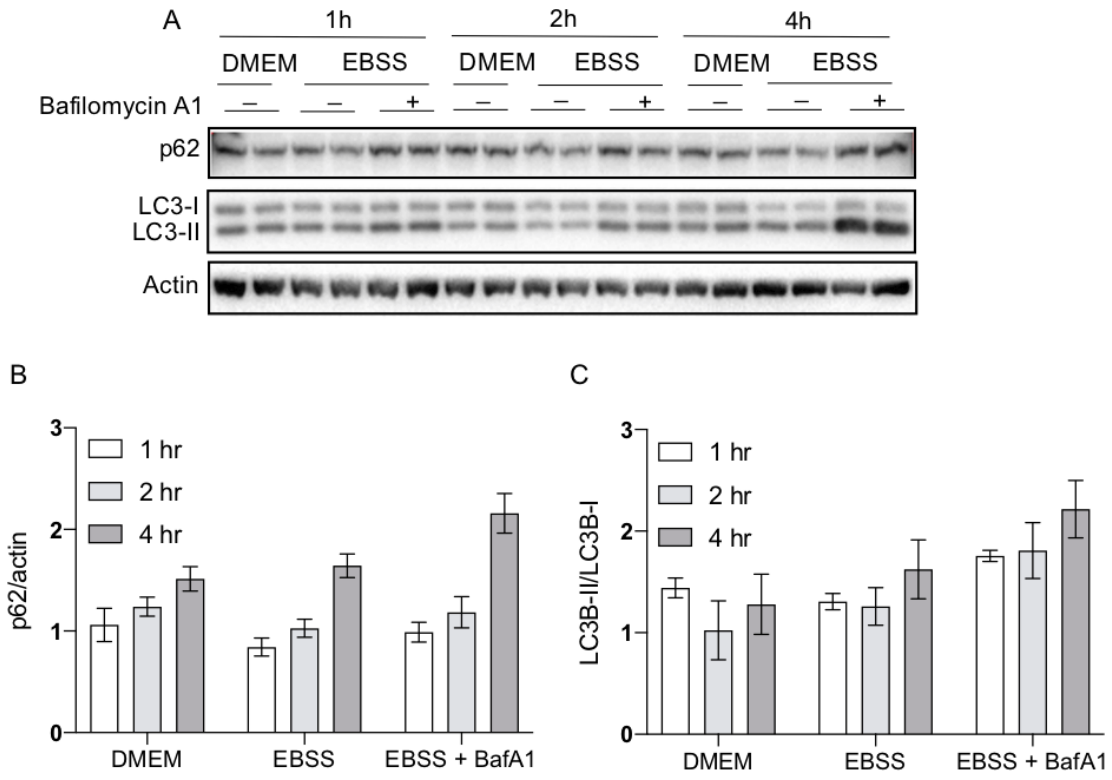

Figure 3.3.11.2: Analysis of autophagy flux with amino acid starvation in IMG cells. Cells were incubated with or without EBSS and with or without 100 nM Baf A1 for the times indicated. Cell lysates were resolved by 10 % SDS-PAGE gel before proteins were electroblotted onto PVDF membrane. Membranes were immunoprobed with antibodies for the proteins indicated. Actin was used as loading control. Results are representative of three independent experiments.

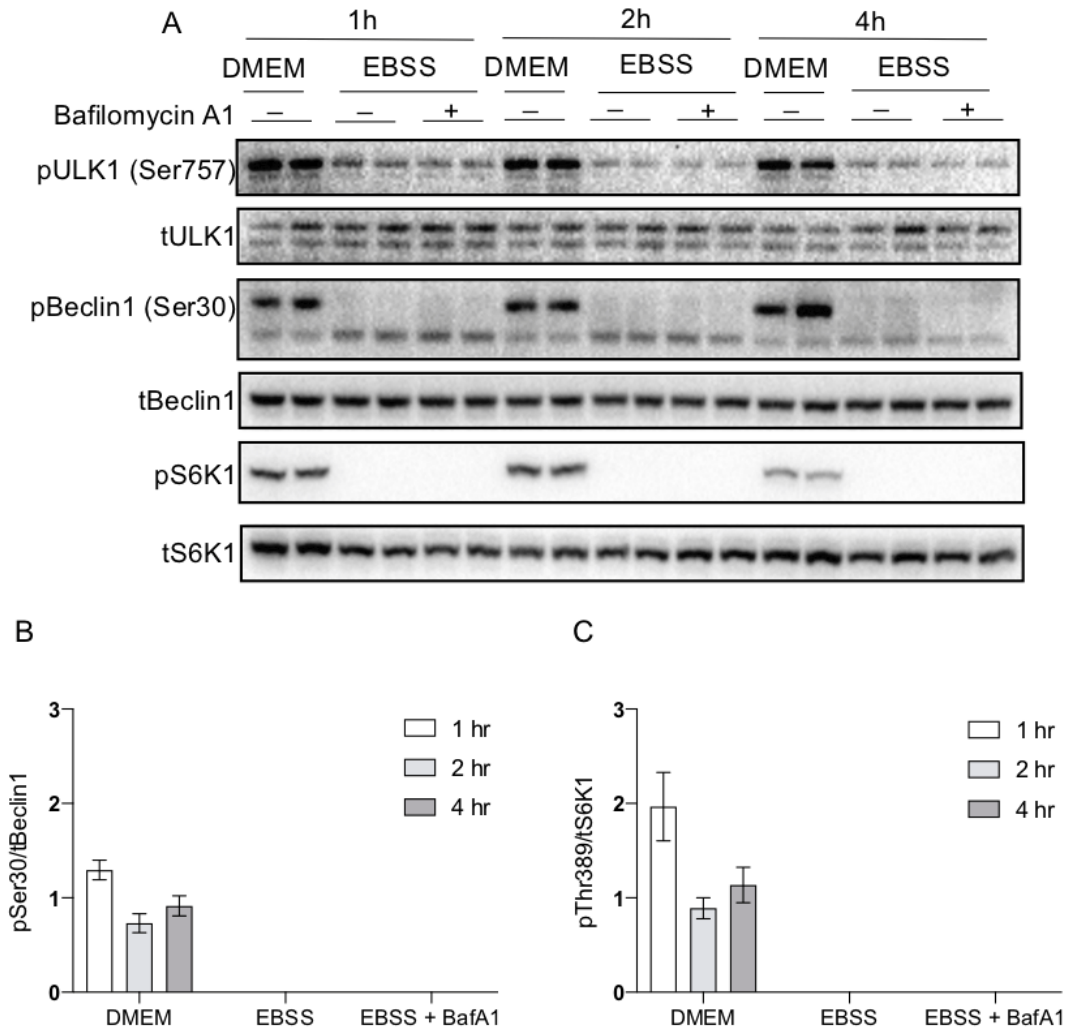

Figure 3.3.12.1: Analysis of autophagy signalling during amino acid starvation in IMG cells. Cells were incubated with or without EBSS and with or without 100 nM Baf A1 for the times indicated. Cell lysates were resolved by 10 % SDS-PAGE gel before proteins were electroblotted onto PVDF membrane. Membranes were immunoprobed with antibodies for the proteins indicated. Actin was used as loading control. Results are representative of three independent experiments.

3.3.13 Immunolocalization of autophagy proteins in IMG cells

An alternative method to assess autophagy qualitatively and quantitatively within cultured cells is immunofluorescence microscopy. In this approach, localisation of LC3B and/or Beclin1 can be used to identify autophagosomes, in a puncta formation assay (Anwar et al., 2019; Runwal et al., 2019). To this end, HEK293 (Figure 3.3.13.1) and IMG (Figure 3.3.13.2) cells were incubated in in the presence or absence of EBSS for 4 hrs, with 100 nM Baf A1 for the final 2 hrs to prevent further lysosomal fusion of autophagosomes. After fixation and permeabilization, cells were probed with anti-LC3B and anti-Beclin1 antibodies, followed by detection with suitable Alexa dye conjugated secondary antibodies on an epifluorescence inverted microscope. Formation of LC3B positive puncta is clearly visible in HEK293 cells, following nutrient removal (Figure 3.3.13.1, compare panels a and d) and this is exacerbated by Baf A1 treatment (Figure 3.3.13.1, panel g). In addition, Beclin1 puncta were also detected, indicating sites of autophagosomal origin (omegasomes) with colocalization detected between Beclin1 positive puncta and LC3B positive puncta (white arrows). Conversely, in IMG cells formation of Beclin1 puncta was not detectable, although diffuse Beclin1 staining was observed (Figure 3.3.13.2, panels b, e and h). Nonetheless, EBSS stimulated the formation of numerous LC3B positive puncta, and this was exacerbated by Baf A1 treatment (Figure 3.3.13.2, compare panels d and g).

Taken together, IMG cells provide a robust system for the study of microglial autophagy, with a prototypical response to nutrient stress. Thus, this cell line offered an opportunity to investigate the impact of CSF1R signalling and its inhibition on autophagy in a microglial model.

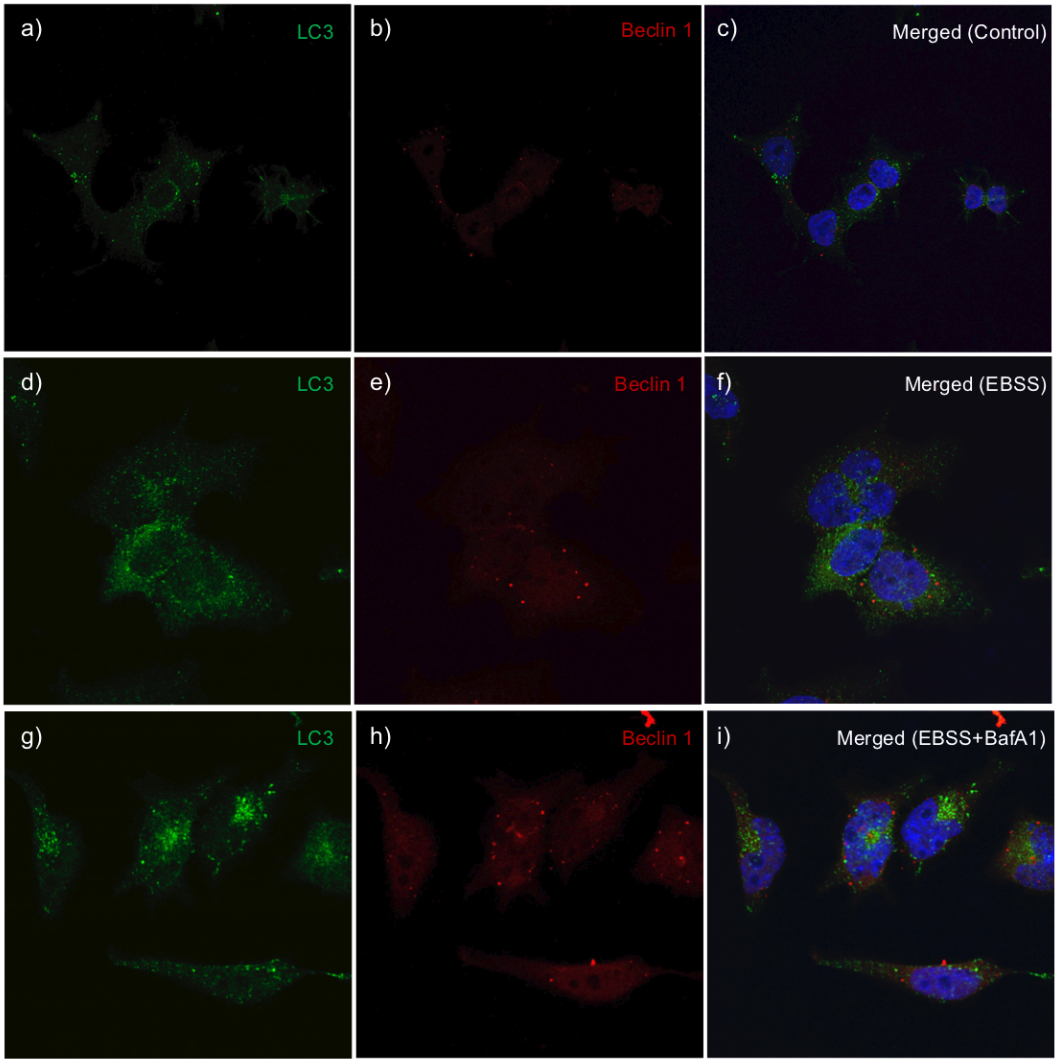

Figure 3.3.13.1: Formation of autophagosomes in HEK293 cells. Cells were incubated in full media (panels a-c) or EBSS for 4 hrs (panels d-f), or incubated EBSS for 4 hrs with 100 nM Baf A1 for the final 2 hrs (panels g-i). After methanol fixation, permeabilization and blocking in BSA, coverslips were incubated with anti-LC3B and anti-Beclin1 antibodies, followed by secondary antibodies with Alexa 488 (green, panels a, d and g) and Alexa594 (red, panels b, e and f) conjugates, respectively. DNA was stained with DAPI (blue, panels c, f and i). Images are representative of three independent experiments.

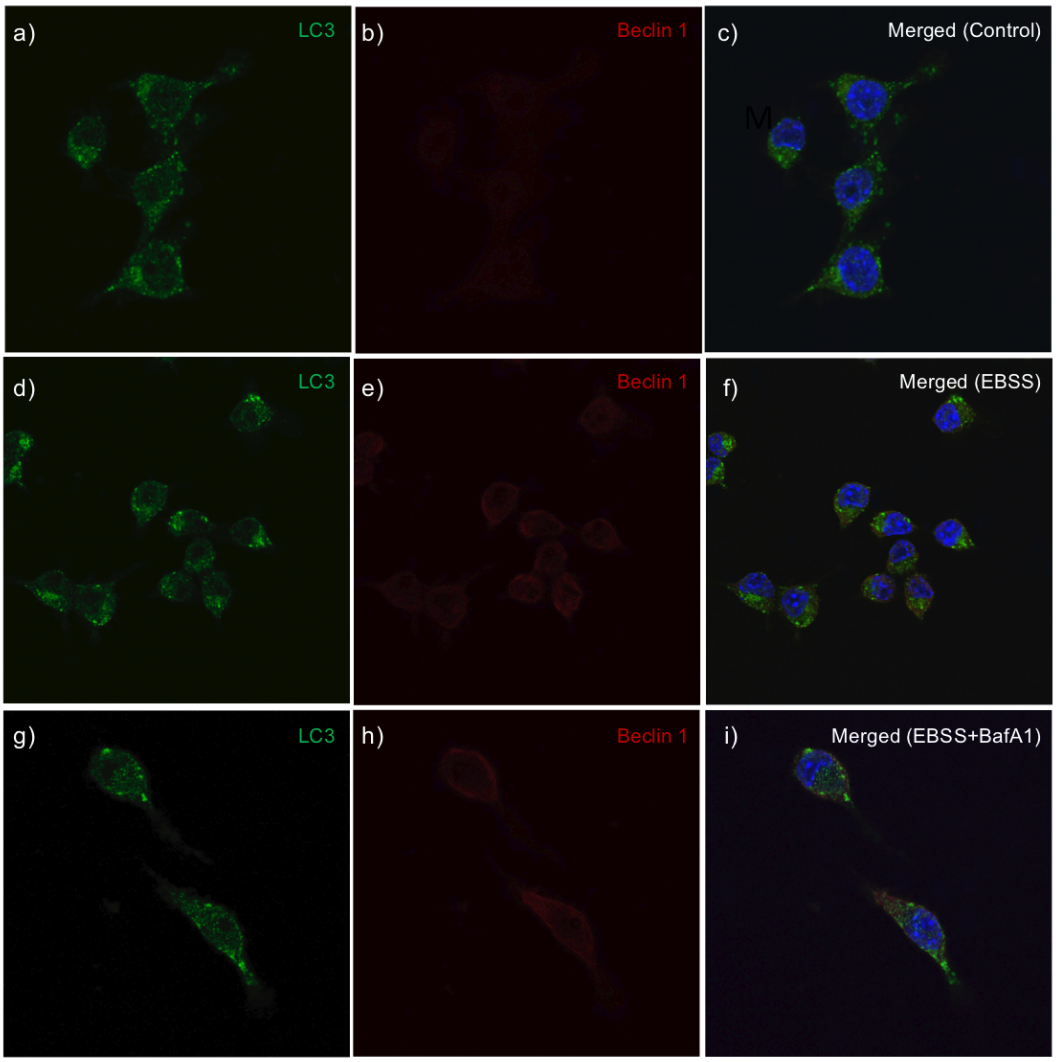

Figure 3.3.13.2: Formation of autophagosomes in IMG cells. Cells were incubated in full media (panels a-c) or EBSS for 4 hrs (panels d-f), or incubated EBSS for 4 hrs with 100 nM Baf A1 for the final 2 hrs (panels g-i). After methanol fixation, permeabilization and blocking in BSA, coverslips were incubated with anti-LC3B and anti-Beclin1 antibodies, followed by secondary antibodies with Alexa 488 (green, panels a, d and g) and Alexa 594 (red, panels b, e and f) conjugates, respectively. DNA was stained with DAPI (blue, panels c, f and i). Images are representative of three independent experiments.

3.3.14 Inhibition of mTORC1 does not induce autophagy in IMG cells

Rapamycin is the prototypical mTORC1 inhibitor that prevents substrate binding by the mTORC1 complex protein, Raptor. In numerous studies, rapamycin has been shown to induce autophagy, by inhibiting the ability of mTORC1 to phosphorylate ULK1 complexes (Wu *et al.*, 2013). To demonstrate this, cells were cultured in full media with or without 100 nM rapamycin for the times indicated (Figure 3.3.14.1). Rapamycin, as expected, inhibited mTORC1-dependent phosphorylation of S6K1 at Thr389. However, no increase in autophagy was detected, either by turnover of LC3B, or SQSTM1/p62.

3.3.15 The CSF1R inhibitor, GW2580 does not induce autophagy in IMG cells

Classically, receptor tyrosine kinase signalling that leads to mTORC1 activation also suppresses autophagy (Hansen *et al.*, 2007; Domigan *et al.*, 2015). If CSF1R signalling suppresses autophagy in IMG cells, then inhibition of the receptor may activate autophagy. To test this, cells were incubated with the small molecular CSF1R inhibitor, GW2580. To do so, cells were starved overnight then stimulated with 50 ng mL^{-1} CSF1 in the absence of FBS for the times indicated, and in the presence or absence of 1 μM GW2580 (1 hr pre-treatment, Figure 3.3.15.1). Western blot analysis showed no loss of LC3B-II expression that would have been expected by activation of autophagy. Additionally, GW2580 did not alter SQSTM1/p62 expression. Overall, GW2580 did not promote increased activation of autophagy following receptor inhibition.

Taken together, these data suggest that regulation of autophagy is uncoupled from mTORC1 signalling, downstream of the CSF1R in IMG cells.

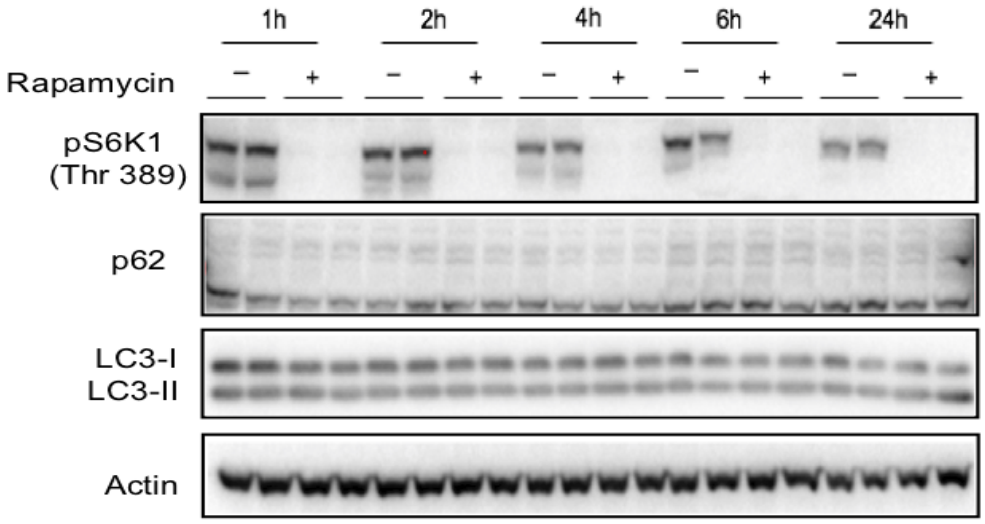

Figure 3.3.14.1: Inhibition of mTORC1 with rapamycin does not induce autophagy in IMG cells. Cells were incubated in full media with or without 100 nM rapamycin for the times indicated. Cell lysates were resolved by 10 % SDS-PAGE gel before proteins were electroblotted onto PVDF membrane. Membranes were immunoprobed with antibodies for the proteins indicated. Actin was used as loading control. Results are representative of two independent experiments.

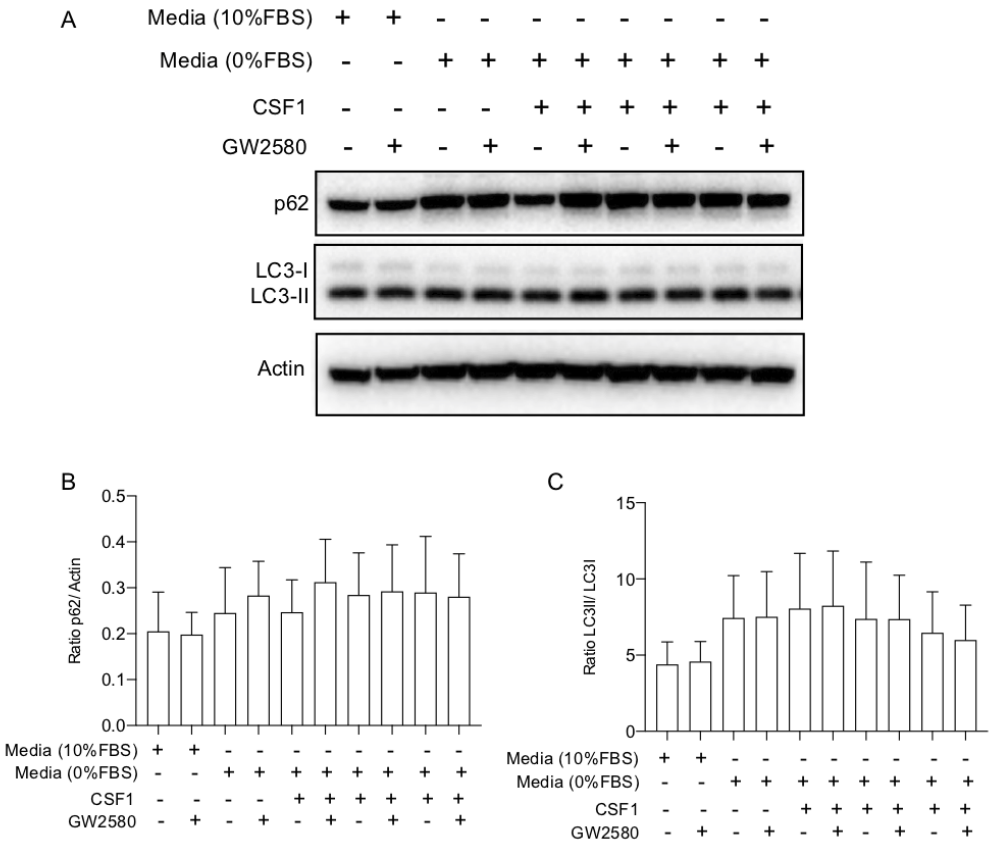

Figure 3.3.15.1: GW2580 does not induce autophagy in IMG cells. Cells were incubated starved of FBS overnight prior to stimulation with 50 ng mL^{-1} CSF1 in the presence or absence of 1 μM GW2580 for the times indicated. Cell lysates were resolved by 10 % SDS-PAGE gel before proteins were electroblotted onto PVDF membrane. Membranes were immunoprobed with antibodies for the proteins indicated. Actin was used as loading control. Results are representative of three independent experiments.

3.4 Discussion

In this chapter, BV2 cells were shown to not be a good model for characterising CSF1R signalling. Instead the IMG cell line provides an excellent model for understanding the mechanisms underlying CSF1R signalling. In IMG cells, CSF1 was shown to activate CSF1R-dependent PI3K/mTORC1 signalling and this was inhibited with GW2580. In addition, IMG cells respond to nutrient stress by inducing autophagy, but mTORC1 does not directly regulate autophagy, despite ULK1 being phosphorylated on the mTORC1 site, Ser757.

3.4.1 CSF1 stimulates CSF1R signalling in IMG, but not BV2 cells

The BV2 microglial cell line, was originally generated from embryonic brain mononuclear cells (Blasi *et al.*, 1990), but remains a controversial cell line to be used in scientific research. One of the major limitations of this cell line is the relatively high baseline level of activity and the inadequacy of responses to pro-and anti-inflammatory stimuli (Horvath *et al.*, 2008; Kim *et al.*, 2014). Studies looking at microglial signalling and functions in the adult brain demands a cell line which is at least comparable to the resident microglia in the adult brain. Initial studies were done in BV2 cells as they were previously uncharacterised in terms of CSF1R signalling. Conversely, the IMG microglial cell line was generated from the immortalisation of microglia from adult murine brain via infection with the v-raf/v-myc retrovirus (McCarthy *et al.*, 2016). In terms of their similarity to resident microglia of the brain, they offer a more “microglial-like” option, and so these were also investigated for CSF1R signalling.

Although CSF1 stimulated proliferation in BV2 cells (1.5-fold of control), it was modest in comparison to the 3.5-fold increase observed in IMG cells. This reason for this was obvious from analysis of the downstream signalling pathways in both cell lines. While IMG cells showed robust, concentration dependent activation of PI3K/Akt/mTOR signalling, CSF1 treatment, even at 100 ng/mL^{-1} did little to stimulate pathway activation. Therefore, BV2 cells, despite having a potent response to nutrient deprivation, did not recapitulate the CSF1R signalling found in IMG or resident microglial cells (Keane *et al.*, 2021).

3.4.2 The use of immortalised cells and caveats associated with this

Like other cell types, microglia go through senescence after a certain number of cell divisions. Telomere shortening occurs upon repeated cell division events and after about ~50 replications (known as the Hayflick limit) cells may lose their mitotic potential (Hayflick, 1965). Therefore, to meet the need for the extensive number of cells needed for research, cells can be 'immortalised' by different approaches such as including ectopic expression of telomerase or telomerase reverse transcriptase (TERT), by mutating the p53 and pRb genes (Maqsood et al., 2013). Introducing viral genes that overrides the cell cycle is another way of immortalising cells. These immortalised cells are genetically manipulated to grow indefinitely and serve as model systems for studying various diseases, including neurodegenerative diseases such as AD. IMG cells were immortalised by transducing isolated primary microglia from adult murine brain with retroviral v-raf/v-myc (McCarthy et al., 2016). Although immortalised cells are easier to grow and maintain, provide more homogenous populations than primary cells and thereby facilitate more reproducible data, immortalisation may also have undesirable consequences. Genetic manipulation may alter cellular phenotype, resulting in, for example, changed functional and mechanistic responses to stimuli (Kohno et al., 2011). For instance, BV2 cells have been reported to resemble an activated microglial state (Bocchini *et al.*, 1992). Sequential passaging of cell lines may further cause genotypic and phenotypic variation over an extended period, with genetic drift introducing heterogeneity in cultures. Moreover, although infrequent, cell lines can become contaminated with more rapidly proliferating cells lines (Nelson-Rees, Daniels and Flandermeyer, 1981).

Although IMG experiments should be repeated in the more physiologically relevant primary microglial cell cultures, this approach also has its limitations. Primary microglia are also broadly regarded as being in a partially activated state, because of their method of isolation. Microglial isolation from CNS tissue to single-cell suspension must pass through mechanical dissociation or enzymatic digestion and different purification methods such as fluorescence or magnetic activated cell sorting (FACS/MACS). This can cause cells to develop altered metabolism or induce their activation (Mattei et al., 2020; Ocañas et al., 2022). Cultured primary microglia exhibit increased motility and altered phagocytosis rates too (Montilla et al., 2020). To obtain a high microglial yield, microglia are often grown as a confluent glial cell

layer from neonatal or embryonic CNS tissue and then mechanically shaken off to acquire a pure microglial monoculture giving them an activated (amoeboid morphology and increased pro-inflammatory cytokine secretion) and immature phenotype. Various growth factor supplements are also needed to maintain the survival and differentiation phenotypes of these primary microglial cultures (Bohlen et al., 2017). Consequently, all these potential impacts on microglial biology mean that data obtained from either cell lines or isolated primary microglia should be interpreted with some degree of caution in light of their in vitro-acquired properties.

3.4.3 IMG cells are refractory to IL-34

Similarly to CSF1, IL-34 is thought to tightly bind to the CSF1R to promote differentiation, proliferation and survival of monocytes, macrophages and osteoclasts (Boulakirba et al. 2018). In fact, IL-34 stimulates a stronger and more rapid phosphorylation of CSF1R than CSF1 itself (Felix *et al.*, 2013). However, biological activity and signal transduction by both ligands has been shown to differ in human monocytes. For instance, the ability for the two ligands to induce the production of chemokines is distinct and IL-34 is known to induce a stronger but transient tyrosine phosphorylation of the CSF1R and downstream molecules (Boulakirba et al. 2018).

In IMG cells, IL-34 treatment did not promote cell proliferation, nor stimulate the CSF1R. No phosphorylation of S6K1 or Akt was observed experiments after 10 mins of incubation with IL-34. Although it is possible that this time point may have been too late to capture the activation of Akt, it would not explain the lack of S6k1 phosphorylation, which is usually sustained following receptor activation. Additionally, IL-34 had no impact on autophagy, suggesting that IMG cells either respond poorly to IL-34 or require some supplementation with FBS, which was omitted in the IL-34 and CSF1 experiments, for IL-34 to stimulate the CSF1R.

3.4.4 Regulation of autophagy is non-canonical in IMG cells

In both BV2 and IMG cells amino acid deprivation induced autophagy. Additionally, amino acid deprivation induced autophagy in IMG cells and this was concomitant with attenuated mTORC1 signalling, characterised by reduced S6K1 phosphorylation on Thr389 (Byfield, Murray and Backer, 2005). Not only that, but

phosphorylation of ULK1 at Ser757 was also impaired. Ser757 is the main mTORC1 phosphorylation site and its dephosphorylation occurs when ULK1 is activated (Kim *et al.*, 2011).

Conversely, Beclin1 phosphorylation at Ser30 was also decreased by amino acid deprivation. Phosphorylation of this site is frequently increased following amino acid deprivation (Park *et al.*, 2018), although unpublished work form this laboratory in neuronal cells also showed decreased Beclin1 phosphorylation at Ser30 following amino acid deprivation (Lois Lee Dekkers, unpublished data from SH-SY-5Y cells). This could be explained by cellular origin such as CNS vs peripheral nervous system (PNS). Indeed, an increase in Beclin1/PIK3C3-independent autophagy has been reported after treatment of SH-SY-5Y neuronal cell line with the neurotoxin 1-methyl-4-phenylpyridinium, which produces mitochondria-targeted injury (Chu, Zhu and Dagda, 2007). Similarly, this neurotoxic compound increased autophagic vacuoles in primary midbrain dopaminergic neurons, which was reversed by inhibition of RAS/Erk1/2 signalling but not PI3K signalling (Zhu *et al.*, 2007). While an increase in Beclin1 at Ser30 phosphorylation has been observed in MEFs, HEK293T cells, and HCT116 cells (Park *et al.*, 2018).

In what is a direct relation to this, the present study has found that the mTORC1 inhibitor, rapamycin (Thoreen and Sabatini, 2009) was capable of attenuating mTORC1 signalling, but failed to induce autophagy in IMG cells. This would suggest that like other cell types, IMG and perhaps microglial cells in general, possess a non-canonical mechanism for inducing autophagy that does not rely solely on signals through mTORC1. Indeed, other kinases, including Akt, AMPK, MAPK and Protein kinase C (PKC) are also involved in the regulation of autophagy (Suffixidharan, Jain and Basu, 2011).

Non-canonical autophagy pathways utilize alternative mechanisms for induction of autophagy and also components of the autophagy machinery to selectively target internal cellular substrate to be degraded. Cheong and colleagues have discovered that one type of autophagy can bypass the canonical ULK1 initiation step in response to raised ammonia levels caused by the increased amino acid catabolism in cells or to glucose deprivation in double deficient ULK1/2 mouse embryo fibroblasts. They reported that ULK1/2 are required for the autophagy response

triggered by the deprivation of nitrogenous amino acids (Cheong *et al.*, 2011). Additionally, resveratrol mediated Beclin1-independent autophagy was shown in human breast cancer cell death. While this process was insensitive towards the knockdown of the PI3KC3 complex components, it was dependent on the ubiquitin-like conjugation system (Scarlatti *et al.*, 2008). Another example of non-canonical autophagy would be the study where autophagy was induced in an Atg5/Atg7-indepepdt and ULK1- and Beclin1- dependent manner in Embryonic Fibroblast (MEF) cells isolated from $ATG5^{-/-}$ mice (Nishida *et al.*, 2009). Two crucial pathways with important roles in myeloid cells: LC3-associted endocytosis (LANDO), described by the LC3 conjugation to clathrin- and Rab5-positive endosomes (Heckmann *et al.*, 2019) and LC3-associated phagocytosis (LAP) are key to the understanding of non-canonical autophagy. LAP will be dealt with experimentally in the following chapter. From these studies it can be said that the observed uncoupling of autophagy from mTORC1 signalling is not surprising due to the existence of non-canonical pathways for autophagy induction.

3.5 Limitations and future work

Repeating these experiments in primary cells would prove a better insight into autophagy signalling in microglia. The inability to obtain sufficient cell numbers for quantitatively assessing LC3B-positive puncta by immunofluorescence in IMG cells, also using this to explore non-canonical autophagy would strengthen the argument for this mode of autophagy in at least the IMG cells. Further investigation of non-canonical forms of autophagy, such as more detailed analysis of ULK1 phosphorylation on activation sites (e.g. autophosphorylation and AMPK sites), combined with alternative inducers of autophagy (e.g. ammonia or glucose deprivation) could resolve the remaining question of how non-canonical autophagy in IMG cells is activated. It should be noted that BV2 cells have a robust autophagy response, but FBS starvation, did not cause attenuation of S6K1 phosphorylation to the same extent as in IMG cells (compare Figure 3.3.1.1 with Figure 3.3.5.1).

Gene silencing of the CSF1R by lentiviral transduction of shRNA could be utilised to study the relationship between CSF1R microglial cell function further. Finally, all these experiments should be replicated in either primary murine and *in vivo* animals to validate the findings in the current study.

3.6 Conclusion

In conclusion, the data presented herein demonstrates that CSF1R regulate mTORC1 signalling and cell proliferation of microglial cells, but not cellular autophagy, despite cells having a robust activatable autophagic response to nutrient stress. Since autophagy would appear uncoupled from CSF1R signalling, this would offer a novel opportunity to pursue receptor antagonists to resolve inappropriate microglial cell proliferation in the AD brain, while also allowing for a normal autophagy response to either occur, or be restored by independent modulation of autophagy. This will be explored, in part in subsequent chapters.

Chapter 4: CSF1R as a regulator of microglial activation and inflammatory responses

4.1 Introduction

In the previous chapter, CSF1R-stimulated mTORC1 activity was shown to be uncoupled from autophagy regulation in IMG cells. However, the effect of inhibiting CSF1R signalling with GW2580 on microglial functions, other than autophagy, is relatively understudied. CSF1R signalling is one of the main regulators of proliferation of mononuclear phagocytes such as microglia. However, direct links between proliferative microglia and functional studies of phagocytosis in this immune cell are limited and require further investigation. Whether CSF1R inhibition by GW2580 in microglia alters phagocytosis or microglial activation, demands attention. In this chapter, the effect of CSF1R stimulation or inhibition by GW2580 on the phagocytosis of latex beads in IMG cells was investigated. Whether stimulation or CSF1R inhibition by GW2580 altered microglial activation was investigated by analysing nitric oxide (NO) production, reactive oxygen species (ROS) generation and cytokine and chemokine expression in response to lipopolysaccharide (LPS), a pro-inflammatory stimulus, was examined herein. The underlying mechanism(s) behind any observed functional alterations by CSF1 or GW2580 were also characterised.

4.2 Phagocytosis

Phagocytosis is a specialised process for the uptake and removal of unwanted targets such as pathogens, apoptotic cells, and cellular debris, and is one of the primary innate functions of microglia. Removal of unwanted material such as pathogens, apoptotic cells, cellular and neuronal debris and dead and dying neurons is essential for normal function of the brain and to prevent the onset of aggregation prone diseases. (Paresce, Ghosh and Maxfield, 1996; Sierra *et al.*, 2010; Sivagnanam, Zhu and Schlichter, 2010). Little is known about whether there are any direct relationships between proliferation and phagocytosis in microglia. Treatment of murine microglia with CSF1 increased microglial phagocytosis of microspheres and amyloid beta (Aβ) (Mitrasinovic *et al.*, 2003). CSF1R overexpression by transfection in BV2 and human microglia also increased phagocytosis of fluorescein conjugated Aβ (Mitrasinovic and Murphy, 2003). Conversely, in tumour associated macrophages (TAMs), simultaneous inhibition of CSF1R and SHP2 (Src homology region 2 (SH2) domain-phosphatase 2) increases their phagocytic capabilities (Ramesh *et al.*, 2019). Thus, to resolve whether IMG cells require CSF1R stimulation to phagocytose latex beads was investigated.

4.2.1 LC3B-Associated Phagocytosis

The intersecting point of two microglial functions, phagocytosis, and autophagy is a hybrid membrane trafficking pathway termed LC3B-Associated Phagocytosis (LAP). LAP occurs when the autophagy machinery is partially translocated to the phagosome to promote an efficient intracellular degradation of engulfed cargo. In contrast to canonical autophagy, LC3B is recruited to single membrane phagosomes, as opposed to double membrane-containing autophagosomes (Florey *et al.*, 2011). Engulfment of bacteria or yeast, by RAW264 macrophages induced the translocation of overexpressed GFP-LC3B to single membrane phagosomes within 10 mins of internalisation (Sanjuan *et al.*, 2007). LAP has also been implicated in the regulation of the inflammatory profile, enhancing the immune response via modulation of antigen presentation. For instance, Toll-Like Receptor (TLR)-stimulated phagocytosis of bacteria in macrophages resulted in LC3B association to phagosomes that enhanced the function of conventional phagosomes (Sanjuan *et al.*, 2007). LC3B recruitment to zymosan-containing phagosomes in human macrophages and dendritic cells was also associated with prolonged presentation of the phagocytosed material on major histocompatibility complex class II (MHC II) (Romao *et al.*, 2013). Despite the growing understanding of the mechanism of phagocytosis in peripheral macrophages, questions remain as to whether LAP is an important form of phagocytosis used by microglia. Phagocytosis of latex beads is an appropriate model system to examine phagocytosis of foreign particulate matter (Gu *et al.*, 2010; Ueno, Yamamoto and Kawasaki, 2021) and was employed in this study.

4.3 Activation of microglia

Microglial activation is characterised by its responses to CNS injury, infection, and diseases with complex reactions and is a hallmark of a wide range of brain pathology. Bacterial endotoxin, Lipopolysaccharide (LPS), is the most used challenge for stimulating a pro-inflammatory response in microglia, both *in vitro* and *in vivo.* LPS activates the innate immune receptor, TLR4, which is highly expressed in microglia, and leads to the induction of pro-inflammatory signalling (Cui *et al.*, 2020). Recognition of bacteria results in the rapid activation of microglia and induces pro-inflammatory responses with generation of NO, ROS, and release of various cytokines. At low concentrations, NO is important for vasodilation and neurotransmission, while at higher concentrations, it plays a negative role

contributing towards pathogenesis in stroke, demyelination, and other neurodegenerative diseases (Levine, Punihaole and Levine, 2012). LPS triggers ROS expression through mechanisms such as constitutively expressed Nicotinamide Adenine Dinucleotide Phosphate Hydrogen (NADPH) oxidase or suppression of the anti-oxidative enzymes involved in ROS clearance (Li *et al.*, 2010).

CSF1 may be a key factor in regulating microglial inflammatory responses. Interestingly, compound 31, a dual inhibitor of Death Associated Protein Kinase (DAPK)1 and CSF1R inhibits tau aggregate formation and reduces neuronal death, as well as reducing NO production by half in LPS-induced BV2 microglia (Farag *et al.*, 2019). Simultaneous and sustained inhibition of CSF1R and MAPK using dual-kinase inhibitor-loaded supramolecular nanoparticles repolarised macrophages from a pro-tumorigenic M2 phenotype to an anti-tumorigenic M1 phenotype in the peripheral nervous system (Ramesh *et al.*, 2020). Thus, interfering with CSF1R signalling to regulate microglial activation may provide a promising drug target for treatment of neuroinflammatory diseases and there are pre-clinical studies, in a number of neurodegenerative diseases, to support this idea (Gómez-Nicola *et al.*, 2013; Martínez-Muriana *et al.*, 2016; Olmos-Alonso *et al.*, 2016). However, those studies are focussed on the curtailing of microglial proliferation and the effect of inhibiting this receptor to target both NO and ROS production in the CNS has not been explored yet.

Microglial activation is achieved through multiple signal transduction pathways, including the PI3K/Akt/mTORC1 and Ras/MEK/ERK pathways, and also kinases such as c-Jun N-terminal protein Kinase (JNK) and p-38 mitogen-activated protein kinase (p-38) (Wang *et al.*, 2011). The convergence, divergence or “crosstalk” properties of these kinase pathways form complex signalling networks that stimulate an array of cellular responses, including the activation of transcription factors such as NFκB (Schulze-Osthoff *et al.*, 1997). Activation of such transcription factors results in the production of various inflammatory mediators, cytokines and/or chemokines necessary for various additional cellular functions and maintenance of homeostasis.

PI3K/Akt/mTORC1 signalling regulates growth factor-dependent proliferation by controlling cell growth and key mechanisms leading to microglial activation. PI3K

inhibition by LY294002 was reported to contribute to brain damage in a mouse model of sepsis by abolishing the ghrelin-induced decrease in TNFα and IL-1β production (Sun *et al.*, 2016). Treatment of cells with LY294002 enhanced the production of IL-1β and inhibited IL-1Ra transcription in LPS-activated monocytes (Molnarfi *et al.*, 2007). More specifically, the expression of the delta isoform of the catalytic subunit p110 - PI3Kδ - accounts for most of the PI3K-dependent signalling involved in the production of IL-1β, IL-6, TNF and IL-1Ra in activated monocytes (Molnarfi *et al.*, 2008). PI3K was also shown to be essential for LPS-induced NADPH oxidase (PHOX) activation, a key enzyme for the production of superoxide, in primary microglial cultures since the PI3K inhibitor, wortmannin, blocked LPS-induced superoxide production (Hu *et al.*, 2012). IL-1a and TNFα production seems to be dependent on PI3K signalling and inhibition of the CSF1R, by proxy, will attenuate PI3K-dependent signalling. Therefore, the direct consequences of inhibition or promotion of this pathway by GW2580, for IL-1β and TNF-α expression in LPS-treated microglia requires further investigation.

In LPS stimulated microglia, JNK signalling is a dominant pathway for cytokine production *in vitro.* The JNK inhibitor, SP600125, prevented LPS-induced TNFα and IL-6 induction, and NO production in BV2 microglia (Lim *et al.*, 2018). While tectorigenin, an isoflavone isolated from various medicinal plants, supressed iNOS, COX-2, TNFα and IL-6 production through JNK signalling in the same cells (Lim *et al.*, 2018). In microglia, the role of the p-38 MAPK pathway is to regulate cellular proliferation, differentiation, development, apoptosis and regulate the expression of various inflammatory genes (Wei and Liu, 2002). Suppression of p-38 MAPK signalling with the specific inhibitor, NJK14047, decreased expression of pro-inflammatory mediators, including TNFα and IL-1β, iNOS and cyclooxygenase 2 (COX2) in LPS-stimulated BV2 microglia (Gee *et al.*, 2018). The inhibition of p-38 MAPK signalling in microglia is not only effective in acute inflammation (Kim *et al.*, 2013), but also markedly mitigated symptoms in chronic neuroinflammatory disease models, including AD (Park *et al.*, 2013).

The transcription factor NFκB is essential for proper cellular functions such as inflammatory gene transcription, cell proliferation and apoptosis for review see (Chen, Castranova and Shi, 2001). Aberrant NFκB activation contributes to the pathogenesis of various autoimmune and inflammation-related diseases such as AD, Multiple Sclerosis (MS) and Inflammatory Bowel Disease (IBD). LPS-induced

TLR4 signalling is capable of activating NF-κB and MAPK pathways through the adaptor molecule MyD88 (Kumar, Kawai and Akira, 2009). NFκB has been shown to regulate pro-inflammatory cytokine such as TNFα and it controls expression of iNOS, thus mediating NO production in macrophages infected with the intracellular bacterial pathogen Listeria monocytogenes (Farlik *et al.*, 2010).

Some of these pro-inflammatory signalling pathways may overlap with proliferation of microglial cells aggravating the CNS microenvironment. Whether CSF1 inhibition impacts on microglial pro-inflammatory and phagocytic functions, independent of effects on proliferation, has not been looked at extensively. Elucidating the relationships between aspects of microglial activation and proliferation signalling would be of significant benefit in understanding microglial activation in a broader sense. It is hypothesized that inhibiting CSF1R with GW2580 may increase the phagocytic function of microglial cells and that treatment of cells with CSF1 or GW2580 may alter microglial responses to LPS.

4.4 Aims and objectives

The aims of this chapter were to investigate the aspects of microglial function, if any, that are affected by CSF1R inhibition using GW2580 in IMG microglia. The specific objectives were to assess whether receptor activation or inhibition:

- affects phagocytosis of latex beads in IMG cells.
- modulates NO and ROS production and microglial cytokine and chemokine secretion in response to acute LPS insult.
- influences cell signalling in response to acute LPS challenge.

4.5 Results

4.5.1 Optimisation of an IMG cell phagocytosis assay

Phagocytosis is an innate immune function of microglia when confronted with foreign particles. To test the phagocytic potential of IMG cells, cells were seeded in 6-well plate at a density of 0.5 x 10^6 cells per well and cultured overnight before exposing them to 1 µm diameter carboxylate-modified polystyrene fluorescent latex beads. Cells were washed and stained with 7-aminoactinomycin D (7-AAD) to distinguish between live and dead cells before quantifying the internalisation of the beads by flow cytometry (BD FACS Canto II). The gating strategy for analysis is demonstrated in Figure 4.5.1.1. The optimal phagocytic conditions were examined by using serum supplemented (10 % FBS) or serum free media; and either adding beads directly to the wells or first opsonising beads by incubating them in 25 % FBS at 37 ˚C for 30 min (Figure 4.5.1.2). Beads were also added to wells at different densities (Stock concentration of 2.5 mg mL^{-1}) and incubated for different periods of time (Figure 4.5.1.3) for optimization purposes. It was evident that microglia internalised one or more fluorescent beads, manifested by multiple smaller clusters of ascending FITC signal. The ideal conditions for 40-50 % phagocytosis in control cells was determined to be non-opsonized beads added to wells at a final concentration of 2.5 µg mL^{-1} and incubated for 2 hrs in serum-free media.

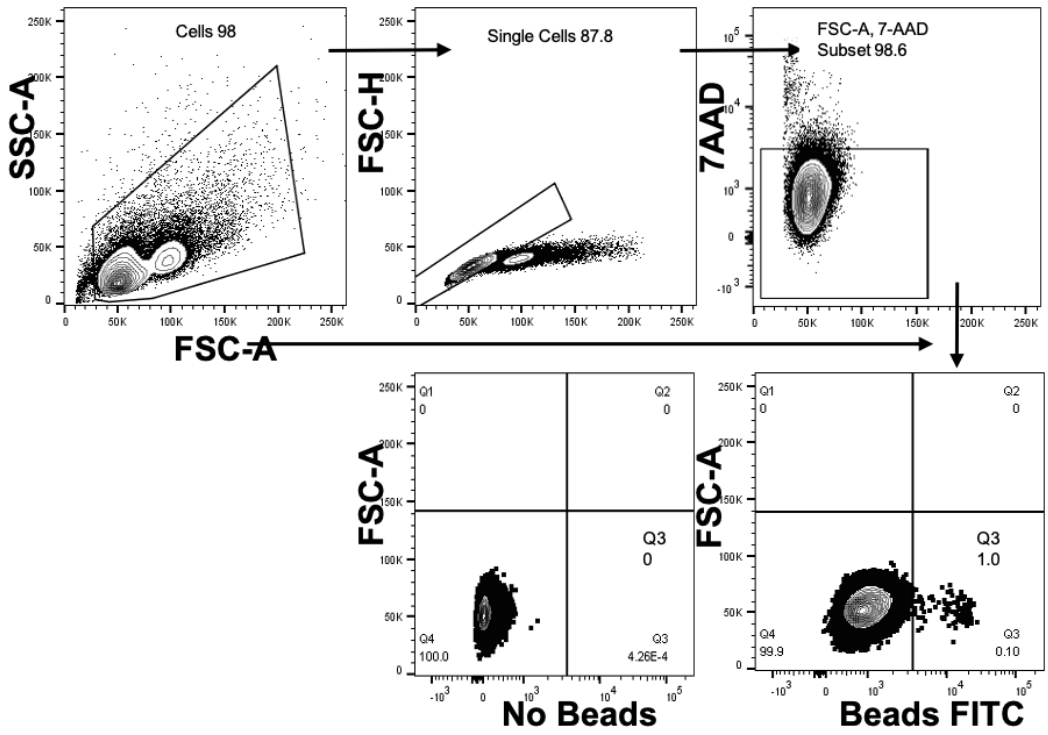

Figure 4.5.1.1: Gating strategy for phagocytosis of latex beads assay in IMG cells. Cells were seeded at a density of 0.5 x 10^6 cells per well in 6-well plates and left to adhere overnight. The following day 1 µm-diameter fluorescent latex beads at a final concentration of 2.5 µg mL^{-1} were added for 60 min. Cells were collected by trypsinisation and stained with 7-AAD to distinguish between live and dead cells. Cells were analysed by flow cytometry (BD FACS Canto II; FlowJo). Single cells were gated excluding debris, doublets, and dead cells. Live cells containing internalised fluorescent beads were then selected, based on high FITC fluorescence for phagocytic analysis. Representative images from one experiment with three replicates per condition.

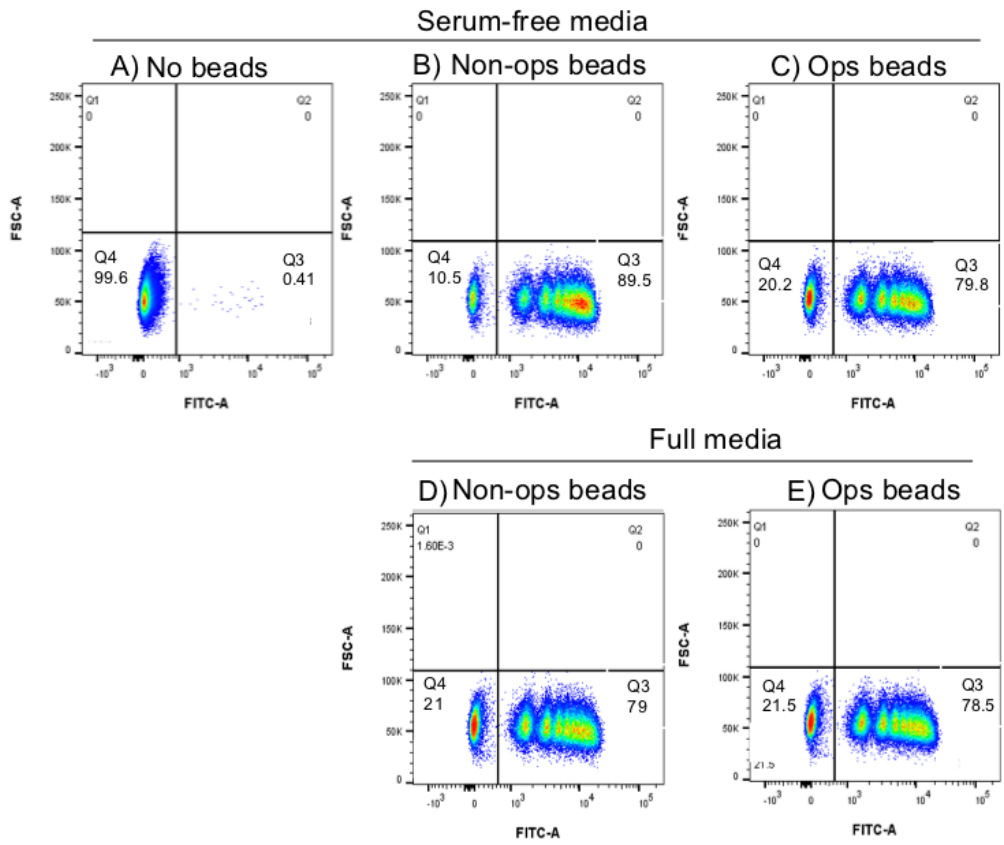

Figure 4.5.1.2: Investigation of the requirement for opsonization of latex beads in phagocytosis assay in IMG cells. Cells were seeded at a density of 0.5 x 10^6 cells per well in 6-well plates and left to adhere overnight. Beads were added either opsonized or directly to wells and incubated for 2 hrs in serum free media (0 % FBS) or in full media with (10 % FBS). Cells were collected and stained with 7-AAD to distinguish between live and dead cells. Cells were analysed by flow cytometry (BD FACS Canto II; FlowJo). Single cells were gated excluding debris, doublets, and dead cells. Live cells containing internalised fluorescent beads were then selected, based on high FITC fluorescence for phagocytic analysis. Representative images from one experiment with three replicates per condition.

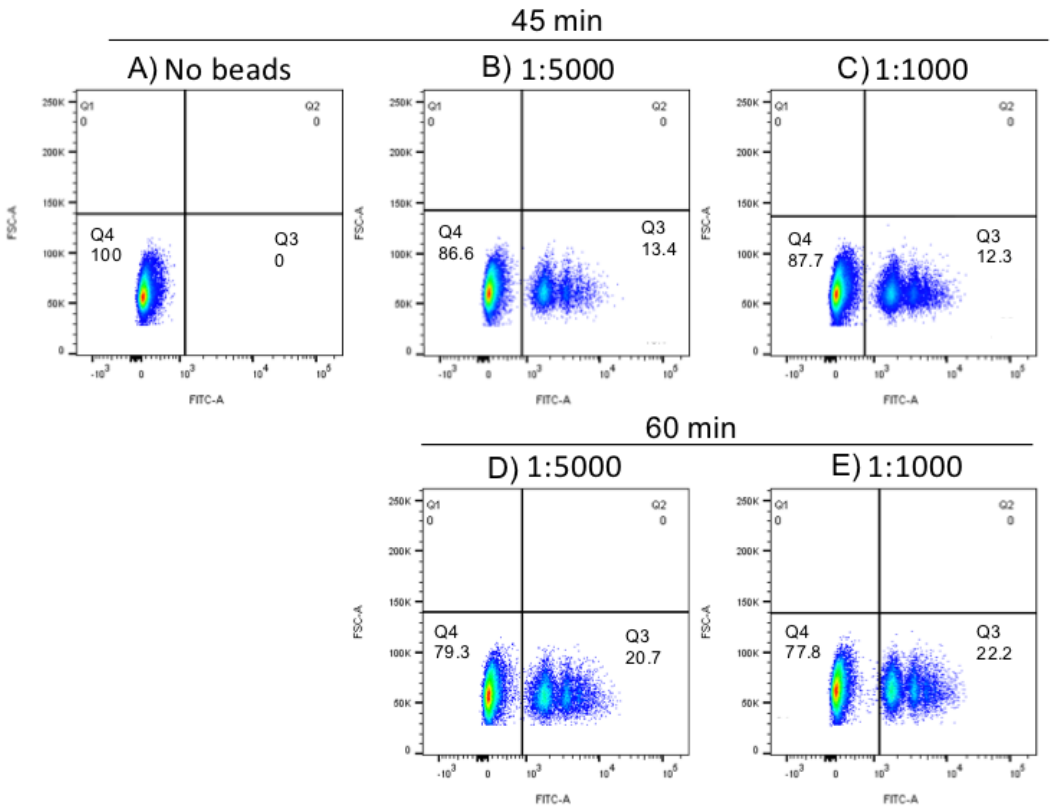

Figure 4.5.1.3: Investigation of the optimal concentration and timing of incubation of latex beads in phagocytosis assay in IMG cells. Cells were seeded at a density of 0.5 x 10^6 cells per well in 6 well plates and left to adhere overnight. Beads were added to a final concentration of either 0.5 µg mL^{-1} (1:5,000) or 2.5 µg mL^{-1} (1:1,000) directly to wells and incubated for 45 or 60 min in serum free media. Cells were collected and stained with 7-AAD to distinguish between live and dead cells. Cells were analysed by flow cytometry (BD FACS Canto II; FlowJo). Single cells were gated excluding debris, doublets, and dead cells. Live cells containing internalised fluorescent beads were then selected, based on high FITC fluorescence for phagocytic analysis. Representative images from one experiment with three replicates per condition.

4.5.2 LAP-independent internalisation of latex beads in IMG cells

IMG cells were seeded on 13 mm coverslips inserted in 6-well plate at a density of 0.5 x 10^6 cells per well and cultured overnight. Cells were incubated with 1 µm-diameter fluorescent latex beads at a final concentration of 2.5 µg mL^{-1} for 2 hrs at 37 °C in serum-free media. Cells were then fixed in methanol before probing for Iba1 to confirm that beads were internalized by Iba1-positive IMG cells (Figure 4.5.2.1; panels A-C). In a separate experiment, IMG cells were prepared as described above and probed for LC3B localisation. Beads internalized by cells were qualitatively analysed for LAP by confocal microscopy to detect co-localization of internalized latex beads with LC3B. However, the internalised beads did not co-localise with LC3B puncta as LC3B staining remained evenly distributed throughout the cell (Figure 4.5.2.1; panel D-F).

Thereafter, to visualise whether the structure engulfing the beads is composed of a single membrane or double membrane, cells were again prepared and exposed to fluorescent latex beads and following incubation for 2 hrs, cells were washed, collected by trypsinization, and pelleted prior to processing for Transmission Electron Microscopy (TEM). The membrane surrounding the internalized beads was found to be a single- membraned structure, visible as a single dark line (Figure 4.5.2.1; panels G-I). Images were compared to previous studies (Eskelinen and Kovács, 2011) to validate the structural differences between single and double-membrane architecture under TEM has been shown in Figure 4.5.2.1; panels J-M. Internalised beads were contained within a single-membraned classical phagosome, as opposed to within either (1) LC3B-positive double-membraned autophagosomes, or (2) LC3B-positive single-membraned phagosomes. These observations ruled out the contribution of LAP, at least under these experimental conditions.

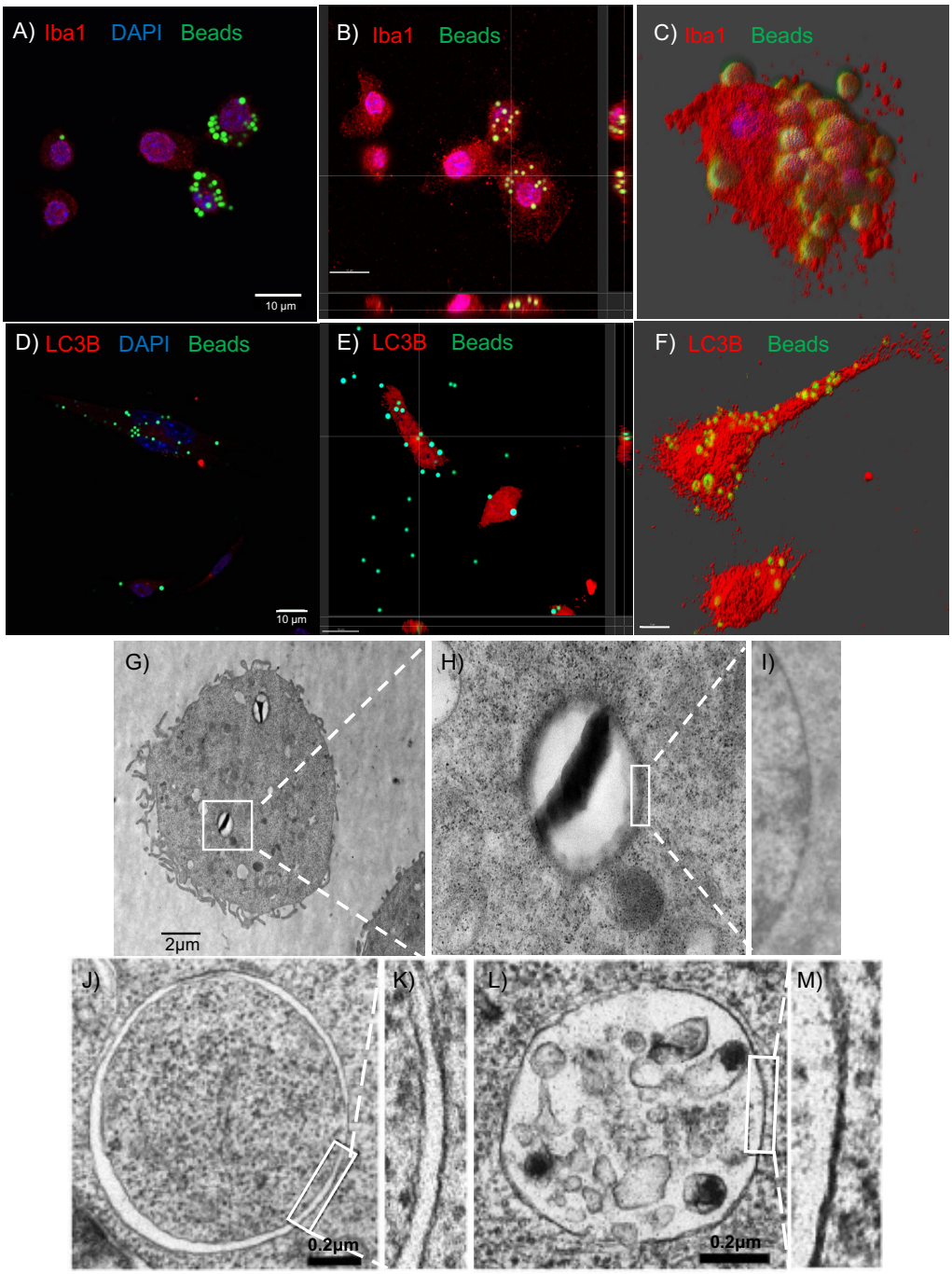

Figure 4.5.2.1: LAP-independent internalisation of latex beads in IMG cells. Cells were seeded at a density of 0.5 x 10^6 cells per well on 10 mm coverslips in 6-well plates and left to adhere overnight. Fluorescent beads (green, 488 nm) were added directly to wells in serum free media for 2 hrs. Cells were then fixed in methanol before labelling for Iba1 (red, 594 nm, panels A-C) or LC3B (red, 594 nm, panels D-F) and imaged by confocal microscopy. (A and D) internalization of latex beads, (B and E) cross-section of cells with internalized beads, and (C and F) 3D construction from multiple Z-stack images of cells with internalized beads. The nuclei of the cell were stained with DAPI (blue). (G-I) TEM of internalised beads at increasing magnification to identify phagosomal membrane characteristics. (J-M) double and single-membraned structure under TEM for comparison, taken from (Eskelinen and Kovács, 2011). Representative images from three independent experiments.

4.5.3 The effect of modulating autophagy on internalization of latex beads

Since LC3B was not directly associated with internalised latex beads, whether promoting autophagy had any impact on bead internalisation was also examined. IMG cells were seeded as before, but this time, the media was replaced with EBSS to stimulate autophagy, but also in the presence or absence of Bafilomycin A1 (BafA1) for 4 hr to inhibit autophagy. Cells were collected, lysed, and probed for autophagy markers to be analysed by western immunoblotting to demonstrate that autophagy was activated and/or inhibited (Figure 4.5.3.1, panel A). In parallel, cells were prepared as described and were incubated with latex bead following the treatments. Cells were then collected and stained with 7-AAD before analysis by flow cytometry.

Western immunoblot analysis showed that after 4 h of EBSS treatment autophagy was induced in IMG cells. This was manifested by LC3B-I disappearance with EBSS alone, and accumulation of LC3B-II and p62 in the presence of BafA1 (Figure 4.5.3.1; A). Stimulation of autophagy with EBSS ($F_{1,8} = 111.8$; $p < 0.0001$) and subsequent inhibition with BafA1 ($F_{1,8} = 215.0$; $p < 0.0001$) significantly affected latex bead uptake (Figure 4.5.3.1; B-C). A significant interaction between the two factors, EBSS and BafA1 ($F_{1,8} = 21.02$; $p = 0.0018$) was also observed. Induction of autophagy by EBSS resulted in a statistically significant increase in latex bead uptake of 15-20 %, compared to control ($p = 0.0171$ by Bonferroni post hoc analysis). BafA1-mediated depolarization of lysosome membrane potential decreased bead uptake by more than 50 %, compared to control ($p < 0.0001$ by Bonferroni post hoc analysis). Inhibition of EBSS-stimulated autophagy with BafA1 significantly decreased internalization of latex beads by 30 %, compared to EBSS alone ($p = 0.0006$ by Bonferroni post hoc analysis). These data show that a functional lysosome is essential for bead uptake and that induction of autophagy further increased uptake of foreign particles.

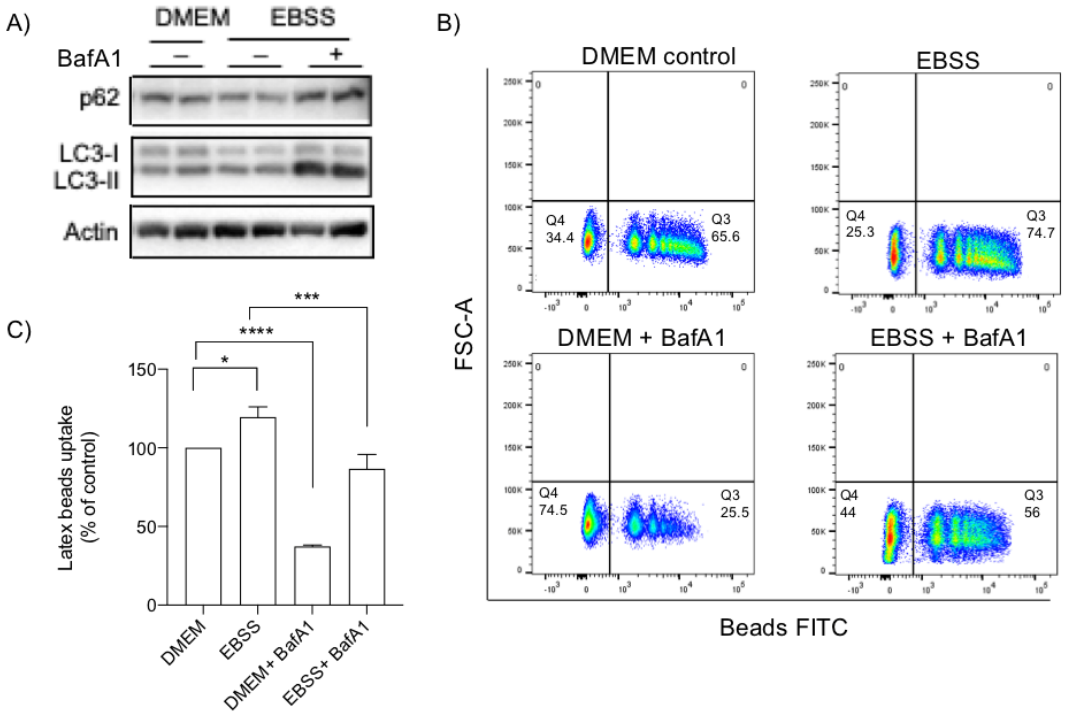

Figure 4.5.3.1: The effect of induction and/or inhibition of autophagy on internalization of latex beads. Cells were seeded at a density of 0.5 x 10^6 cells per well in 6-well plates and left to adhere overnight. Following treatment with EBSS for 4hrs with and without 100 ng mL^{-1} BafA1, fluorescent beads, at a final concentration of 2.5 µg mL^{-1}, were added directly to wells for 2 hrs in serum free media. Cells were collected and stained with 7-AAD to distinguish between live and dead cells. (A) Western immunoblot analysis showed EBSS-induced autophagy induction is blocked by BafA1. (B) EBSS- and BafA1- induced autophagy stimulation or inhibition, respectively, altered latex bead uptake. Single cells were gated excluding debris, doublets, and dead cells. Live cells containing internalised fluorescent beads were then selected, based on high FITC fluorescence for phagocytic analysis (BD FACS Canto II; FlowJo). (C) Densitometric analysis of uptake of beads from panel B. All data are plotted as mean ± SEM of three independent experiments and analysed by two-way ANOVA. Significant differences are denoted by *$p < 0.05$, ***$p < 0.001$ and ***$p < 0.0001$ by Bonferroni post hoc analysis.

4.5.4 Effect of CSF1R stimulation and inhibition with GW2580 on latex bead uptake

In the previous chapter, CSF1 stimulated mTORC1 signalling, although mTORC1 signalling was uncoupled from autophagy regulation. Whether inhibiting CSF1R with GW2580 influenced latex bead uptake was examined next. IMG cells were seeded in 6-well dishes as before. The following day cells were pre-treated with GW2580 for 1 hr before incubation with or without CSF1 in the presence or absence of GW2580 for a further 24 hrs (Figure 4.5.4.1). Cells were incubated with latex beads following the treatments before collecting and staining with 7-AAD and analysing by flow cytometry.

CSF1 and GW2580 affected the uptake of latex beads. There was a significant main effect of CSF1 ($F_{1,8} = 8.113$; $p = 0.0251$) and a significant interaction between CSF1 and GW2580 ($F_{1,8} = 11.20$; $p = 0.0101$). Stimulation of cells with CSF1 reduced phagocytic activity by almost 10 % compared to control ($p = 0.0141$ by Bonferroni post hoc analysis). Pre-treatment of cells with GW2580 prevented the CSF1-dependent decrease in phagocytosis in IMG cells ($p = 0.0267$ by Bonferroni post hoc analysis).

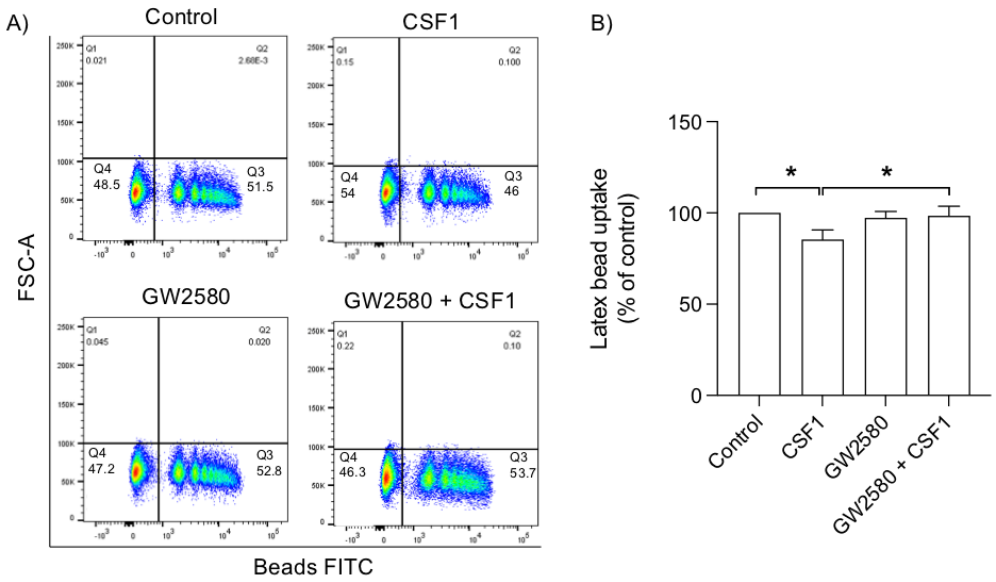

Figure 4.5.4.1: The effect of CSF1 and/or GW2580 on internalisation of latex beads. Cells were seeded at a density of 0.5 x 10^6 cells per well in 6-well plates and left to adhere overnight. Following pre-treatment with 1 μM GW2580 for 1 hr and treatment with CSF1 for 24 hrs, fluorescent bead at a final concentration of 2.5 μg mL^{-1} were added directly to wells for 2 hrs in serum free media. Cells were collected and stained with 7-AAD to distinguish between live and dead cells. (A) Cells were analysed by flow cytometry (BD FACS Canto II; FlowJo). Single cells were gated excluding debris, doublets, and dead cells. Live cells containing internalised fluorescent bead were then selected, based on high FITC fluorescence for phagocytic analysis. (B) Densitometric analysis of uptake of bead followed by treatments shown. All data are plotted as mean ± SEM of three independent experiments and analysed by two-way ANOVA. Significant differences are denoted by *$p < 0.05$ by Bonferroni post hoc analysis.

4.5.5 Optimisation of LPS dose and timepoint

Neal et al found that LPS and 1-Methyl-4-phenyl-1,2,3,6-tetrahydropyridine (MPTP), a dopaminergic neurotoxicant, both increased CSF1R signalling in animal models of Parkinson's disease (PD) and GW2580 abolished the MPTP-induced neuroinflammation, dopaminergic neurotoxicity and behavioural deficits (Neal *et al.*, 2020). However, the effect of CSF1R inhibition by GW2580 on LPS-induced NO, ROS production and pro-inflammatory cytokine/chemokine secretion has not been explored. Therefore, having established that CSF1, itself, modestly reduced bead uptake and that CSF1R inhibition reversed this, the effect of CSF1R inhibition on the response of acute LPS challenge was examined. To do so, the optimal LPS dose and duration for incubation with IMG cells was determined. IMG cells were seeded at 0.5 x 10^5 cells per well in 96 well plate and left to adhere overnight. The following day cells were incubated with LPS at various concentrations in serum free media for 24 hrs to determine the optimal dose. The media was then collected and analysed for NO by Griess reagent for nitrite determination. Cells were also assessed for ROS production analysis and viability. ROS levels were determined by the conversion of non-fluorescent (2',7'-dichlorofluorescein diacetate) H_2DCFDA, to highly fluorescent 2',7'-dichlorofluorescein (DCF) and the fluorescence emission was read using a plate reader at a 485 nm excitation and 535 nm emission wavelength.

NO production started to increase at 5 ng mL^{-1} of LPS treatment compared to control, reached the optimal level at 100 ng mL^{-1} before plateauing at 200 ng mL^{-1} (Figure 4.5.5.1). ROS production was significantly increased with 100 ng mL^{-1} of LPS treatment compared to control.

To determine the optimal timepoint for LPS incubation, cells were set up as described above and analysed for NO and ROS production. Both NO and ROS production increased significantly after 24 hrs of LPS treatment compared to control before starting to diminish at 48 hrs (Figure 4.5.5.2).

Cell viability was assessed by Alamar blue assay during both LPS dose and time optimisation assays. The viability of the cells remained almost at 100 % throughout all the doses of LPS and almost 95 % cells were alive after 24 hrs of LPS treatment before starting to die at 48 hrs.

Taken together, the optimum dose for LPS treatment of IMG cells was determined to be 100 ng mL^{-1} and the optimum time point for LPS treatment of IMG cells was found to be 24 hrs and this combination of LPS treatment was selected for further experiments.

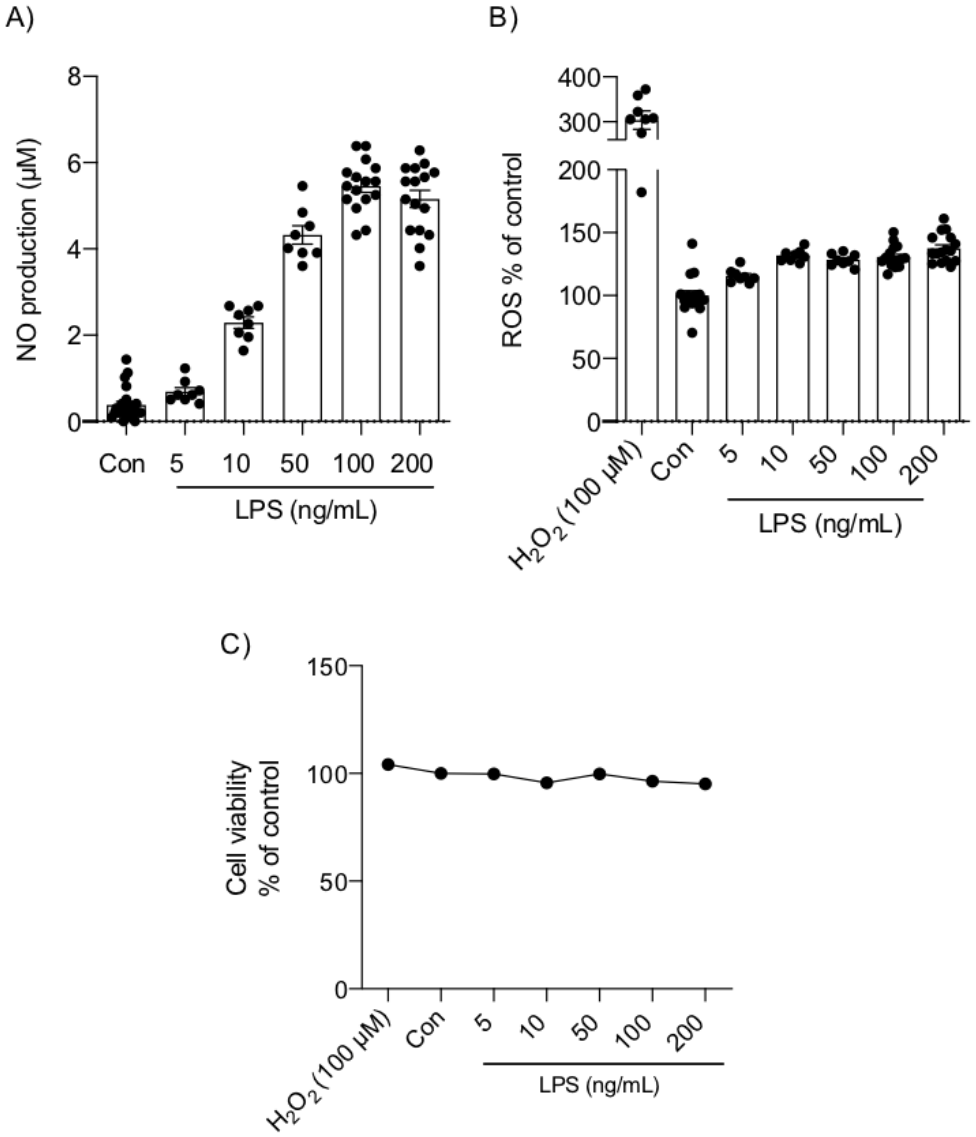

Figure 4.5.5.1: Dose optimisation of assays for LPS-stimulated NO and ROS production in IMG cells. Cells were seeded at 0.5 x 10^5 cells per well in 96-well plates and left to adhere overnight. The following day cells were incubated with LPS at various concentrations in serum free media for 24 h. The media was then collected and analysed for NO by Griess reagents for nitrite determination (A). The cells were used for ROS production analysis by determining the conversion of H_2DCFDA to DCF (B) and viability of cells were determined by Alamar blue assay (C). Results represent mean ± SEM of three independent experiments.

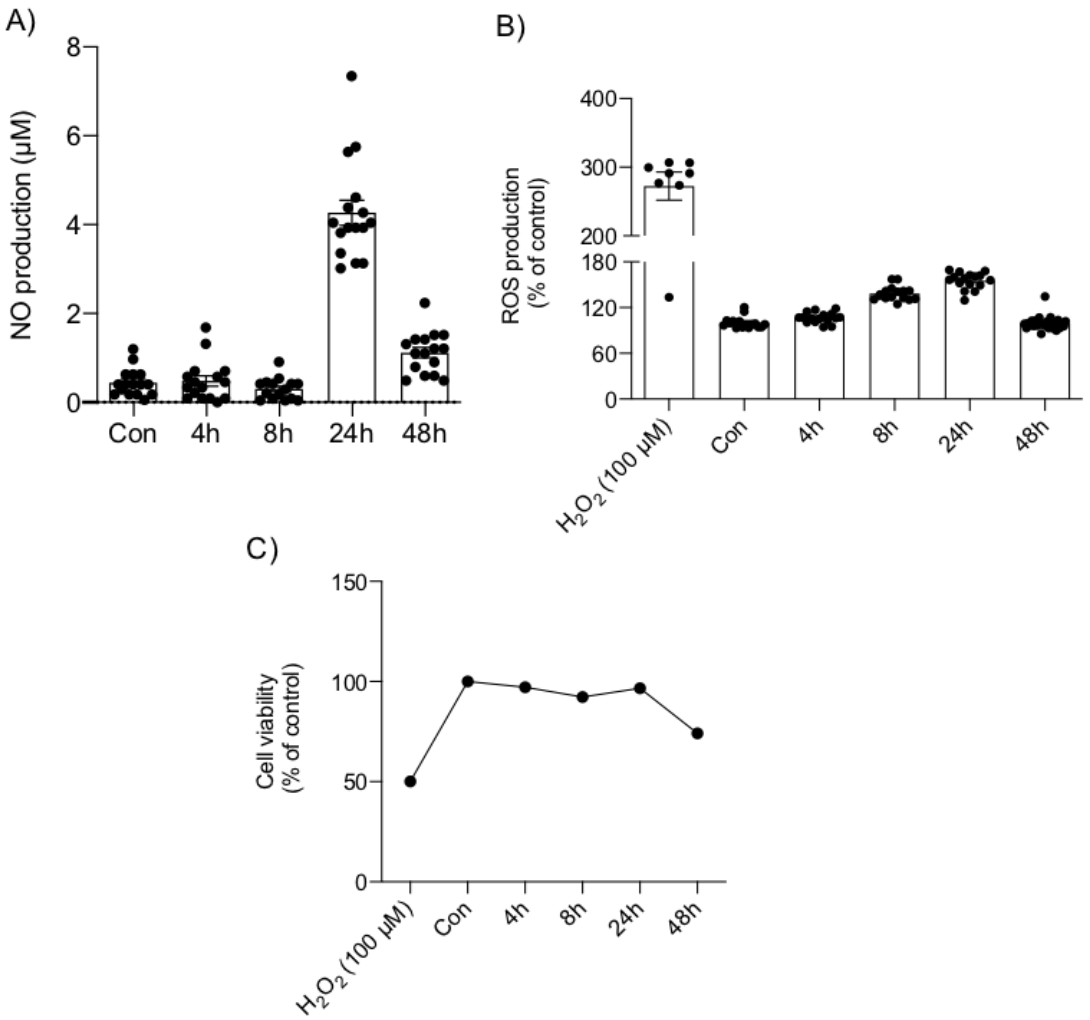

Figure 4.5.5.2 Time optimisation of assays for LPS-stimulated NO and ROS production in IMG cells. Cells were seeded at 0.5 x 10^5 cells per well in 96-well plates and left to adhere overnight. The following day cells were incubated with 100 ng mL^{-1} LPS in serum free media over various timepoints. The media was then collected and analysed for NO by Griess reagents for nitrite determination (A). The cells were used for ROS production analysis by determining the conversion of H_2DCFDA to DCF (B) and viability of cells were determined by Alamar blue assay (C). Results represent mean ± SEM of three independent experiments.

4.5.6 Effect of stimulation or inhibition of CSF1R on LPS-induced NO and ROS production

Following treatment optimisation, the effect of GW2580 on microglial activation with LPS challenge was investigated. IMG cells were cultured and pre-treated with GW2580 for 1 hr. Cells were then incubated with LPS and CSF1 with or without GW2580 for 24 hrs. After this time, the media and cells were collected and analysed for NO and ROS production as before.

Nitric Oxide

LPS treatment showed a significant increase in NO production in IMG cells compared to control as analysed by one-way ANOVA (Figure 4.5.6.1 (A); $F_{7, 64}$ = 319.7, p <0.0001). Given that the response to LPS was as expected and was sufficiently large to mask other effects, the induction by LPS (vs non LPS) was not included in the statistical hypothesis and only the hypothesis that CSF1 or GW2580 would affect LPS-induced NO production was tested by two-way ANOVA. CSF1 was observed to increase LPS-induced NO production by approximately 20 %, while GW2580 was able to reduce LPS-induced NO by >25 %. ANOVA revealed a main effect of CSF1 treatment ($F_{1, 28}$ = 1192, p =0.0018), a main effect of treatment with GW2580 ($F_{1, 28}$ = 59.83, p <0.0001) but no interaction of these 2 factors ($F_{1, 28}$ = 2.947, p =0.0971). In post-hoc, pairwise comparisons, co-treatment of LPS with CSF1 significantly increased NO production compared to LPS control (p =0.0063 by Bonferroni post hoc analysis) while co-treatment of LPS with GW2580, without or with CSF1, significantly reduced this increase in NO levels compared to LPS control (p=0.0013; p =0.0314 respectively) or LPS+CSF1 control (p <0.0001; p <0.0001 respectively, by Bonferroni post hoc analysis). Co-treatment with LPS and GW2580, with or without CSF1, significantly reduced this increase in NO levels compared to the LPS and CSF1 co-treated group. These indicate that CSF1 can facilitate LPS-induced NO production and since GW2580 significantly abolishes this effect in IMG cells, there may even be basal CSF1R effects in this regard.

Once the LPS-treated groups were statistically analysed, the hypothesis that CSF1 or GW2580 may affect basal NO production was tested separately (i.e., in groups not treated with LPS; Figure 4.5.6.1; panel B); Two-way ANOVA analysis revealed a main effect of GW2580 treatment ($F_{1, 36}$ = 1192, p =0.0002). However, there was no main effect of CSF1 treatment ($F_{1, 36}$ = 2.473, p =0.1246) or an interaction

between these 2 factors ($F_{1, 36}$ = 0.1512, p =0.6997). GW2580 alone reduced NO levels compared to control and compared to CSF1 treatment alone (p =0.0088, p =0.0035 respectively, by Bonferroni post hoc analysis). This implies that GW2580 reduces basal NO production, regardless of the presence or absence of exogenous CSF1, again suggesting either some basal CSF1R activity or off-target effects of GW2580.

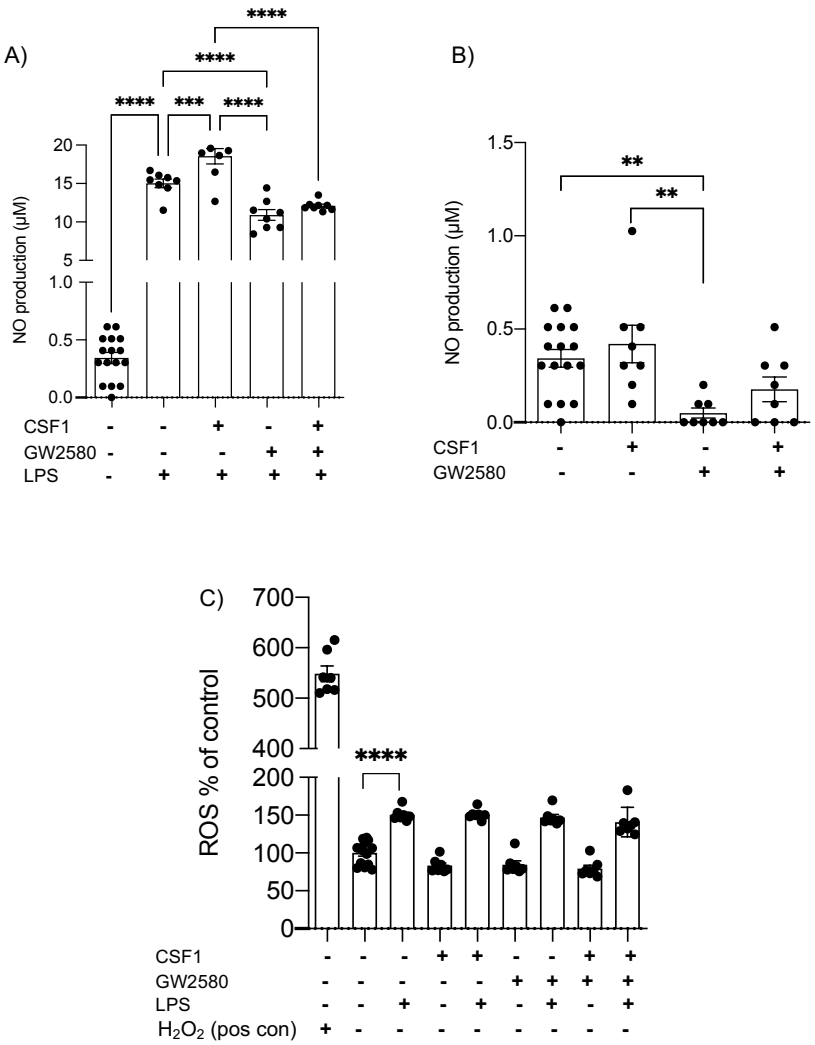

Figure 4.5.6.1: Effect of stimulation or inhibition of the CSF1R on LPS-induced NO and ROS production. IMG cells were seeded at 0.5 x 10^5 cells per well in 96-well plates and left to adhere overnight. The following day cells were pre-treated for 1 hr with or without 1 μM GW2580 before incubating with or without 50 ng mL^{-1} CSF1 or 100 ng mL^{-1} LPS in serum free media for 24 hrs. The media was then collected and analysed for NO. Cells were used for ROS production analysis and viability assay. Results shown are for *n*= 8 technical replicates. The data shown are representative of three independently repeated experiments with similar results. Significant differences are denoted $^{**}p < 0.01$, $^{****}p < 0.0001$ by Bonferroni post hoc analysis.

ROS

LPS treatment showed a significant increase in ROS production in IMG cells compared to control as analysed by one-way ANOVA (Figure 4.5.6.1 (C); $F_{8, 61}$ = 490.8, p <0.0001). As justified earlier, a two-way ANOVA was used to test the hypothesis that CSF1 or GW2580 would affect LPS-induced ROS production in these cells. No significant differences were observed between any groups with LPS challenge. ANOVA revealed no main effect of GW2580 treatment ($F_{1, 24}$ = 1192, p =0.1512), no main effect of CSF1 treatment ($F_{1, 24}$ = 0.4058, p =0.5302) and no interaction ($F_{1, 24}$ = 0.4999, p =0.4863).

After statistically analysing only the LPS-treated groups, the hypothesis that CSF1 or GW2580 might affect basal ROS production (i.e., among groups not treated with LPS) was examined. Although two-way ANOVA analysis showed a main effect of GW2580 treatment ($F_{1, 31}$ =4.285, p =0.0469), a main effect of CSF1 treatment ($F_{1, 31}$ = 5.620, p =0.0242) the reduction, compared to control, was trivial (and showed the same directional change for CSF1 and GW2580). Therefore, it is unlikely that there is any biological effect of CSF1R activation or inhibition on ROS production in this experimental system.

4.5.7 Effect of stimulation or inhibition of the CSF1R on LPS-induced cytokine production

Next, the effect of inhibiting CSF1R on LPS-induced secretion of cytokines in IMG cells was examined. IMG cells were cultured and pre-treated with GW2580 for 1 hr. Cells were then incubated with LPS and CSF1 with or without GW2580 for 24 hrs. Normal growth media was used as a control. After this time, the media was collected and analysed by ELISA for cytokine production. (Figure 4.5.7.1).

TNFα

LPS substantially increased TNFα production compared to control. GW2580, but not CSF1, treatment altered this LPS-induced response. Given that there were three factors of interest, LPS, CSF1 and GW2580, a three-way ANOVA was performed for statistical analysis. The ANOVA indicated a main effect of treatment with LPS and a main effect of treatment with GW2580 in TNFα production ($F_{1, 16}$ = 2195, p <0.0001; $F_{1, 16}$ = 8.391, p = 0.0105, respectively). That is, LPS very markedly

increased the secretion of TNFα, while GW2580, to a much lesser extent, tended to reduce the expression of TNFα in groups to which it was administered. No main effect of CSF1 was observed ($F_{1, 16}$ = 1.515, p = 0.2361) in the three-way ANONA analysis. Three-way ANOVA also indicated a significant interaction effect between LPS x GW2580 ($F_{1, 16}$ = 8.314, p = 0.0108) implying that LPS has a different effect on the production of this cytokine in the presence or absence of GW2580. However post-hoc, pairwise comparison did not indicate a significant difference between LPS and LPS+GW2580 (p = 0.2134 by Bonferroni post hoc analysis), co-treatment of CSF1+GW2580 reduced TNFα production compared to LPS treatment alone (p = 0.0206 by Bonferroni post hoc analysis).

Then, whether CSF1 or GW2580 affected basal TNFα production in the absence of LPS was looked at. Treatment of cells with CSF1 on its own significantly increased TNFα production indicated by the main effect of CSF1 ($F_{1, 20}$ = 24.21, p < 0.0001) but GW2580 on its own did not have an impact on basal production of this cytokine ($F_{1, 20}$ = 0.6774, p = 0.4202). There was a significant interaction between CSF1 x GW2580 ($F_{1, 20}$ = 17.52, p = 0.0005), thus CSF1 has a different effect depending on the presence or absence of its inhibitor GW2580 in non-LPS treated group.

IL-6

LPS increased IL-6 production compared to control and GW2580 modestly reduced this LPS-induction, even in the presence of CSF1. In groups not treated with LPS, neither CSF1 nor GW2580 had any significant effect on IL-6. Three-way ANOVA analysis indicated a main effect of treatment with LPS, and main effect of treatment with GW2580 on IL-6 production ($F_{1, 16}$ = 49880, p <0.0001; $F_{1, 16}$ = 92.48, p <0.0001, respectively) as well as an interaction between LPS x GW2580 ($F_{1, 16}$ = 77.62, p <0.0001). In post-hoc, pairwise comparisons, GW2580 and LPS co-treatment significantly reduced this cytokine production compared to LPS treatment alone (p = 0.0043 by Bonferroni post hoc analysis) and this reduction with respect to LPS alone persisted when cells were co-treated with GW2580, CSF1 and LPS (p < 0.0001 by Bonferroni post hoc analysis).

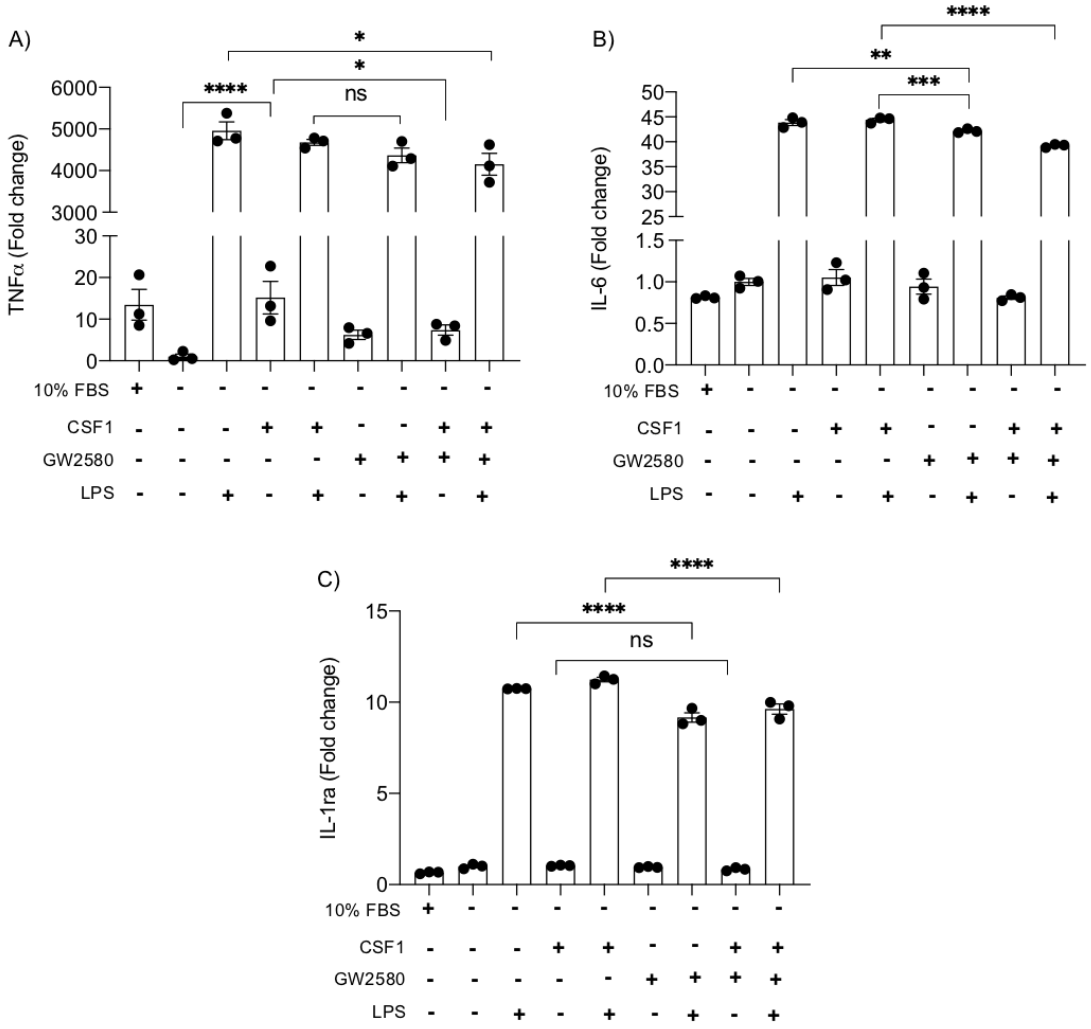

Figure 4.5.7.1: Effect of stimulation or inhibition of the CSF1R on LPS-induced cytokines. IMG cells were seeded at 0.5 x 10^6 cells per well in 6-well plates and left to adhere overnight. The following day cells were pre-treated with or without 1 μM GW2580 for 1 hr before incubating with or without 50 ng mL^{-1} CSF1 or 100 ng mL^{-1} LPS in serum free media for 24 hrs. The media was then collected and analysed for secretion of cytokines indicated by ELISA. Results represent mean ± SEM of three independent experiments, with each dot representing the mean of two technical replicates from each experiment. Significant differences are denoted by $^{**}p < 0.01$, $^{***}p < 0.001$ and $^{****}p < 0.0001$ by Bonferroni post hoc analysis.

IL-1ra

LPS increased IL-1ra production compared to control and GW2580 showed a very modest ability to reduce this effect regardless of the presence or absence of CSF1 in LPS treated group. No significant differences between treatments were noticed in the non-LPS treated groups. Three-way ANOVA analysis indicated a main effect of treatment with LPS and a main effect of treatment with GW2580 on IL-1ra production ($F_{1, 16}$ = 7940, p <0.0001; $F_{1, 16}$ = 68.38 and p <0.0001 respectively). That indicates that LPS markedly increased the secretion of IL-1ra, while GW2580, to a much lesser extent, tended to decrease the expression of IL-1ra in groups to which it was administered.

4.5.8 Effect of stimulation or inhibition of the CSF1R on LPS-induced chemokine production

Next, the effect of inhibiting CSF1R on the secretion of LPS-induced chemokine production was investigated. IMG cells were prepared as before with media collected and analysed by ELISA for chemokine expression levels. Given that there were three factors of interest, a three-way ANOVA was performed for statistical analysis, similarly to the cytokines above (Figure 4.5.8.1).

Chemokine ligand 2 (CCL2; also known as monocyte chemoattractant protein-1, (MCP-1))

CCL2 production was increased with LPS treatment compared to control. GW2580 very markedly reduced the CCL2 response to LPS while CSF1 had no significant effect. GW2580 also reduced LPS-induced CCL2 whether alone or in the presence of CSF1. Three-way ANOVA analysis indicated a main effect of treatment with LPS and a main effect of treatment with GW2580 in CCL2 production ($F_{1, 16}$ = 68.97, p <0.0001; $F_{1, 16}$ = 44.46, p <0.0001, respectively). There was a significant interaction effect between LPS x GW2580 ($F_{1, 16}$ = 33.58, p <0.0001) indicating that GW2580 reduces CCL2 expression selectively in the LPS-treated group. In post-hoc, pairwise comparisons, GW2580 co-treatment decreased LPS-induced CCL2 expression compared to LPS alone whether in the absence (p < 0.0001 by Bonferroni post hoc analysis) or presence of CSF1 (p = 0.003 by Bonferroni post hoc analysis). No significant effects between treatments were noticed in the non-LPS treated groups.

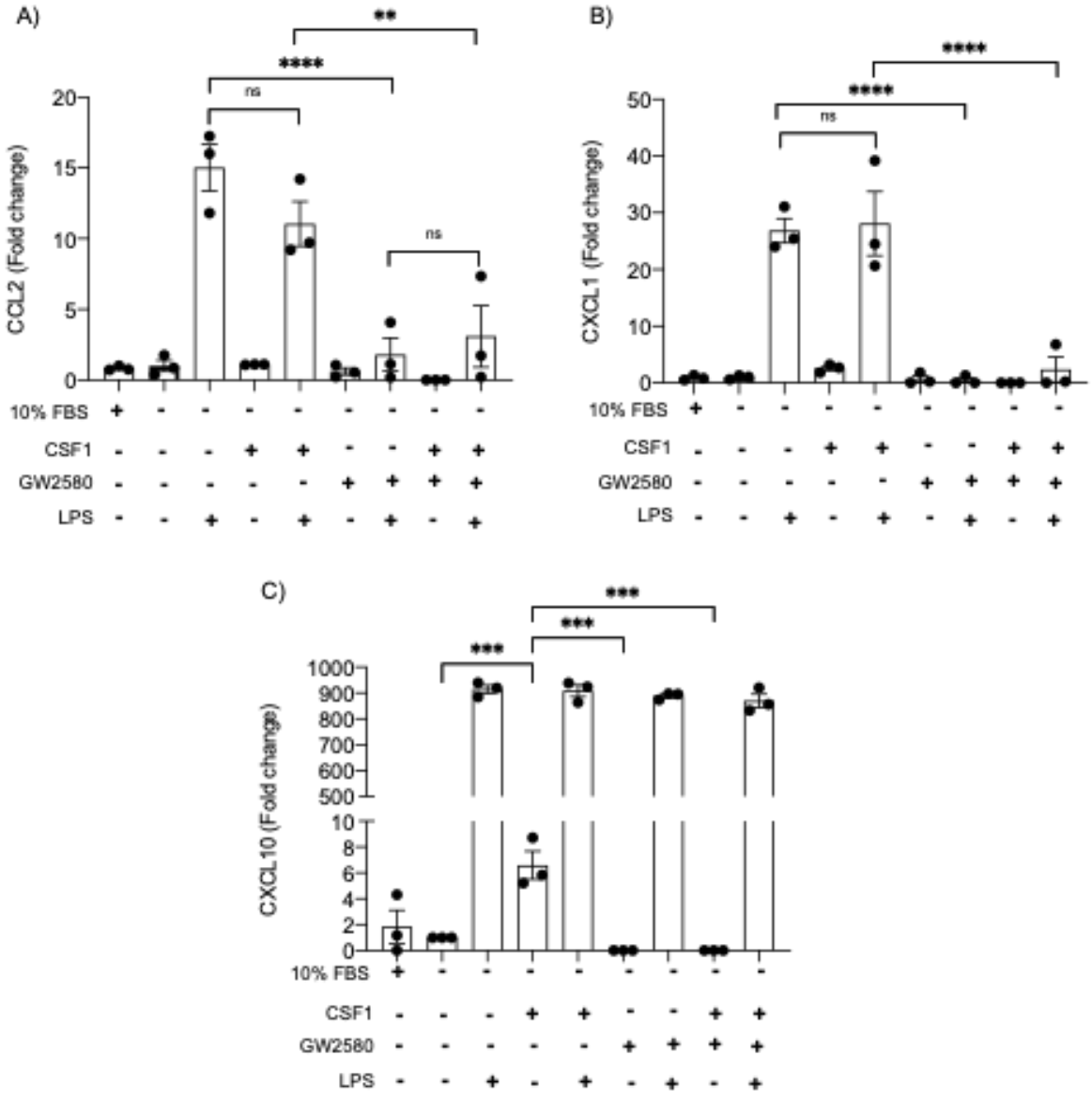

Figure 4.5.8.1: Effect of stimulation or inhibition of the CSF1R on LPS-induced chemokines. IMG cells were seeded at 0.5 x 106 cells per well in 6 well plates and left to adhere overnight. The following day cells were pre-treated with or without 1 μM GW2580 for 1 hr before incubating with or without 50 ng mL-1 CSF1 or 100 ng mL-1 LPS in serum free media for 24 hrs. The media was then collected and analysed for secretion of chemokines indicated by ELISA results represent mean ± SEM of three independent experiments, with each dot representing the mean of the two technical replicates from each individual experiment. Significant differences are denoted by **p < 0.01, ***p < 0.001 ****p < 0.0001 by Bonferroni post hoc analysis.

Chemokine (C-X-C motif) ligand 1 (CXCL1)

A very similar pattern was observed for CXCL1. LPS increased CXCL1 production compared to control and GW2580 treatment significantly reduced this LPS-induced response, illustrated by a main effect of treatment with LPS ($F_{1,16}$ = 67.85, p <0.0001), a main effect of treatment with GW2580 ($F_{1,16}$ = 71.89, p <0.0001) and a significant interaction effect between LPS x GW2580 ($F_{1,16}$ = 57.57, p <0.0001). CSF1 had no significant main effect ($F_{1,16}$ = 0.3910, p = 0.5406) and nor were there any significant interactions between CSF1 and LPS, GW2580 or LPS x GW2580. Thus, GW2580 co-treatment decreased LPS-induced CXCL1 expression (p < 0.0001 compared to LPS control by Bonferroni post hoc analysis) and this reduction persisted whether CSF1 was present (p < 0.0001 by Bonferroni post hoc analysis) or not.

Chemokine (C-X-C motif) ligand 10 (CXCL10, also known as interferon-γ–inducible α-chemokine/inducing protein–10 (IP10))

This strong inhibition of chemokine induction was not observed when examining CXCL10. LPS treatment showed a significant increase in CXCL10 production in IMG cells compared to control but GW2580 had limited ability to reduce this CXCL10 response. Three-way ANOVA analysis showed only a main effect of LPS (Figure 4.5.8.1 (C); $F_{7, 64}$ = 319.7, p <0.0001). Even when only LPS-treated groups were analysed, no significant effects of CSF1, or GW2580 treatment, nor any interaction between them were found ($F_{1,8}$ = 0.4094, p =0.5402; $F_{1,8}$ = 2.750, p =0.1359; $F_{1,8}$ = 1189, p =0.7391, respectively).

Testing the hypothesis that CSF1 or GW2580 might alter basal CXCL10 production among groups not treated with LPS, two-way ANOVA analysis showed that CSF1 treatment, on its own, significantly increased CXCL10 production compared to control (p=0.0005 by Bonferroni post hoc analysis after significant main effect of CSF1; $F_{1,8}$ = 26.75, p =0.0009). GW2580 completely blocked this effect despite having no impact on its own: there was an interaction between the GW2580 and CSF1 ($F_{1, 8}$ = 26.75, p =0.0009). Thus, CSF1 modestly induces CXCL10 at baseline (p=0.0002 by Bonferroni post hoc analysis) and treatment of cells with GW2580 reduces this induction (p=0.0002).

4.5.9 Effect of stimulation or inhibition of the CSF1R on LPS-induced MAPK signalling

Cellular stressors such as heat shock, UV irradiation, pro-inflammatory cytokines such as IL-1 and TNFα and LPS are known to activate the MAPK pathway (Wei and Liu, 2002). Therefore, the effect of activating or inhibiting the CSF1R following LPS challenge on this pathway was investigated. IMG cells were cultured before being treated with LPS in serum free media for 24 hrs. After this time, cells were pre-treated with GW2580 for 1h before incubating with CSF1 for 10 min. This timepoint was chosen for signalling experiments because previously 10 min was shown to have the maximal CSF1-induced mTORC1 activation, indicated by phosphorylation of S6K1 at Thr389, in IMG cells. Cells were then collected, lysed, and resolved by 10 % SDS-PAGE gel and Western immunoblotting. Membranes were probed for total and phosphorylated Erk1/2 at Thr202/Tyr204, total and phosphorylated JNK at Thr183/Tyr185 and total and phosphorylated p38 MAPK at Thr180/Tyr182. Given that there were three factors of interest, three-way ANOVA was performed for statistical analysis of densitometry data (Figure 4.5.9.1).

Erk1/2

Phosphorylation of Erk1/2 was not significantly affected 10 mins post-LPS treatment (unpaired t test between control and LPS treated group: $p = 0.0931$). In three-way ANOVA, neither LPS, CSF1 nor GW2580 had any effect on Erk1/2 phosphorylation at the sites examined.

p38 MAPK

Likewise, p38 MAPK was also not affected by LPS treatment (unpaired t-test between control and LPS treated group: $p = 0.4840$). Statistical analysis by three-way ANOVA showed that neither LPS, CSF1 nor GW2580 had any effect on p38 MAPK activation.

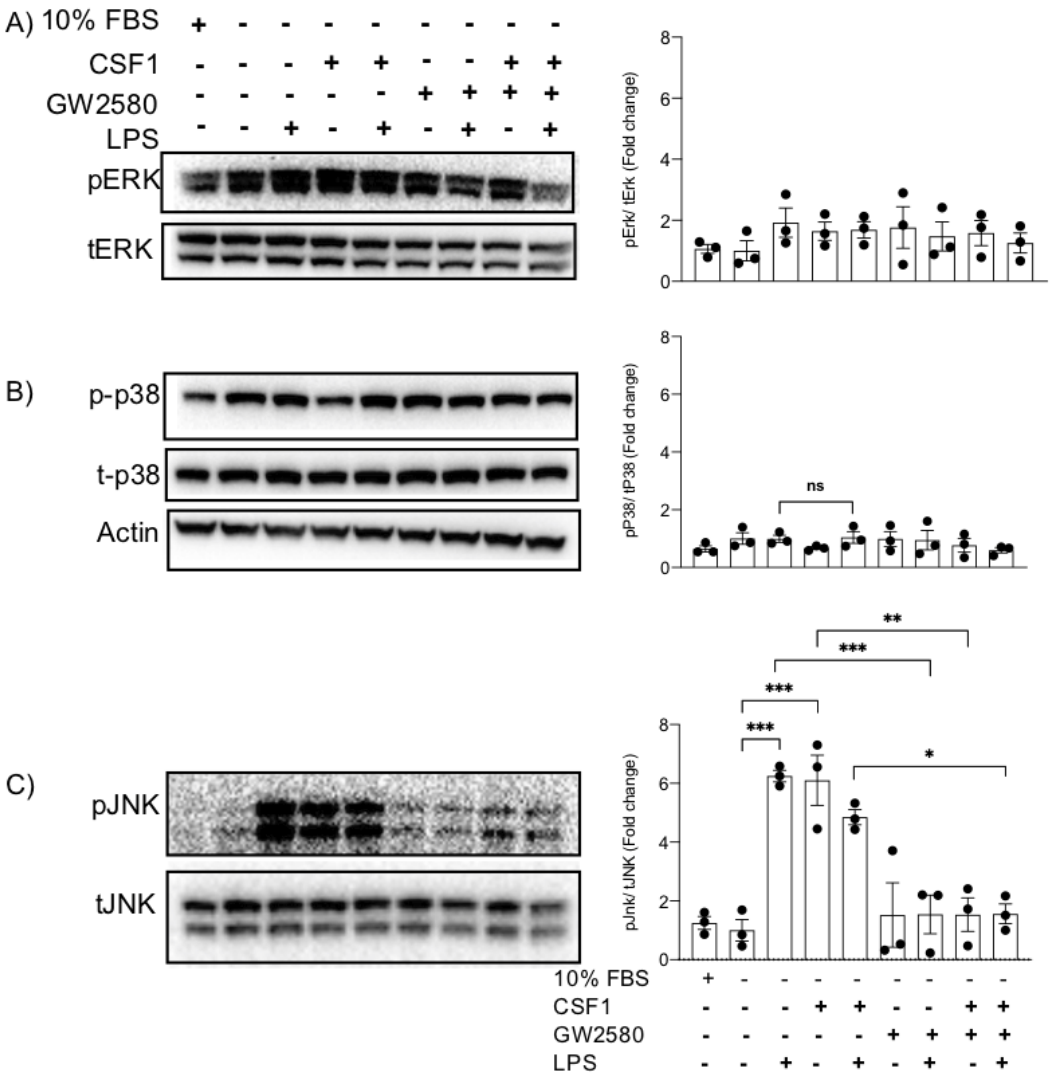

Figure 4.5.9.1: Effect of stimulation or inhibition of the CSF1R on LPS-induced MAPK activation. IMG cells were seeded and grown to 75 % confluency in 10 cm dishes. The following day cells were treated with 100 ng mL^{-1} LPS in serum free media for 24 hrs. After this time, cells were pre-treated with 1 μM GW2580 for 1 hr before incubating with 50 ng mL^{-1} CSF1 for 10 min. Cell lysates were collected and analysed by western immunoblot to detect the expression of phosphorylated and total protein and quantification of Erk1/2 (A), p38 (B) and JNK (C). Actin was used as loading control. Results represent mean ± SEM of three independent experiments. Significant differences are denoted by *p < 0.05, **p < 0.01, ***p < 0.001 by Bonferroni post hoc analysis.

JNK

LPS, CSF1 and GW2580 all altered JNK signalling. LPS and CSF1 were both sufficient to increase JNK phosphorylation compared to control and GW2580 markedly reduced these LPS- and CSF1-induced responses. Statistical analysis by three-way ANOVA analysis indicated a main effect of LPS, a main effect of GW2580 and a main effect CSF1 on JNK phosphorylation ($F_{1,16}$ = 5.300, p=0.0351; $F_{1,16}$ = 47.49, p <0.0001, $F_{1,16}$ = 4.676, p=0.0461 respectively). A significant interaction between LPS and GW2580 ($F_{1, 16}$ = 4.924, p = 0.0413), showed that LPS affected the cells differently in the presence of GW2580. A similar significant interaction showed that CSF1 also affected the cells differently (i.e., less) in the presence of GW2580 ($F_{1,16}$ = 13.94, 0.0018). There was also an interaction of all three factors (LPS x GW2580 x CSF1: $F_{1,16}$ =13.22, p = 0.0022), indicating that the impacts of any of these molecules is highly contingent on the presence of the others. In pairwise comparisons, GW2580 significantly reduced JNK phosphorylation induced by LPS + CSF1 (p=0.0208) and by LPS (p=0.0008). Thus, both LPS and CSF1 induce phosphorylation of JNK and GW2580 was sufficient to block this effect in both cases.

4.5.10 Effect of stimulation or inhibition of the CSF1R on PI3K/Akt/mTORC1 signalling in LPS-treated cells

In chapter 3 it was shown that CSF1 induces PI3K/Akt/mTORC1 signalling in IMG cells under normal conditions. Here, the effect of stimulating or inhibiting the CSF1R in conjunction with LPS treatment was investigated. Cells were prepared and treated as before and membranes were probed for total Akt and Akt phosphorylated at Ser473, and total S6K1 and S6K1 phosphorylated at Thr389. Actin was used as loading control. Three-way ANOVA was performed for statistical analysis as before (Figure 4.5.10.1).

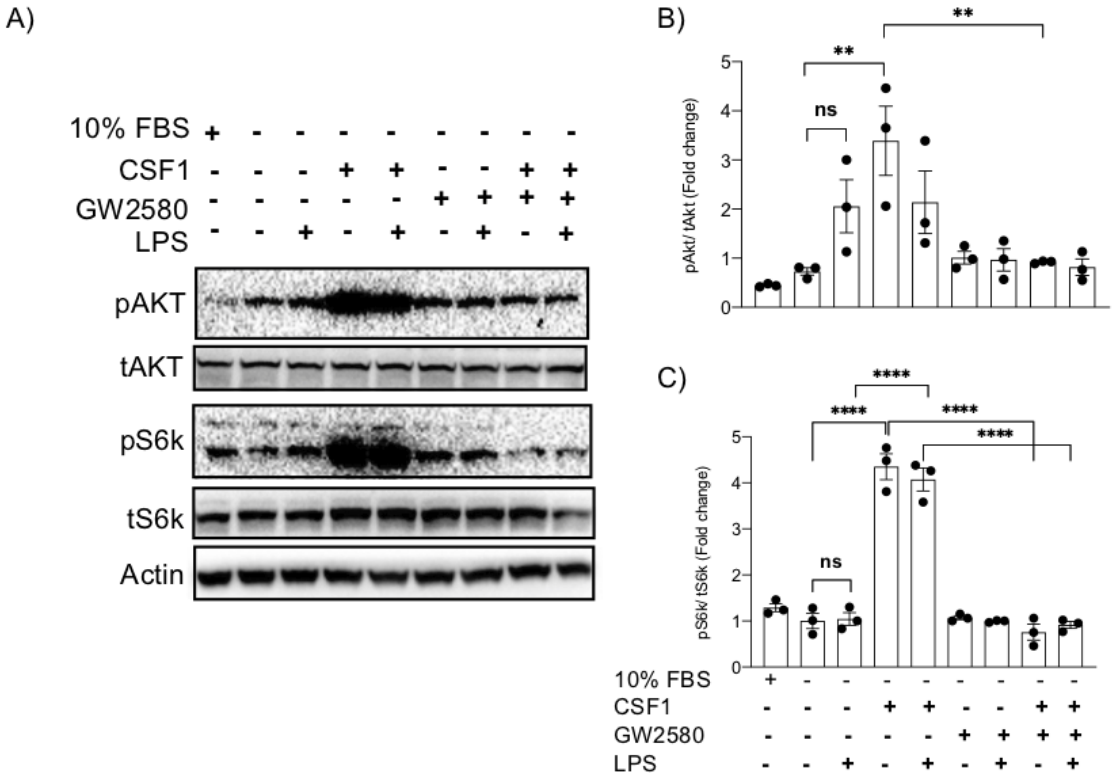

Figure 4.5.10.1: Effect of stimulation or inhibition of the CSF1R on LPS-induced PI3K/Akt/mTOR pathway activation. IMG cells were seeded and grown to 75 % confluency in 10 cm dishes. The following day cells were treated with 100 ng mL^{-1} LPS in serum free media for 24 hrs. After this time, cells were pre-treated with 1 μM GW2580 for 1 hr before incubating with 50 ng mL^{-1} CSF1 for 10 min. Cell lysates were collected and analysed by western immunoblot to detect phosphorylation of Akt, S6K1, and total proteins of Akt and S6K1. Actin was used as loading control (A). pAkt quantified using densitometric analysis and normalised to tAkt (B). pS6K1 quantified using densitometric analysis and normalised to tS6K1 (C). Results represent mean ± SEM of three independent experiments. Significant differences are denoted by $^{**}p < 0.01$, $^{****}p < 0.0001$ by Bonferroni post hoc analysis.

Akt

CSF1 increased Akt phosphorylation compared to control and GW2580 treatment inhibited this phosphorylation as expected but LPS showed only a modest, but non-significant, trend of increasing phosphorylation of Akt at Ser473. Three-way ANOVA analysis indicated a main effect of GW2580 and a main effect of CSF1 but no significant effect of LPS on Akt phosphorylation ($F_{1, 16}$ = 16.36, p = 0.0009; $F_{1, 16}$ = 4.838, p = 0.0429, $F_{1, 16}$ = 0.003783, p = 0.9517, respectively). There was also a significant interaction between GW2580 and CSF1 ($F_{1, 16}$ = 6.871, p = 0.0185) indicating that CSF1 has a different effect on pAkt depending on the presence or absence of GW2580. Pairwise comparisons confirmed that CSF1 significantly increased the phosphorylation of Akt compared to control (p = 0.0030 by Bonferroni post hoc analysis) and that GW2580 returned this CSF1-induced Akt phosphorylation to baseline levels (p = 0.0061 by Bonferroni post hoc analysis).

S6K1

Similarly, to the outcome observed with Akt, CSF1 increased S6K1 phosphorylation compared to control and GW2580 treatment inhibited this phosphorylation. Three-way ANOVA analysis indicated a main effect of treatment with GW2580, a main effect of treatment with CSF1 on S6K1 phosphorylation ($F_{1, 16}$ = 201.5, p < 0.0001; $F_{1, 16}$ = 159.3, p < 0.0001 respectively) and a significant interaction effect between GW2580 x CSF1 ($F_{1, 16}$ = 203.9, p < 0.0001). This indicates that CSF1 increases S6K1 phosphorylation and that this effect is blocked by GW2580. This is borne out by Bonferroni post hoc analysis showing that GW2580 decreased this CSF1-induced S6K1 phosphorylation (p < 0.0001). LPS did not have any effect on S6K1 phosphorylation ($F_{1, 16}$ = 0.1045, p = 0.7507) and treatment with LPS, CSF1 and GW2580 also left S6K1 phosphorylation equivalent to baseline levels (and reduced with respect to the CSF1 and CSF1 + LPS groups; p < 0.0001 by Bonferroni post hoc analysis). Thus, CSF1 robustly increases S6K1 phosphorylation in a CSF1R-dependent fashion, but LPS does not impact on these effects.

4.5.11 Effect of stimulation or inhibition of the CSF1R on LPS-induced NFκB activation

Finally, the NFκB pathway was investigated. Cells were prepared as before, and membranes were probed for IκB with actin was used as loading control. Degradation

of IκB is a metric of NFκB activation because IκB is the inhibitor of NFκB (Nasuhara *et al.*, 1999). NFκB resides in the cytoplasm in an inactivate complex of p65 and p50 bound to IκB. Receptor activation leads to phosphorylation of IκB, triggered by IκB kinase (IKK). This results in IκB ubiquitination and degradation and translocation of p65 and p50 to the nucleus for gene transcription. Effects of LPS, CSF1 and GW2580 were very limited 10 min after treatment. Three-way ANOVA was performed for overall statistical analysis, but no statistical differences were observed among groups. However, an unpaired t test was performed to demonstrate that some effect of LPS on NFκB activation could at least be detected with a statistically significant difference between control and LPS treated groups (p =0.0461), (Figure 4.5.11.1). Thus, at least at 24 hrs post-LPS treatment, 10 min post-CSF1 or 1 hr post-GW2580, there were no significant effects on NFκB activation.

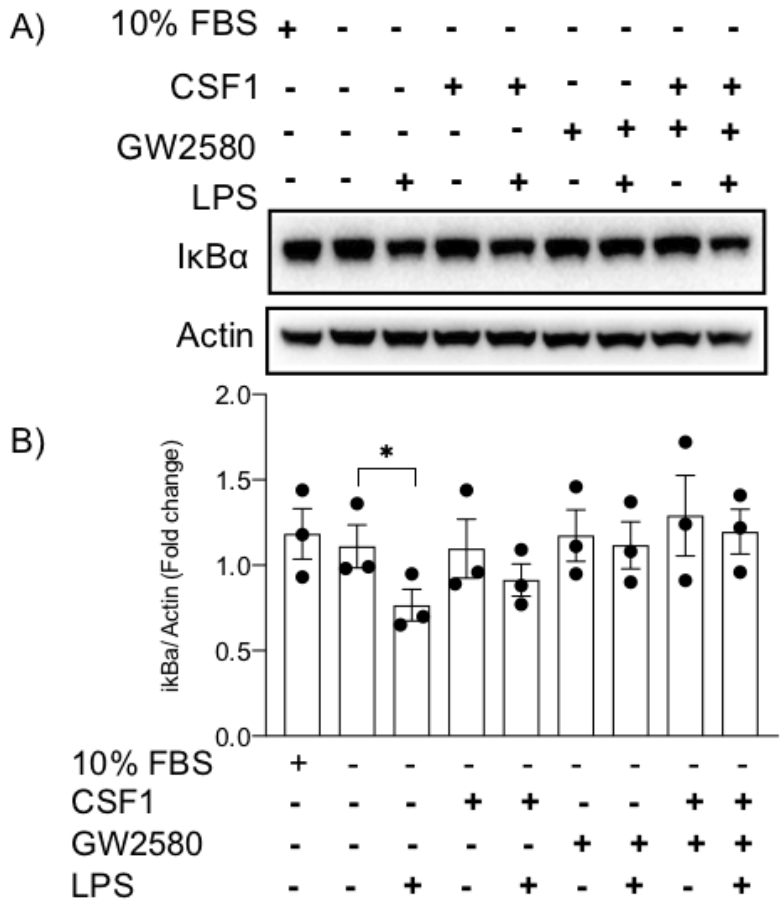

Figure 4.5.11.1: Effect of stimulation or inhibition of the CSF1R on LPS-induced NFκB activation (IkBa degradation). IMG cells were seeded and grown to 75 % confluency in 10 cm dishes. The following day cells were treated with 100 ng mL^{-1} LPS in serum free media for 24 hrs. After this time, cells were pre-treated with 1 μM GW2580 for 1 hr before incubating with 50 ng mL^{-1} CSF1 for 10 min. Cell lysates were collected and analysed by western immunoblot to detect expression of IκBα and actin was used as loading control (A). IκBα degradation was quantified using densitometric analysis and normalised to actin (B) Results represent mean ± SEM of three independent experiments. Significant differences are denoted by $*p < 0.05$ by unpaired t test.

4.6 Discussion

In this study, it was demonstrated that LPS increases cytokines, chemokines, NO and ROS production and increased JNK signalling in IMG cells. Exogenous CSF1, on its own, was sufficient to increase JNK signalling, Akt and S6K phosphorylation and GW2580 prevented these effects whether in the presence or absence of LPS. Inhibition of CSF1R robustly inhibited LPS-induced CCL2 and CXCL1 (but not CXCL10) secretion and modestly reduced LPS-induced TNFα and IL-6, despite minimal effects of CSF1 on these mediators when applied alone. NO production was also modestly reduced by GW2580 treatment of cells but no effect on ROS was observed. It was also shown that the internalisation of latex beads by IMG cells was modestly reduced by CSF1, and this was reversed by GW2580. However, this uptake was not LAP-dependent and was not affected by induction of autophagy. Collectively the data indicate that CSF1 and CSF1R inhibition affect multiple facets of microglial activation.

Table 4.6.1: Effect of LPS, CSF1 and GW2580 on different parameters measured in the chapter. Alterations are expressed as % increase or % decrease from the 'baseline'. Baseline for samples without LPS and LPS itself is 'Cell only control' and baseline for samples with LPS is 'LPS only control'.

Main effects	TNF	IL-6	IL-1ra	CCL2	CXCL1	CXCL10	JNK	PI3K/AKT/S6K1	NO	Phagocytosis
CSF1	up 1500%	-	-	-	-	up 600%	up 600%	up 100%	-	down 200%
GW2580	up 500%	-	-	-	-	-	-	-	down 40%	-
GW2580+CSF1	up 500%	-	-	-	-	-	-	down 100%	down 30%	-
LPS	up 500000%	up 4500%	up 1000%	up 1500%	up 2500%	up 90000%	up 600%	up 400%	up 1500%	-
LPS+CSF1	-	-	up 1000%	down 500%	-	-	down 100%	up 300%	up 1800%	-
LPS+GW2580	down 100000%	down 500%	down 200%	down 1300%	down 2400%	-	down 400%	down 300%	down 500%	-
GW2580+LPS+CSF1	down 100000%	down 500%	down 200%	down 1200%	down 2400%	-	down 400%	down 300%	down 500%	-

4.6.1 GW2580 suppresses CCL2 and CXCL1 expression but not CXCL10

LPS-induced expression of the chemokines CCL2 and CXCL1 was robustly suppressed by CSF1R inhibition, whether in the presence or absence of CSF1, while GW2580 had no impact on LPS-induced CXCL10 production. This differential inhibition of cytokine and chemokine expression using CSF1R inhibition is not easily explained. It is possible that it is due to differences in the regulation of these inducible mediators. The regulation of cytokine or chemokine expression starts at the transcriptional level and is stimulus- and cell-type dependent. The transcription factor NFκB is important for the maximal expression of CCL2 after LPS challenge, as pre-exposure of human monocytes to caffeic acid phenethyl ester (CAPE), prevented the nuclear binding of the NF-κB p65 subunit, and thereby reduced the

chemokine expression in a dose-dependent manner (Fietta *et al.*, 2002). The MAPK pathway plays an important role in chemokine expression. LPS-induced CCL2 production and secretion have previously been shown to be attenuated by inhibitors of JNK and p38 MAPK in microglia isolated from rat brain (Zhou, Ling and Dheen, 2007). These findings are consistent with the CSF1-induced and GW2580-inhibited JNK and place GW2580 in a position to inhibit LPS-induced CCL2 expression, but do not explain why CSF1 treatment does not then induce CCL2 expression/secretion. There are cellular outputs such as inflammation and apoptosis which can be altered solely by manipulating JNK activity. For example JNK activation is indispensable for modulating ApoE to regulate LPS-induced NO production primary mouse microglia and in BV2 microglia (Pocivavsek, Burns and Rebeck, 2009). JNK signalling has also been shown to be necessary for neurons in the CNS (Björkblom *et al.*, 2008). However, it seems likely that despite a CSF1-dependent contribution to CCL2 secretion observed herein, that CSF1-dependent JNK activation, alone, is not sufficient to drive CCL2 expression.

A similar difficulty arises in reconciling the inhibition of LPS-induced CXCL1 by GW2580. This chemokine is not significantly induced by CSF1 and yet LPS-induced CXCL1 expression is robustly suppressed by GW2580, even in the absence of exogenous CSF1. Expression of many CXC chemokines is also dependent on NFκB and the transcription rate of these secretory genes may be determined by the interaction of NFκB with other factors. Some *in vitro* studies suggest that the transcriptional regulation of CXCL1 requires NFκB to interact with STAT1 (Burke *et al.*, 2014). Treatment of isolated rat islet cells with IL-1β induced CXCL1 gene transcription and this IL-1β-induced transcription of CXCL1 gene required NFκB and STAT1 to bind to genomic regulatory sequences within the proximal gene promoters in these cells (Burke *et al.*, 2014). NFκB transcriptional activation has also been shown to upregulate CXCL1 expression by interacting with STAT3 in tumour cells (Fang *et al.*, 2021). However, no studies were found examining the requirement for JAK/STAT signalling in the regulation of CXCL1 expression in microglial cells.

Despite the effects observed for CSF1 and GW2580 on CCL2 and CXCL1, this was not matched by similar effects on CXCL10. MAPK pathways mediate transcriptional and post-transcriptional changes in gene expression in response to proinflammatory stimuli such as LPS. CXCL10 expression, in particular, has been shown to be

regulated by MAPK cascades (Hommes, Peppelenbosch and Van Deventer, 2003). LPS- and IFNγ-induced CXCL10 expression correlated with activation of JNK and p38 MAPK signalling and pre-treatment with the JNK inhibitor SP600125 or the p38 inhibitor SB203580, separately or together, almost completely prevented CXCL10 expression in BV2 microglial cells (Shen, Zhang and Bhat, 2006). Despite this propensity for JNK to mediate LPS-induced CXCL10, in the current study GW2580 almost completely ablated LPS-induced JNK activation but this had minimal impact on microglial CXCL10. Therefore, microglia appear to robustly synthesise CXCL10 in the absence of JNK activity, suggesting regulation that relies on additional signalling factors.

The transcription factor STAT1 was shown to be crucial for IFN-γ-mediated induction of CXCL10 genes in primary microglia and astrocytes (Ellis *et al.*, 2010). The JAK/STAT pathway is important for the regulation of CXCL10 expression in virus- and cytokine-stimulated human astrocytes (Williams *et al.*, 2009). Similarly, Dhillon and colleagues have shown that co-treatment with IFNγ and PDGF induced synergistic increase of CXCL10 expression in monocyte-derived macrophages through phosphorylation of STAT1 at Tyr701 by JAK1, in addition to a contribution from the PI3K pathway (Dhillon *et al.*, 2007).

Gene silencing of either the p65/RelA subunit of NF-κB or STAT1 revealed that p65/RelA and STAT1 are necessary for activation of IL-1β- and IFNγ-mediated CXCL10 gene expression in rat pancreatic β cells (Burke *et al.*, 2013). Conversely, for cytokine-induced CXCL1 expression in rat pancreatic β cells (Burke *et al.*, 2014) and CCL2 expression in microglia isolated from a mouse model of epilepsy (Tian *et al.*, 2017), STAT signalling was proposed to contribute to, but not be essential for, their expression. Although not performed in microglia, it is notable that an unbiased gene-expression profile array performed after inhibition of CSF1R (PLX3397, 1μM) in a T-cell lymphoma cell line showed changes in the expression of several genes that are involved in cytokine (JAK/STAT) signalling accompanied by several changes in PI3K/Akt in phospho-proteomic screens (Murga-Zamalloa *et al.*, 2020). Thus, even if STAT signalling may be a more significant contributor to CXCL10 induction than to that of CCL2 and CXCL1, there are data to suggest that CSF1R inhibition should also be expected to impinge on JAK/STAT signalling. Thus, while it is a possibility that control of expression of CXCL10 diverges from that of CXCL1

and CCL2, how GW2580 inhibition of CSF1R might achieve this is not clear at this point.

When looking at the signalling pathways in this study, both LPS and CSF1 increased phosphorylation of JNK. JNKs are strongly activated in cells by various stresses such as UV radiation, heat shock, osmotic shock, DNA-damaging agents, and metabolic inhibitors as well as pro-inflammatory cytokines, including TNFα, and IL-1β, so the significant increase in JNK phosphorylation with LPS in IMG cells was expected. JNK, as part of the MAPK family, has an important role in relaying extracellular signals from the membrane to the nucleus to phosphorylate several transcription factors and regulate gene expression. In LPS stimulated microglia, JNK signalling is one of the dominant pathways for cytokine production *in vitro* (Uesugi et al., 2006). In partial agreement with the results in this chapter, previous reports showed that LPS stimulated phosphorylation of the JNK substrate and transcription factor, c-jun, by activating both 46-kDa and 54-kDa JNK splice variants in primary microglia cultures from neonatal rat brain and inhibition of JNK, using SP600125, reduced LPS-induced TNFα, IL-6 and CCL2 transcript expression, but not protein expression (Waetzig et al., 2005). However, differences could be explained by choice of model, mouse IMG cells versus primary rat microglia.

JNK1, one of the three JNK-encoding genes, was shown to be necessary for the induction of the mitogen-activated protein kinase phosphatase 1 (*Mkp1)* gene when cells were treated with LPS and CSF1, and this was inhibited by SP600125, leading to a G_1 cell cycle arrest in murine bone marrow macrophages (Himes *et al.*, 2006). Inhibition of JNK by SP600125 also reduced CSF1R expression in macrophages and stopped CSF1-dependent differentiation of bone marrow cells to macrophages (Himes *et al.*, 2006). The response of macrophages to JNK inhibitors has been linked to phosphorylation of the PU.1 transcription factor (Celada *et al.*, 1996). These studies support a link between CSF1R and JNK signalling and the observed effect that GW2580 had on JNK signalling in this chapter. Indeed, SP600125 also attenuated LPS-induced CCL2 up-regulation in rat astrocytoma C6 cells (Zhang *et al.*, 2012). LPS also induced an up-regulation in CXCL1 and CCL2 expression as well as an increase in phosphorylation in JNK, Erk and p38 MAPK in astrocytes (Liu *et al.*, 2018). Inhibition of JNK and Erk, but not p38 MAPK with SB203580 also blocked the LPS-induced expression of these two chemokines (Liu *et al.*, 2018). In

microglial cells activated with an inhibitor of c-GMP-selective phosphodiesterase, zaprinast, and LPS side by side, LPS also induced up-regulation of CXCL1 and CCL2 (Lee *et al.*, 2012). These studies illustrate the importance of JNK signalling in CCL2 and CXCL1 expression and are consistent with the observation, in the current study, of CSF1-mediated JNK signalling contributing to LPS-induced CCL2 and CXCL1. It is important, however, to reiterate that while CSF1 was sufficient, alone, to robustly induce JNK activation, this was not sufficient to robustly induce these chemokines.

Finally, despite the implied contribution of JNK to chemokine expression in the current study, JNK has also been shown to be involved in CXCL10 induction by double stranded RNA (dsRNA) in the Ra2 microgial cell line (Nakamichi *et al.*, 2005). Since CXCL10 secretion persisted in the current study, despite the absence of JNK activation (in GW2580-inhibited microglia), a differential activation of JNK cannot explain divergent effects of CSF1R inhibition on CCL2/CXCL1 and CXCL10.

Regardless of the ability of CSF1R inhibition to suppress LPS-induced CCL2 and CXCL1, exogenous CSF1 only modestly induced TNFα, CXCL1 and CXCL10. There is evidence that JNK activation can drive CXCL10 and/or TNFα expression in macrophages (Comalada *et al.*, 2003; Swantek, Cobb and Geppert, 1997(Nayak *et al.*, 2019), mast cells (Alrashdan *et al.*, 2012), in ATP stimulated microglia (Suzuki *et al.*, 2004) or Bisphenol A-induced BV2 microglia (Zhu *et al.*, 2015), and in IFN-γ activated BV2 microglia (Shen, Zhang and Bhat, 2006). TNFα and CXCL10 expression is also regulated by PI3K/Akt/mTORC1 signalling since inhibition with either LY294002, rapamycin or torin1 decreased LPS- and ATP-induced TNFα and BDNF production in primary rat microglia (Hu *et al.*, 2020). Translation of the mRNA encoding CXCL10 is regulated by eIF4E-binding proteins 1 and 2 (4E-BP1/2), two of the main mTORC1 effector proteins, and inhibition of mTORC1 by rapamycin or torin1 also reduced CXCL10 expression, at least in macrophages (William *et al.*, 2019).

Taken together these data support the notion that CSF1 can stimulate TNFα and CXCL10 expression through JNK and PI3K signalling and this is attenuated with the CSF1R inhibitor, GW2580. The differential size of the effects on CSF-induced TNFα and CXCL10 expression between studies may be explained by the model specific properties.

4.6.2 Endogenous CSF1 activity in IMG cells or off-target effects of GW2580?

CSF1 had minimal effects on CCL2 and CXCL1 expression. Conversely, LPS treatment strongly induced CCL2 and CXCL1 expression and the sensitivity of this effect to GW2580 inhibition suggested a contribution of CSF1 to this chemokine induction. Moreover, some effects such as induction of NO occurred in IMGs treated only with GW2580, suggesting some CSF1 activity in the absence of exogenously added CSF1. One possible explanation is that some basal autocrine CSF1 activity facilitates their expression but further exogenous CSF1 does not enhance it. Endogenous CSF1 production is evident in pure microglial cultures. For example, Hagan and colleagues have shown that the level of CSF1 is higher in mixed glial cultures, compared to the low levels of CSF1 found in pure primary microglial cultures but it is the highest in pure astrocyte cultures (Hagan *et al.*, 2020). In another study, differentiated BMDMs were supplemented with CSF1 supplement in the media for 7 days before withdrawal for two weeks, where upon endogenously expressed CSF1 was detectable in the media (Chen *et al.*, 2021). Thus, it is possible that some endogenous CSF1 production occurs in IMG cultures, although this was not assessed in the current study.

Alternatively, GW2580 could have off-target effects. For example, GW2580 can inhibit the tropomyosin related kinases A and B (Trk A/B) in addition to CSF1R (Davis *et al.*, 2011). In this chapter, GW2580 was used at a concentration of 1 μM in culture, while against isolated enzymes GW2580 has an IC_{50} for CSF1R of 10 nM (Priceman *et al.*, 2010) and TrkA of 88 nM (Conway *et al.*, 2008). Routinely, for cell culture experiments drug concentrations of 10-fold are frequently found to recapitulate on-target inhibition. Therefore, in the current study, it would not be unreasonable for GW2580 to also be inhibiting TrkA or TrkB too. The TrkB receptor, for instance, is activated by brain derived neurotrophic factor (BDNF), also supports growth, survival, and differentiation of cells (Puehringer *et al.*, 2013). TrkB receptor can also be activated independently in the absence of its ligand, via transactivation involving GPCRs (Rajagopal *et al.*, 2004). In primary astrocytes TrkB-mediated STAT3 signalling increased CCL2 expression and inhibition of STAT3 by shStat3 resulted in a 50% reduction in CCL2 mRNA (Ni *et al.*, 2017). Although, no evidence could be found, at the present time, on whether TrkB may influence CCL2 or CXCL1 expression in microglia. Immunohistochemical analysis revealed increased mRNA levels of chemokine receptors CCR5, CXCR3 and CXCR4 in the TrkB-positive

neurons in cerebral cortex, hippocampus and striatum of 6 and 18 months old $BDNF^{+/-}$ mice compared to WT animals (Ahmed *et al.*, 2008). Inhibition of the CSF1R by Ki20227 up-regulated BDNF, and potentially also TrkB signalling, to enhance neuro-behavioural function in cerebral ischemia (Du *et al.*, 2020). It is possible that in the current case, GW2580 may have blocked CCL2 and CXCL1 expression by inhibiting TrkB receptors. A possible consequence of inappropriate TrkB inhibition is attenuation of the same signalling pathways as found downstream of the CSF1R. For instance, activation of PI3K/Akt pathway, that are also required for signals promoting pro-inflammatory mediators like chemokine production (Saponaro *et al.*, 2012). Other off target effects of GW2580, other than TrkA/B may yet be identified.

4.6.3 *NO*

NO, produced from L-arginine in a reaction catalysed by inducible Nitric Oxide synthase (iNOS), is a crucial inflammatory effector molecule produced by human and rodent microglia (Xue *et al.*, 2018). In this chapter, LPS stimulation of IMG cells increased NO production. Interestingly, the presence of CSF1 synergistically, but only modestly, augmented the LPS-induced NO production. Inhibiting CSF1R signalling with GW2580, whether in the presence or absence of CSF1, was able to mitigate increased NO levels in IMG cells. Earlier in this chapter it was observed that LPS treatment of IMG cells led to activation of JNK, and this was also inhibited by GW2580. In BV2 cells, LPS induced iNOS expression and this was abolished with JNK inhibition, but not inhibition of Erk1/2 or p38 MAPK (SB203580) (Svensson *et al.*, 2010). In addition, BV2 cells when treated Aβ also increased NO production and addition of CSF1 dramatically augmented the Aβ-induced iNOS mRNA expression in these microglia (Murphy, Yang and Cordell, 1998). Therefore, taken together, the observed effects on NO production as a result of LPS and CSF1 is likely related to JNK signalling in IMG cells.

4.6.4 Effects of CSF1 on phagocytosis

IMG cells were found to be effective in engulfing 1 μm latex beads. However, the question remains as to whether the process of 1 μm latex bead uptake specifically requires phagocytosis, since small particles can be internalised by other mechanisms such as macropinocytosis. The literature suggests that the size of the latex bead is critical in determining the process of uptake. Yet, it has not yet been

determined as to what size of particle is too large for uptake by pinocytosis and/or too small to initiate phagocytosis and understanding of this is still dependent historical studies (Pratten and Lloyd, 1986). Nonetheless, it has been suggested that during phagocytosis, 1-2 μm sized particles are internalised, while in pinocytosis, 0.1-0.2 μm sized liquid droplets are ingested (Lakna, 2017; for review, see Kruth, 2011). Polystyrene microspheres having a size ranging between 1-2 μm have been shown to be most effectively phagocytosed by the mouse peritoneal macrophage after 30 min and 1 hr of treatment in the presence of FBS (Tabata and Ikada, 1988). Lian and colleagues have also used fluorescent latex beads of 1 μm diameter to show the effect of purified recombinant complement C3 protein on latex bead phagocytosis: showing that 1 hr treatment with C3 enhances phagocytosis while, 24 hrs treatment diminished this function in primary microglia isolated from mouse cortex and hippocampus (Lian *et al.*, 2016). Taken together, it is likely that 1 μm hydrophobic solid latex beads used in this chapter were likely internalised by phagocytosis, as there was no evidence of involvement of LC3B precluding LAP and that the size of bead used would be at the expected limit of pinocytosis.

The latex-bead internalisation that was observed was reduced by CSF1 treatment of cells compared to control and GW2580 treatment of cells reversed this effect. Phagocytosis may be impaired in many neurodegenerative diseases, including AD. Impaired microglial proliferation has been connected with deficient microglial phagocytosis of Aβ by research demonstrating an amplification of microglia population in response to Aβ in *Trem2*$^{+/-}$ mice on an APP/PS1 background (Ulrich *et al.*, 2014). On the contrary, CSF1 treatment of primary adult human microglia has been shown to increase phagocytic function of Aβ1-42 peptide *in vitro* (Smith et al., 2013). Our findings and the results demonstrated by Ulrich and colleagues are similar in the sense that both labs found that microglial proliferation which can be targeted by CSF1R signalling, has the potential to restore microglial phagocytosis. This indicates inhibition of CSF1R signalling may prove to be a beneficial strategy for induction of efficient phagocytosis and thus, improvement of aggregation-prone disease conditions. The betterment of phagocytic function may be the consequence of the controlled CNS inflammatory microenvironment, which is now free from excessive proliferative microglia. No proliferative microglia would mean less inflammatory mediators and a homeostatically balanced CNS with intact microglial functions. Moreover, GW2580 was found to reduce NO and pro-inflammatory

cytokines such as TNFα in IMG cells. Therefore, one might argue that GW2580 improves microglial phagocytic function, potentially by reducing inflammatory mediator production. However, this is speculative and needs formal testing.

4.6.5 Caveats of using latex beads vs Aβ for phagocytosis experiments

Latex beads were used to assess the mechanism of phagocytosis in IMG cells, to determine whether they employed canonical phagocytosis, or LAP. Latex bead uptake is widely used as a cost-effective model for investigating phagocytosis that provides uniformity, stability and consistency of results, and is easy to incorporate in the experiments, but does have its limitations (Sierra et al., 2013). Importantly, latex beads are a synthetic phagocytic target and so only recapitulate a physical structure, they do not release any chemoattractant(s) and therefore do not activate conventional 'finding mechanisms' in phagocytes (Park et al., 2011). Using latex beads in assays also means the phagocytic process remains incomplete as the material cannot be degraded. Although sometimes these particles are opsonized with serum to facilitate their recognition, it is not clear whether there is any interaction of *in vivo* microglia with serum components (Hellwig, Heinrich and Biber, 2013). Consequentially, phagocytosis of Aβ may be considered as a more realistic model to analyse microglial phagocytic function. However, in this study only the mechanism(s) by which IMG cells perform phagocytosis (i.e. engulfment and internalisation, followed by fusion with the lysosome) was explored. The more physiologically relevant question of how microglia phagocytose Aβ was not an objective in this study. However, investigating Aβ phagocytosis by IMG cells in the presence or absence of CSF1R agonist and antagonist will be the focus of future research.

4.6.6 Differential experimental design for secretory and siganllig analysis

There was a difference in design of experiments that measured cytokine/chemokine secretion by ELISA compared to experiments where signalling mechanisms were examined. In short, a 24 hr incubation was used to examine secretory activity of cells post-challenge, whereas much shorter incubations were employed to observe early receptor signalling events. For the cytokine secretion assays, IMG cells were seeded and left to adhere overnight. The following day cells were pre-treated with or without GW2580 for 1 hr before incubating with or without CSF1 or LPS in serum free media for 24 hrs before the media was collected and analysed by ELISA.

Conversely, in signalling experiments, cells were treated with LPS in serum free media the day after seeding, for a further 24 hrs. After this time, cells were pre-treated with GW2580 for 1 hr before incubating with CSF1 for 10 min. Cell lysates were collected and analysed by Western immunoblot to detect expression signalling proteins and to determine their phosphorylation status. Although the 24 hr LPS treatment may be suitable for secretory analysis, this was not appropriate for signalling experiments where acute signalling events that occur transiently within the first hour of receptor activation can be missed. For instance, LPS-stimulated phosphorylation of P38 MAPK was observed as early as 5 min and of ERK1/2 and JNK was observed after 15 min of LPS treatment in BV2 microglial cells line (Wen, Ribeiro and Zhang, 2011). Similar patterns in LPS-stimulated signalling are evident in the peripheral nervous system too, with LPS-stimulated phosphorylation and the activation of ERK, P38 MAPK and JNK occurring at 10 mins, in ovine oviduct epithelial cells (Li et al., 2016). Additionally, optimal NFkB signalling in microglia occurs within minutes of LPS stimulation in vitro (Subedi et al., 2019). Another difference between the two experimental designs was that for secretory analysis cells were treated with CSF1 for 24 hrs, whereas, for the signaling experiments cells were stimulated with CSF1 only 10 min. Classical CSF1R studies in macrophages and other systems has demonstrated that the CSF1R activates the PI3K pathway within minutes (Murray et al., 2000) and in the present study was illustrated by phosphorylation of S6K1 as early as 10 min following stimulation with CSF1, in IMG cells. However, given the possibility that GW2580 may have off-target effects, and the difference in time of protein expression compared to acute signalling events, then these results must be interpreted with some caution.

4.7 Conclusion

Overall, this chapter demonstrates that CSF1R modulates several aspects of microglial function. CSF1 modestly reduced internalisation of latex beads, which was prevented by GW2580 inhibition of CSF1R. Predictably LPS increased cytokine, chemokine, NO and ROS production in IMG cells but CSF1R inhibition substantially inhibited the LPS-induction of CCL2 and CXCL1 and the activation of JNK. Despite robust activation of JNK by CSF1, this was not sufficient to produce substantial increases in these chemokines, although limited induction of TNF-α and

CXCL10 did occur after CSF1 treatment. The possibility of endogenous CSF1 production in IMG cells and off target effects of GW2580 cannot be ruled out.

Chapter 5: Effect of CSF1R inhibition on microglial activation in APP/PS1 mice

5.1 Introduction

In a healthy CNS, microglia remains in a homeostatic state and performs the normal function of monitoring the brain parenchyma to sense alterations in brain microenvironment, regulating neuronal excitability, synaptic activity and pruning, neurogenesis and clearance of apoptotic cells (for review see Casali and Reed-Geaghan, 2021). Gene profiling and quantitative mass spectrometry analysis have revealed that the homeostatic microglial signature is driven by the expression of transforming growth factor beta (TGFβ) (Butovsky *et al.*, 2014). Microglia are the mediator of neuroinflammatory responses in the brain. These cells alter their state as required for their optimal function and activation of these cells is a hallmark of CNS pathology.

5.2 Microglial activation

Upon recognition of danger signals, a lack of normal signals from neurons or other glial cells, microglia become activated with morphological and functional changes. Phenotypical features of these activated microglia include amoeboid cell body with large nucleus and little cytoplasm, and thickening and branching of the processes (Das Sarma *et al.*, 2013). Although whether microglial activation plays a favourable or detrimental role in neuropathological conditions still remains a controversial topic, much of the current literature suggests that chronic, long term microglial activation is damaging to the brain causing cognitive impairment, synaptic loss or excessive neurodegeneration (Mass *et al.*, 2017; Zhang *et al.*, 2021).

5.2.1 Microglial activation phenotypes

Various damage- and pathogen-associated molecular patterns (DAMPs and PAMPs, respectively) such as heat-shock proteins like HMGB1, ATP, bacterial LPS, peptidoglycan etc. can activate microglia and activated microglia can assume different activated phenotypes. By analogy to pre-existing concepts in macrophage activation, microglia in aging, injury or pathology were originally broadly divided into two subgroups depending on their upregulated cytokines, proteins and functions: a cytotoxic pro-inflammatory phenotype (activated, M1 microglia) and a more neuroprotective anti-inflammatory phenotype (alternative, M2 microglia). However, from various transcriptomic analysis it is now well accepted that these two descriptions

of microglial status rarely occur in the brain and are actually the very extreme ends of a continuous spectrum of microglia activation phenotypes. Many relatively newly characterised microglial phenotypes have been established. This has stemmed from the observation that microglia present in the non-plaque brain areas differ in phenotype from the microglia seen around the Aβ plaques. Microglia associated with Aβ plaques have a pro-inflammatory phenotype and are termed as disease-associated microglia (DAM) (Krasemann *et al.*, 2017). The development of this microglial phenotype involves a two-step activation process. Stage 1 DAM is a TREM2-independent process where microglia convert from homeostatic to an intermediate stage and the progression from the intermediate stage to Stage 2 DAM is a TREM2-dependent process (Keren-Shaul *et al.*, 2017). Due to the pro-inflammatory phenotype, DAM microglia are predominantly associated with the neuroinflammation in AD. These microglial cells become reprogrammed in response to neurodegeneration or altered homeostasis in the brain (Keren-Shaul *et al.*, 2017). Another phenotype of microglia, somewhat overlapping with DAM, is known as microglia neurodegenerative phenotype (MGnD). These microglia promote the expression of ApoE signalling-related genes and suppresses TGFβ signalling in microglia and may contribute to neurodegeneration in the brain (Krasemann *et al.*, 2017). Activation of TREM2-ApoE signalling via phosphatidylserine exposed on the apoptotic neurons regulates this phenotype in microglia (Krasemann *et al.*, 2017).

Build-up of lipids have been observed in more than 50 % of all microglia in the aged hippocampus, leading to this subset being called as lipid droplet accumulating microglia (LDAM), with a pro-inflammatory phenotype and severe functional abnormalities (Marschallinger *et al.*, 2019). It is striking that the transcriptional signature of these subsets of microglia is very distinctive to the subsets described above or expected aging-related gene expression pattern. For instance, an upregulation in TREM2-ApoE axis is observed in DAM or MgND but is not regulated in this subset at all (Holtman *et al.*, 2015). A very recently identified subtype of microglia has been termed as Activated Response Microglia (ARM). This subtype of microglia express genes involved in MHC-II presentation (*Cd74, Ctsb, Cstd*), inflammatory processes (*Cst7, Clec7a, Itgax*) putative tissue repair genes (*Dkk 1, Spp1, Gpnmb*) and AD risk genes like ApoE (Sala Frigerio *et al.*, 2019). This core signature emphasises that many of the ‘new’ phenotypes emerging from single cell

RNA sequencing studies share strong overlap with each other, as previously described for primed microglia (Holtman *et al.*, 2015).

5.3 Microglial proliferation and CSF1

Importantly, microglial activation is directly connected with their proliferation and their elevated production/expression of inflammatory factors and surface proteins (Graeber, 2010). Excessive proliferation of microglia is a common feature in many neurodegenerative disorders. Expression of proliferation markers such as cyclin A and B1, and Ki-67 increase in activated human microglia (Böttcher *et al.*, 2019). Aβ has been shown to bind to several receptors expressed on microglia such as TLR2, TLR4, TLR6, Receptor for Advanced Glycation End-products (RAGE), low density lipoprotein receptor-related protein (LRP) etc. (Stewart *et al.*, 2010) and proliferative $Iba1^+$ microglia are found surrounding the Aβ plaques in the hippocampus of AD brains (Marlatt *et al.*, 2014). Ponomarev and colleagues have shown that activated microglial cells proliferate early, before any manifestation of clinical symptoms of experimental autoimmune encephalomyelitis (EAE), and that this proliferation was seen with an upregulation of MHC II, CD86 and CD40 in a mouse model of EAE (Ponomarev *et al.*, 2005). These studies portray that microglial proliferation is strongly correlated with microglial activation and intervention targeting the signalling pathways governing proliferation seems likely to impact other features of activation.

The literature suggests that proliferation of cells is strongly controlled by CSF1R signalling and inhibition of this signalling by CSF1R inhibitor to regulate microglial elimination or proliferation has been shown to be effective in mitigating neuropathology in animal models of neurodegeneration. CSF1R inhibitors can prevent microglia survival rather than simply limiting their proliferation. Administration of PLX3397 (290 mg kg^{-1}), a CSF1R inhibitor, showed 50 % reduction in microglia after just 3 days and the brains were essentially devoid of microglia by 21 days in 12 month-old mice, illustrating the critical role of CSF1R in microglial survival. This group also showed that the microglial cells repopulated through nestin-positive cells within 1 week after cessation of the CSF1R inhibitor, indicating the importance of CSF1R in microglial differentiation and proliferation (Elmore *et al.*, 2014). Dagher and colleagues have reported that inhibition of CSF1R by PLX5622 (300 mg kg^{-1}) for 3 months saw a 30 %

reduction in microglial numbers and improved cognition in the 3xTg-AD mice, (Dagher *et al.*, 2015). Treatment with PLX3397 (290 mg kg^{-1}), for 3 months, reduced 70-80 % of $Iba1^{+}$ cells and 99 % of the area fraction occupied by the cells. This manipulation decreased amyloid plaque deposition and improved cognitive function as measured by fear conditioning in 5 month-old 5xFAD mice (Sosna *et al.*, 2018) illustrating the potential benefits of targeting microglial proliferation as a strategy to treat or prevent neurodegeneration.

CSF1R inhibition improves disease phenotype in mouse models of other neurogenerative diseases as well and the depletion of microglia has measurable effects on other neuronal and glia populations. For instance, 5-day treatment with BLZ945 (169 mg kg^{-1}) in the 5 week-old murine cuprizone model of multiple sclerosis (MS), maximally depleted microglial number and increased remyelination in the striatum or cortex. The study showed a positive correlation with microglial reduction, with increased numbers of oligodendrocytes and astrogliosis (Beckmann *et al.*, 2018). Microglial activation in the hippocampal and cortical region of mice was associated with rotenone-induced cognitive decline assessed by Morris Water Maze (MWM), object recognition test and passive avoidance test in a dose-dependent manner. Inhibition of CSF1R by PLX3397 (40 mg kg^{-1}) for 7 days diminished approx. 70 % of microglia, improved cognitive performance as well as reduced neuronal damage in eight week old rotenone-injected mice (Zhang *et al.*, 2021).

All the studies above take the approach of ablating the microglial population, affecting the survival of the cells. However, the current work targets microglia proliferation, so the basal population survives but the proliferation does not occur, as was done in the study performed by Olmos-Alonso and colleagues. They demonstrated that administration of GW2580 (0.1 % or 1000 ppm) for 3 months to inhibit CSF1R signalling improved AD-like pathology in 9 months old APP/PS1 mouse model of AD. They showed that inhibition of CSF1R signalling reduced inflammatory mediators such a *Tgfβ* and *IL-1β* at the mRNA levels. Some pro-inflammatory cytokines such as IL-1A, IL12, CCL2, CXCL13, measured using quantitative antibody arrays, were reduced by the treatment of GW2580 at protein levels (Olmos-Alonso et al. 2016). However, the investigation of these inflammatory markers was done in homogenates from the cortex of the APP/PS1 mice and did not look at the effect of the drug specifically in

microglial cells. Therefore, building up on this study, the effect of chronic CSF1R inhibition on microglial activation will be examined in the microglia isolated from APP/PS1 model of AD in this chapter.

5.4 Aims and objectives

The overall aims of this chapter were to characterise microglial phenotype, affected by CSF1R inhibition using chronic GW2580 treatment, in the APP/PS1 model of AD. Specific objectives were to assess whether CSF1R inhibition:

- protects against APP/PS1 strain-dependent cognitive deficits in APP/PS1 mice.
- alters expression of multiple genes in microglial isolates from APP/PS1 hippocampus
- alters levels of protein markers of neuroinflammation and neurodegeneration in hippocampal homogenates from APP/PS1 and WT mice.

5.5 Experimental design

To address these aims 3 cohorts of APP/PS1 mice were cognitively assessed at baseline (6 months), assigned to CSF1R inhibitor (GW2580) and control diets and assessed for disease progression and changes in microglial phenotype after 3 months of treatment (Figure 5.5.1, panel A).

A)

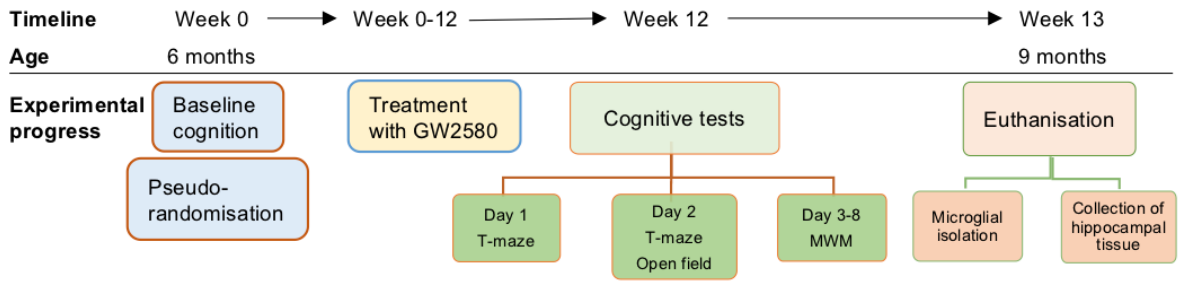

B)

	N.chow				GW2580				Total
	WT		Tg		WT		Tg		
	Male	Female	Male	Female	Male	Female	Male	Female	
Animal in behaviour studies	10	10	6	10	4	8	5	8	61
Animal for microglial isolate (PCR)	8	5	6	8	2	4	3	5	41
Animal for brain homogenate (WB)	0	10	0	10	0	8	0	8	36

Figure 5.5.1: Experimental scheme showing the study design and the number of animals used for different purposes in the study. (A) 6 month-old mice were analysed for their baseline cognition before pseudo-randomizing them into groups of equivalent cognitive baseline to start the GW2580/ placebo treatment for 12 weeks. On week 12 post-treatment cognitive tests were performed before sacrificing the mice for isolation of microglia or collection for hippocampal tissue for homogenization. (B) The number of mice used for cognitive tests, gene and protein expression analysis is listed in the table.

5.6 Results

5.6.1 Cognitive performance and assignment of animals into treatment groups

In order to assign animals to groups of equivalent baseline cognition, animals were assessed on a visuospatial memory task reliant on hippocampal function. The performance of 6 month-old APP/PS1 (Tg) mice (n=36) and WT (n= 32) was assessed in a reference memory Y-maze task across a total of 48 trials over 4 days with 12 trials taken by each mouse per day (Figure 5.6.1.1, panel A). Two-way repeated measure ANOVA with genotype as between subject factor and days of learning as within subject factor indicated that APP/PS1 mice were not different compared to their WT controls on this task, at this point in disease. ANOVA revealed a significant effect of days in training ($F_{2.414,\ 159.4}$ = 88.74, p <0.0001), where performance of both genotypes improved over 4 days, but there was no effect of genotype ($F_{1,\ 66}$ = 0.8175, p = 0.3692), nor any interaction between genotype and time ($F_{3,\ 198}$ = 01.550, p = 0.2027).

On day 5, the 'correct' exit arm was moved to a new location and learning of this reversal was assessed across 3 blocks of 4 trials, a total of 12 trials per mouse, on a single day (Figure 5.6.1.1, panel B). Two-way repeated measures ANOVA indicated that APP/PS1 were slower to learn the new 'correct' exit arm compared to WT controls. ANOVA revealed a significant effect of genotype ($F_{1,\ 66}$ = 21.19, p <0.0001) and trial block ($F_{1.956,\ 129.1}$ = 48.14, p <0.0001) but no significant interaction between the two ($F_{2,\ 132}$ = 0.4010, p = 0.6705) was observed, indicating that while both strains can learn the reversal, the APP/PS1 mice do so more slowly.

Animals were assigned to drug or placebo treatment groups based on their (i) genotype (ii) sex and (iii) baseline cognitive status. Cognition was determined from their rate of adjusting strategy once the exit arm was reversed, based off their 12 trials following reversal of the escape arm, which was broken into 3 blocks of 4 trials. The average percentage correct over the 3 blocks was calculated for each animal. Animals were then split equally across the 2 groups, for treatment with GW2580 or placebo diet, such that the average percentage correct within a diet group would be roughly equal. Animals were assigned to drug (diet containing 0.1 % of GW2580) or placebo diet and animals continued solely on these diets for 3 months before performing any further behavioural tests.

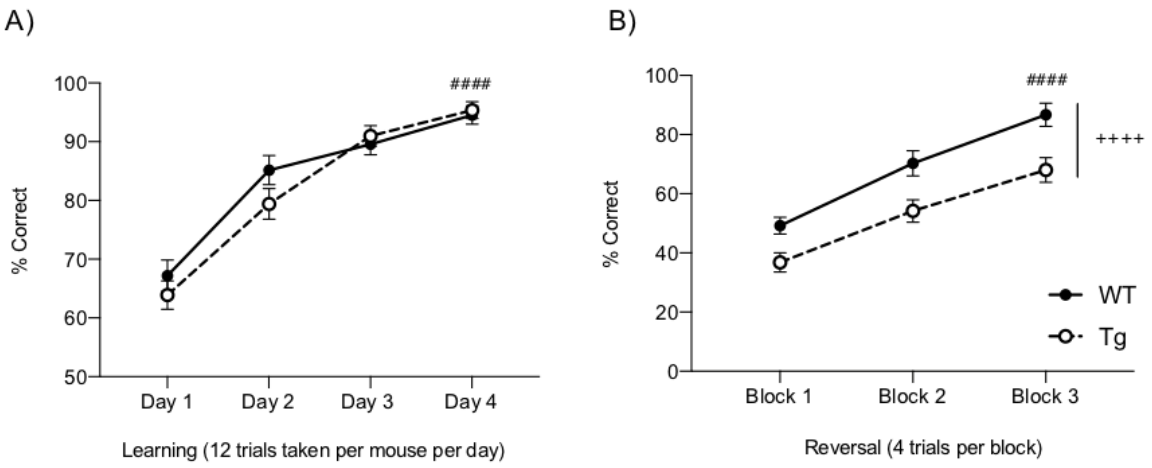

Figure 5.6.1.1: Performance of APP/PS1 versus WT mice on a visuo-spatial reference memory task. Learning on the visuo-spatial working memory was assessed using the Y-maze across a total of 48 trials, 12 trials taken by each mouse per day over 4 days, in APP/PS1 (n= 36) compared to WT mice (n= 32) (A). Reversal learning in the Y-maze was assessed across a total of 12 trials per mouse- each block representing 4 trials in APP/PS1 (n= 36) compared to WT mice (n= 32) (B). Data are shown as mean ± SEM and were analysed by two-way repeated measure ANOVA with strain as between subject factors and days or trial blocks as within subject factors for Learning and Reversal, respectively. Main effects of days of Learning and main effects of trial blocks are depicted by $^{\#\#\#\#}p < 0.0001$, and main effect of genotype is depicted by $^{++++}p < 0.0001$.

5.6.2 Learning and memory in the Morris Water Maze (MWM)

The ability of Tg n.chow (n=15), Tg GW2580 (n=14) and WT n.chow (n=20), WT GW2580 (n=12) at 9 months of age to locate the hidden platform in the MWM spatial memory task was assessed across 20 trials over 5 days with 4 trials per day, per mouse. The latency to reach the platform (Figure 5.6.2.1, panels A-C) and the swim speed (Figure 5.6.2.1, panel D) were recorded. Data were analysed by two-way repeated measures ANOVA with drug as the between subject factor and training days as the within subject factor for males, females and both sexes combined for Figure 5.6.2.1, panels A-C and by three-way ANOVA with strain, sex and drug treatment as factors for Figure 5.6.2.1, panels D-F.

Although the Tg females were somewhat slower to reach the hidden platform compared to Tg males, all groups learnt the task in the water maze. Treatment of Tg mice with GW2580 appeared to shorten the latency to reach the platform compared to Tg normal chow group. Two-way ANOVA of the latency in Tg mice from both sexes combined showed a significant effect of training day ($F_{2.868, 77.44} = 31.76$, $p < 0.0001$) but no significant effect of drug ($F_{1, 27} = 2.317$, $p = 0.1396$) or interaction ($F_{4, 108} = 0.9926$, $p = 0.4149$) was observed. Two-way ANOVA of the latency in Tg females showed a significant effect of training days ($F_{3.094, 49.50} = 19.21$, $p < 0.0001$). There was also no effect of drug ($F_{1, 16} = 2.245$, $p = 0.1535$) but the interaction of training and treatment showed a trend towards improved cognitive performance in GW2580 treated mice ($F_{4, 46} = 2.135$, $p = 0.0866$). The data suggest that Tg female mice may be worse at locating the hidden platform and that GW2580 may improve disease-associated spatial memory in Tg female mice, but the experiment was underpowered to detect this effect in females only (n=9 per group). Average swim speed of mice from each group on day 3 was calculated as a control parameter and three-way ANOVA was used for the statistical analysis. There was no main effect of drug ($F_{1, 53} = 3.142$, $p = 0.0821$), of strain ($F_{1, 53} = 2.601$, $p = 0.1127$), sex ($F_{1, 53} = 3.817$, $p = 0.0560$) or drug x strain x sex interaction ($F_{1, 53} = 1.008$, $p = 0.3200$) on swim speed, indicating that any observable motor deficits associated with the maze test and the 'longer' escape latency in the Tg mice was not explained by motor dysfunction.

In a probe test conducted after 5 days of training, during which the platform was removed from the water maze (Figure 5.6.2.1 panel E), three-way ANOVA revealed

that all groups spent an equal amount of time in the target quadrant where the platform was located during the training days and less time in all other quadrants, indicating that all animals learned the location of the platform, with respect to visuospatial cues. Statistically, there was no main effect of drug ($F_{1, 52} = 0.4175$, $p = 0.5210$), of strain ($F_{1, 52} = 0.8691$, $p = 0.3555$), of sex ($F_{1, 52} = 0.003784$, $p = 0.9512$) or drug x strain x sex interaction ($F_{1, 52} = 1.339$, $p = 0.2525$) between the groups. In the non-spatial flag test, in which a flag was added to the platform located in the quadrant opposite to their original exit quadrant (trial 1) and in their original exit quadrant (trial 2), all groups reached the platform faster than in the hidden platform version of the maze (Figure 5.6.2.1, panel F) and no differences within the groups were observed in this test. ANOVA revealed no main effect of drug ($F_{1, 53} = 2.844$, $p = 0.0976$), strain ($F_{1, 53} = 2.039$, $p = 0.1592$), sex ($F_{1, 53} = 0.08634$, $p = 0.7700$), or drug x strain x sex interaction ($F_{1, 53} = 0.06667$, $p = 0.7973$) between the groups analysed.

Collectively these data indicate that female Tg mice performed slightly better than the control Tg mice when treated with the CSF1R inhibitor GW2580, but this different was not significant and all groups performed with equal efficiency in probe test.

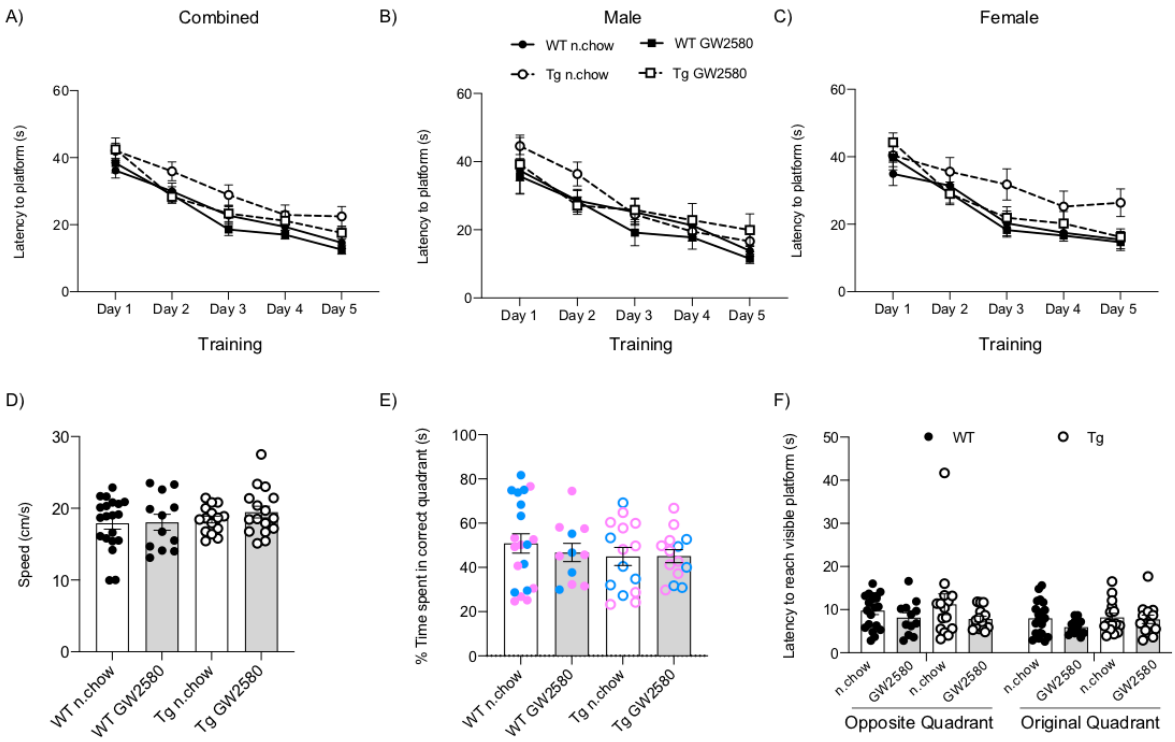

Figure 5.6.2.1: Performance of APP/PS1 versus WT mice on a spatial and non-spatial memory task in Morris Water Maze (MWM). The latency to reach the hidden platform in combined sex (A), Male (B) and Female (C) and swim speed (D) was assessed in Tg n.chow (n=15) and Tg GW2580 (n=14) mice and WT n.chow (n=20) and WT GW2580 (n=12) mice in the spatial memory water maze task across 20 trials over 5 days. Probe test performed after the 20 training trials (E) and non-spatial memory (flag trial; F) in Tg and WT mice. Data are shown as mean ± SEM and were analysed by two-way repeated measure ANOVA with drug treatment as between subject factors and training days as within subject factors (A, B, C) or by two-way ANOVA (D, E, F).

5.6.3 Working memory in the T-maze

Animals were assigned to drug (diet containing (w/w) 0.1 % of GW2580) or placebo treatment groups and left on the treatment for 3 months before performing any behavioural tests. In the T-maze working memory task, memory was assessed in Tg n.chow (n=16), Tg GW2580 (n=14) and WT n.chow (n=20), WT GW2580 (n=12) mice by spontaneous alternation, over 2 days, 5 trials per day. Tg n.chow were impaired on the task compared to WT controls, validating the animal model used, but GW2580 did not have any effect on improving this observation (Figure 5.6.3.1). Two-way ANOVA with genotype and drug as factors revealed a significant effect of genotype ($F_{1, 58} = 4.076$, $p = 0.0481$) but no significant effect of drug ($F_{1, 58} = 0.1734$, $p = 0.6786$) or interaction between these two factors ($F_{1, 58} = 1.386$, $p = 0.2438$).

Having observed worse performance of Tg female mice than Tg male mice in the MWM learning task, a separate two-way ANOVA with drug and sex as factors in Tg animals only was performed here to see whether the Tg female mice were worse in this task too. However, the performance of Tg female and Tg male mice were not different in T-maze spontaneous alternation task. No significant main effect of sex ($F_{1, 26} = 0.5369$, $p = 0.4703$) or drug ($F_{1, 26} = 0.7635$, $p = 0.3902$) or interaction ($F_{1, 26} = 0.7911$, $p = 0.3819$) was found.

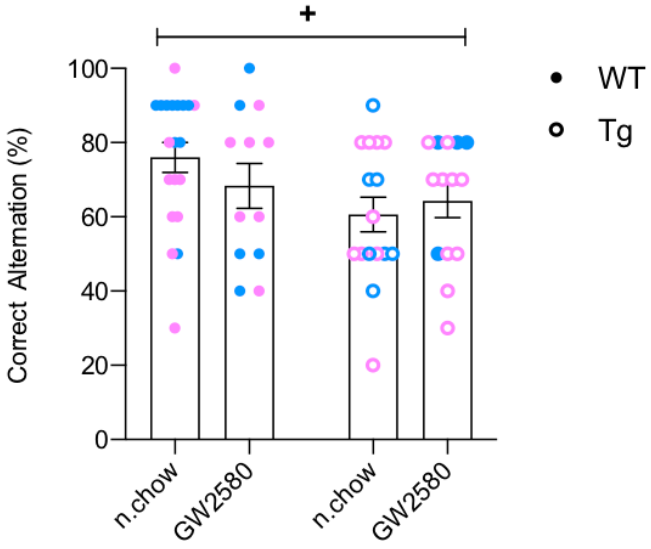

Figure 5.6.3.1: Performance of APP/PS1 versus WT mice on a working memory task. Working memory was assessed in Tg n.chow (n=16) and Tg GW2580 (n=14) mice and WT n.chow (n=20) and WT GW2580 (n=12) mice by spontaneous T-maze alternation, over 2 days, 5 trials per day. Data are shown as mean ± SEM and were analysed by two-way ANOVA. Main effects of genotype are depicted by $^{+}p < 0.05$.

5.6.4 Open field activity and anxiety like behaviour

Animals were assigned to drug (diet containing 0.1 % (w/w) of GW2580) or placebo treatment groups and left on the treatment for 3 months before performing any behavioural tests. Distance travelled (Figure 5.6.4.1, panel A) and number and time in rears (Figure 5.6.4.1, panels B-C) in the open field were recorded for 5 mins in mice from Tg n.chow (n=15), Tg GW2580 (n=14) and WT n.chow (n=20), WT GW2580 (n=12) mice. APP/PS1 mice were slightly more active in the open field compared to WT controls and GW2580 reduced activity in both genotypes. Two-way ANOVA with genotype and drug as factors reveled a significant effect of genotype ($F_{1, 57}$ = 7.079, p = 0.0101) and drug ($F_{1, 57}$ = 5.852, p = 0.0188) but no significant interaction between these two factors ($F_{1, 57}$ = 0.09059, p = 0.7645) was observed.

No difference was observed in the number of rears in any of the groups. Two-way ANOVA with genotype and drug as factors revealed no significant effect of genotype ($F_{1, 57}$ = 7.079, p = 3.216), drug ($F_{1, 57}$ = 0.1535, p = 0.6967) or interaction between these two factors ($F_{1, 57}$ = 1.440, p = 0.2351). Although there were no differences in the number of rears, WT were found to spend more time in rearing than APP/PS1 mice. Two-way ANOVA with genotype and drug as factors revealed a significant effect of genotype ($F_{1, 57}$ = 74.753, p = 0.0344) but no significant effect of drug ($F_{1, 57}$ = 0.01308, p = 0.9093) or interaction between these two factors ($F_{1, 57}$ = 3.162, p = 0.0807) was observed.

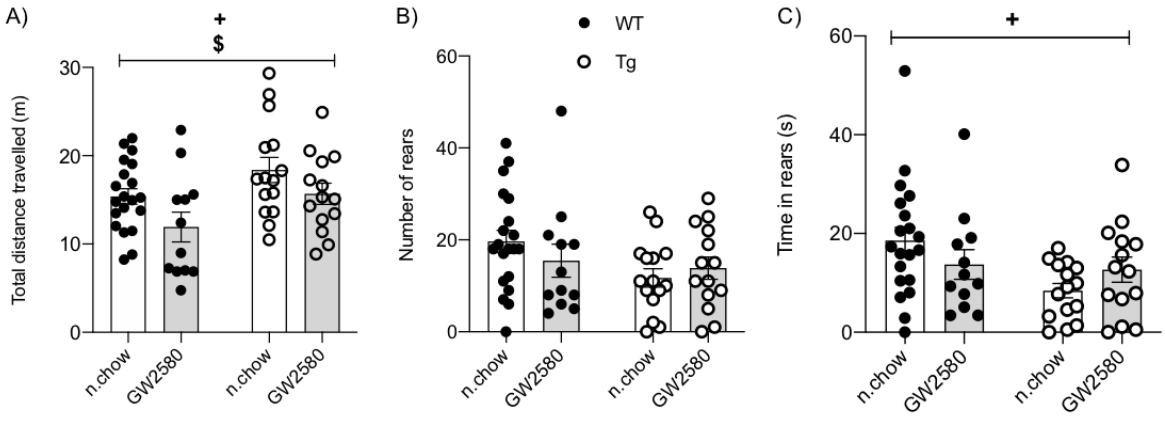

Figure 5.6.4.1: Open field activity in APP/PS1 versus WT mice. Distance travelled in open field by Tg n.chow (n=15) and Tg GW2580 (n=14) mice and WT n.chow (n=20) and WT GW2580 (n=12) mice (A). The number of rears recorded in open field, across 5 min (B). The amount of time spent in rearing during this 5 min (C). Data are shown as mean ± SEM and were analysed by two-way ANOVA. Main effects of genotype and drug are depicted by $^{+}p < 0.05$ and $^{\$}p < 0.05$, respectively.

5.6.5 Effect of GW2580 on Aβ in APP/PS1 mice

After 3 months of treatment, and following behavioural analysis, animals were euthanised. Extraction of protein from hippocampal homogenate was performed by homogenising the tissue in CHAPS lysis buffer before centrifuging it to collect the supernatant. Protein concentration in the supernatant was determined and samples were prepared. Resulting from the female-selective effects observed in cognitive testing, and published literature on more advanced pathology in female APP/PS1 mice, female mice only were used in the analysis of expression of proteins associated with AD-like disease in this model. The effect of GW2580 on Aβ levels was examined by Western immunoblot using anti-Aβ antibody (6E10) in female mice from Tg n.chow (n=10), Tg GW2580 (n=8) and WT normal chow (n=10) and WT GW2580 (n=8) groups. The results for Aβ monomer and probable dimer levels were normalised to actin as loading control (Figure 5.6.5.1) for all mice analysed.

As the 6E10 antibody specifically detects human Aβ, APP/PS1 Tg mice showed a very robust expression of human Aβ monomer and dimer with this antibody, while the WT mice did not show any human Aβ expression. GW2580 did not make any difference to Aβ expression levels in Tg mice as shown by unpaired t-test (p = 0.5394).

5.6.6 Effect of GW2580 on synapses in APP/PS1 mice

The effect of GW2580 on synaptic markers PSD95 and synaptophysin was examined by Western immunoblot in female mice from Tg n.chow (n=10), Tg GW2580 (n=8) and WT n.chow (n=10) and WT GW2580 (n=8) groups. The resultant bands for these two markers were normalised to actin as loading control (Figure 5.6.6.1) and examples from half of each cohort are presented.

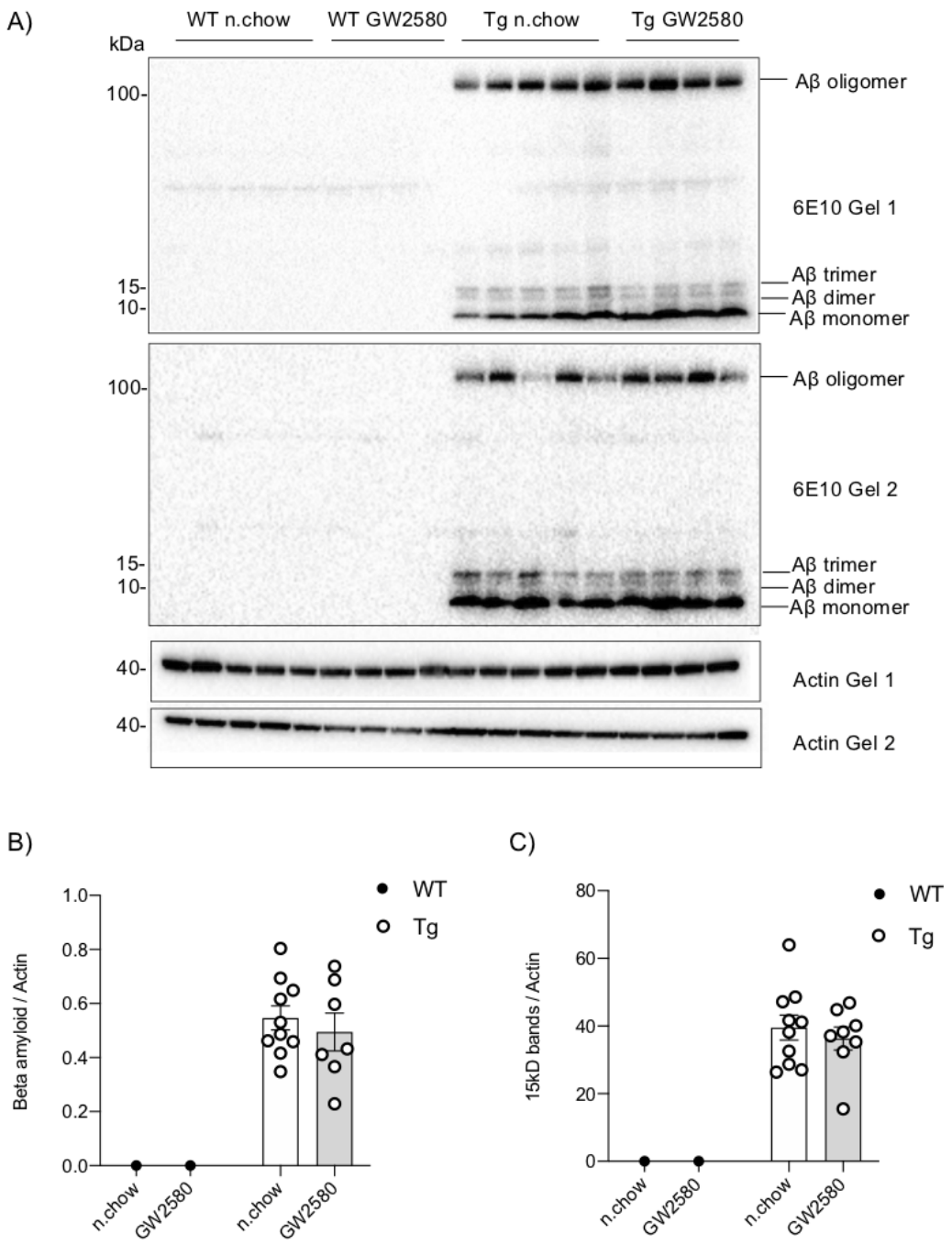

Figure 5.6.5.1: Effect of GW2580 on Aβ in female APP/PS1 mice. Expression of APP and Aβ (A). Extracts were equally distributed and resolved on two identical SDS-PAGE gels (Tg n.chow (n=10) and Tg GW2580 (n=8) and WT n.chow (n=10) and WT GW2580 (n=8)) and blotted with 6E10, an antibody directed against a synthetic sequence from human APP, present in Aβ. Bands were quantified by densitometry and normalized to actin for both the 10 kDa bands (B) and 15 kDa bands (C). Data are shown as mean ± SEM and were analysed by unpaired-t test.

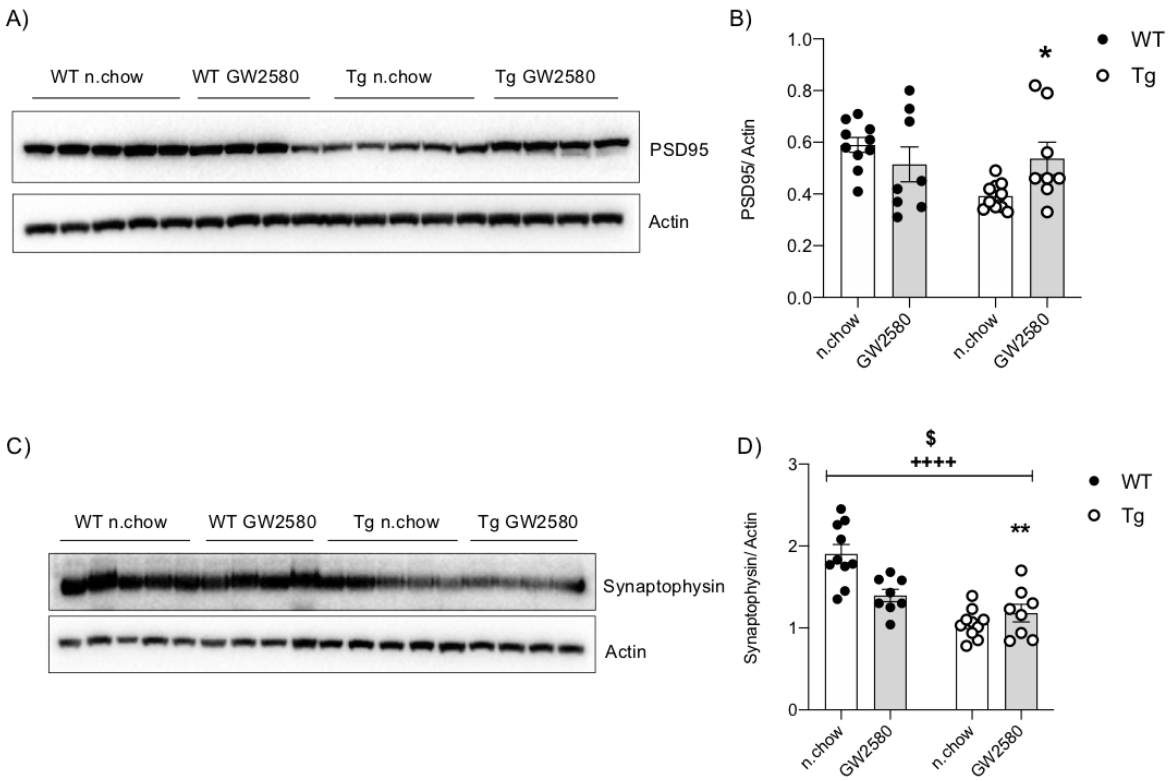

Figure 5.6.6.1: Effect of GW2580 on synapses in female APP/PS1 and WT mice. Expression of PSD95 and synaptophysin (A, C). Extracts were equally distributed and resolved on two identical SDS-PAGE gels (Tg n.chow (n=10) and Tg GW2580 (n=8) and WT n.chow (n=10) and WT GW2580 (n=8)) and blotted with antibodies against PSD95 and Synaptophysin (only one gel from each analysis is presented). Bands from both sets of gels were quantified by densitometry and normalized to actin for both PSD95 and synaptophysin (B, D). Data are shown as mean ± SEM and were analysed by two-way ANOVA. Main effects of genotype and drug are depicted by $^{++++}p < 0.0001$ and $^{\$}p < 0.05$, respectively and interaction between drug and genotype are depicted by $*p < 0.05$, $**p < 0.01$.

A decrease in PSD95 expression was noticed in Tg n.chow mice and GW2580 reverted this WT levels. Two-way ANOVA with genotype and drug as factors showed a genotype-associated decrease that was not quite significant ($F_{1,32}$ =3.703, p = 0.0632) but there was a significant interaction between genotype and drug ($F_{1, 32}$ = 6.012, p = 0.0198) reflecting the increased PSD95 levels in drug-treated APP/PS1 mice. A similar trend was observed in the expression of synaptophysin. Two-way ANOVA with genotype and drug as factors revealed a significant effect of genotype ($F_{1, 32}$ = 33.40, p <0.0001) and a significant interaction between genotype and drug ($F_{1, 32}$ = 11.92, p = 0.0016).

5.6.7 Effect of GW2580 on astrocytes in APP/PS1

The effect of GW2580 on astrocyte marker, GFAP expression was examined next by Western immunoblot in the same homogenates prepared from female Tg n.chow (n=10), Tg GW2580 (n=8) and WT n.chow (n=10) and WT GW2580 (n=8) groups. The resultant bands for GFAP were normalised to actin as loading control (Figure 5.6.7.1) and examples from half of each cohort are presented. Expression of GFAP increased in Tg n.chow mice compared to WT control and GW2580 brought it down to WT expression levels. Two-way ANOVA with genotype and drug as factors revealed a trend, but no significant effect of genotype ($F_{1, 32}$ = 0.1136, p = 0.7383) but a significant interaction between genotype and drug ($F_{1, 32}$ = 22.84, p <0.0001) reflecting the reduction in GFAP levels in GW2580-treated Tg mice.

5.6.8 Effect of GW2580 on microglia in APP/PS1

The effect of GW2580 on microglial marker, Iba1 expression, was examined by Western immunoblot in female mice from Tg n.chow (n=10), Tg GW2580 (n=8) and WT n.chow (n=10) and WT GW2580 (n=8) groups. The resultant bands for Iba1 were normalised to actin as loading control (Figure 5.6.8.1) and examples from half of each cohort are presented. As expected, the number of microglia was increased robustly in Tg normal chow mice compared to WT controls and GW2580 appeared to return it towards control levels. Two-way ANOVA with genotype and drug as factors revealed a significant effect of genotype ($F_{1, 32}$ = 9.524, p = 0.0042) and a trend towards an effect of drug ($F_{1, 32}$ = 3.190, p = 0.0836). No significant interaction ($F_{1, 32}$ = 0.08558, p = 0.7718) was observed and Bonferronni post-hoc analysis revealed no significant differences between Tg normal chow vs Tg GW2580 mice (p = 0.9084).

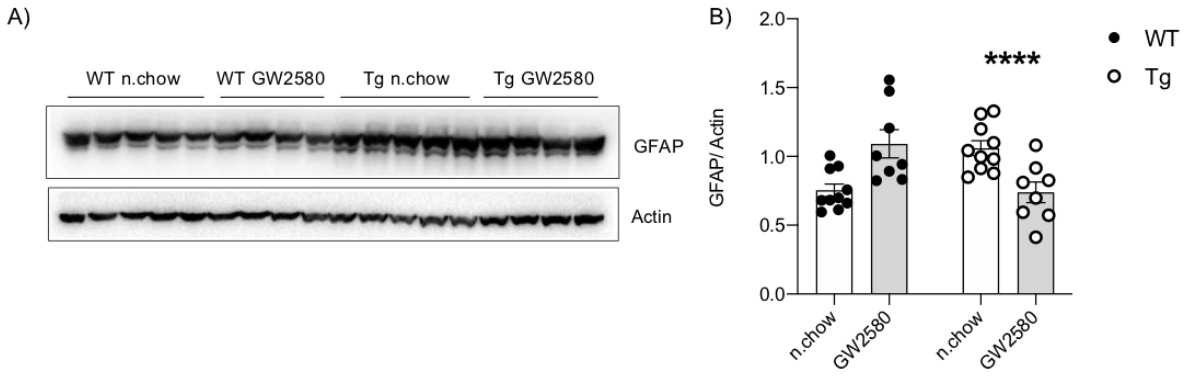

Figure 5.6.7.1: Effect of GW2580 on astrocytes in female APP/PS1 and WT mice. Expression of GFAP(A). Extracts were equally distributed and resolved on two identical SDS-PAGE gels (Tg n.chow (n=10) and Tg GW2580 (n=8) and WT n.chow (n=10) and WT GW2580 (n=8)) and blotted with antibodies against GFAP (only one gel from each analysis is presented). Bands from both sets of gels were quantified by densitometry and normalized to actin (B). Data are shown as mean ± SEM and were analysed by two-way ANOVA. Interaction between drug and genotype are depicted by ****$p < 0.0001$.

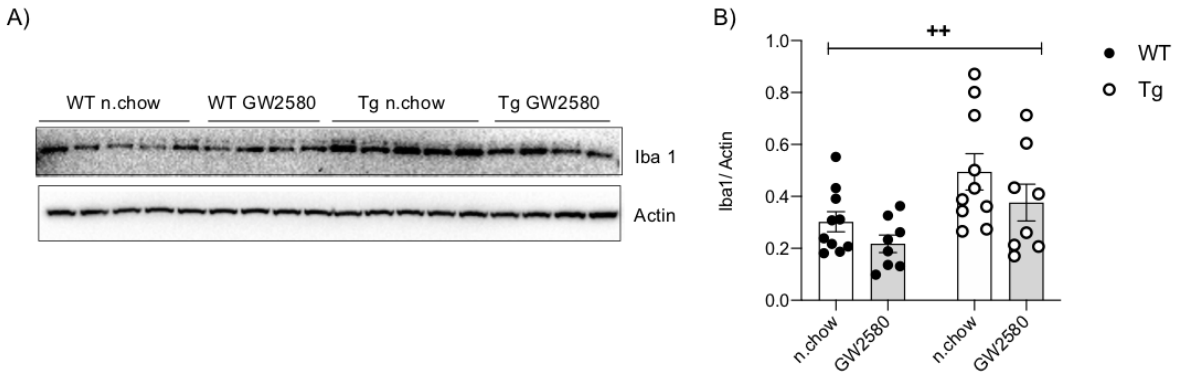

Figure 5.6.8.1: Effect of GW2580 on Iba1 in female APP/PS1 and WT mice. Expression of Iba1 (A). Extracts were equally distributed and resolved on two identical SDS-PAGE gels (Tg n.chow (n=10) and Tg GW2580 (n=8) and WT n.chow (n=10) and WT GW2580 (n=8)) and blotted with antibodies against Iba 1 (only one gel from each analysis is presented). Bands from both sets of gels were quantified by densitometry and normalized to actin (B). Data are shown as mean ± SEM and were analysed by two-way ANOVA with Bonferroni post-hoc tests. Main effects of genotype are depicted by $^{++}p < 0.01$.

5.6.9 GW2580 inhibits hippocampal microglial proliferation in APP/PS1 mouse

Animals assigned to drug (diet containing 0.1 % (w/w) of GW2580) or placebo treatment for 3 months were euthanised for the isolation of microglia from the mouse hippocampus of male and female mice. Microglia were isolated using fluorescence activated cell sorting (FACS) and their frequency in the population among dissociated cells in Tg n.chow (n=14), Tg GW2580 (n=7) and WT n.chow (n=12), WT GW2580 (n=5) was analysed (Figure 5.6.9.1).

A trend of increased microglial number was noticed in Tg normal chow mice compared to WT controls, although this did not reach significance (effect of genotype, $F_{1, 34} = 2.777$, $p = 0.1048$) and this appeared to be mitigated by GW2580 treatment, validating the efficacy of the drug. Two-way ANOVA with genotype and drug as factors revealed a significant interaction between genotype and drug ($F_{1, 34} = 10.06$, $p = 0.0032$), meaning that the drug has had a different effect contingent on the genotype. However, Bonferroni pairwise comparison did not show a significant difference between Tg GW2580 and Tg normal chow ($p = 0.2070$).

When analysis of microglial number was performed only in female mice, there was a significant main effect of genotype ($F_{1, 15} = 5.869$, $p = 0.0285$) and an interaction between genotype and drug ($F_{1, 15} = 13.08$, $p = 0.0025$) and this was not the case when a separate analysis was performed in male mice (genotype: $F_{1, 15} = 0.041220$, $p = 0.8419$ and interaction: ($F_{1, 15} = 1.533$, $p = 0.2348$). When the full Tg data set was analysed to examine whether two-way ANOVA analysis detected a main effect of sex on microglial number, the observed trend was not significant: no significant main effect of sex ($F_{1, 17} = 2.601$, $p = 0.1252$) or drug ($F_{1, 17} = 4.091$, $p = 0.0591$) or interaction between the two factors ($F_{1, 17} = 2.023$, $p = 0.1730$) was observed.

Taken together, this shows that although the study lacked statistical power to demonstrate a significant sex difference, microglial proliferation increases are significant in female APP/PS1 mice but not in male APP/PS1 mice and that GW2580 did mitigate this disease-associated increase in microglial numbers. While all the subsequent real-time quantitative polymerase chain reaction (RT-qPCR) analysis were performed on both sexes, since the number of microglial isolates available was relatively limited, only female animals were used in Western immunoblot analyses earlier in this chapter.

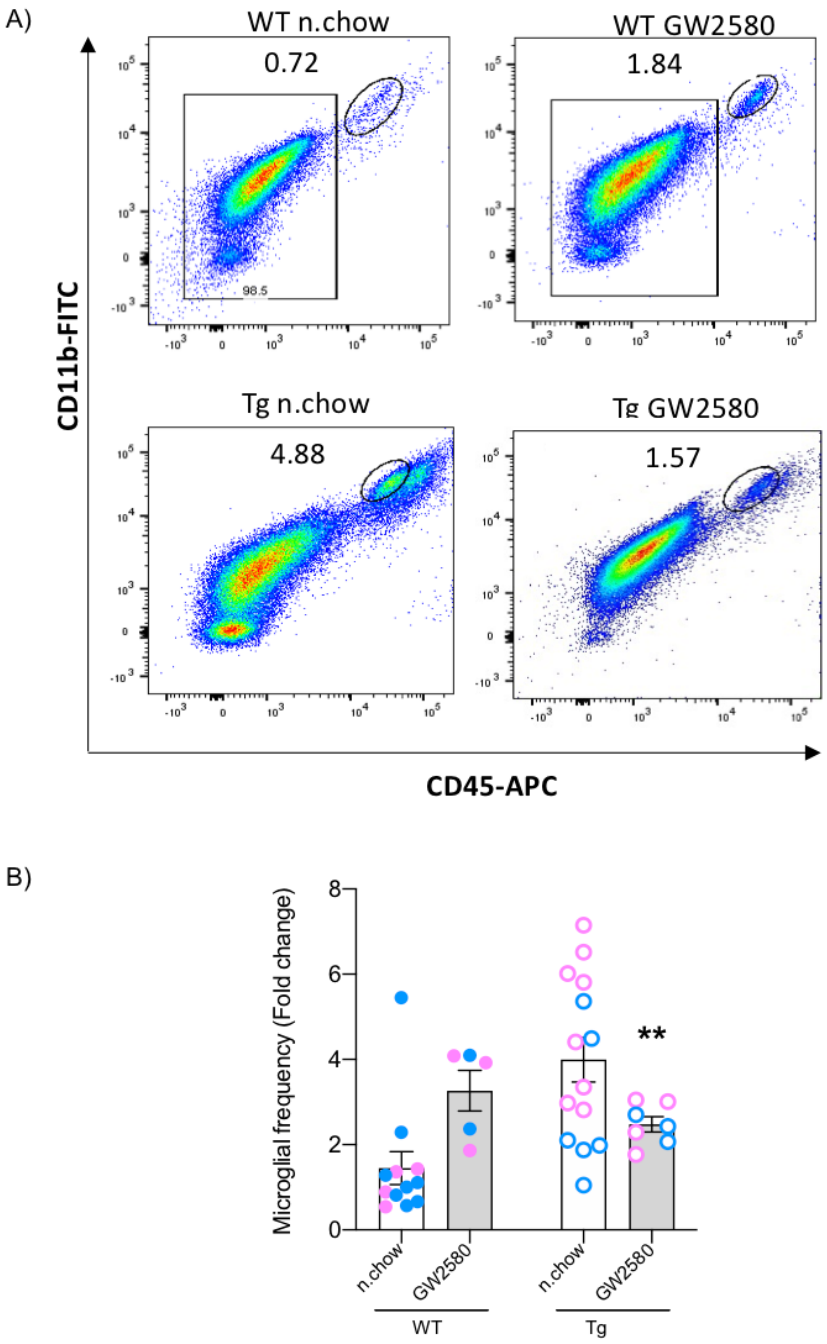

Figure 5.6.9.1: Fluorescence-activated cell sorted (FACS) microglial frequency in normal and APP/PS1 mouse hippocampus. Representative flow cytometry images showing frequency of CD44lowCD11b+ microglia. Graph showing frequency of microglia from Tg n.chow (n=14) and Tg GW2580 (n=7), WT n.chow (n=12) and WT GW2580 (n=5) (B). Data are shown as mean ± SEM, pink representing microglial frequency in female and blue representing microglial frequency in male mice and were analysed by two-way ANOVA with Bonferroni post-hoc tests. Interaction between drug and genotype are depicted by **p = 0.0032.

5.6.10 Effect of GW2580 on the expression of microglial and neuroinflammatory genes in microglia isolated by FACS

RNA was extracted from microglia isolated by FACS to examine their phenotype and to assess whether GW2580 (0.1 %) affects the mRNA expression of certain constitutive and neuroinflammatory microglial genes in Tg n.chow (n=14), Tg GW2580 (n=7) and WT n.chow (n=12), WT GW2580 (n=5) mice. Gene expression was analysed by RT-qPCR. Two-way ANOVA was used with genotype and drug as factors for statistical analysis performed on both sexes combined. To determine whether GW2580 affected gene expression differentially in male and female mice, two-way ANOVA with sex and drug as factors was performed in Tg mice only. These statistical analyses are shown (for all genes analysed) in Tables 5.6.10.1 – 5.6.14.1 and the data are represented in Figures 5.6.10.1 – 5.6.14.1.

Tyrobp and *Trem2* mRNA expression were modestly increased in Tg mice on normal chow compared to WT controls and GW2580 treatment lowered expression of both towards WT levels, although this did not reach statistical significance. *Trem2* expression was higher in male Tg mice and GW2580 lowered this more markedly in male Tg mice. Sex differences were not apparent with *Tyrobp*. A trend towards reduced *Sall1* was seen in Tg mice compared to WT mice but there were no effects of drug or sex on *Sall1* expression. *P2ry12* expression was lower in Tg mice on normal chow compared to WT controls but GW2580 treatment of Tg mice did not affect its expression. However, GW2580 was found to have a significantly larger effect in WT mice than in Tg mice. Indicating a change to the baseline homeostatic state.

	(i) 2-way ANOVA			(ii) 2-way ANOVA		
	Strain x Drug			Drug x Sex (in Tg only)		
Gene	**Factor**	***F***	***P***	**Factor**	***F***	***P***
Tyrobp	Strain	$F_{1, 34} = 0.09383$	0.7612	GW2580	$F_{1, 17} = 3.125$	0.095
	GW2580	$F_{1, 34} = 1.063$	0.3097	Sex	$F_{1, 17} = 0.1858$	0.6719
	Interaction	$F_{1, 34} = 2.355$	0.1341	Interaction	$F_{1, 17} = 0.5590$	0.4649
Sall1	Strain	$F_{1, 34} = 2.923$	0.0964	GW2580	$F_{1, 17} = 0.8877$	0.3593
	GW2580	$F_{1, 34} = 0.07210$	0.7899	Sex	$F_{1, 17} = 0.8951$	0.3574
	Interaction	$F_{1, 34} = 0.9076$	0.3475	Interaction	$F_{1, 17} = 0.8356$	0.3734
Trem2	Strain	$F_{1, 34} = 0.04789$	0.8281	GW2580	$F_{1, 17} = 6.071$	**0.0247**
	GW2580	$F_{1, 34} = 1.142$	0.2927	Sex	$F_{1, 17} = 7.014$	**0.0169**
	Interaction	$F_{1, 34} = 1.011$	0.3217	Interaction	$F_{1, 17} = 5.651$	**0.0295**
P2ry12	Strain	$F_{1, 34} = 5.969$	**0.0199**	GW2580	$F_{1, 17} = 0.3602$	0.5563
	GW2580	$F_{1, 34} = 2.869$	0.0994	Sex	$F_{1, 17} = 3.934$	0.0637
	Interaction	$F_{1, 34} = 4.154$	**0.0494**	Interaction	$F_{1, 17} = 0.2976$	0.5925

Table 5.6.10.1: mRNA expression of Tyrobp, Sall1, Trem2 and P2ry12 gene in hippocampal microglial isolates from APP/PS1 and WT mice. Statistical analysis examined (i) main effects of strain, drug and interaction of strain and drug and (ii) main effects of drug, sex and interaction between drug and sex by two-way ANOVA. Data in bold indicate significant effects.

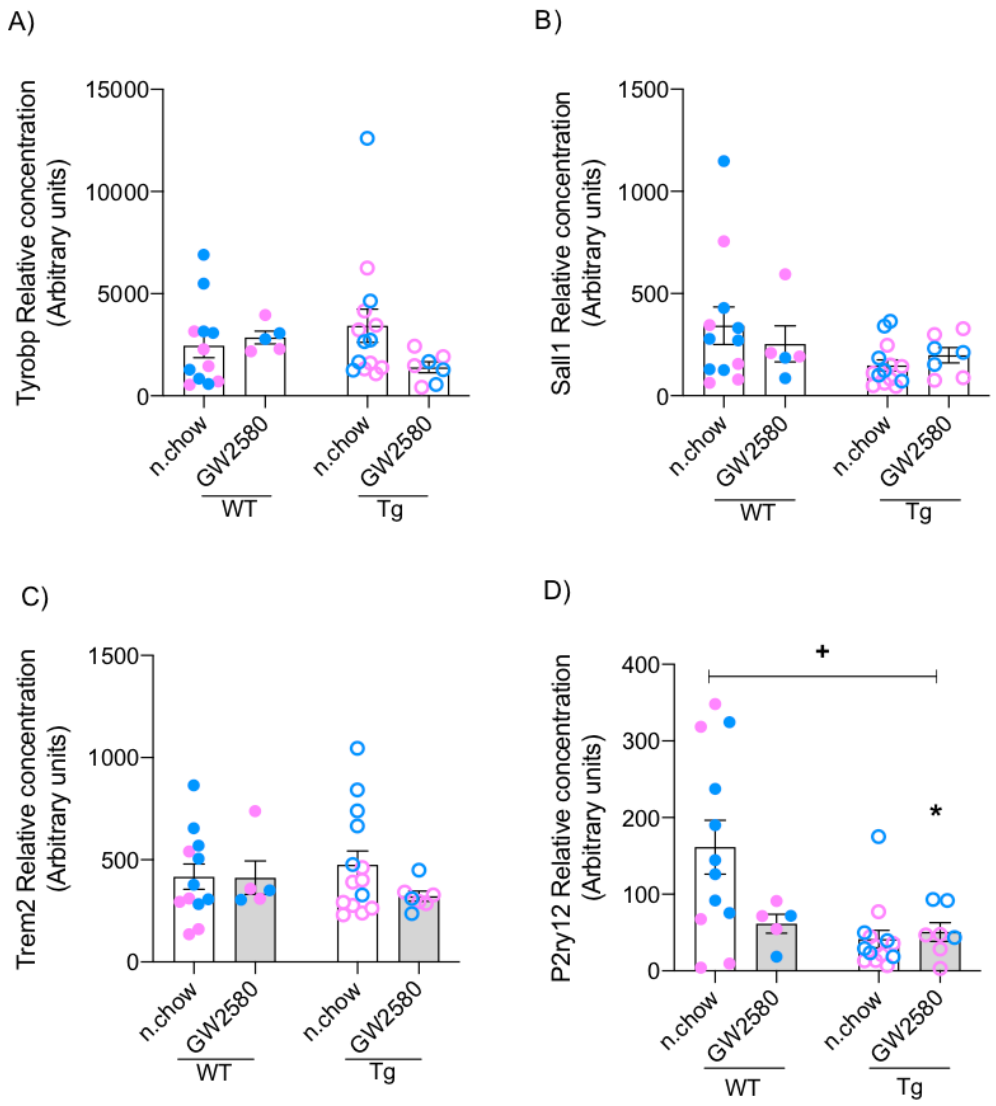

Figure 5.6.10.1: Effect of GW2580 on the expression of constitutive genes in microglia isolated from WT and APP/PS1 mouse hippocampus by FACS. mRNA expression of *Tyrobp* (A), *Sall1* (B), *Trem2* (C) and *P2ry12* (D) in microglia isolated from Tg n.chow (n=14) and Tg GW2580 (n=7), WT n.chow (n=12) and WT GW2580 (n=5) mice. Data are shown as mean ± SEM, pink representing microglial isolates from female and blue representing microglial isolates from male mice. Data were analysed by two-way ANOVA. Main effects of genotype and interaction between drug and genotype are depicted by $^{+}p < 0.05$ and by $*p < 0.05$, respectively.

5.6.11 Effect of GW2580 on the expression of primed/DAM genes in microglia isolated by FACS

Whether GW2580 (0.1 %) affects the mRNA expression of microglial genes implicated in the expression profile of primed and/or DAM phenotypes was examined.

Itgax mRNA expression increased in Tg mice on normal chow compared to WT controls and Tg mice treated with GW2580 lowered their expression back to WT control levels. GW2580 was not seen to differentially affect the expression of this gene in male or in female mice.

Clec7a mRNA expression increased in Tg mice on normal chow compared to WT controls and Tg mice treated with GW2580 showed a trend to lower its expression. GW2580 showed a trend towards lowering of *Clec7a* in male mice, though this was not significant.

Apoe mRNA expression increased in Tg mice on normal chow compared to WT controls and Tg mice treated with GW2580 reduced its expression. However, GW2580 was not found to differentially affect the expression of this gene in male vs. female mice.

Lpl mRNA expression increased in Tg mice on normal chow compared to WT controls and Tg mice treated with GW2580 reduced its expression, although this did not reach statistical significance. GW2580 was not observed to differentially affect the expression of this gene according to sex.

Overall, GW2580 reduced expression of most DAM genes in Tg mice and there was a tendency for this to be more marked in male mice.

	(i) 2-way ANOVA			(ii) 2-way ANOVA		
	Strain x Drug			Drug x Sex (in Tg only)		
Gene	**Factor**	***F***	***P***	**Factor**	***F***	***P***
Itgax	Strain	$F_{1, 33} = 4.504$	**0.0414**	GW2580	$F_{1, 17} = 6.068$	**0.0247**
	GW2580	$F_{1, 33} = 3.580$	0.0673	Sex	$F_{1, 17} = 0.4121$	0.5295
	Interaction	$F_{1, 33} = 5.804$	**0.0217**	Interaction	$F_{1, 17} = 0.1577$	0.6962
Clec7a	Strain	$F_{1, 34} = 7.670$	**0.009**	GW2580	$F_{1, 17} = 1.728$	0.2061
	GW2580	$F_{1, 34} = 0.2716$	0.6057	Sex	$F_{1, 17} = 0.001374$	0.9709
	Interaction	$F_{1, 34} = 1.317$	0.2592	Interaction	$F_{1, 17} = 3.961$	0.0629
Apoe	Strain	$F_{1, 34} = 8.175$	**0.0072**	GW2580	$F_{1, 17} = 6.814$	**0.0183**
	GW2580	$F_{1, 34} = 3.411$	0.0735	Sex	$F_{1, 17} = 0.004744$	0.9459
	Interaction	$F_{1, 34} = 4.438$	**0.0426**	Interaction	$F_{1, 17} = 2.479$	0.1338
Lpl	Strain	$F_{1, 34} = 3.650$	0.0645	GW2580	$F_{1, 17} = 4.995$	**0.0391**
	GW2580	$F_{1, 34} = 1.538$	0.2234	Sex	$F_{1, 17} = 0.7620$	0.3949
	Interaction	$F_{1, 34} = 3.367$	0.0753	Interaction	$F_{1, 17} = 3.053$	0.0986

Table 5.6.11.1: mRNA expression of Itgax, Clex7a, Apoe and Lpl gene in hippocampal microglial isolates from APP/PS1 and WT mice. Statistics depicts (i) main effects of strain, drug and interaction of strain and drug and (ii) main effects of drug, sex and interaction between drug and sex by two-way ANOVA. Data in bold indicate significant effects.

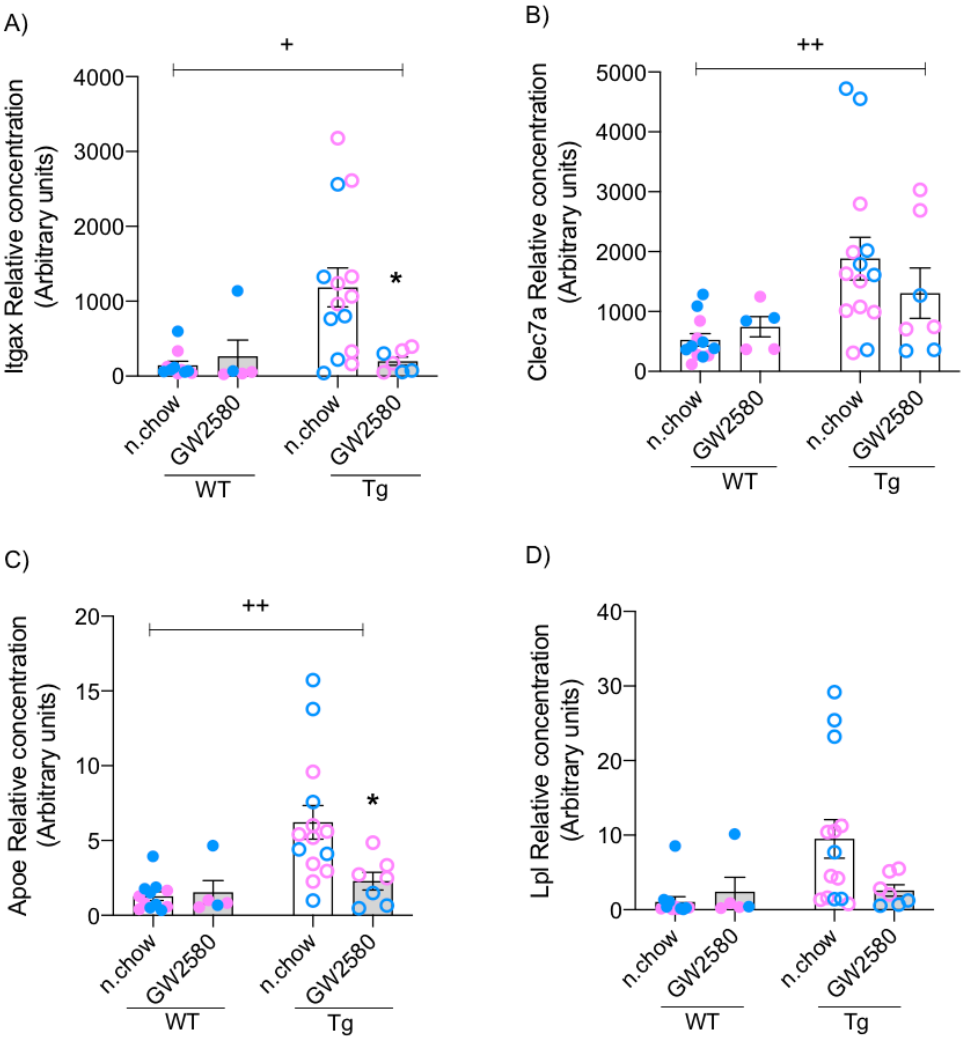

Figure 5.6.11.1: Effect of GW2580 on the expression of primed/DAM genes in microglia isolated from WT and APP/PS1 mouse hippocampus by FACS. mRNA expression of *Itgax* (A), *Clec7a* (B), *Apoe* (C) and *Lpl* (D) in microglia isolated from Tg n.chow (n=14) and Tg GW2580 (n=7), WT n.chow (n=12) and WT GW2580 (n=5) mice. Data are shown as mean ± SEM, pink representing microglial isolates from female and blue representing microglial isolates from male mice, Data were analysed by two-way ANOVA. Main effects of genotype are depicted by $^{+}p < 0.05$ and $^{++}p < 0.01$ and interaction between genotype and drug are depicted by $*p < 0.05$.

5.6.12 Effect of GW2580 on the expression of other neuroinflammatory genes in microglia isolated by FACS.

The mRNA expression of further microglial genes: *Cybb* (NADPH oxidase subunit), complement factor 1q (*C1q*) and *Tgfb*, were analysed by RT-qPCR in isolated microglia (Table 5.6.12.1 and Figure 5.6.12.1).
Cybb mRNA expression increased markedly in Tg mice on normal chow compared to WT controls and GW2580 reduced this expression in Tg mice, although this did not reach statistical significance. GW2580 did significantly affect expression when examined in Tg mice only but an apparent selective effect on male mice did not reach statistical significance.

C1q mRNA expression remained unchanged in Tg mice compared to WT controls but GW2580 showed a trend to reduce *C1q* expression in both WT and Tg mice, although this was also not quite significant. *C1q* also tended to be higher in males but this also was not quite significant.

There was not a significant difference in *Tgfb* mRNA expression between Tg and WT mice. However, GW2580 decreased *Tgfb* mRNA expression selectively in WT mice and this was not different according to sex.

The data indicate that *Tgfb*, which is a controller of the homeostatic state, is reduced by GW2580 in normal mice and that GW2580 can reduce other aspects of the activated phenotype in Tg mice but in ways that are quite different depending on the gene examined.

	(i) 2-way ANOVA			(ii) 2-way ANOVA		
	Strain x Drug			Drug x Sex (in Tg only)		
Gene	**Factor**	***F***	***P***	**Factor**	***F***	***P***
Cybb	Strain	$F_{1, 30} = 1.713$	0.2006	GW2580	$F_{1, 17} = 5.580$	**0.0304**
	GW2580	$F_{1, 30} = 1.639$	0.2103	Sex	$F_{1, 17} = 0.01459$	0.9053
	Interaction	$F_{1, 30} = 2.986$	0.0942	Interaction	$F_{1, 17} = 2.634$	0.123
C1q	Strain	$F_{1, 34} = 1.496$	0.2298	GW2580	$F_{1, 17} = 2.441$	0.1366
	GW2580	$F_{1, 34} = 3.455$	0.0717	Sex	$F_{1, 17} = 4.243$	0.0551
	Interaction	$F_{1, 34} = 0.03460$	0.8535	Interaction	$F_{1, 17} = 1.516$	0.2349
Tgfb	Strain	$F_{1, 34} = 0.4872$	0.4899	GW2580	$F_{1, 17} = 1.261$	0.2771
	GW2580	$F_{1, 34} = 1.765$	0.1928	Sex	$F_{1, 17} = 0.7833$	0.3885
	Interaction	$F_{1, 34} = 4.790$	**0.0356**	Interaction	$F_{1, 17} = 0.0002351$	0.9879

Table 5.6.12.1: mRNA expression of Cybb, C1q, Tgfb gene in hippocampal microglial isolates from APP/PS1 and WT mice. Statistics depicts (i) main effects of strain, drug and interaction of strain and drug and (ii) main effects of drug, sex and interaction between drug and sex by two-way ANOVA. Data in bold indicate significant effects.

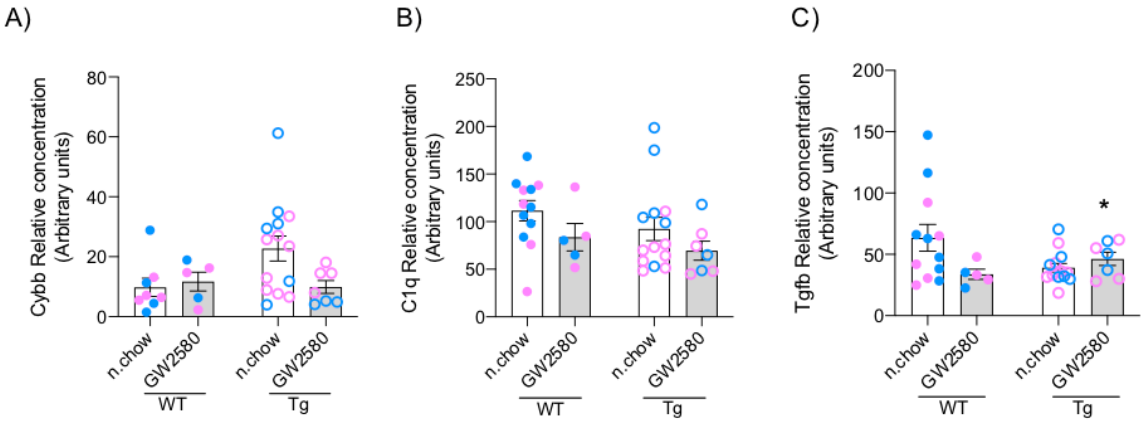

Figure 5.6.12.1: Effect of GW2580 on the expression of other neuroinflammatory genes in microglia isolated from WT and APP/PS1 mouse hippocampus by FACS. mRNA expression of *Cybb* (A) and *C1q* (B) and *Tgfb* (C) in microglia isolated from Tg n.chow (n=14) and Tg GW2580 (n=7), WT n.chow (n=12) and WT GW2580 (n=5) mice. Data are shown as mean ± SEM, pink representing microglial isolates from female and blue representing microglial isolates from male mice, only in graphs where GW2580 affected gene expression significantly in either male or in female group. Data were analysed by two-way ANOVA. Interaction between genotype and drug are depicted by *$p < 0.05$.

5.6.13 Effect of GW2580 on levels of Cathepsin D and Cystatin F gene expression and protein levels in APP/PS1 and WT hippocampal homogenates

The lysosomal genes, *Ctsd (cathepsin D)* and *Cst7 (cystatin F),* were analysed in microglial isolates by RT-qPCR (Table 5.6.13.1 and Figure 5.6.13.1, panels A and B). The effect of GW2580 on cathepsin D and cystatin F protein expression was also examined here, by Western immunoblot in hippocampal homogenates from female Tg n.chow (n=10), Tg GW2580 (n=8) and WT n.chow (n=10) and WT GW2580 (n=8) groups. The resultant bands for these proteins were normalised to actin as loading control (Figure 5.6.13.1, panels C and D).

Ctsd mRNA expression increased in Tg mice on normal chow compared to WT controls, and GW2580 reversed this expression pattern back to WT control levels. A significant effect of drug was apparent in an analysis of all Tg mice. The trend that GW2580 reduced disease induced *Ctsd* was not quite significant. However, cathepsin D protein expression, when examined in hippocampal homogenates, did not show a difference between Tg and WT mice on normal chow and no effect of GW2580 was found.

Cst7 mRNA expression showed a large increase in Tg mice on normal chow compared to WT controls, and GW2580 reduced its expression back to WT control levels. A significant reduction of *Cst7* expression was apparent in an analysis of all Tg mice and this appeared to be more marked in male mice, although the interaction of drug and sex was not significant. The expression of cystatin F protein showed a similar pattern, where a robust increase in cystatin F was observed in Tg mice compared to WT controls and GW2580 treatment of Tg mice lowered cystatin F expression. However, this did not reach statistical significance.

	(i) 2-way ANOVA			(ii) 2-way ANOVA		
	Strain x Drug			Drug x Sex (in Tg only)		
Gene	**Factor**	***F***	***P***	**Factor**	***F***	***P***
Ctsd	Strain	$F_{1, 34} = 3.455$	0.0717	GW2580	$F_{1, 17} = 6.983$	**0.0171**
	GW2580	$F_{1, 34} = 2.462$	0.1259	Sex	$F_{1, 17} = 1.098$	0.3093
	Interaction	$F_{1, 34} = 2.773$	0.1051	Interaction	$F_{1, 17} = 4.042$	0.0605
Cst7	Strain	$F_{1, 34} = 3.719$	0.0622	GW2580	$F_{1, 17} = 5.755$	**0.0282**
	GW2580	$F_{1, 34} = 2.217$	0.1457	Sex	$F_{1, 17} = 0.5859$	0.4545
	Interaction	$F_{1, 34} = 2.790$	0.104	Interaction	$F_{1, 17} = 4.113$	0.0585

Table 5.6.13.1: mRNA expression of Ctsd and Cst7 gene in hippocampal microglial isolates from APP/PS1 and WT mice. Statistics depicts (i) main effects of strain, drug and interaction of strain and drug and (ii) main effects of drug, sex and interaction between drug and sex by two-way ANOVA. Data in bold indicate significant effects.

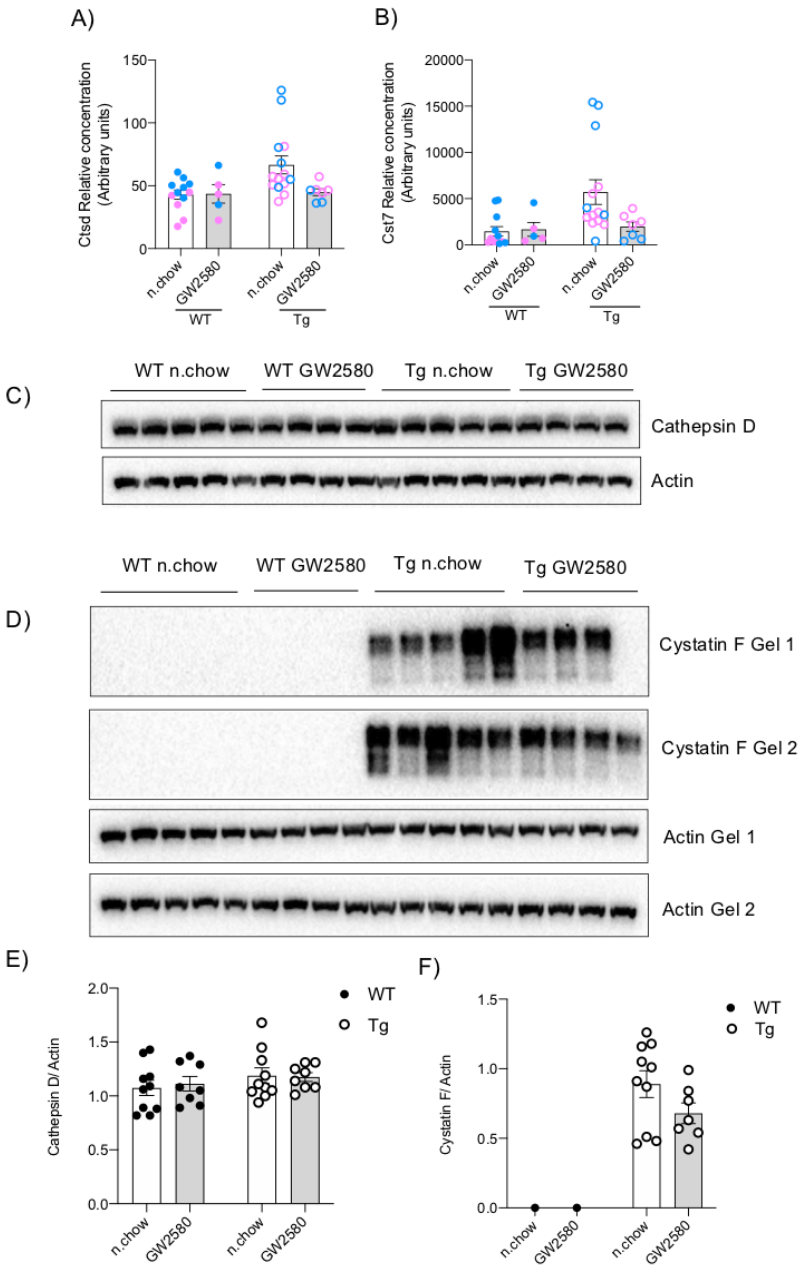

Figure 5.6.13.1: Effect of GW2580 on the expression of lysosomal genes in isolated microglia and lysosomal protein expression in WT and APP/PS1 mouse hippocampal homogenates. mRNA expression of *Ctsd* (A) and *Cst7* (B) in microglia isolated from Tg n.chow (n=14) and Tg GW2580 (n=7), WT n.chow (n=12) and WT GW2580 (n=5) mice. Data are shown as mean ± SEM, pink representing microglial isolates from female and blue representing microglial isolates from male mice. For protein expression of cathepsin D, extracts were equally distributed and resolved on two identical SDS-PAGE gels (Tg n.chow (n=10) and Tg GW2580 (n=8) and WT n.chow (n=10) and WT GW2580 (n=8)) and blotted with antibodies against cathepsin D (only one gel from each analysis is presented) (C). For cystatin F, extracts were equally distributed and resolved on two identical SDS-PAGE gels (Tg n.chow (n=10) and Tg GW2580 (n=8) and WT n.chow (n=10) and WT GW2580 (n=8)) and probed for cystatin F (D). Bands were quantified from both sets of gels by densitometry and normalized to actin for both cathepsin D and cystatin F (E, F). Data are shown as mean ± SEM. Data were analysed by unpaired t-test for cystatin F protein expression and by two-way ANOVA for both mRNA and cathepsin D protein expression.

5.6.14 Effect of GW2580 on autophagy-related genes and proteins in the APP/PS1 mice

Autophagy-related genes, *Tfeb,* a transcription factor controlling gene expression of specific autophagy and lysosomal genes and *Lc3b,* a gene encoding LC3B necessary for autophagosome biogenesis, were analysed in microglial isolates by RT-qPCR and the result presented statistically and graphically as before (Table 5.6.14.1 and Figure 5.6.14.1, panels A and B). The effect of GW2580 on LC3B and p62 protein expression was also examined by Western immunoblot in hippocampal homogenates from female mice: Tg n.chow (n=10), Tg GW2580 (n=8) and WT n.chow (n=10) and WT GW2580 (n=8) groups. The resolved protein bands were normalised to the actin loading control (Figure 5.6.13.1, panel C).

Tfeb mRNA expression was examined as its transcription can be a readout of new expression of *Tfeb*-regulated autophagy and lysosomal genes and an indicator of increased autophagy. GW2580 decreased *Tfeb* mRNA expression in WT mice but to increase it in Tg mice and this differential effect (drug x sex interaction) was significant. Moreover, this effect was sex-dependent: the induction of *Tfeb* in Tg mice occurred in males more than in females and was a significant interaction.

Transcriptional expression of *Lc3b,* which is a *Tfeb*-regulated gene*,* mimicked *Tfeb* (Figure 5.6.14.1, compare panels A and B). *Lc3b* mRNA expression decreased in Tg mice on normal chow compared to WT controls, and GW2580 reversed this expression pattern, although this did not reach statistical significance. Interestingly, a similar pattern for LC3B protein expression to *Lc3b* mRNA expression was observed. LC3B protein expression decreased in Tg mice on normal chow compared to WT controls, and GW2580 reversed this expression pattern, although this did not reach statistical significance.

A trend of reduced SQSTM1/p62 protein expression was noticed in Tg n.chow mice versus WT controls and GW2580 appeared to increase this protein expression. However, SQSTM1/p62 mRNA expression was not analysed in this experiment. Although not always showing statistical significance, both transcripts examined in microglia and both proteins examined in homogenates tentatively suggest an increased expression of factors associated with increased autophagy in microglia. More formal measures of cell-specific autophagy indicators would be necessary to confirm this.

	(i) 2-way ANOVA			(ii) 2-way ANOVA		
	Strain x Drug			Drug x Sex (in Tg only)		
Gene	**Factor**	***F***	***P***	**Factor**	***F***	***P***
Tfeb	Strain	$F_{1, 33} = 0.01523$	0.9025	GW2580	$F_{1, 17} = 3.226$	0.0903
	GW2580	$F_{1, 33} = 0.7573$	0.3905	Sex	$F_{1, 17} = 0.8851$	0.36
	Interaction	$F_{1, 33} = 4.444$	**0.0427**	Interaction	$F_{1, 17} = 8.401$	**0.01**
Lc3b	Strain	$F_{1, 34} = 1.103$	0.301	GW2580	$F_{1, 17} = 3.095$	0.0965
	GW2580	$F_{1, 34} = 0.03100$	0.8613	Sex	$F_{1, 17} = 0.05266$	0.8212
	Interaction	$F_{1, 34} = 3.615$	0.0657	Interaction	$F_{1, 17} = 1.122$	0.3043

Table 5.6.14.1: mRNA expression of Tfeb and Lc3b gene in hippocampal microglial isolates from APP/PS1 and WT mice. Statistics depicts (i) main effects of strain, drug and interaction of strain and drug and (ii) main effects of drug, sex and interaction between drug and sex by two-way ANOVA. Data in bold indicate significant effects.

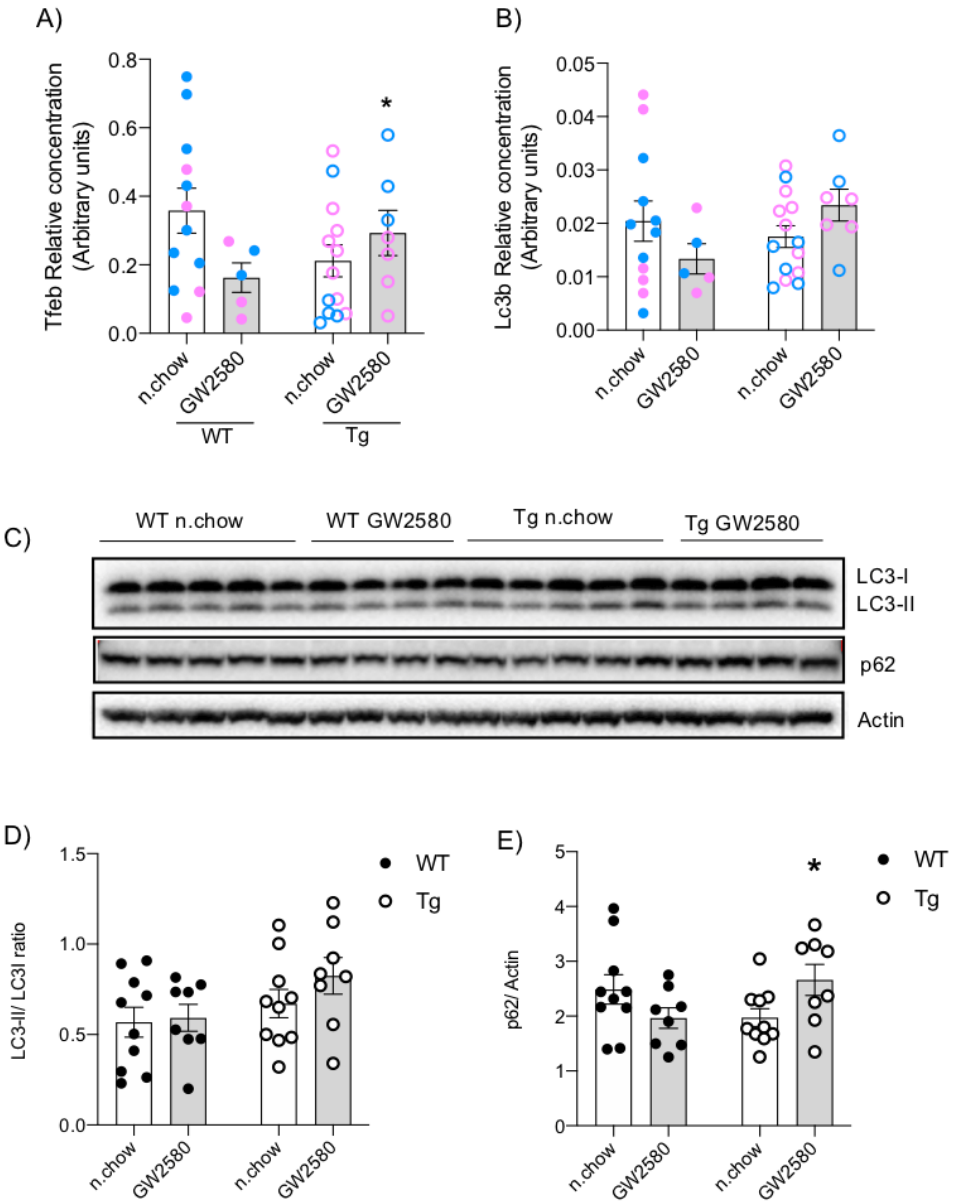

Figure 5.6.14.1: Effect of GW2580 on the expression of autophagy related genes in FACS sorted microglia and proteins from WT and APP/PS1 mouse hippocampus. mRNA expression of *Tfeb* (A) and *LC3* (B) in microglia isolated from Tg n.chow (n=14) and Tg GW2580 (n=7), WT n.chow (n=12) and WT GW2580 (n=5) mice. Data are shown as mean ± SEM, pink representing microglial isolates from female and blue representing microglial isolates from male mice. Data were analysed by two-way ANOVA. Interaction between genotype and drug are depicted by *p < 0.05. Expression of LC3B and p62 in hippocampal homogenate (C) was detected in extracts equally distributed and resolved on two identical SDS-PAGE gels (Tg n.chow (n=10) and Tg GW2580 (n=8) and WT n.chow (n=10) and WT GW2580 (n=8)) and blotted with antibodies against p62 and LC3B (only one gel shown). Bands from both sets of gels were quantified by densitometry and normalized to actin for both p62 and LC3B (D, E). Data are shown as mean ± SEM and were analysed by two-way ANOVA. Interaction between drug and genotype are depicted by *p < 0.05.

5.6.15 Effect of GW2580 on CSF1R signalling in APP/PS1 mice

The effect of GW2580 on PI3K/Akt/mTOR signalling downstream of the CSF1R, was examined by Western immunoblot in mice from Tg n.chow (n=10), Tg GW2580 (n=8) and WT n.chow (n=10) and WT GW2580 (n=8) groups. Membranes were probed with antibodies for the proteins and phosphorylated sites indicated in Figure 5.6.15.1, with resolved protein bands normalised to the actin loading control.

A decreased phosphorylation of Akt on Ser473 was observed in Tg mice compared to WT mice (main effect of genotype: $F_{1, 32} = 8.003$, $p = 0.0080$). However, GW2580 treatment of the Tg mice did not seem to affect Akt expression. No main effect of drug ($F_{1, 32} = 0.1478$, $p = 0.7032$) or interaction ($F_{1, 32} = 0.7362$, $p = 0.3972$) was observed for this protein.

Phosphorylation of S6K1 showed a similar pattern to Akt expression in Tg mice on normal chow. S6K1 was reduced in Tg mice on normal chow compared to WT controls (main effect of genotype: $F_{1, 32} = 0.1175$, $p = 0.7340$). However, unlike the effect of GW2580 on Akt, GW2580 treatment of Tg mice increased S6K1 expression (main effect of drug: $F_{1, 32} = 0.01443$, $p = 0.9051$). No statistically significant interaction between drug and genotype ($F_{1, 32} = 3.551$, $p = 0.0686$) was observed herein.

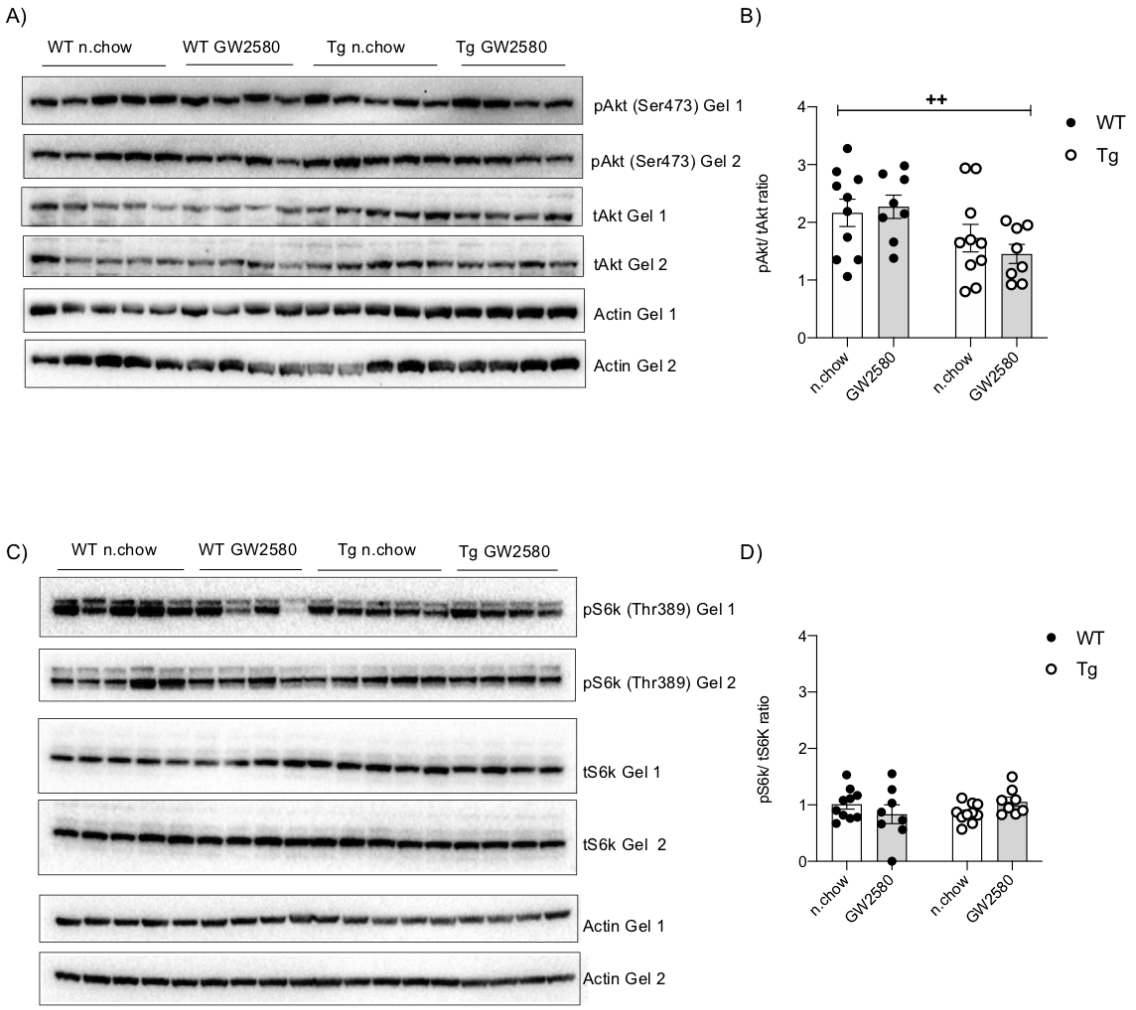

Figure 5.6.15.1: Effect of GW2580 on signaling of CSF1R in APP/PS1 and WT mice. Expression of phosphorylated and total Akt and phosphorylated and total S6K1 (A, C). Western immunoblotting of extracts equally distributed and resolved on two identical SDS-PAGE gels (Tg n.chow (n=10) and Tg GW2580 (n=8) and WT n.chow (n=10) and WT GW2580 (n=8)) and probed with indicated antibodies (only one set of gels shown). Bands from both sets of gels were quantified by densitometry and normalized to actin for both Akt and S6K1 and expressed as ratio of phosphorylated to total proteins (B, D). Data are shown as mean ± SEM and were analysed by two-way ANOVA. Main effects of genotype are depicted by $^{++}p < 0.01$.

5.7 Discussion

It has been shown in this chapter that inhibition of CSF1R signalling, using GW2580, to suppress microglial proliferation ameliorates microglial DAM phenotype, with the drug tending to be more effective in altering gene expression in male mice compared to females. However, Microglial proliferation was found to be more abundant in female APP/PS1 mice and GW2580 reduced this observation. Although GW2580 did not affect levels of Aβ, its impact on microglial proliferation and phenotype was moderately effective in preventing synaptic degeneration, depicted by the improvement in synaptophysin and PSD95 protein levels with the drug. GW2580 had no effect on working memory task in APP/PS1 mice but there was a modest effect on hippocampal-dependent, visuospatial cognitive function assessed by MWM. However, this effect was only apparent in female mice. Thus, inhibition of microglial proliferation by targeting CSF1R signalling affects multiple features of disease phenotype in APP/PS1 mice.

5.8 Study limitations

This research is subject to some limitations. Given the sex differences that emerged, the sample size in this study turned out to be insufficient for robust statistical interrogation of impacts on cognitive function and microglial phenotype. An unforeseen technical problem resulted in the loss of microglial isolates from a cohort of 25 animals. Furthermore, although increased mortality in female Tg mice is a documented feature of the strain (Giménez-Llort *et al.*, 2021). The effect of sex differences was underestimated before conducting the study and the selectivity of loss in the female subjects compounded the difficulty in accounting for observed sex differences. These limitations have implications for the data obtained in the MWM, where a clear disease-associated effect was observed only in females and although the drug appeared protective against these deficits, statistically significant effects of strain or treatment were difficult to confirm because there were only 9 female Tg mice on normal chow and GW2580 treatment in the groups assessed on this task. These sex-differences in cognitive function were mimicked by the numbers of microglia isolated by FACS. Consistent with more developed disease in females, these female transgenic animals showed higher numbers of microglia and only females appeared to benefit from GW2580 treatment. As a direct result of these cognitive and microglial findings, only female mice were chosen for Western blotting analyses. Although several interesting results emerged from these analyses of

protein expression, the subsequent analysis of gene expression in the microglial isolates indicated very clearly that CSF1R inhibition had very marked effects on microglial phenotype and that these were more marked in male mice. One might conclude that CSF1R inhibition was more likely to reduce microglial numbers in females, since the disease was more progressed, and microglial proliferation more robust, in females but that the microglia that were left, after depletion, were more strongly affected by CSF1R in males than in females. However, despite the large effect sizes for most of those analyses (i.e., high F values in ANOVA), effects for many genes did not come out as statistically significant and this may be explained largely by insufficient statistical power. There were several effects that might be biologically significant, based on the large F values, but the failure to find these effects statistically significant reflects variability in the data, which the small sample size could not overcome. Therefore, small sample size in this research, arising from sex-selective mortality and technical errors during cell isolations, has affected the confidence with which some conclusions can be drawn, and these caveats should be borne in mind throughout the discussion of the data obtained. This also calls for further work to repeat key findings with larger sample sizes.

5.9 Microglial DAM or MGnD phenotypes is ameliorated by GW2580

In the gene expression analysis performed here, up-regulation of several genes associated with the DAM signature such as *Itgax, Clec7a, Trem2, Tyrobp, Apoe, Lpl, Ctsd, Cst7* were identified. *Itgax* and *Clec7a* are upregulated in the first stage of TREM2-independent DAM activation (Keren-Shaul *et al.*, 2017) and their mRNA expression was observed to increase in Tg mice in the current work. *Itgax* and *Clec7a* are also known as primed microglial markers. Microglial priming was first described, in functional terms, as the propensity of microglia, activated by prior pathology, to show exaggerated pro-inflammatory responses to secondary inflammatory stimulation (Cunningham et al., 2005) and its gene expression profile was first described, in transcriptomic studies, by Holtman and colleagues in multiple different animal models of ageing and neurodegenerative disease (Holtman *et al.*, 2015). The profile includes several indicators of lysosomal and phagocytic activation, antigen presentation, cell surface ligand-binding receptors, lipid metabolism and oxidative phosphorylation. There are strong overlapping patterns of gene expression between what has been termed ‘priming’ and what has more recently been described as ‘DAM’.

Although not reaching statistical significance, likely due to limiting statistical power, the gene encoding TREM2, a phagocytosis receptor (Takahashi, Rochford and Neumann, 2005), that's involved in inflammation (Piccio *et al.*, 2007), and is essential for the DAM phenotype, (Keren-Shaul *et al.*, 2017) was upregulated in Tg mice in this study. Whether association of TREM2 with Aβ phagocytosis by microglia plays a beneficial or detrimental roles is still a matter of debate (Jay *et al.*, 2015; Wang *et al.*, 2015). The influence of TREM2 on neuroinflammation is also contradictory in the literature. For example, a lack of TREM2 expression was shown to reduce the pro-inflammatory phenotype in APP/PS1 mice (Jay *et al.*, 2015), while *Trem2* overexpression by transduction of FLAG-tagged *Trem2* vector in microglia was found to reduce pro-inflammatory features such as TNFα and iNOS secretion (Takahashi, Rochford and Neumann, 2005). Therefore, both increased activation and decreased activation of TREM2 may have anti-inflammatory effects. Nonetheless, the involvement of this gene in AD is well established. A rare TREM2 missense variant in exon 2 of TREM2, R47H, is associated with increased risk for LOAD (Guerreiro *et al.*, 2013; Jonsson *et al.*, 2013). TREM2 regulates ApoE signalling in microglia in ALS and AD mouse model and is a powerful target for restoring homeostatic microglia (Krasemann *et al.*, 2017). It is notable that the mRNA expression of *Tyrobp*, the gene coding for DAP12, an intracellular adaptor molecule which TREM2 binds to, to initiate signal transduction, was also found to be upregulated in the Tg mice in the study. These changes in *Trem2* and *Tyrobp* support an increased activation of TREM2 signalling, which is consistent with the co-ordinated up-regulation of DAM or MGnD markers inspected herein. Evidence supporting this includes expression of *Apoe* and *Lpl*, which also showed heightened expression in Tg mice and GW2580 decreased these expression levels, suggesting that GW2580 can suppress the primed/DAM/MGnD phenotype in microglia.

Lpl codes for lipoprotein lipase, a triglyceride hydrolase and also an assistant for lipid transport between lipoprotein particles and cells (i.e., lipoprotein uptake). Its precise contribution to neuroinflammation in AD is unclear but it is present in/at amyloid plaques and single-nucleotide polymorphisms (SNPs) in the coding region of the *Lpl* gene do increase risk for developing AD (Blain *et al.*, 2006). It may be related to the need for significant phagocytosis-associated membrane degradation in microglia and/or the possible need for fatty acid oxidation to fuel microglial

activation during neurodegeneration (Keren-Shaul *et al.*, 2017). The significance of its reduction in microglia by CSF1R inhibition requires investigation.

Upregulated expression of lysosomal genes such as *Ctsd*, coding for cathepsin D and *Cst7,* coding for cystatin F was observed in microglia isolated from Tg mice. Cathepsin D is a lysosomal aspartic protease known to increase in AD (Chai *et al.*, 2019). Cathepsin D plays an important role in intralysosomal Aβ and tau degradation (Suire *et al.*, 2020). Mutations within the *Ctsd* gene might interfere with the appropriate function of proteolytic degradation, thus *Ctsd* may be a risk factor for developing LOAD (Suire *et al.*, 2020). In the current work, approx. 30% increase in mRNA expression of *Ctsd* was observed in Tg mice and GW2580 restored expression to basal levels. However, this increase in *Ctsd* mRNA expression was only seen at transcriptional level. At protein levels, the amount of cathepsin D remained the same between APP/PS1 and WT mice. This differential observation between mRNA and protein levels is not necessarily surprising. The gene expression analysis was done in isolated microglia in this current study, while the proteins were looked at in homogenates from mouse hippocampus and overlying cortex. Given the ubiquitous nature of Cathepsin D expression, homogenates cannot resolve cell-type specific changes and thus the analysis was limited in ability to detect microglia-specific alterations in protein expression.

Cystatin F, a protease inhibitor of papain-like cysteine proteases such as cathepsins B, H, L and S (Rawlings, Morton and Barrett, 2006). *Cst7* was also examined at mRNA and protein levels and in both cases their expression was increased in Tg mice. Particularly at protein levels, a dramatic increase in its expression was observed in Tg mice compared to WT controls. *Cst7* is amongst the top genes regulated in CD11b+/CD45+ microglia, with a 15.3 fold higher expression in 15-18 months old APP/PS1 mice compared to WT controls (Orre *et al.*, 2014). Cystatin F is not expressed in the brain in physiological conditions and thus no protein bands were observed in the WT mice, while, a striking increase in its expression is evident in activated microglia from the APP/PS1 mice (Ma *et al.*, 2011), similar to what was seen here. Cystatin F has been shown to dramatically increase in pre-symptomatic mouse model of prion disease and hence has been proposed to be used as a biomarker of disease (Nuvolone *et al.*, 2017). Increased expression of Cystatin F in

protein accumulation-prone diseases indicates the importance of dysregulated proteolytic activities in these types of disease.

Consistent with upregulation in the above genes, there was a strong trend towards reduced expression of homeostatic genes such as *Sall1* or *P2ry12* in Tg mice herein. Microglia play a vital role in the maintenance of homeostasis in the CNS, and lose this ability in neurodegenerative diseases such as AD (Sobue *et al.*, 2021). Loss of homeostatic function by microglia may disrupt neuronal function. SALL1 is a zinc finger transcriptional repressor. SALL1 is important in the maintenance of microglial physiological properties as *Sall1*-deficient microglia are known to be more pro-inflammatory (Buttgereit *et al.*, 2016). P2ry12, a receptor involved in chemotaxis, is one of the most abundantly expressed genes in microglia whose expression is reduced in microglia with a reactive status (Haynes *et al.*, 2006). Microglia located around the vicinity of amyloid plaques lack P2ry12 receptor expression (Jay *et al.*, 2015). Microglial homeostasis is also tightly regulated by TGFβ in the CNS. *Tgfb* has been shown to be a key regulator of the homeostatic phenotype – loss of TGFβ is a driver of the switch to MGnD phenotype (Krasemann *et al.*, 2017; Zöller *et al.*, 2018). *Tgfb* gene expression levels were observed to decrease (modestly) in Tg mice in the current work. TGFβ is neuroprotective against cellular excitotoxicity, hypoxia, and ischemia. Impaired signalling induced by TGFβ1, a growth factor involved in cell proliferation and differentiation is well documented in neurodegeneration and is associated with increased Aβ deposition in AD brain and in mouse model of AD (Tesseur *et al.*, 2006). TGFβ1 receptor expression in microglia inhibited microglial activation (Buttgereit *et al.*, 2016). Microglial secretion of TGFβ reduces the release of inflammatory mediators such as O_2^- and NO by microglia (Herrera-Molina *et al.*, 2012). It was striking that GW2580 treatment markedly reduced expression of both *Tgfb* and *P2yr12*, in the current work, suggesting that CSR1R may be important for the maintenance of homeostatic phenotype. In fact, in support of this idea, a very recent study performed on CSF1R $^{+/-}$ mouse model of adult-onset leukoencephalopathy demonstrated that CSF1R haploinsufficiency in microglia decreased homeostatic proteins such as P2RY12 and Transmembrane protein 119 (TMEM119) in the mouse cortex. A corresponding loss of presynaptic markers such as Synaptophysin, SV2A, and Bassoon, measured by quantifying cortical synaptic integrity was shown and CSF1R inhibitor, PLX5622, prevented these observed effects (Arreola *et al.*, 2021).

Taken together these data suggest that the microglia isolated from APP/PS1 mice display in a primed, DAM, MGnD phenotype with suppressed homoeostatic gene expression pattern. Inhibition of CSF1R signalling with GW2580 showed a strong trend towards reverting this Tg phenotype towards that of WT controls herein. Our finding is in agreement with Gomez-Nicola and colleagues who demonstrated that blocking microglial proliferation with GW2580 (1000 ppm) for 3 months drove the cells towards an anti-inflammatory phenotype analysed by cytokine array analysis. This group showed that protein expression of pro-inflammatory cytokines/chemokine such as IL-1A, IL12, CCL2, CXCL13 etc were restored to control levels with GW2580 treatment of APP/PS1 mice. While anti-inflammatory cytokine/chemokine such as IL-4, CCL9 were increased and some molecules such as IL-7, TNFR2, CCL11 and CCL24 remined unchanged as a result of the treatment (Olmos-Alonso *et al.*, 2016). During the preparation of this thesis, the above research group has published that isolated microglia display a DAM phenotype with $CLEC7A^+$, $CD11C^+$ and $MHCII^+$ cells near Aβ plaques, they displayed signs of senescence, including telomere shortening and a senescent transcriptomic profile of 164 genes analysed by RNA sequencing. Inhibition of microglial proliferation prevented the development of DAM phenotype as well as reducing Aβ plaque density in 10 month-old APP/ PS1 mice (Hu *et al.*, 2021). Taken together, these suggest that inhibition of CSF1R signalling ameliorated the DAM phenotype in microglia isolated from diseased mice. Therefore, GW2580 may be an effective disease-modifying drug for the treatment of AD.

5.10 Synaptic loss is recovered by GW2580

Analysis of PSD95 and synaptophysin showed that expression of these proteins was markedly reduced in Tg mice. Inhibition of CSF1R with GW2580 increased PSD95 and synaptophysin protein expression in Tg mice. Although not statistically significant, there was an apparent decrease in the density of both pre- and post-synaptic markers when WT mice were treated with GW2580. This phenomenon could be related to an alteration of the continuous turnover of hippocampal synaptic terminals by microglia in health. Microglia play a crucial role in facilitating the elimination of dendritic spine and axon terminals in physiological conditions (Paolicelli *et al.*, 2011). Complement proteins play a crucial role in facilitating phagocytosis to engulf and degrade pathogens or abnormal synaptic connections by phagocytes such as microglia and C1q is required for the refinement of sensory

motor circuits and synaptic dysfunction during development (Vukojicic *et al.*, 2019). The expression of microglial *C1q* gene was, therefore, also examined herein but, if anything, its expression also decreased upon GW2580 treatment. Moreover, linear regression analysis was performed to test for correlation between *C1q* and pre- and post-synaptic markers, but this did not show any significant relationship. Therefore, an alteration in C1q would not appear to explain a reduction in synaptic density upon GW2580 treatment in normal animals.

The literature indicates that the complement system, especially complement proteins such as C1q and C3 are also associated with synaptic phagocytosis in neurodegenerative diseases, including AD and MS (Dejanovic *et al.*, 2018; Werneburg *et al.*, 2020). The complement C1q has been shown to aberrantly prune the synapses in AD and deletion of the gene rescues synaptic pruning in progranulin-null mice (Lui *et al.*, 2016). These observations are also not easily reconciled with the disease-associated decrease in synaptic density seen here, since C1q was also not robustly decreased in disease, *per se*. Nonetheless, the possibility of the synaptic loss seen here being linked with an increase in other complement proteins, such as C3, cannot be ruled out. C3 is mostly produced by astrocytes (Liddelow *et al.*, 2017) and it is likely that astrocyte phenotype is also altered by CSF1R inhibition, as a secondary effect of altered microglial phenotype. Astrocytes have been isolated in the current experiments and analysis of these remains a possibility for future work. Whether synaptic pruning is altered in GW2580-treated animals requires clarification, but apparent changes in microglial phenotype in those wild type animals does offer the possibility that these contribute to excessive synaptic removal or impaired synaptogenesis.

5.11 Differences exist between microglial isolates from male and female APP/PS1 mice

It is now accepted that sex-specific diversity in microglia exists due to genetic, epigenetic, and hormonal contributions (Han *et al.*, 2021). Literature suggests that female microglia are more inflammatory than male microglia in both health and in disease. Guillot-Sestier and collagues have shown that many inflammatory genes and gnes related to oxidative stress such as *Ubqin1, App, Hmox, Nkiras1, Mef2a and Panx1* etc. was increased in female microglia (Guillot-Sestier *et al.*, 2021). This is consistent with our findings in the current study, female APP/PS1 mice showed a

higher microglial frequency than in male APP/PS1 mice of the same age, reflecting a constantly activated state and administration of GW2580 reduced this microglial frequency.

On the other hand, most of the microglial activation genes analysed in this chapter, were observed to be upregulated in Tg mice, particularly in microglia from male Tg mice. GW2580 was more effective in ameliorating this effect in microglia isolated from the male APP/PS1 mice compared to females. Therefore, it appears that microglia from male APP/PS1 have a more DAM-like, dysfunctional phenotype in our case. As the proliferating microglia is removed by the GW2580 treatment of mice, amongst the remaining 'normal' microglia, the ones isolated from male mice may be more pro-inflammatory. A small number of evidence indirectly support this finding. For instance, microglia isolated from male mice has been reported to display an amoeboid morphology (Leyns *et al.*, 2017; Guillot-Sestier *et al.*, 2021) and amoeboid microglia are characteristic of an 'activated' phenotype. Amoeboid cells are also associated with enhanced phagocytosis and increased mobility in microglia with the ability of taking up more Aβ and latex beads, further signs of the activated states of microglia (Szabo and Gulya, 2013; Fu *et al.*, 2014).

The differences observed in sex-specific gene expression is not due to hormonal control of microglia as reduction in circulating oestrogen by ovariectomy did not have any effect on gene expression in microglia from adult female mice (Villa *et al.*, 2016). Additionally, Gene expression pattern remained the same when microglia were transplanted into the brains of the opposite sex (Wood, 2018). Thus, our observation that female has more proliferative microglia than male mice but the drug works better in males may simply be because the male and female are in different stages of the disease/plaque pathology, where microglia from female $App^{NL\text{-}G\text{-}F}$ reaching the dysfunctional activated response microglia (ARM) phenotype, characterised by upregulated gene expression such as *Trem2, Cst7, Aplp2, Axl* etc., faster than microglia from male $App^{NL\text{-}G\text{-}F}$ mice (Sala Frigerio *et al.*, 2019). Moreover, male microglia were reported to reach adult phenotype later than female microglia (Villapol et al., 2019), Thus, GW2580, being an anti-inflammatory drug, was more efficient in targeting the amoeboid-shaped microglia isolated from male mice.

These sex-linked differences are evident in rodent microglia in early stages of life which resolves by adolescence but comes back in adult stages of life as seen in our APP/PS1 mouse model of AD (9 months of age). Male rats have a higher number of microglia in the hippocampus, cortex and amygdala than female rats during early postnatal development period (P4), while, microglial number increases in these regions in female during the late adolescent period and adulthood (P30-60) (Ruggiero *et al.*, 2018). Microglial isolates from the whole brain was shown to have higher expression of inflammatory cytokines TNFα, IL-1β, and IL-6 in female compared to male microglia but this diversity disappeared by P21 (Crain, Nikodemova and Watters, 2013). A lower number of purinergic receptors, P2X4 and P2Y4, which are associated with microglial activation, was found in male microglia over the early postnatal days (Koizumi *et al.*, 2013).

However, this sex-specificity seems to influence prevalence of AD, with women being more prone to developing it than men (Viña and Lloret, 2010). In a study isolating microglia from both male and female APP/PS1 mice, microglia from female mice were found to be more glycolytic, less phagocytic and were associated with increased amyloidosis, while microglia isolated from male mice had a more amoeboid morphology (Guillot-Sestier *et al.*, 2021). Female APP/PS1 mice showed a heavier amyloid burden, with more amyloid deposits in the hippocampus than males and this developed at an earlier age in females than in age-matched males (Wang et al., 2003). In another study, glucose and insulin intolerance and higher levels of cholesterol and triglycerides were found to develop faster in male APP/PS1 mice than in age-matched female APP/PS1 mice, while female APP/PS1 mice had more Aβ deposits and poorer learning ability and memory function (Li *et al.*, 2016). The exact contributing factor to notion is not defined. However, this sex-related differences observed in microglia from APP/PS1 mice may be related to how the microglia from different sexes react to the amyloid plaque present in the CNS. The relationship between microglia and Aβ is discussed in the following section in detail.

5.12 The lack of behavioural deficiency between WT and Tg animals

Although there was not a statistically significant cognitive impairment in APP/PS1 in the mice used in this study, it is important to emphasize that a trend towards cognitive deficit was observed in Tg female mice compared to WT controls and that GW2580 seemed to reverse this impairment in Tg female mice. The experiments

were powered to detect statistically significant impairments in Tg animals and were sex balanced (6 male and 9 female Tg mice w/o drug and 10 male and 10 female WT mice w/o drug. However, in retrospect, reported sex differences between male and female APP/PS1 mice might have predicted the observed findings. 12-month-old female APP/PS1 and 3x Tg-AD mice have been reported to perform worse than age-matched male mice in MWM spatial memory task (Yang et al., 2018; Mifflin et al., 2021). Wang and colleagues have shown that female APP/PS1 mice accumulate amyloid at an earlier age and that they build up more amyloid deposits in the hippocampus than age-matched (12 and 17 months) male mice (Wang et al., 2003). It is known that increased amyloid load is strongly correlated with memory and cognitive impairment in APP/PS1 mice (Bruce-Keller et al., 2011). That is, a lack of effect of the transgene on visuospatial navigation at 9 months in male APP/PS1 might not be surprising given the 'lag' in disease progression observed in males. The inclusion of similar numbers of male mice meant that the number of female mice included was insufficient to accommodate the variability observed and the data suggest that these experiments would either need to be focused on female animals or need to factor in increased statistical power. The work is currently being repeated with additional mice to supplement these data.

5.13 Aβ levels is not altered by GW2580

Microglial association with Aβ is debatable. For example, Aβ deposits in the brain but no observed cognitive impairment or any uncontrolled or severe systemic illness (Harrington et al., 2017). Treatment of APP/PS1 mice with GW2580 (0.1 % (w/w) for 3 months) also did not produce any changes in Aβ plaque formation (Harrington et al., 2017). This finding agreed with Olmos-Alonso and colleagues where the number of Aβ plaques in APP/PS1 mice were also unaltered after 3 months of treatment with GW2580 (0.1 % (w/w)) (Olmos-Alonso et al., 2016b). Reported in this chapter, inhibition of CSF1R signalling improved cognitive function and synaptic integrity, without altering Aβ levels in the APP/PS1 mice. This indicates that controlling excessive microglial proliferation and switching of microglial phenotype from an activated, DAM or MGnD phenotype to a more 'homeostatic' phenotype is sufficient to ameliorate AD disease phenotypes. It is therefore implied that it may not be the amount of Aβ which is the culprit, but the inflammatory response to it that matters in aggravated AD pathology and progression. In support of this notion, clinical studies of AD patients showed that those with higher inflammatory status are

more likely to develop disease than those with similar Aβ levels, but no inflammation (Pascoal *et al.*, 2021).

With regards to Aβ clearance observed in other AD mouse models, the age at which the CSF1R inhibition treatment is administrated to the mice may be an important factor to consider. Microglial proliferation starts early in the disease phase and if the disease has already progressed to an advanced stage, reducing microglial proliferation at this point may not have any beneficial effect. For example, microglial depletion by PLX3397 (290 mg kg^{-1}) administration for 3 months stopped Aβ plaque formation in 5 month-old 5xFAD mice (Sosna et al., 2018), Therefore, this research directs us to the possibility that inhibition of CSF1R signalling is plausibly only effective before the start of pathology. Moreover, microglia may not even be the key source of Aβ clearance in AD (Spangenberg et al., 2016). Knockout and overexpression studies reveal other mechanisms such as the existence of Aβ-degrading enzymes for Aβ plaque clearance (Poirier et al., 2006; Hafez et al., 2011).

5.13 Conclusion

Taken together the data suggest that inhibition of CSF1R by GW2580 ameliorates amyloid-associated cognitive deficits and synaptic degeneration in the APP/PS1 mouse model of AD. Microglia isolated from APP/PS1 mice display a DAM/MGnD phenotype and GW2580 both reduces microglial proliferation and shifts the remaining microglia towards a more 'homeostatic' state. The data suggest that the amount of Aβ may not be the key determinant of disease-associated symptoms in AD, rather it is the neuroinflammatory response towards Aβ that may be a major determinant of AD progression. Moreover, microglia from the APP/PS1 mice show sex-selectivity in patterns of disease-associated gene expression. Therefore, the findings herein reiterate microglial CSF1R as a therapeutic target, although differences between the sexes could be a complicating factor. It will be important to investigate those sex differences more fully in future studies of AD, both *in vitro* and *in vivo*, and clinically.

The current study showed altered microglial phenotypes with CSF1R inhibition but did not assess the impacts of such changes on the phenotype of astrocytes in APP/PS1 mice. The effect of GW2580 on microglia-astrocyte interactions in AD background may provide further insights into whether microglial impacts on disease

features may be mediated via astrocytes or whether the key interaction is between microglia and neurons.

Finally, a much more focused study will be necessary to determine whether autophagy activity is truly altered in microglia from APP/PS1 mice. An initial examination of LC3B and SQSTM1/p62 puncta formation by immunohistochemistry in the APP/PS1 brain would provide the starting point to examine altered autophagy in this model and the ability of GW2580 to increase or decrease microglial autophagy.

Chapter 6: General discussion

6.1 Rationale and brief summary of results

As the brain ages, multiple changes occur such as neuronal synaptic loss, impairments in white matter integrity, activation of microglia and astrocytes, and multiple cellular processes including phagocytosis, proteostasis and metabolism become less efficient (Mattson and Arumugam, 2018). These abnormalities can lead to a gradual decline in cognitive and other functions and, in many cases, to chronic neurodegenerative conditions like Alzheimer's disease (AD). Currently there are 50 million people suffering from AD (or another dementia) worldwide and, as longevity increases in the population, the number of people suffering with AD is projected to triple by 2050 (Scheltens et al., 2021). Despite this there are still no disease-modifying therapies for AD.

Inflammation is a consistent feature of neurodegenerative diseases, and microglia have become a focus of interest. In particular, microglial proliferation and survival, which are regulated by CSF1R, may be valid targets for delaying AD progression. At the inception of this project, it was hypothesised that inhibiting CSF1R signalling may promote microglial autophagy and may modulate microglial phenotype and function *in* vitro and *in vivo*.

Data obtained in the current study have expanded knowledge on microglial activation and function *in vitro* and *in vivo* with three main conclusions. Firstly, CSF1R signalling does not directly regulate microglial autophagy in immortalised microglia. Secondly inhibition of CSF1R signalling influences several aspects of microglial function *in vitro*, including suppressing LPS-induced chemokine and NO secretion, while CSF1 itself modestly inhibits phagocytosis and basal cytokine/chemokine synthesis. Thirdly, inhibiting CSF1R signalling *in vivo* altered microglial function: ameliorating the chronic microglial DAM phenotype in APP/PS1 mice and mitigating synaptic loss and cognitive impairment.

6.2 CSF1R signalling, and regulation of phagocytosis and autophagy in microglia

One of the innate and essential functions of microglial cells is phagocytosis of foreign material. Treatment of cells with CSF1 (50 ng mL^{-1}) for 24 hr moderately reduced

phagocytosis of latex beads by IMG cells compared to vehicle control, whereas CSF1R inhibition restored latex bead uptake. In contrast, a prior study showed that exposure of human microglia to CSF1 (25 ng mL^{-1}) for 72 hrs increased phagocytosis of Aβ1-42 compared to vehicle controls (Smith *et al.*, 2013). However, reduced CSF1R signalling, achieved by siRNA targeting of *Csf1r,* had no effect on primary mouse microglial phagocytosis of pre-opsonised latex beads (Delaney *et al.*, 2021). The difference between these studies and the findings presented herein might be explained by (1) differences in duration and concentration of CSF1 exposure, (2) the substrate and/or size of latex beads used, and (3) by the potency, duration, or mechanism of receptor attenuation. Taken together, these data point towards involvement of CSF1R signalling in modulating microglial phagocytosis but the question requires further investigation to ascertain whether the observed CSF1 effect is cargo- and/or time-dependent and what mechanism may be involved.

Activation of CSF1R signalling attenuated phagocytosis slightly, whereas CSF1R inhibition restored this activity. The PI3K/Akt/mTORC1 pathway is activated by CSF1R signalling and this regulates cytoskeletal rearrangements (Bao *et al.*, 2020). Phagocytosis also requires rearrangement of the actin cytoskeleton through activation of various signalling pathways including PI3K signalling (Baranov *et al.*, 2016). It might be hypothesised that perhaps CSF1-mediated reduction of phagocytosis was due, in part, to competition in signalling for cytoskeletal changes. Moreover, CSF1R signalling activates mTORC1 (Stanley and Chitu, 2014), which is widely reported as a negative regulator of autophagy (Wan *et al.*, 2018). Not only that, but phagocytosis itself has multiple points of crosstalk with the autophagy pathway, including the ability of phagocytic cells to perform LC3B-Associated Phagocytosis (LAP). In BV2 microglial cells, reduced expression of the autophagy-regulating protein Beclin1, by shRNA targeting, attenuated phagocytosis of 6 μm pre-opsonised latex beads (Lucin *et al.*, 2013). Taken together, it is possible that CSF1R activation inhibits phagocytosis through two possible avenues: (1) modification of the actin cytoskeleton, and (2) appropriation of endocytic trafficking machinery.

Perhaps one of the most surprising results reported herein is that microglial cells possess a non-canonical autophagy phenotype. This was characterised by uncoupling of mTORC1 from autophagy regulation *in vitro*: CSF1R activated mTORC1 signalling

but this did not affect microglial autophagy. Consistent with this, rapamycin was unable to activate autophagy in IMGs despite mTORC1 inhibition. Therefore, mTORC1 is uncoupled from autophagy regulation in IMG cells. *In vivo* the scenario is perhaps more complex. There are two main regulatory mechanisms for autophagy: (i) non-transcriptional regulation by mTORC1, whose activation/inhibition is triggered by environmental stressors such as nutrient availability, hypoxia etc. and (ii) transcriptional-dependent upregulation of certain transcription factors such as TFEB, genes of the class O forkhead box transcription factors (FOXO) family (Webb and Brunet, 2014), E2F1 and NF-kB (Gang *et al.*, 2011). These transcription factors regulate the expression of autophagy-related genes associated with the various stages of the autophagy process. In this regard, gene expression analysis in hippocampal isolates of *Tfeb* and *Lc3b,* and LC3B protein expression showed they were decreased in APP/PS1 mice, compared to wild type littermates, while CSF1R inhibition upregulated their expression. Since, at least *in vitro*, CSF1R signalling is uncoupled from autophagy regulation, it is likely that inhibiting the receptor could result in 'gene priming', which entails cells reacting to changes in environment by upregulating mRNA transcripts in preparation for invoking adaptive changes, but this would require further analysis. Additionally, increased expression of *Tfeb* and *Lc3b* in the APP/PS1 mouse could also indicate a response to accumulation of toxic protein aggregates (Bécot *et al.*, 2020; Long *et al.*, 2020). In terms of LC3B protein expression in the APP/PS1 mouse, this could reflect either enhanced autophagy or inhibited autophagy, since increased synthesis of LC3B can indicate a higher rate of autophagy but may also accumulate due to defective autophagy. Despite these findings from *in vivo* analysis, it does not alter the fact that, in IMG cells, autophagy regulation is not functionally downstream of CSF1R signalling, even if expression of autophagy-related genes may be.

Unfortunately, microglial autophagy was not properly assessed *in vivo*. Although some limited data were obtained by examining the effect of GW2580 on autophagy-related transcripts in isolated microglial gene expression and in hippocampal homogenate protein expression, these findings are inadequate to reach to any concrete conclusions. Not enough autophagy genes have been looked at in microglial isolates and the protein work is done on hippocampal homogenates, meaning that the results obtained by Western immunoblotting cannot resolve the contributions of multiple

different cell types. Whether all the genes examined translate into proteins also would need to be assessed. Immunohistochemical analysis of APP/PS1 brains could be analysed for autophagy-related markers such as LC3B and P62 puncta formation with and without GW2580. The distribution pattern of LC3B in relation to Aβ plaques would be an interesting addition to identify whether there are any relationships between the two. In fact, some of these assays were originally planned to be part of this thesis but due to the loss of animals arising from failed glial-isolation protocols meant that these questions could not be addressed and are now required to be pursued in future work.

Autophagy is thought to be an essential process in both the generation and clearance of Aβ in AD and an accumulation of Aβ occurs as a consequence of dysfunctional autophagic turnover of APP-rich organelles (Steele *et al.*, 2013). Changes in autophagy in AD mouse models has been mostly studied in neuronal cells. For instance, immature autophagic vacuoles have been found to increase in the hippocampal neuron of 4-6 month-old PS1M146L/APP751SL mouse model long before the occurrence of any synaptic an neuronal loss occurred (Sanchez-Varo *et al.*, 2012). Literature is limited on research investigating microglial autophagy in AD mice. There was a report drawing a link to accumulation of abnormally abundant autophagy vesicles and impaired mTORC1 signalling as seen by decreased phosphorylation of 4EBP1, Akt at Ser473 and NDRG1 in Trem2 deficient microglia isolated from $Trem2^{-/-}$ 5XFAD mice, affecting ATP level and bioenergetic pathways (Ulland *et al.*, 2017). Rapamycin-induced autophagy induction was associated with amelioration of a defective Aβ degradation in microglia isolated from 5XFAD mice (Daily and Amer, 2020). The lack of microglia autophagy studies in AD mouse models demands attention for conducting experiments to look at whether autophagy is indeed non-canonical in microglia *in vivo.* For example, as LAP is a common form of non-canonical autophagy, this could be studied by looking at LC3B puncta formation in microglia and the relationship of LC3B protein with Aβ accumulation by immunhistomechemical anasyis of AD mouse brain following pharmacologically- or genetically-induced autophagy induction in the mice. Addition of a CSF1R inhibitor such as GW2580 in this setting could address whether CSF1R may be invoved in the process.

It is also interesting to know whether acute stimuli, which have been shown to improve or to exacerbate AD pathological features in different experiments (see Lopez-

Rodriguez et al. 2021 for review) may exert some of these effects through alteration of autophagic flux in microglia. One study administering LPS (1 mg/kg) for 18 weeks in 12-14 week old male senescence-accelerated prone 8 (SAMP8) mice, exhibiting most features of AD pathogenesis, has been shown to suppress glucose and lipid build-up in isolated microglial cells, pro-inflammatory cytokine secretion in blood and decrease Aβ load with memory improvement (Kobayashi *et al.*, 2018). Moreover, a single challenge of APP/PS1 mice with bacterial LPS produces an exaggerated acute microglial IL-1β response selectively in the APP/PS1 mice and can acutely disrupt cognitive function in those mice (Lopez-Rodriguez et al., 2021). Since we know that microglial autophagy is impaired in the 5XFAD model (Ulland *et al.*, 2017) and that the proliferation and survival of these cells is regulated by CSF1R, it is plausible that CSF1R-mediated changes in autophagy could provide mechanistic links related to this improved phenotype (with 18 weeks of LPS) or the exacerbated phenotype (with a single LPS challenge) and this could also be examined in future. Such studies would be contingent on first carefully confirming and elucidating the changes in autophagy in microglia from APP/PS1 mice.

6.3 Sexual dimorphism in microglial gene expression in APP/PS1 microglia

Various neuroinflammatory microglial genes related to primed/DAM phenotype were investigated herein. The expression of most of these DAM genes increased in male APP/PS1 mice in particular and GW2580 mitigated these alterations more efficiently in the male microglia. It is generally accepted that female microglia are more pro-inflammatory and a recent publication by Guillot-Sestier and colleagues showed that microglia from female mice were more glycolytic, less phagocytic and were associated with increased amyloidosis, while microglia isolated from male mice had a more amoeboid morphology. The study also showed that many inflammatory genes and genes related to oxidative stress such as *Ubqin1, App, Hmox, Nkiras1, Mef2a and Panx1* etc. were increased in female microglia with respect to male microglia (Guillot-Sestier *et al.*, 2021). Female are also known to be more prone to developing AD than men (Viña and Lloret, 2010). This literature agrees in part with our findings that a greater microglial frequency was observed in female mice, consistent with an activated state. However, in contrast to the literature, male microglia displayed more

dysfunctional phenotype in the current work. As discussed in Chapter 5, these differential findings do not appear to be not related to circulating sex hormones (Villa *et al.*, 2016) and maybe instated be attributed to the male and female being at different stages of the disease with female APP/PS1 mice developing Aβ burden and poorer learning ability and memory function faster, than age-matched male APP/PS1 mice (Li et al., 2016). Recent studies using CSF1R inhibition strategy to deplete microglia in the 5xFAD AD model reported that microglial elimination before plaque formation was sufficient to halt the progression of plaque pathology (Sosna *et al.*, 2018; Spangenberg *et al.*, 2019). It is a possibility that as males are at a less advanced stages of the disease, so the GW2580 is more effective in microglia from male mice. The data suggest that, though not currently practical, it may be necessary to target microglial CSF1R early in the disease before the development of plaque pathology to achieve maximum benefit. One might also speculate that how the microglia react to Aβ may also play a role in the contradictory findings observed: more amyloid plaques and higher levels of soluble Aβ occur in female AD mice regardless of the brain area examined (Wang *et al.*, 2003). Microglia in the vicinity of the plaques are more reactive and amoeboid compared to the homeostatic microglia in the rest of the parenchyma (Krabbe *et al.*, 2013). Genes that are upregulated in AD mice matched the transcript expression pattern in tissues isolated from the near the Aβ plaques than tissues further away (Orre *et al.*, 2014). Thus, the increased number of plaques may dictate that there are higher numbers of microglia in proximity to Aβ plaques and may be a contributing factor in determining sex differences in microglia phenotype. Taken together, efficiency of GW2580 as a drug relies of various factors, including sex, stages of disease etc. and if it were to develop into a preventative AD treatment, then all these factors need to be considered thoroughly.

This study came with a major limitation in that the sample size was not large enough. Although large effect sizes of the drug treatment were observed in many of the parameters examined here, due to the insufficient number of mice, many of them failed to reach statistical significance. Therefore, the study needs repeated with a larger number of animals that would allow a thorough examination of sex differences with GW2580 treatment and would be sufficient to detect effects that may only occur in females (cognitive dysfunction, synaptic degeneration) or more prominently in males (aspects of the microglial phenotype). Some of the differentially expressed genes such

as *Trem2, Ctsd, Cst7* etc. may be confirmed using visualisation methods such as immunohistochemical analysis of the diseased brain slices. The Western immunoblots were pursued only in female mice hippocampal homogenate based on the cognitive data, but the gene expression analysis on microglial isolates had more profound effects in male mice. Due to time constraints homogenate from male mice were not looked at but this must be done in future to reach a firm conclusion. Therefore, the discussion on sex differences must also take this caveat into consideration.

6.4 Direct and indirect effects of CSF1R inhibition on additional cell types

Given the beneficial effects of removing proliferating microglia from the amyloid-laden brain, it would be important to explore whether CSF1R inhibition exerts these benefits through direct microglial effects on neurons, or via other cell types such as astrocytes. While isolating microglia from the APP/PS1 mice, astrocytes were also isolated, and the RNA has been stored. Interaction between microglia and astrocytes happen via glial contacts as well as via secreted factors to maintain their physiological functions (Liddelow, Marsh and Stevens, 2020). Microglial TREM2 is involved in the uptake of lipoparticles, such as cholesterol, secreted by astrocytes (Bohlen *et al.*, 2017) and a lack of cholesterol from astrocytes may alter microglial phenotype. Secretion of IL-1α, TNFα, and C1q by activated microglia were shown to be sufficient to robustly influence the phenotype of reactive A1 astrocytes. They also reported that A1 astrocytes cause neuronal and oligodendrocyte death in postnatal rats and mice and inhibition of A1 formation by using (IL-1α$^{-/-}$TNFα$^{-/-}$C1q$^{-/-}$) knock-out mice stopped this axotomized neuronal death (Liddelow *et al.*, 2017). Treatment of microglia with chemotherapeutic drug, methotrexate, drives cytokine (ILs and TNF) release by microglia and these cytokines in turn may drive the production of reactive astrocytes (Gibson *et al.*, 2019). Therefore, knowing how the CSF1R-induced changes in microglia would change the phenotype of astrocytes would be a useful addition to our understanding of the function effects of CSF1R inhibition. The effect of inhibition of microglial CSF1R on the astrocyte phenotype should be examined in co-culture experiments with microglia and astrocytes. The influence, on astrocytes, of microglia-secreted factors in the media following CSF1R inhibition should be analysed. Moreover, the same sorts of conditions could also be used to assess whether the microglial secretory profile, as

altered by CSF1R inhibition, would have differential effects on neuronal synapse integrity, following up the effects, observed herein, on synaptic density in vivo.

Despite the unequivocal effects of CSF1R inhibition on brain microglia, it is important to recognise that CSF1R inhibition can also have significant effects on macrophage populations outside the CNS and thus examining the effect of peripheral changes arising from GW2580 administration in APP/PS1 mice would be important. Administration of GW2580 in the SOD1G93A transgenic mouse model of amyotrophic lateral sclerosis (ALS), resulted in protection of skeletal muscle from denervation with GW2580 treatment and restriction of macrophage entry into the nerves (Martínez-Muriana *et al.*, 2016). CSF1R inhibition by PLX5622 also had significant effects on bone marrow derived macrophages, abolishing IL-1β and CD68 production and inhibiting phagocytosis of Zymosan-A BioParticles. Moreover, a decrease in proliferation of resident and interstitial macrophages of peritoneum, lung, and liver but not spleen was observed with PLX5622 treatment in 6-12 month-old C57BL/6J mice (Lei *et al.*, 2020). Another study has reported no difference in blood monocyte numbers with CSF1R inhibition by PLX3397 in mouse model of *cmo* (a gene causing mutation in proline serine threonine phosphatase-interacting protein 2 leading to auto-inflammatory disease) (Chitu *et al.*, 2012). It is important to know whether there are any adverse effects of the drug in the peripheral nervous system and to understand whether some of the beneficial CNS effects may arise from effects on peripheral cells. Even if the putative drug has beneficial effects in the CNS, any negative effects in the peripheral immune system, or peripheral nervous system could present an obstacle to therapeutically targeting CSF1R for treatment or prevention of CNS conditions.

6.5 Inhibition of CSF1R signalling may be beneficial against acute neuroinflammation

In this current study, while CSF1R inhibition was able to demonstrate beneficial effects in an AD mouse model, its inhibition in IMG cells was found to suppress LPS-induced chemokines, such as, CCL2 and CXCL1 expression. The involvement of chemokines (chemotactic cytokines) in CNS injury is well established. Chemokines are released by activated microglia to stimulate migration of the influx of inflammatory cells such as neutrophils (CXCL1) and monocytes (CCL2) to the site of inflammation by following

the chemokine gradient (Hughes and Nibbs, 2018). They also showed that chemokines are subject to post-translational modifications (Hughes and Nibbs, 2018) and their altered expression have been observed in both acute neurodegeneration and in chronic conditions like AD. However, whether the effects of chemokines are necessary for neuroprotection or are detrimental under acute insults remains to be agreed upon.

Acute inflammatory stimulus such as peptidoglycan- or LPS-induced upregulation of chemokines seems to be an unfavourable outcome for the CNS either through direct deleterious effects or through the negative effects of the infiltrating cells that they attract to the CNS. CCL2 has also been reported to increase BBB permeability, in an *in vitro* BBB model of astrocytes and brain endothelial cells co-culture, by 200 fold by redistributing tight junction proteins (Dimitrijevic *et al.*, 2006). CXCL1 has been associated with ROS production and CXCL1 has been shown to be essential for neutrophil migration, expression of proinflammatory mediators such as IL-1β, IL-17 and IL-6 in a mouse model of sepsis (Jin *et al.*, 2014). Analysis of mouse brain 24 hrs post LPS injection (2 mg kg^{-1}) increased CCL2, IL-1β, IL-6, TNFα at mRNA and protein levels and CCL2 induced phagocyte activation and an elevated number of $CCR2^{+}$ inflammatory monocytes in the brain (Cazareth *et al.*, 2014). Taken together, these studies imply that upregulation of chemokines may play a negative role in CNS homeostasis and blocking this upregulation by CSF1R may prove to have a protective effect.

An effort was made in Chapter 4 to reconcile how CSF1R inhibition might inhibit expression of some chemokines such as CCL2 and CXCL1 but not others like CXCL10. While speculating that differential regulatory mechanism between the chemokines might be responsible, currently no concrete conclusion was reached as to what that could be. A well-known transcription factor for chemokine and cytokine regulation is NFkB (Liu *et al.*, 2017). In this study the role of this pathway on CXCL1 and CCL2 expression following 24 hr LPS treatment was looked at. However, 24 hr may be too late to capture any NFkB signalling events. Therefore, the effect of NFkB activation on chemokine secretion over a period of time should be explored experimentally in future. Likewise, it has been shown that both JNK and STAT signalling play roles in the timing and magnitude of chemokine expression in other cell

populations, *in vitro*, and it will be useful to examine whether there are differential effects of JNK and STAT inhibitors on the secretion of chemokines by microglia in the presence and absence of CSF1R inhibition.

6.6 Conclusion

Overall, this work demonstrated that inhibition of CSF1R signalling, a pathway linked to microglial proliferation, mitigates several potentially detrimental facets of microglial function including suppression of LPS-induced chemokine and NO secretion and amelioration of phagocytosis. CSF1R inhibition also prevented synaptic loss and improved memory functions and detrimental DAM phenotype in microglia *in vivo*. Advancement of health science over the recent past century has seen a steady rise in life expectancy and thus an increase in AD prevalence. However, there remains no effective preventative or disease-modifying treatment. It is becoming increasingly clear targeting Aβ might not be sufficient as a treatment for AD. Microglia, the main macrophage population of the brain, which is regulated by CSF1R, should be a key focus in developing new therapies. Therefore, CSF1R is a promising target to provide disease-modifying therapy.

Chapter 7: Bibliography

Ahmed, F. et al. (2008) ‘Brain-derived neurotrophic factor modulates expression of chemokine receptors in the brain’, Brain Research. doi: 10.1016/j.brainres.2008.05.086.
Aizenstein, H. J. et al. (2008) ‘Frequent amyloid deposition without significant cognitive impairment among the elderly’, Archives of Neurology. doi: 10.1001/archneur.65.11.1509.
Ajami, B. et al. (2007) ‘Local self-renewal can sustain CNS microglia maintenance and function throughout adult life’, Nature Neuroscience. doi: 10.1038/nn2014.
Alrashdan, Y. A. et al. (2012) ‘Asthmatic airway smooth muscle CXCL10 production: Mitogen-activated protein kinase JNK involvement’, American Journal of Physiology - Lung Cellular and Molecular Physiology. doi: 10.1152/ajplung.00232.2011.
Angelova, D. M. and Brown, D. R. (2019) ‘Microglia and the aging brain: are senescent microglia the key to neurodegeneration?’, Journal of Neurochemistry. doi: 10.1111/jnc.14860.
Anwar, T. et al. (2019) ‘ER-Targeted Beclin 1 Supports Autophagosome Biogenesis in the Absence of ULK1 and ULK2 Kinases’, Cells. doi: 10.3390/cells8050475.
Arreola, M. A. et al. (2021) ‘Microglial dyshomeostasis drives perineuronal net and synaptic loss in a CSF1R+/− mouse model of ALSP, which can be rescued via CSF1R inhibitors’, Science Advances. doi: 10.1126/sciadv.abg1601.
Axe, E. L. et al. (2008) ‘Autophagosome formation from membrane compartments enriched in phosphatidylinositol 3-phosphate and dynamically connected to the endoplasmic reticulum’, Journal of Cell Biology. doi: 10.1083/jcb.200803137.
Bao, H. R. et al. (2020) ‘Relationship between pi3k/mtor/rhoa pathway-regulated cytoskeletal rearrangements and phagocytic capacity of macrophages’, Brazilian Journal of Medical and Biological Research. doi: 10.1590/1414-431x20209207.
Baranov, M. V. et al. (2016) ‘SWAP70 Organizes the Actin Cytoskeleton and Is Essential for Phagocytosis’, Cell Reports. doi: 10.1016/j.celrep.2016.10.021.
Bartocci, A. et al. (1987) ‘Macrophages specifically regulate the concentration of their own growth factor in the circulation.’, Proceedings of the National Academy of Sciences of the United States of America. doi: 10.1073/pnas.84.17.6179.
Beckmann, N. et al. (2018) ‘Brain region-specific enhancement of remyelination and prevention of demyelination by the CSF1R kinase inhibitor BLZ945’, Acta neuropathologica communications. doi: 10.1186/s40478-018-0510-8.

Bécot, A. et al. (2020) ‘The Transcription Factor EB Reduces the Intraneuronal Accumulation of the Beta-Secretase-Derived APP Fragment C99 in Cellular and Mouse Alzheimer’s Disease Models’, Cells. doi: 10.3390/cells9051204.

Belinson, H. et al. (2008) ‘Activation of the amyloid cascade in apolipoprotein E4 transgenic mice induces lysosomal activation and neurodegeneration resulting in marked cognitive deficits’, Journal of Neuroscience. doi: 10.1523/JNEUROSCI.5633-07.2008.

Bennett, J. M. et al. (2018) ‘Inflammation-nature’s way to efficiently respond to all types of challenges: Implications for understanding and managing “the epidemic” of chronic diseases’, Frontiers in Medicine. doi: 10.3389/fmed.2018.00316.

Von Bernhardi, R., Tichauer, J. E. and Eugenín, J. (2010) ‘Aging-dependent changes of microglial cells and their relevance for neurodegenerative disorders’, Journal of Neurochemistry. doi: 10.1111/j.1471-4159.2009.06537.x.

Bertram, L., Lill, C. M. and Tanzi, R. E. (2010) ‘The genetics of alzheimer disease: Back to the future’, Neuron. doi: 10.1016/j.neuron.2010.10.013.

Bien-Ly, N. et al. (2012) ‘Reducing human apolipoprotein E levels attenuates age-dependent Aβ accumulation in mutant human amyloid precursor protein transgenic mice.’, The Journal of neuroscience : the official journal of the Society for Neuroscience. doi: 10.1523/JNEUROSCI.0033-12.2012.

Björkblom, B. et al. (2008) ‘All JNKs can kill, but nuclear localization is critical for neuronal death’, Journal of Biological Chemistry. doi: 10.1074/jbc.M707744200.

Blain, J. F. et al. (2006) ‘A polymorphism in lipoprotein lipase affects the severity of Alzheimer’s disease pathophysiology’, European Journal of Neuroscience. doi: 10.1111/j.1460-9568.2006.05007.x.

Blasi, E. et al. (1990) ‘Immortalization of murine microglial cells by a v-raf / v-myc carrying retrovirus’, Journal of Neuroimmunology. doi: 10.1016/0165-5728(90)90073-V.

Blommaart, E. F. C. et al. (1995) ‘Phosphorylation of ribosomal protein S6 is inhibitory for autophagy in isolated rat hepatocytes’, Journal of Biological Chemistry. doi: 10.1074/jbc.270.5.2320.

Bocchini, V. et al. (1992) ‘An immortalized cell line expresses properties of activated microglial cells’, Journal of Neuroscience Research. doi: 10.1002/jnr.490310405.

Bohlen, C. J. et al. (2017) ‘Diverse Requirements for Microglial Survival, Specification, and Function Revealed by Defined-Medium Cultures’, Neuron. doi: 10.1016/j.neuron.2017.04.043.

Boissonneault, V. et al. (2009) ‘Powerful beneficial effects of macrophage colony-stimulating factor on beta-amyloid deposition and cognitive impairment in Alzheimer’s disease.’, Brain : a journal of neurology, 132(Pt 4), pp. 1078–92. doi: 10.1093/brain/awn331.

Bollag, G. et al. (2012) ‘Vemurafenib: The first drug approved for BRAF-mutant cancer’, Nature Reviews Drug Discovery. doi: 10.1038/nrd3847.

Bonilla, F. A. and Oettgen, H. C. (2010) ‘Adaptive immunity’, Journal of Allergy and Clinical Immunology. doi: 10.1016/j.jaci.2009.09.017.

Böttcher, C. et al. (2019) ‘Human microglia regional heterogeneity and phenotypes determined by multiplexed single-cell mass cytometry’, Nature Neuroscience. doi: 10.1038/s41593-018-0290-2.

Boulakirba, S. et al. (2018) ‘IL-34 and CSF-1 display an equivalent macrophage differentiation ability but a different polarization potential’, Scientific Reports. doi: 10.1038/s41598-017-18433-4.

Boya, P. et al. (2005) ‘Inhibition of Macroautophagy Triggers Apoptosis Inhibition of Macroautophagy Triggers Apoptosis †’, Molecular and Cellular Biology. doi: 10.1128/MCB.25.3.1025.

Brendecke, S. M. and Prinz, M. (2015) ‘Do not judge a cell by its cover—diversity of CNS resident, adjoining and infiltrating myeloid cells in inflammation’, Seminars in Immunopathology. doi: 10.1007/s00281-015-0520-6.

Brown, G. C. and Neher, J. J. (2012) ‘Eaten alive! Cell death by primary phagocytosis: “Phagoptosis”’, Trends in Biochemical Sciences. doi: 10.1016/j.tibs.2012.05.002.

Bruce-Keller, A. J. et al. (2011) ‘Cognitive impairment in humanized APP×PS1 mice is linked to Aβ 1-42 and NOX activation’, Neurobiology of Disease. doi: 10.1016/j.nbd.2011.07.012.

Burgess, A. W. and Metcalf, D. (1980) ‘The nature and action of granulocyte - macrophage colony stimulating factors’, Blood. doi: 10.1182/blood.v56.6.947.947.

Burke, S. J. et al. (2013) ‘ Synergistic Expression of the CXCL10 Gene in Response to IL-1β and IFN-γ Involves NF-κB, Phosphorylation of STAT1 at Tyr 701 , and Acetylation of Histones H3 and H4 ’, The Journal of Immunology. doi: 10.4049/jimmunol.1300344.

Burke, S. J. et al. (2014) ‘NF-κB and STAT1 control CXCL1 and CXCL2 gene transcription’, American Journal of Physiology - Endocrinology and Metabolism. doi: 10.1152/ajpendo.00347.2013.
Butovsky, O. et al. (2014) ‘Identification of a unique TGF-β-dependent molecular and functional signature in microglia’, Nature Neuroscience. doi: 10.1038/nn.3599.
Buttgereit, A. et al. (2016) ‘Sall1 is a transcriptional regulator defining microglia identity and function’, Nature Immunology. doi: 10.1038/ni.3585.
Byfield, M. P., Murray, J. T. and Backer, J. M. (2005) ‘hVps34 is a nutrient-regulated lipid kinase required for activation of p70 S6 kinase’, Journal of Biological Chemistry. doi: 10.1074/jbc.M507201200.
Caccamo, A. et al. (2010) ‘Molecular interplay between mammalian target of rapamycin (mTOR), amyloid-β, and Tau: Effects on cognitive impairments’, Journal of Biological Chemistry. doi: 10.1074/jbc.M110.100420.
Caccamo, A. et al. (2017) ‘p62 improves AD-like pathology by increasing autophagy’, Molecular Psychiatry. doi: 10.1038/mp.2016.139.
Casali, B. T. and Reed-Geaghan, E. G. (2021) ‘Microglial function and regulation during development, homeostasis and alzheimer’s disease’, Cells. doi: 10.3390/cells10040957.
Cataldo, A. M. et al. (1997) ‘Increased Neuronal Endocytosis and Protease Delivery to Early Endosomes In Sporadic Alzheimers-Disease - Neuropathologic Evidence For a Mechanism Of Increased β-Amyloidogenesis’, Journal of Neuroscience, 17(16), pp. 6142–6151.
Cazareth, J. et al. (2014) ‘Molecular and cellular neuroinflammatory status of mouse brain after systemic lipopolysaccharide challenge: Importance of CCR2/CCL2 signaling’, Journal of Neuroinflammation. doi: 10.1186/1742-2094-11-132.
Celada, A. et al. (1996) ‘The transcription factor PU.1 is involved in macrophage proliferation’, Journal of Experimental Medicine. doi: 10.1084/jem.184.1.61.
Chai, Y. L. et al. (2019) ‘Lysosomal cathepsin D is upregulated in Alzheimer’s disease neocortex and may be a marker for neurofibrillary degeneration’, Brain Pathology. doi: 10.1111/bpa.12631.
Chalhoub, N. and Baker, S. J. (2009) ‘PTEN and the PI3-kinase pathway in cancer’, Annual Review of Pathology: Mechanisms of Disease. doi: 10.1146/annurev.pathol.4.110807.092311.

Chen, F., Castranova, V. and Shi, X. (2001) ‘New insights into the role of nuclear factor-κB in cell growth regulation’, American Journal of Pathology. doi: 10.1016/S0002-9440(10)61708-7.
Chen, P., Cescon, M. and Bonaldo, P. (2014) ‘Autophagy-mediated regulation of macrophages and its applications for cancer’, Autophagy. doi: 10.4161/auto.26927.
Chen, Y. C. et al. (2021) ‘Withholding of M-CSF supplement reprograms macrophages to M2-like via endogenous CSF-1 activation’, International Journal of Molecular Sciences. doi: 10.3390/ijms22073532.
Cheong, H. et al. (2011) ‘Ammonia-induced autophagy is independent of ULK1/ULK2 kinases’, Proceedings of the National Academy of Sciences of the United States of America. doi: 10.1073/pnas.1107969108.
Chihara, T. et al. (2010) ‘IL-34 and M-CSF share the receptor Fms but are not identical in biological activity and signal activation’, Cell Death and Differentiation. doi: 10.1038/cdd.2010.60.
Chitu, V. et al. (2012) ‘PSTPIP2 deficiency in mice causes osteopenia and increased differentiation of multipotent myeloid precursors into osteoclasts’, Blood. doi: 10.1182/blood-2012-04-425595.
Chitu, V. et al. (2016) ‘Emerging Roles for CSF-1 Receptor and its Ligands in the Nervous System’, Trends in Neurosciences. doi: 10.1016/j.tins.2016.03.005.
Chitu, V. and Stanley, E. R. (2006) ‘Colony-stimulating factor-1 in immunity and inflammation’, Current Opinion in Immunology. doi: 10.1016/j.coi.2005.11.006.
Cho, M. H. et al. (2014) ‘Autophagy in microglia degrades extracellular β-amyloid fibrils and regulates the NLRP3 inflammasome’, Autophagy, 10(10), pp. 1761–1775. doi: 10.4161/auto.29647.
Chu, C. T., Zhu, J. and Dagda, R. (2007) ‘Beclin 1-independent pathway of damage-induced mitophagy and autophagic stress: Implications for neurodegeneration and cell death’, Autophagy. doi: 10.4161/auto.4625.
Colonna, M. and Butovsky, O. (2017) ‘Microglia Function in the Central Nervous System During Health and Neurodegeneration’, Annual Review of Immunology. doi: 10.1146/annurev-immunol-051116-052358.
Comalada, M. et al. (2003) ‘PKCε is involved in JNK activation that mediates LPS-induced TNF-α, which induces apoptosis in macrophages’, American Journal of Physiology - Cell Physiology. doi: 10.1152/ajpcell.00228.2003.

Condello, C. et al. (2015) ‘Microglia constitute a barrier that prevents neurotoxic protofibrillar Aβ42 hotspots around plaques’, Nature Communications. doi: 10.1038/ncomms7176.

Conway, J. G. et al. (2005) ‘Inhibition of colony-stimulating-factor-1 signaling in vivo with the orally bioavailable cFMS kinase inhibitor GW2580.’, Proceedings of the National Academy of Sciences of the United States of America. doi: 10.1073/pnas.0502000102.

Conway, J. G. et al. (2008) ‘Effects of the cFMS kinase inhibitor 5-(3-methoxy-4-((4-methoxybenzyl)oxy)benzyl)pyrimidine-2,4-diamine (GW2580) in normal and arthritic rats.’, The Journal of pharmacology and experimental therapeutics. doi: 10.1124/jpet.107.129429.

Crain, J. M., Nikodemova, M. and Watters, J. J. (2013) ‘Microglia express distinct M1 and M2 phenotypic markers in the postnatal and adult central nervous system in male and female mice’, Journal of Neuroscience Research. doi: 10.1002/jnr.23242.

Cui, W. et al. (2020) ‘Inhibition of TLR4 Induces M2 Microglial Polarization and Provides Neuroprotection via the NLRP3 Inflammasome in Alzheimer’s Disease’, Frontiers in Neuroscience. doi: 10.3389/fnins.2020.00444.

Dagher, N. N. et al. (2015) ‘Colony-stimulating factor 1 receptor inhibition prevents microglial plaque association and improves cognition in 3xTg-AD mice’, Journal of Neuroinflammation, 12(1), p. 139. doi: 10.1186/s12974-015-0366-9.

Dai, X. M. et al. (2004) ‘Incomplete restoration of colony-stimulating factor 1 (CSF-1) function in CSF-1-deficient Csf1op/Csf1op mice by transgenic expression of cell surface CSF-1’, Blood. doi: 10.1182/blood-2003-08-2739.

Daily, K. P. and Amer, A. (2020) ‘Microglial autophagy-mediated clearance of amyloid-beta plaques is dysfunctional in Alzheimer’s disease mice’, Alzheimer’s & Dementia. doi: 10.1002/alz.044120.

Davies, C. A. et al. (1987) ‘A quantitative morphometric analysis of the neuronal and synaptic content of the frontal and temporal cortex in patients with Alzheimer’s disease’, Journal of the Neurological Sciences. doi: 10.1016/0022-510X(87)90057-8.

Davis, M. I. et al. (2011) ‘Comprehensive analysis of kinase inhibitor selectivity’, Nature Biotechnology. doi: 10.1038/nbt.1990.

Dejanovic, B. et al. (2018) ‘Changes in the Synaptic Proteome in Tauopathy and Rescue of Tau-Induced Synapse Loss by C1q Antibodies’, Neuron. doi: 10.1016/j.neuron.2018.10.014.

Delaney, C. et al. (2021) ‘Attenuated CSF-1R signalling drives cerebrovascular pathology’, EMBO Molecular Medicine. doi: 10.15252/emmm.202012889.
Deretic, V., Saitoh, T. and Akira, S. (2013) ‘Autophagy in infection, inflammation and immunity’, Nature Reviews Immunology. doi: 10.1038/nri3532.
Dhillon, N. K. et al. (2007) ‘PDGF Synergistically Enhances IFN-γ-Induced Expression of CXCL10 in Blood-Derived Macrophages: Implications for HIV Dementia’, The Journal of Immunology. doi: 10.4049/jimmunol.179.5.2722.
Dibble, C. C. and Cantley, L. C. (2015) ‘Regulation of mTORC1 by PI3K signaling’, Trends in Cell Biology. doi: 10.1016/j.tcb.2015.06.002.
Digiacomo, G. et al. (2015) ‘Prostaglandin E2 transactivates the colony-stimulating factor-1 receptor and synergizes with Colony-stimulating factor-1 in the induction of macrophage migration via the mitogen-activated protein kinase ERK1/2’, FASEB Journal. doi: 10.1096/fj.14-258939.
Dimitrijevic, O. B. et al. (2006) ‘Effects of the chemokine CCL2 on blood-brain barrier permeability during ischemia-reperfusion injury’, Journal of Cerebral Blood Flow and Metabolism. doi: 10.1038/sj.jcbfm.9600229.
Domigan, C. K. et al. (2015) ‘Autocrine VEGF maintains endothelial survival through regulation of metabolism and autophagy’, Journal of Cell Science. doi: 10.1242/jcs.163774.
Dorsey, F. C. et al. (2009) ‘Mapping the phosphorylation sites of Ulk1’, Journal of Proteome Research. doi: 10.1021/pr900583m.
Douglass, T. G. et al. (2008) ‘Macrophage colony stimulating factor: Not just for macrophages anymore! A gateway into complex biologies’, International Immunopharmacology. doi: 10.1016/j.intimp.2008.04.016.
Du, X. et al. (2020) ‘Combinational pretreatment of colony-stimulating factor 1 receptor inhibitor and triptolide upregulates BDNF-AKT and autophagic pathways to improve cerebral ischemia’, Mediators of Inflammation. doi: 10.1155/2020/8796103.
Duran, A. et al. (2011) ‘P62 Is a Key Regulator of Nutrient Sensing in the mTORC1 Pathway’, Molecular Cell. doi: 10.1016/j.molcel.2011.06.038.
Düvel, K. et al. (2010) ‘Activation of a metabolic gene regulatory network downstream of mTOR complex 1’, Molecular Cell. doi: 10.1016/j.molcel.2010.06.022.
Easley-Neal, C. et al. (2019) ‘CSF1R Ligands IL-34 and CSF1 Are Differentially Required for Microglia Development and Maintenance in White and Gray Matter Brain Regions’, Frontiers in Immunology. doi: 10.3389/fimmu.2019.02199.

Ellis, S. L. et al. (2010) ‘The Cell-Specific Induction of CXC Chemokine Ligand 9 Mediated by IFN-γ in Microglia of the Central Nervous System Is Determined by the Myeloid Transcription Factor PU.1’, The Journal of Immunology. doi: 10.4049/jimmunol.1000900.

Elmore, M. R. P. et al. (2014) ‘Colony-stimulating factor 1 receptor signaling is necessary for microglia viability, unmasking a microglia progenitor cell in the adult brain’, Neuron, 82(2), pp. 380–397. doi: 10.1016/j.neuron.2014.02.040.

Fang, L. et al. (2021) ‘LAMC1 upregulation via TGFβ induces inflammatory cancer-associated fibroblasts in esophageal squamous cell carcinoma via NF-κB–CXCL1–STAT3’, Molecular Oncology. doi: 10.1002/1878-0261.13053.

Farag, A. K. et al. (2019) ‘First-in-class DAPK1/CSF1R dual inhibitors: Discovery of 3,5-dimethoxy-N-(4-(4-methoxyphenoxy)-2-((6-morpholinopyridin-3-yl)amino)pyrimidin-5-yl)benzamide as a potential anti-tauopathies agent’, European Journal of Medicinal Chemistry. doi: 10.1016/j.ejmech.2018.10.057.

Farlik, M. et al. (2010) ‘Nonconventional initiation complex assembly by STAT and NF-κB transcription factors regulates nitric oxide synthase expression’, Immunity. doi: 10.1016/j.immuni.2010.07.001.

Felix, J. et al. (2013) ‘Human IL-34 and CSF-1 establish structurally similar extracellular assemblies with their common hematopoietic receptor’, Structure. doi: 10.1016/j.str.2013.01.018.

Fietta, A. M. et al. (2002) ‘Pharmacological analysis of signal transduction pathways required for mycobacterium tuberculosis-induced iL-8 and MCP-1 production in human peripheral monocytes’, Cytokine. doi: 10.1006/cyto.2002.1968.

Flex, A. et al. (2014) ‘Effect of proinflammatory gene polymorphisms on the risk of Alzheimer’s disease’, Neurodegenerative Diseases. doi: 10.1159/000353395.

Florey, O. et al. (2011) ‘Autophagy machinery mediates macroendocytic processing and entotic cell death by targeting single membranes’, Nature Cell Biology. doi: 10.1038/ncb2363.

Fu, R. et al. (2014) ‘Phagocytosis of microglia in the central nervous system diseases’, Molecular Neurobiology. doi: 10.1007/s12035-013-8620-6.

Fujita, N. et al. (2008) ‘The Atg16L complex specifies the site of LC3 lipidation for membrane biogenesis in autophagy’, Molecular Biology of the Cell. doi: 10.1091/mbc.E07-12-1257.

Gallo, R. L. and Nakatsuji, T. (2011) 'Microbial symbiosis with the innate immune defense system of the skin', Journal of Investigative Dermatology. doi: 10.1038/jid.2011.182.

Gang, H. et al. (2011) 'Epigenetic regulation of E2F-1-dependent Bnip3 transcription and cell death by nuclear factor-κB and histone deacetylase-1', in Pediatric Cardiology. doi: 10.1007/s00246-011-9893-z.

Garceau, V. et al. (2010) 'Pivotal Advance: Avian colony-stimulating factor 1 (CSF-1), interleukin-34 (IL-34), and CSF-1 receptor genes and gene products', Journal of Leukocyte Biology. doi: 10.1189/jlb.0909624.

Gee, M. S. et al. (2018) 'A Novel and Selective p38 Mitogen-Activated Protein Kinase Inhibitor Attenuates LPS-Induced Neuroinflammation in BV2 Microglia and a Mouse Model', Neurochemical Research. doi: 10.1007/s11064-018-2661-1.

Gibson, E. M. et al. (2019) 'Methotrexate Chemotherapy Induces Persistent Tri-glial Dysregulation that Underlies Chemotherapy-Related Cognitive Impairment', Cell. doi: 10.1016/j.cell.2018.10.049.

Giménez-Llort, L. et al. (2021) 'Survival bias and crosstalk between chronological and behavioral age: Age- and genotype-sensitivity tests define behavioral signatures in middle-aged, old, and long-lived mice with normal and ad-associated aging', Biomedicines. doi: 10.3390/biomedicines9060636.

Ginhoux, F. et al. (2013) 'Origin and differentiation of microglia', Frontiers in Cellular Neuroscience. doi: 10.3389/fncel.2013.00045.

Gómez-Nicola, D. et al. (2013) 'Regulation of microglial proliferation during chronic neurodegeneration', Journal of Neuroscience. doi: 10.1523/JNEUROSCI.4440-12.2013.

Graeber, M. B. (2010) 'Changing face of microglia', Science. doi: 10.1126/science.1190929.

Greter, M. et al. (2012) 'Stroma-Derived Interleukin-34 Controls the Development and Maintenance of Langerhans Cells and the Maintenance of Microglia', Immunity. doi: 10.1016/j.immuni.2012.11.001.

Gu, B. J. et al. (2010) 'The P2X7-nonmuscle myosin membrane complex regulates phagocytosis of nonopsonized particles and bacteria by a pathway attenuated by extracellular ATP', Blood. doi: 10.1182/blood-2009-11-251744.

Guerreiro, R. et al. (2013) 'TREM2 Variants in Alzheimer's Disease ', New England Journal of Medicine. doi: 10.1056/nejmoa1211851.

Guillonneau, C., Bézie, S. and Anegon, I. (2017) 'Immunoregulatory properties of the cytokine IL-34', Cellular and Molecular Life Sciences. doi: 10.1007/s00018-017-2482-4.

Guillot-Sestier, M. V. et al. (2021) 'Microglial metabolism is a pivotal factor in sexual dimorphism in Alzheimer's disease', Communications Biology. doi: 10.1038/s42003-021-02259-y.

Hagan, N. et al. (2020) 'CSF1R signaling is a regulator of pathogenesis in progressive MS', Cell Death and Disease. doi: 10.1038/s41419-020-03084-7.

Han, J. et al. (2021) 'Uncovering sex differences of rodent microglia', Journal of Neuroinflammation. doi: 10.1186/s12974-021-02124-z.

Hansen, D. V., Hanson, J. E. and Sheng, M. (2018) 'Microglia in Alzheimer's disease', Journal of Cell Biology. doi: 10.1083/jcb.201709069.

Hansen, K. et al. (2007) 'Autophagic cell death induced by TrkA receptor activation in human glioblastoma cells', Journal of Neurochemistry. doi: 10.1111/j.1471-4159.2007.04753.x.

Hao, A. J., Dheen, S. T. and Ling, E. A. (2002) 'Expression of macrophage colony-stimulating factor and its receptor in microglia activation is linked to teratogen-induced neuronal damage', Neuroscience, 112(4), pp. 889–900. doi: 10.1016/S0306-4522(02)00144-6.

Hashimoto, D. et al. (2013) 'Tissue-resident macrophages self-maintain locally throughout adult life with minimal contribution from circulating monocytes', Immunity. doi: 10.1016/j.immuni.2013.04.004.

Hayflick, L. (1965) 'The limited in vitro lifetime of human diploid cell strains', Experimental Cell Research. doi: 10.1016/0014-4827(65)90211-9.

Haynes, S. E. et al. (2006) 'The P2Y12 receptor regulates microglial activation by extracellular nucleotides', Nature Neuroscience. doi: 10.1038/nn1805.

Heckmann, B. L. et al. (2019) 'LC3-Associated Endocytosis Facilitates β-Amyloid Clearance and Mitigates Neurodegeneration in Murine Alzheimer's Disease', Cell. doi: 10.1016/j.cell.2019.05.056.

Hellwig, S., Heinrich, A. and Biber, K. (2013) 'The brain's best friend: Microglial neurotoxicity revisited', Frontiers in Cellular Neuroscience. doi: 10.3389/fncel.2013.00071.

Hensley, K. (2010) ‘Neuroinflammation in Alzheimer’s disease: Mechanisms, pathologic consequences, and potential for therapeutic manipulation’, Journal of Alzheimer’s Disease, pp. 1–14. doi: 10.3233/JAD-2010-1414.
Herrera-Molina, R. et al. (2012) ‘Modulation of interferon-γ-induced glial cell activation by transforming growth factor β1: A role for STAT1 and MAPK pathways’, Journal of Neurochemistry. doi: 10.1111/j.1471-4159.2012.07887.x.
Himes, S. R. et al. (2006) ‘The JNK Are Important for Development and Survival of Macrophages’, The Journal of Immunology. doi: 10.4049/jimmunol.176.4.2219.
Hindupur, S. K., González, A. and Hall, M. N. (2015) ‘The opposing actions of target of rapamycin and AMP-Activated protein kinase in cell growth control’, Cold Spring Harbor Perspectives in Medicine. doi: 10.1101/cshperspect.a019141.
Hollingworth, P. et al. (2011) ‘Common variants at ABCA7, MS4A6A/MS4A4E, EPHA1, CD33 and CD2AP are associated with Alzheimer’s disease’, Nature Genetics. doi: 10.1038/ng.803.
Holmes, C. et al. (2008) ‘Long-term effects of Abeta42 immunisation in Alzheimer’s disease: follow-up of a randomised, placebo-controlled phase I trial.’, Lancet. doi: 10.1016/S0140-6736(08)61075-2.
Holtman, I. R. et al. (2015) ‘Induction of a common microglia gene expression signature by aging and neurodegenerative conditions: a co-expression meta-analysis’, Acta neuropathologica communications. doi: 10.1186/s40478-015-0203-5.
Hommes, D. W., Peppelenbosch, M. P. and Van Deventer, S. J. H. (2003) ‘Mitogen activated protein (MAP) kinase signal transduction pathways and novel anti-inflammatory targets’, Gut. doi: 10.1136/gut.52.1.144.
Horvath, R. J. et al. (2008) ‘Differential migration, LPS-induced cytokine, chemokine, and NO expression in immortalized BV-2 and HAPI cell lines and primary microglial cultures’, Journal of Neurochemistry. doi: 10.1111/j.1471-4159.2008.05633.x.
Hosokawa, N. et al. (2009) ‘Nutrient-dependent mTORC1 Association with the ULK1 – Atg13 – FIP200 Complex Required for Autophagy’, Molecular Biology of the Cell. doi: 10.1091/mbc.E08.
Hu, X. et al. (2012) ‘Clozapine protects dopaminergic neurons from inflammation-induced damage by inhibiting microglial overactivation’, Journal of Neuroimmune Pharmacology. doi: 10.1007/s11481-011-9309-0.

Hu, Y. et al. (2020) ‘mTOR-mediated metabolic reprogramming shapes distinct microglia functions in response to lipopolysaccharide and ATP’, GLIA. doi: 10.1002/glia.23760.
Hu, Y. et al. (2021) ‘Replicative senescence dictates the emergence of disease-associated microglia and contributes to Aβ pathology’, Cell Reports. doi: 10.1016/j.celrep.2021.109228.
Hubbard, S. R., Mohammadi, M. and Schlessinger, J. (1998) ‘Autoregulatory mechanisms in protein-tyrosine kinases’, Journal of Biological Chemistry, pp. 11987–11990. doi: 10.1074/jbc.273.20.11987.
Hughes, C. E. and Nibbs, R. J. B. (2018) ‘A guide to chemokines and their receptors’, FEBS Journal. doi: 10.1111/febs.14466.
Hume, D. A. and MacDonald, K. P. A. (2012) ‘Therapeutic applications of macrophage colony-stimulating factor-1 (CSF-1) and antagonists of CSF-1 receptor (CSF-1R) signaling’, Blood. doi: 10.1182/blood-2011-09-379214.
Imai, Y. and Kohsaka, S. (2002) ‘Intracellular signaling in M-CSF-induced microglia activation: Role of Iba1’, GLIA, pp. 164–174. doi: 10.1002/glia.10149.
Imbimbo, B. P. (2009) ‘An update on the efficacy of non-steroidal anti-inflammatory drugs in Alzheimer’s disease’, Expert Opinion on Investigational Drugs. doi: 10.1517/13543780903066780.
Itakura, E., Kishi-Itakura, C. and Mizushima, N. (2012) ‘The hairpin-type tail-anchored SNARE syntaxin 17 targets to autophagosomes for fusion with endosomes/lysosomes’, Cell. doi: 10.1016/j.cell.2012.11.001.
Jack, C. et al. (2013) ‘O3–03–01: Update on hypothetical model of Alzheimer’s disease biomarkers’, Alzheimer’s & Dementia. doi: 10.1016/j.jalz.2013.04.248.
Jacquel, A. et al. (2009) ‘Colony-stimulating factor-1-induced oscillations in phosphatidylinositol-3 kinase/AKT are required for caspase activation in monocytes undergoing differentiation into macrophages’, Blood. doi: 10.1182/blood-2009-03-208843.
Jay, T. R. et al. (2015) ‘TREM2 deficiency eliminates TREM2+ inflammatory macrophages and ameliorates pathology in Alzheimer’s disease mouse models’, Journal of Experimental Medicine. doi: 10.1084/jem.20142322.
Ji, M. et al. (2011) ‘Highly frequent promoter methylation and PIK3CA amplification in non-small cell lung cancer (NSCLC)’, BMC Cancer, 11. doi: 10.1186/1471-2407-11-147.

Jiang, T. et al. (2016) ‘A rare coding variant in TREM2 increases risk for Alzheimer’s disease in Han Chinese’, Neurobiology of Aging. doi: 10.1016/j.neurobiolaging.2016.02.023.
Jin, L. et al. (2014) ‘CXCL1 Contributes to Host Defense in Polymicrobial Sepsis via Modulating T Cell and Neutrophil Functions’, The Journal of Immunology. doi: 10.4049/jimmunol.1401138.
Jin, S. C. et al. (2014) ‘Coding variants in TREM2 increase risk for Alzheimer’s disease’, Human Molecular Genetics. doi: 10.1093/hmg/ddu277.
Jonsson, T. et al. (2013) ‘Variant of TREM2 associated with the risk of Alzheimer’s disease.’, The New England journal of medicine, 368(2), pp. 107–116. doi: 10.1056/NEJMoa1211103.
Kabeya, Y. et al. (2004) ‘LC3, GABARAP and GATE16 localize to autophagosomal membrane depending on form-II formation’, Journal of Cell Science. doi: 10.1242/jcs.01131.
Kamat, C. D. et al. (2008) ‘Antioxidants in central nervous system diseases: Preclinical promise and translational challenges’, Journal of Alzheimer’s Disease. doi: 10.3233/JAD-2008-15314.
Keane, L. et al. (2021) ‘mTOR-dependent translation amplifies microglia priming in aging mice’, Journal of Clinical Investigation. doi: 10.1172/JCI132727.
Kennedy, R. H. and Silver, R. (2015) ‘Neuroimmune Signaling: Cytokines and the CNS’, in Neuroscience in the 21st Century. doi: 10.1007/978-1-4614-6434-1_174-1.
Keren-Shaul, H. et al. (2017) ‘A Unique Microglia Type Associated with Restricting Development of Alzheimer’s Disease’, Cell. doi: 10.1016/j.cell.2017.05.018.
Kettenmann, H., Kirchhoff, F. and Verkhratsky, A. (2013) ‘Microglia: New Roles for the Synaptic Stripper’, Neuron. doi: 10.1016/j.neuron.2012.12.023.
Kielian, T. (2014) ‘Neuroinflammation: Good, bad, or indifferent?’, Journal of Neurochemistry. doi: 10.1111/jnc.12755.
Kierdorf, K. et al. (2013) ‘Microglia emerge from erythromyeloid precursors via Pu.1- and Irf8-dependent pathways’, Nature Neuroscience. doi: 10.1038/nn.3318.
Kim, E. et al. (2008) ‘Regulation of TORC1 by Rag GTPases in nutrient response’, Nature Cell Biology. doi: 10.1038/ncb1753.
Kim, E. A. et al. (2014) ‘Anti-inflammatory mechanisms of N-adamantyl-4-methylthiazol-2-amine in lipopolysaccharide-stimulated BV-2 microglial cells’, International Immunopharmacology. doi: 10.1016/j.intimp.2014.06.022.

Kim, J. et al. (2011) ‘AMPK and mTOR regulate autophagy through direct phosphorylation of Ulk1’, Nature Cell Biology. doi: 10.1038/ncb2152.
Kim, M. J. et al. (2013) ‘Floridoside suppresses pro-inflammatory responses by blocking MAPK signaling in activated microglia’, BMB Reports. doi: 10.5483/BMBRep.2013.46.8.237.
Kirisako, T. et al. (2000) ‘The reversible modification regulates the membrane-binding state of Apg8/Aut7 essential for autophagy and the cytoplasm to vacuole targeting pathway’, Journal of Cell Biology. doi: 10.1083/jcb.151.2.263.
Klionsky, D. J. et al. (2012) ‘Guidelines for the use and interpretation of assays for monitoring autophagy’, Autophagy. doi: 10.4161/auto.19496.
Kobayashi, Y. et al. (2018) ‘Oral administration of Pantoea agglomerans-derived lipopolysaccharide prevents metabolic dysfunction and Alzheimer’s disease-related memory loss in senescence-accelerated prone 8 (SAMP8) mice fed a high-fat diet’, PLoS ONE. doi: 10.1371/journal.pone.0198493.
Koenigsknecht-Talboo, J. (2005) ‘Microglial Phagocytosis Induced by Fibrillar -Amyloid and IgGs Are Differentially Regulated by Proinflammatory Cytokines’, Journal of Neuroscience. doi: 10.1523/JNEUROSCI.1808-05.2005.
Kohno, S. et al. (2011) ‘Establishment and characterization of a noradrenergic adrenal chromaffin cell line, tsAM5NE, immortalized with the temperature-sensitive SV40 T-antigen’, Cell Biology International. doi: 10.1042/cbi20090344.
Koizumi, S. et al. (2013) ‘Purinergic receptors in microglia: Functional modal shifts of microglia mediated by P2 and P1 receptors’, GLIA. doi: 10.1002/glia.22358.
Krabbe, G. et al. (2013) ‘Functional Impairment of Microglia Coincides with Beta-Amyloid Deposition in Mice with Alzheimer-Like Pathology’, PLoS ONE. doi: 10.1371/journal.pone.0060921.
Krasemann, S. et al. (2017) ‘The TREM2-APOE Pathway Drives the Transcriptional Phenotype of Dysfunctional Microglia in Neurodegenerative Diseases’, Immunity. doi: 10.1016/j.immuni.2017.08.008.
Kruth, H. S. (2011) ‘Receptor-independent fluid-phase pinocytosis mechanisms for induction of foam cell formation with native low-density lipoprotein particles’, Current Opinion in Lipidology. doi: 10.1097/MOL.0b013e32834adadb.
Kumar, H., Kawai, T. and Akira, S. (2009) ‘Toll-like receptors and innate immunity’, Biochemical and Biophysical Research Communications. doi: 10.1016/j.bbrc.2009.08.062.

Lamark, T. et al. (2009) ‘NBR1 and p62 as cargo receptors for selective autophagy of ubiquitinated targets’, Cell Cycle. doi: 10.4161/cc.8.13.8892.
Laplante, M. and Sabatini, D. M. (2009) ‘An Emerging Role of mTOR in Lipid Biosynthesis’, Current Biology. doi: 10.1016/j.cub.2009.09.058.
Lawson, L. J. et al. (1990) ‘Heterogeneity in the distribution and morphology of microglia in the normal adult mouse brain’, Neuroscience. doi: 10.1016/0306-4522(90)90229-W.
Lee, H. S. et al. (2012) ‘Zaprinast activates MAPKs, NFκB, and Akt and induces the expressions of inflammatory genes in microglia’, International Immunopharmacology. doi: 10.1016/j.intimp.2012.04.013.
Lei, F. et al. (2020) ‘CSF1R inhibition by a small-molecule inhibitor is not microglia specific; Affecting hematopoiesis and the function of macrophages’, Proceedings of the National Academy of Sciences of the United States of America. doi: 10.1073/pnas.1922788117.
Leissring, M. a et al. (2003) ‘Enhanced proteolysis of beta-amyloid in APP transgenic mice prevents plaque formation, secondary pathology, and premature death.’, Neuron. doi: 10.1016/S0896-6273(03)00787-6.
Lemmon, M. A. and Schlessinger, J. (2010) ‘Cell signaling by receptor tyrosine kinases’, Cell, pp. 1117–1134. doi: 10.1016/j.cell.2010.06.011.
Levenga, J. et al. (2021) ‘Immunohistological Examination of AKT Isoforms in the Brain: Cell-Type Specificity That May Underlie AKT’s Role in Complex Brain Disorders and Neurological Disease’, Cerebral Cortex Communications. doi: 10.1093/texcom/tgab036.
Levine, A. B., Punihaole, D. and Levine, T. B. (2012) ‘Characterization of the role of nitric oxide and its clinical applications’, Cardiology (Switzerland). doi: 10.1159/000338150.
Leyns, C. E. G. et al. (2017) ‘TREM2 deficiency attenuates neuroinflammation and protects against neurodegeneration in a mouse model of tauopathy’, Proceedings of the National Academy of Sciences of the United States of America. doi: 10.1073/pnas.1710311114.
Li, D. and Wu, M. (2021) ‘Pattern recognition receptors in health and diseases’, Signal Transduction and Targeted Therapy. doi: 10.1038/s41392-021-00687-0.
Li, L. et al. (2010) ‘Molecular mechanism underlying LPS-induced generation of reactive oxygen species in macrophages’, The FASEB Journal.

Li, M. et al. (2004) ‘Macrophage colony stimulatory factor and interferon-gamma trigger distinct mechanisms for augmentation of beta-amyloid-induced microglia-mediated neurotoxicity.’, Journal of neurochemistry, 91(3), pp. 623–633. doi: 10.1111/j.1471-4159.2004.02765.x.

Li, Q. et al. (2016) ‘Lipopolysaccharide induces SBD-1 expression via the P38 MAPK signaling pathway in ovine oviduct epithelial cells’, Lipids in Health and Disease. doi: 10.1186/s12944-016-0294-4.

Li, X. et al. (2016) ‘Sex differences between APPswePS1dE9 mice in a-beta accumulation and pancreatic islet function during the development of Alzheimer’s disease’, Laboratory Animals. doi: 10.1177/0023677215615269.

Lian, H. et al. (2016) ‘Astrocyte-microglia cross talk through complement activation modulates amyloid pathology in mouse models of alzheimer’s disease’, Journal of Neuroscience. doi: 10.1523/JNEUROSCI.2117-15.2016.

Liddelow, S. A. et al. (2017) ‘Neurotoxic reactive astrocytes are induced by activated microglia’, Nature, 541(7638). doi: 10.1038/nature21029.

Liddelow, S. A., Marsh, S. E. and Stevens, B. (2020) ‘Microglia and Astrocytes in Disease: Dynamic Duo or Partners in Crime?’, Trends in Immunology. doi: 10.1016/j.it.2020.07.006.

Lim, H. S. et al. (2018) ‘The anti-neuroinflammatory activity of tectorigenin pretreatment via downregulated NF-κB and ERK/JNK pathways in BV-2 microglial and microglia inactivation in mice with lipopolysaccharide’, Frontiers in Pharmacology. doi: 10.3389/fphar.2018.00462.

Liu, S. et al. (2018) ‘Hyperbaric Oxygen Alleviates the Inflammatory Response Induced by LPS Through Inhibition of NF-κB/MAPKs-CCL2/CXCL1 Signaling Pathway in Cultured Astrocytes’, Inflammation. doi: 10.1007/s10753-018-0843-2.

Liu, T. et al. (2017) ‘NF-κB signaling in inflammation’, Signal Transduction and Targeted Therapy. doi: 10.1038/sigtrans.2017.23.

Long, X. et al. (2005) ‘Rheb binds and regulates the mTOR kinase’, Current Biology. doi: 10.1016/j.cub.2005.02.053.

Long, Z. et al. (2020) ‘Dynamic changes of autophagic flux induced by Abeta in the brain of postmortem Alzheimer’s disease patients, animal models and cell models’, Aging. doi: 10.18632/aging.103305.

Lucin, K. M. et al. (2013) ‘Microglial Beclin 1 Regulates Retromer Trafficking and Phagocytosis and Is Impaired in Alzheimer’s Disease’, Neuron, 79(5), pp. 873–886. doi: 10.1016/j.neuron.2013.06.046.

Lui, H. et al. (2016) ‘Progranulin Deficiency Promotes Circuit-Specific Synaptic Pruning by Microglia via Complement Activation’, Cell. doi: 10.1016/j.cell.2016.04.001.

Ma, J. et al. (2011) ‘Microglial cystatin F expression is a sensitive indicator for ongoing demyelination with concurrent remyelination’, Journal of Neuroscience Research. doi: 10.1002/jnr.22567.

Maqsood, M. I. et al. (2013) ‘Immortality of cell lines: Challenges and advantages of establishment’, Cell Biology International. doi: 10.1002/cbin.10137.

Marlatt, M. W. et al. (2014) ‘Proliferation in the alzheimer hippocampus is due to microglia, not astroglia, and occurs at sites of amyloid deposition’, Neural Plasticity. doi: 10.1155/2014/693851.

Marschallinger, J. et al. (2019) ‘Lipid droplet accumulating microglia represent a dysfunctional and pro-inflammatory state in the aging brain’, bioRxiv. doi: 10.1101/722827.

Martínez-Muriana, A. et al. (2016) ‘CSF1R blockade slows the progression of amyotrophic lateral sclerosis by reducing microgliosis and invasion of macrophages into peripheral nerves’, Scientific Reports, 6. doi: 10.1038/srep25663.

Mass, E. et al. (2017) ‘A somatic mutation in erythro-myeloid progenitors causes neurodegenerative disease’, Nature. doi: 10.1038/nature23672.

Mathern, D. R. and Heeger, P. S. (2015) ‘Molecules great and small: The complement system’, Clinical Journal of the American Society of Nephrology. doi: 10.2215/CJN.06230614.

Mattei, D. et al. (2020) ‘Enzymatic dissociation induces transcriptional and proteotype bias in brain cell populations’, International Journal of Molecular Sciences. doi: 10.3390/ijms21217944.

Mattson, M. P. and Arumugam, T. V. (2018) ‘Hallmarks of Brain Aging: Adaptive and Pathological Modification by Metabolic States’, Cell Metabolism. doi: 10.1016/j.cmet.2018.05.011.

Mauvezin, C. and Neufeld, T. P. (2015) ‘Bafilomycin A1 disrupts autophagic flux by inhibiting both V-ATPase-dependent acidification and Ca-P60A/SERCA-dependent autophagosome-lysosome fusion’, Autophagy. doi: 10.1080/15548627.2015.1066957.

Mayilyan, K. R. et al. (2008) ‘The Complement System in Innate Immunity’, in. doi: 10.1007/978-3-540-73930-2_10.
McCarthy, R. C. et al. (2016) ‘Characterization of a novel adult murine immortalized microglial cell line and its activation by amyloid-beta’, Journal of Neuroinflammation. doi: 10.1186/s12974-016-0484-z.
Mifflin, M. A. et al. (2021) ‘Sex differences in the IntelliCage and the Morris water maze in the APP/PS1 mouse model of amyloidosis’, Neurobiology of Aging. doi: 10.1016/j.neurobiolaging.2021.01.018.
Mitrasinovic, O. M. et al. (2003) ‘Macrophage colony stimulating factor promotes phagocytosis by murine microglia’, Neuroscience Letters, 344(3), pp. 185–188. doi: 10.1016/S0304-3940(03)00474-9.
Mitrasinovic, O. M. and Murphy, G. M. (2003) ‘Microglial overexpression of the M-CSF receptor augments phagocytosis of opsonized Aβ’, Neurobiology of Aging. doi: 10.1016/S0197-4580(02)00237-3.
Mizushima, N. (2007) ‘Autophagy: Process and function’, Genes and Development, pp. 2861–2873. doi: 10.1101/gad.1599207.
Mizushima, N. (2010) ‘The role of the Atg1/ULK1 complex in autophagy regulation’, Current Opinion in Cell Biology. doi: 10.1016/j.ceb.2009.12.004.
Mizushima, N., Yoshimori, T. and Ohsumi, Y. (2011) ‘The Role of Atg Proteins in Autophagosome Formation’, Annual Review of Cell and Developmental Biology. doi: 10.1146/annurev-cellbio-092910-154005.
Mohammadi, M. H. and Kariminik, A. (2021) ‘CC and CXC chemokines play key roles in the development of polyomaviruses related pathological conditions’, Virology Journal. doi: 10.1186/s12985-021-01582-4.
Molnarfi, N. et al. (2007) ‘Opposite Regulation of IL-1β and Secreted IL-1 Receptor Antagonist Production by Phosphatidylinositide-3 Kinases in Human Monocytes Activated by Lipopolysaccharides or Contact with T Cells’, The Journal of Immunology, 178(1), pp. 446–454. doi: 10.4049/jimmunol.178.1.446.
Molnarfi, N. et al. (2008) ‘Differential regulation of cytokine production by PI3Kδ in human monocytes upon acute and chronic inflammatory conditions’, Molecular Immunology. doi: 10.1016/j.molimm.2008.04.001.
Montilla, A. et al. (2020) ‘Functional and Metabolic Characterization of Microglia Culture in a Defined Medium’, Frontiers in Cellular Neuroscience. doi: 10.3389/fncel.2020.00022.

Murga-Zamalloa, C. et al. (2020) ‘Colony-stimulating factor 1 receptor (CSF1R) activates Akt/mTOR signaling and promotes T-cell lymphoma viability’, Clinical Cancer Research. doi: 10.1158/1078-0432.CCR-19-1486.

Murman, D. L. (2015) ‘The Impact of Age on Cognition’, Seminars in Hearing. doi: 10.1055/s-0035-1555115.

Murphy, G. M., Yang, L. and Cordell, B. (1998) ‘Macrophage colony-stimulating factor augments β-amyloid-induced interleukin-1, interleukin-6, and nitric oxide production by microglial cells’, Journal of Biological Chemistry. doi: 10.1074/jbc.273.33.20967.

Murray, J. T. et al. (2000) ‘Mechanism of phosphatidylinositol 3-kinase-dependent increases in BAC1.2F5 macrophage-like cell density in response to M-CSF: Phosphatidylinositol 3-kinase inhibitors increase the rate of apoptosis rather than inhibit DNA synthesis’, Inflammation Research. doi: 10.1007/s000110050638.

Murray, J., Wilson, L. and Kellie, S. (2000) ‘Phosphatidylinositol-3’ kinase-dependent vesicle formation in macrophages in response to macrophage colony stimulating factor’, Journal of Cell Science. doi: 10.1242/jcs.113.2.337.

Nakamichi, K. et al. (2005) ‘Double-stranded RNA stimulates chemokine expression in microglia through vacuolar pH-dependent activation of intracellular signaling pathways’, Journal of Neurochemistry. doi: 10.1111/j.1471-4159.2005.03354.x.

Nakamura, S. and Yoshimori, T. (2017) ‘New insights into autophagosome-lysosome fusion’, Journal of Cell Science. doi: 10.1242/jcs.196352.

Namba, Y. et al. (1991) ‘Apolipoprotein E immunoreactivity in cerebral amyloid deposits and neurofibrillary tangles in Alzheimer’s disease and kuru plaque amyloid in Creutzfeldt-Jakob disease’, Brain Research. doi: 10.1016/0006-8993(91)91092-F.

Nandi, S. et al. (2013) ‘Receptor-type protein-tyrosine phosphatase ζ is a functional receptor for interleukin-34’, Journal of Biological Chemistry. doi: 10.1074/jbc.M112.442731.

Nasuhara, Y. et al. (1999) ‘Differential IκB Kinase Activation and IκBα Degradation by Interleukin-1β and Tumor Necrosis Factor-α in Human U937 Monocytic Cells’, Journal of Biological Chemistry. doi: 10.1074/jbc.274.28.19965.

Nayak, T. K. et al. (2019) ‘P38 and JNK Mitogen-Activated Protein Kinases Interact with Chikungunya Virus Non-structural Protein-2 and Regulate TNF Induction during Viral Infection in Macrophages’, Frontiers in Immunology. doi: 10.3389/fimmu.2019.00786.

Neal, M. L. et al. (2020) ‘Pharmacological inhibition of CSF1R by GW2580 reduces microglial proliferation and is protective against neuroinflammation and dopaminergic neurodegeneration’, FASEB Journal. doi: 10.1096/fj.201900567RR.

Nelson-Rees, W. A., Daniels, D. W. and Flandermeyer, R. R. (1981) ‘Cross-contamination of cells in culture’, Science. doi: 10.1126/science.6451928.

Ni, J. et al. (2017) ‘Tyrosine receptor kinase B is a drug target in astrocytomas’, Neuro-Oncology. doi: 10.1093/neuonc/now139.

Nilsson, P. et al. (2013) ‘Aβ Secretion and Plaque Formation Depend on Autophagy’, Cell Reports. doi: 10.1016/j.celrep.2013.08.042.

Nishida, Y. et al. (2009) ‘Discovery of Atg5/Atg7-independent alternative macroautophagy’, Nature. doi: 10.1038/nature08455.

Nixon, R. A. (2007) ‘Autophagy, amyloidogenesis and Alzheimer disease’, Journal of Cell Science, 120(23), pp. 4081–4091. doi: 10.1242/jcs.019265.

Nuvolone, M. et al. (2017) ‘Cystatin F is a biomarker of prion pathogenesis in mice’, PLoS ONE. doi: 10.1371/journal.pone.0171923.

Nwadike, C. et al. (2018) ‘AMPK Inhibits ULK1-Dependent Autophagosome Formation and Lysosomal Acidification via Distinct Mechanisms’, Molecular and Cellular Biology. doi: 10.1128/mcb.00023-18.

Ocañas, S. R. et al. (2022) ‘ Minimizing the Ex Vivo Confounds of Cell-Isolation Techniques on Transcriptomic and Translatomic Profiles of Purified Microglia ’, eneuro. doi: 10.1523/eneuro.0348-21.2022.

Ohno, H. et al. (2006) ‘A c-fms tyrosine kinase inhibitor, Ki20227,suppresses osteoclast differentiation and osteolytic bone destruction in a bone metastasis model’, Molecular Cancer Therapeutics. doi: 10.1158/1535-7163.MCT-05-0313.

Olmos-Alonso, A. et al. (2016a) ‘Pharmacological targeting of CSF1R inhibits microglial proliferation and prevents the progression of Alzheimer’s-like pathology’, Brain, 139(3), pp. 891–907. doi: 10.1093/brain/awv379.

Olmos-Alonso, A. et al. (2016b) ‘Pharmacological targeting of CSF1R inhibits microglial proliferation and prevents the progression of Alzheimer’s-like pathology’, Brain. doi: 10.1093/brain/awv379.

Ordentlich, P. (2021) ‘Clinical evaluation of colony-stimulating factor 1 receptor inhibitors’, Seminars in Immunology. Elsevier Ltd, 54(October), p. 101514. doi: 10.1016/j.smim.2021.101514.

Orre, M. et al. (2014) ‘Isolation of glia from Alzheimer’s mice reveals inflammation anddysfunction’, Neurobiology of Aging. doi: 10.1016/j.neurobiolaging.2014.06.004.
Pankiv, S. et al. (2007) ‘p62/SQSTM1 binds directly to Atg8/LC3 to facilitate degradation of ubiquitinated protein aggregates by autophagy*[S]’, Journal of Biological Chemistry. doi: 10.1074/jbc.M702824200.
Paolicelli, R. C. et al. (2011) ‘Synaptic pruning by microglia is necessary for normal brain development’, Science. doi: 10.1126/science.1202529.
Paresce, D. M., Ghosh, R. N. and Maxfield, F. R. (1996) ‘Microglial cells internalize aggregates of the Alzheimer’s disease amyloid β-protein via a scavenger receptor’, Neuron, 17(3), pp. 553–565. doi: 10.1016/S0896-6273(00)80187-7.
Park, D. et al. (2011) ‘Continued clearance of apoptotic cells critically depends on the phagocyte Ucp2 protein’, Nature. doi: 10.1038/nature10340.
Park, J. M. et al. (2018) ‘ULK1 phosphorylates Ser30 of BECN1 in association with ATG14 to stimulate autophagy induction’, Autophagy. doi: 10.1080/15548627.2017.1422851.
Park, S. Y. et al. (2013) ‘α-Iso-cubebene exerts neuroprotective effects in amyloid beta stimulated microglia activation’, Neuroscience Letters. doi: 10.1016/j.neulet.2013.09.053.
Pascoal, T. A. et al. (2021) ‘Microglial activation and tau propagate jointly across Braak stages’, Nature Medicine. doi: 10.1038/s41591-021-01456-w.
Patwardhan, P. P. et al. (2014) ‘Sustained inhibition of receptor tyrosine kinases and macrophage depletion by PLX3397 and rapamycin as a potential new approach for the treatment of MPNSTs’, Clinical Cancer Research. doi: 10.1158/1078-0432.CCR-13-2576.
Piccio, L. et al. (2007) ‘Blockade of TREM-2 exacerbates experimental autoimmune encephalomyelitis’, European Journal of Immunology. doi: 10.1002/eji.200636837.
Pickford, F. et al. (2008) ‘The autophagy-related protein beclin 1 shows reduced expression in early Alzheimer disease and regulates amyloid β accumulation in mice’, Journal of Clinical Investigation, 118(6), pp. 2190–2199. doi: 10.1172/JCI33585.
Pocivavsek, A., Burns, M. P. and Rebeck, G. W. (2009) ‘Low-density lipoprotein receptors regulate microglial inflammation through c-Jun N-terminal kinase’, GLIA. doi: 10.1002/glia.20772.

Polito, V. A. et al. (2014) ‘Selective clearance of aberrant tau proteins and rescue of neurotoxicity by transcription factor EB’, EMBO Molecular Medicine. doi: 10.15252/emmm.201303671.

Pollard, J. W. (1997) ‘Role of colony-stimulating factor-1 in reproduction and development’, Molecular Reproduction and Development, 46(1), pp. 54–61. doi: 10.1002/(SICI)1098-2795(199701)46:1<54::AID-MRD9>3.0.CO;2-Q.

Ponomarev, E. D. et al. (2005) ‘Microglial cell activation and proliferation precedes the onset of CNS autoimmunity’, Journal of Neuroscience Research. doi: 10.1002/jnr.20488.

Porstmann, T. et al. (2008) ‘SREBP Activity Is Regulated by mTORC1 and Contributes to Akt-Dependent Cell Growth’, Cell Metabolism. doi: 10.1016/j.cmet.2008.07.007.

Prakash, P. et al. (2021) ‘Monitoring phagocytic uptake of amyloid β into glial cell lysosomes in real time’, Chemical Science. doi: 10.1039/d1sc03486c.

Pratten, M. K. and Lloyd, J. B. (1986) ‘Pinocytosis and phagocytosis: the effect of size of a particulate substrate on its mode of capture by rat peritoneal macrophages cultured in vitro’, BBA - General Subjects. doi: 10.1016/0304-4165(86)90020-6.

Priceman, S. J. et al. (2010) ‘Targeting distinct tumor-infiltrating myeloid cells by inhibiting CSF-1 receptor: Combating tumor evasion of antiangiogenic therapy’, Blood. doi: 10.1182/blood-2009-08-237412.

Puehringer, D. et al. (2013) ‘EGF transactivation of Trk receptors regulates the migration of newborn cortical neurons’, Nature Neuroscience. doi: 10.1038/nn.3333.

Pugsley, H. R. (2017) ‘Assessing autophagic flux by measuring LC3, p62, and LAMP1 co-localization using multispectral imaging flow cytometry’, Journal of Visualized Experiments. doi: 10.3791/55637.

Rad, E., Murray, J. T. and Tee, A. R. (2018) ‘Oncogenic signalling through mechanistic target of rapamycin (mTOR): A driver of metabolic transformation and cancer progression’, Cancers. doi: 10.3390/cancers10010005.

Rajagopal, R. et al. (2004) ‘Transactivation of Trk neurotrophin receptors by G-protein-coupled receptor ligands occurs on intracellular membranes’, Journal of Neuroscience. doi: 10.1523/JNEUROSCI.0010-04.2004.

Ramesh, A. et al. (2019) ‘CSF1R- and SHP2-Inhibitor-Loaded Nanoparticles Enhance Cytotoxic Activity and Phagocytosis in Tumor-Associated Macrophages’, Advanced Materials. doi: 10.1002/adma.201904364.

Ramesh, A. et al. (2020) ‘Dual inhibition of CSF1R and MAPK pathways using supramolecular nanoparticles enhances macrophage immunotherapy’, Biomaterials. doi: 10.1016/j.biomaterials.2019.119559.

Rawlings, N. D., Morton, F. R. and Barrett, A. J. (2006) ‘MEROPS: the peptidase database.’, Nucleic acids research. doi: 10.1093/nar/gkj089.

Rettenmier, C. W., Roussel, M. F. and Sherr, C. J. (1988) ‘The colony-stimulating factor 1 (CSF-1) receptor (c-fms proto-oncogene product) and its ligand.’, Journal of cell science. Supplement, 9, pp. 27–44.

Romao, S. et al. (2013) ‘Autophagy proteins stabilize pathogen-containing phagosomes for prolonged MHC II antigen processing’, Journal of Cell Biology. doi: 10.1083/jcb.201308173.

Rostami, J. et al. (2021) ‘Crosstalk between astrocytes and microglia results in increased degradation of α-synuclein and amyloid-β aggregates’, Journal of Neuroinflammation. doi: 10.1186/s12974-021-02158-3.

Roth, P. and Richard Stanley, E. (1996) ‘Colony stimulating factor-1 expression is developmentally regulated in the mouse’, Journal of Leukocyte Biology. doi: 10.1002/jlb.59.6.817.

Rubinsztein, D. C., Mariño, G. and Kroemer, G. (2011) ‘Autophagy and aging’, Cell. doi: 10.1016/j.cell.2011.07.030.

Ruggiero, M. J. et al. (2018) ‘Sex Differences in Early Postnatal Microglial Colonization of the Developing Rat Hippocampus Following a Single-Day Alcohol Exposure’, Journal of Neuroimmune Pharmacology. doi: 10.1007/s11481-017-9774-1.

Runwal, G. et al. (2019) ‘LC3-positive structures are prominent in autophagy-deficient cells’, Scientific Reports. doi: 10.1038/s41598-019-46657-z.

Russell, R. C. et al. (2013) ‘ULK1 induces autophagy by phosphorylating Beclin-1 and activating VPS34 lipid kinase’, Nature Cell Biology, 15(7), pp. 741–750. doi: 10.1038/ncb2757.

Sahani, M. H., Itakura, E. and Mizushima, N. (2014) ‘Expression of the autophagy substrate SQSTM1/p62 is restored during prolonged starvation depending on transcriptional upregulation and autophagy-derived amino acids’, Autophagy. doi: 10.4161/auto.27344.

Sala Frigerio, C. et al. (2019) ‘The Major Risk Factors for Alzheimer’s Disease: Age, Sex, and Genes Modulate the Microglia Response to Aβ Plaques’, Cell Reports. doi: 10.1016/j.celrep.2019.03.099.

Sampaio, N. G. et al. (2011) ‘Phosphorylation of CSF-1R Y721 mediates its association with PI3K to regulate macrophage motility and enhancement of tumor cell invasion’, Journal of Cell Science. doi: 10.1242/jcs.075309.

Sanchez-Varo, R. et al. (2012) ‘Abnormal accumulation of autophagic vesicles correlates with axonal and synaptic pathology in young Alzheimer’s mice hippocampus’, Acta Neuropathologica, 123(1), pp. 53–70. doi: 10.1007/s00401-011-0896-x.

Sanjuan, M. A. et al. (2007) ‘Toll-like receptor signalling in macrophages links the autophagy pathway to phagocytosis’, Nature. doi: 10.1038/nature06421.

Saponaro, C. et al. (2012) ‘The PI3K/Akt pathway is required for LPS activation of microglial cells’, Immunopharmacology and Immunotoxicology. doi: 10.3109/08923973.2012.665461.

Sarbassov, D. D. et al. (2005) ‘Phosphorylation and regulation of Akt/PKB by the rictor-mTOR complex’, Science. doi: 10.1126/science.1106148.

Das Sarma, S. et al. (2013) ‘Cytomorphological and Cytochemical Identification of Microglia’, ISRN Immunology. doi: 10.1155/2013/205431.

Sbarba, P. Dello and Rovida, E. (2002) ‘Transmodulation of cell surface regulatory molecules via ectodomain shedding’, Biological Chemistry. doi: 10.1515/BC.2002.007.

Scarlatti, F. et al. (2008) ‘Role of non-canonical Beclin 1-independent autophagy in cell death induced by resveratrol in human breast cancer cells’, Cell Death and Differentiation. doi: 10.1038/cdd.2008.51.

Schmelzle, T. and Hall, M. N. (2000) ‘TOR, a central controller of cell growth’, Cell. doi: 10.1016/S0092-8674(00)00117-3.

Schulze-Osthoff, K. et al. (1997) ‘Regulation of NF-κB activation by MAP kinase cascades’, Immunobiology. doi: 10.1016/S0171-2985(97)80025-3.

Schulze, H., Kolter, T. and Sandhoff, K. (2009) ‘Principles of lysosomal membrane degradation. Cellular topology and biochemistry of lysosomal lipid degradation’, Biochimica et Biophysica Acta - Molecular Cell Research. doi: 10.1016/j.bbamcr.2008.09.020.

Segaliny, A. I. et al. (2015) ‘Syndecan-1 regulates the biological activities of interleukin-34’, Biochimica et Biophysica Acta - Molecular Cell Research. doi: 10.1016/j.bbamcr.2015.01.023.

Selkoe, D. J. and Hardy, J. (2016) ‘The amyloid hypothesis of Alzheimer’s disease at 25 years’, EMBO Molecular Medicine. doi: 10.15252/emmm.201606210.

Sengupta, S., Peterson, T. R. and Sabatini, D. M. (2010) ‘Regulation of the mTOR Complex 1 Pathway by Nutrients, Growth Factors, and Stress’, Molecular Cell. doi: 10.1016/j.molcel.2010.09.026.

Serbina, N. V. et al. (2008) ‘Monocyte-mediated defense against microbial pathogens’, Annual Review of Immunology. doi: 10.1146/annurev.immunol.26.021607.090326.

Shen, Q., Zhang, R. and Bhat, N. R. (2006) ‘MAP kinase regulation of IP10/CXCL10 chemokine gene expression in microglial cells’, Brain Research. doi: 10.1016/j.brainres.2006.02.116.

Sherr, C. J. et al. (1985) ‘The c-fms proto-oncogene product is related to the receptor for the mononuclear phagocyte growth factor, CSF 1’, Cell, 41(3), pp. 665–676. doi: 10.1016/S0092-8674(85)80047-7.

Sherr, C. J. (1988) ‘The fms oncogene’, BBA - Reviews on Cancer, pp. 225–243. doi: 10.1016/0304-419X(88)90011-X.

Sierra, A. et al. (2010) ‘Microglia shape adult hippocampal neurogenesis through apoptosis-coupled phagocytosis’, Cell Stem Cell. doi: 10.1016/j.stem.2010.08.014.

Sierra, A. et al. (2013) ‘Janus-faced microglia: Beneficial and detrimental consequences of microglial phagocytosis’, Frontiers in Cellular Neuroscience. doi: 10.3389/fncel.2013.00006.

Sivagnanam, V., Zhu, X. and Schlichter, L. C. (2010) ‘Dominance of E. coli phagocytosis over LPS in the inflammatory response of microglia’, Journal of Neuroimmunology. doi: 10.1016/j.jneuroim.2010.06.021.

Skytte Rasmussen, M. et al. (2017) ‘ATG4B contains a C-terminal LIR motif important for binding and efficient cleavage of mammalian orthologs of yeast Atg8’, Autophagy. doi: 10.1080/15548627.2017.1287651.

Smith, A. M. et al. (2013) ‘M-CSF increases proliferation and phagocytosis while modulating receptor and transcription factor expression in adult human microglia’, Journal of Neuroinflammation. doi: 10.1186/1742-2094-10-85.

Sobue, A. et al. (2021) ‘Microglial gene signature reveals loss of homeostatic microglia associated with neurodegeneration of Alzheimer’s disease’, Acta Neuropathologica Communications. doi: 10.1186/s40478-020-01099-x.
Sorkin, A. and Goh, L. K. (2009) ‘Endocytosis and intracellular trafficking of ErbBs’, Experimental Cell Research, pp. 683–696. doi: 10.1016/j.yexcr.2008.07.029.
Sosna, J. et al. (2018) ‘Early long-term administration of the CSF1R inhibitor PLX3397 ablates microglia and reduces accumulation of intraneuronal amyloid, neuritic plaque deposition and pre-fibrillar oligomers in 5XFAD mouse model of Alzheimer’s disease’, Molecular Neurodegeneration. doi: 10.1186/s13024-018-0244-x.
Spangenberg, E. et al. (2019) ‘Sustained microglial depletion with CSF1R inhibitor impairs parenchymal plaque development in an Alzheimer’s disease model’, Nature Communications. doi: 10.1038/s41467-019-11674-z.
Spangenberg, E. E. et al. (2016) ‘Eliminating microglia in Alzheimer’s mice prevents neuronal loss without modulating amyloid-β pathology’, Brain. doi: 10.1093/brain/aww016.
Spilman, P. et al. (2010) ‘Inhibition of mTOR by rapamycin abolishes cognitive deficits and reduces amyloid-beta levels in a mouse model of Alzheimer’s disease.’, PloS one. doi: 10.1371/journal.pone.0009979.
Stanley, E. R. and Chitu, V. (2014a) ‘CSF-1 receptor signaling in myeloid cells’, Cold Spring Harbor Perspectives in Biology. doi: 10.1101/cshperspect.a021857.
Stanley, E. R. and Chitu, V. (2014b) ‘CSF-1 receptor signaling in myeloid cells’, Cold Spring Harbor Perspectives in Biology. doi: 10.1101/cshperspect.a021857.
Steele, J. W. et al. (2013) ‘Modulation of autophagy as a therapeutic target for Alzheimer’s disease’, Postdoc Journal. doi: 10.14304/surya.jpr.v1n2.3.
Stewart, C. R. et al. (2010) ‘CD36 ligands promote sterile inflammation through assembly of a Toll-like receptor 4 and 6 heterodimer’, Nature Immunology. doi: 10.1038/ni.1836.
Subedi, L. et al. (2019) ‘Anti-Inflammatory Effect of Sulforaphane on LPS-Activated Microglia Potentially through JNK/AP-1/NF-κB Inhibition and Nrf2/HO-1 Activation’, Cells. doi: 10.3390/cells8020194.
Suffixidharan, S., Jain, K. and Basu, A. (2011) ‘Regulation of autophagy by kinases’, Cancers. doi: 10.3390/cancers3022630.

Suire, C. N. et al. (2020) ‘Cathepsin D regulates cerebral Aβ42/40 ratios via differential degradation of Aβ42 and Aβ40’, Alzheimer’s Research and Therapy. doi: 10.1186/s13195-020-00649-8.

Sun, N. et al. (2016) ‘Ghrelin attenuates brain injury in septic mice via PI3K/Akt signaling activation’, Brain Research Bulletin. doi: 10.1016/j.brainresbull.2016.06.002.

Suzuki, T. et al. (2004) ‘Production and Release of Neuroprotective Tumor Necrosis Factor by P2X 7 Receptor-Activated Microglia’, Journal of Neuroscience. doi: 10.1523/JNEUROSCI.3792-03.2004.

Svensson, C. et al. (2010) ‘LPS-induced iNOS expression in Bv-2 cells is suppressed by an oxidative mechanism acting on the JNK pathway-A potential role for neuroprotection’, Brain Research. doi: 10.1016/j.brainres.2010.01.082.

Svensson, J. et al. (2011) ‘Macrophages at the Fetal–Maternal Interface Express Markers of Alternative Activation and Are Induced by M-CSF and IL-10’, The Journal of Immunology. doi: 10.4049/jimmunol.1100130.

Swantek, J. L., Cobb, M. H. and Geppert, T. D. (1997) ‘Jun N-terminal kinase/stress-activated protein kinase (JNK/SAPK) is required for lipopolysaccharide stimulation of tumor necrosis factor alpha (TNF-alpha) translation: glucocorticoids inhibit TNF-alpha translation by blocking JNK/SAPK’, Molecular and Cellular Biology. doi: 10.1128/mcb.17.11.6274.

Szabo, M. and Gulya, K. (2013) ‘Development of the microglial phenotype in culture’, Neuroscience. doi: 10.1016/j.neuroscience.2013.03.033.

Tabata, Y. and Ikada, Y. (1988) ‘Effect of the size and surface charge of polymer microspheres on their phagocytosis by macrophage’, Biomaterials. doi: 10.1016/0142-9612(88)90033-6.

Takahashi, K., Rochford, C. D. P. and Neumann, H. (2005) ‘Clearance of apoptotic neurons without inflammation by microglial triggering receptor expressed on myeloid cells-2’, The Journal of Experimental Medicine. doi: 10.1084/jem.20041611.

Terry, R. D. et al. (1991) ‘Physical basis of cognitive alterations in alzheimer’s disease: Synapse loss is the major correlate of cognitive impairment’, Annals of Neurology. doi: 10.1002/ana.410300410.

Tesseur, I. et al. (2006) ‘Deficiency in neuronal TGF-β signaling promotes neurodegeneration and Alzheimer’s pathology’, Journal of Clinical Investigation. doi: 10.1172/JCI27341.

Thoreen, C. C. and Sabatini, D. M. (2009) ‘Rapamycin inhibits mTORC1, but not completely’, Autophagy. doi: 10.4161/auto.5.5.8504.
Tian, D. S. et al. (2017) ‘Chemokine CCL2-CCR2 signaling induces neuronal cell death via STAT3 activation and IL-1β production after status epilepticus’, Journal of Neuroscience. doi: 10.1523/JNEUROSCI.0315-17.2017.
Ueno, T., Yamamoto, Y. and Kawasaki, K. (2021) ‘Phagocytosis of microparticles increases responsiveness of macrophage-like cell lines U937 and THP-1 to bacterial lipopolysaccharide and lipopeptide’, Scientific Reports. doi: 10.1038/s41598-021-86202-5.
Ulland, T. K. et al. (2017) ‘TREM2 Maintains Microglial Metabolic Fitness in Alzheimer’s Disease’, Cell, 170(4), pp. 649-663.e13. doi: 10.1016/j.cell.2017.07.023.
Ulrich, J. D. et al. (2014) ‘Altered microglial response to Aβ plaques in APPPS1-21 mice heterozygous for TREM2’, Mol. Neurodegener, 9(1), p. 20. doi: 10.1186/1750-1326-9-20.
Ulrich, J. D. et al. (2017) ‘Elucidating the Role of TREM2 in Alzheimer’s Disease’, Neuron. doi: 10.1016/j.neuron.2017.02.042.
Valvezan, A. J. et al. (2017) ‘mTORC1 Couples Nucleotide Synthesis to Nucleotide Demand Resulting in a Targetable Metabolic Vulnerability’, Cancer Cell. doi: 10.1016/j.ccell.2017.09.013.
in ’t Veld, B. A. et al. (2001) ‘Nonsteroidal Antiinflammatory Drugs and the Risk of Alzheimer’s Disease’, New England Journal of Medicine. doi: 10.1056/nejmoa010178.
Villa, A. et al. (2016) ‘Estrogens, neuroinflammation, and neurodegeneration’, Endocrine Reviews. doi: 10.1210/er.2016-1007.
Villapol, S., Faivre, V., Joshi, P., Moretti, R., Besson, V. and Charriaut-Marlangue, C., 2019. Early Sex Differences in the Immune-Inflammatory Responses to Neonatal Ischemic Stroke. *International Journal of Molecular Sciences*, 20(15), p.3809.
Villemagne, V. L. et al. (2013) ‘Amyloid β deposition, neurodegeneration, and cognitive decline in sporadic Alzheimer’s disease: A prospective cohort study’, The Lancet Neurology. doi: 10.1016/S1474-4422(13)70044-9.
Viña, J. and Lloret, A. (2010) ‘Why women have more Alzheimer’s disease than men: Gender and mitochondrial toxicity of amyloid-β peptide’, Journal of Alzheimer’s Disease. doi: 10.3233/JAD-2010-100501.

Vukojicic, A. et al. (2019) ‘The Classical Complement Pathway Mediates Microglia-Dependent Remodeling of Spinal Motor Circuits during Development and in SMA’, Cell Reports. doi: 10.1016/j.celrep.2019.11.013.

Walker, D. G., Tang, T. M. and Lue, L. F. (2017) ‘Studies on colony stimulating factor receptor-1 and ligands colony stimulating factor-1 and interleukin-34 in Alzheimer’s disease brains and human microglia’, Frontiers in Aging Neuroscience. doi: 10.3389/fnagi.2017.00244.

Wan, W. et al. (2018) ‘mTORC1-Regulated and HUWE1-Mediated WIPI2 Degradation Controls Autophagy Flux’, Molecular Cell. doi: 10.1016/j.molcel.2018.09.017.

Wang, J. et al. (2003) ‘Gender differences in the amount and deposition of amyloidβ in APPswe and PS1 double transgenic mice’, Neurobiology of Disease. doi: 10.1016/j.nbd.2003.08.009.

Wang, W. Y. et al. (2015) ‘Role of pro-inflammatory cytokines released from microglia in Alzheimer’s disease’, Annals of Translational Medicine. doi: 10.3978/j.issn.2305-5839.2015.03.49.

Wang, Y. et al. (2012) ‘IL-34 is a tissue-restricted ligand of CSF1R required for the development of Langerhans cells and microglia’, Nature Immunology. doi: 10.1038/ni.2360.

Wang, Y. et al. (2015) ‘TREM2 lipid sensing sustains the microglial response in an Alzheimer’s disease model’, Cell, 160(6), pp. 1061–1071. doi: 10.1016/j.cell.2015.01.049.

Wang, Y. P. et al. (2011) ‘Aspirin-triggered lipoxin A4attenuates LPS-induced pro-inflammatory responses by inhibiting activation of NF-κB and MAPKs in BV-2 microglial cells’, Journal of Neuroinflammation. BioMed Central Ltd, 8(1), p. 95. doi: 10.1186/1742-2094-8-95.

Wang, Y. and Zhang, H. (2019) ‘Regulation of Autophagy by mTOR Signaling Pathway’, in Advances in Experimental Medicine and Biology. doi: 10.1007/978-981-15-0602-4_3.

Webb, A. E. and Brunet, A. (2014) ‘FOXO transcription factors: Key regulators of cellular quality control’, Trends in Biochemical Sciences. doi: 10.1016/j.tibs.2014.02.003.

Wei, Z. and Liu, H. T. (2002) ‘MAPK signal pathways in the regulation of cell proliferation in mammalian cells’, Cell Research. doi: 10.1038/sj.cr.7290105.

Wen, J., Ribeiro, R. and Zhang, Y. (2011) 'Specific PKC isoforms regulate LPS-stimulated iNOS induction in murine microglial cells', Journal of Neuroinflammation. doi: 10.1186/1742-2094-8-38.

Werneburg, S. et al. (2020) 'Targeted Complement Inhibition at Synapses Prevents Microglial Synaptic Engulfment and Synapse Loss in Demyelinating Disease', Immunity. doi: 10.1016/j.immuni.2019.12.004.

Wiktor-Jedrzejczak, W. et al. (1990) 'Total absence of colony-stimulating factor 1 in the macrophage-deficient osteopetrotic (op/op) mouse', Proceedings of the National Academy of Sciences of the United States of America. doi: 10.1073/pnas.87.12.4828.

William, M. et al. (2019) 'Translational repression of Ccl5 and Cxcl10 by 4E-BP1 and 4E-BP2 restrains the ability of mouse macrophages to induce migration of activated T cells', European Journal of Immunology. doi: 10.1002/eji.201847857.

Williams, R. et al. (2009) 'Proinflammatory cytokines and HIV-1 synergistically enhance CXCL10 expression in human astrocytes', GLIA. doi: 10.1002/glia.20801.

Wolfe, D. M. et al. (2013) 'Autophagy failure in Alzheimer's disease and the role of defective lysosomal acidification', European Journal of Neuroscience, 37(12), pp. 1949–1961. doi: 10.1111/ejn.12169.

Wood, H. (2018) 'Microglia show sex-specific gene expression profiles', Nature reviews. Neurology. doi: 10.1038/s41582-018-0040-9.

Woodling, N. S. et al. (2016) 'Cyclooxygenase inhibition targets neurons to prevent early behavioural decline in Alzheimer's disease model mice', Brain. doi: 10.1093/brain/aww117.

Wu, L. et al. (2013) 'Rapamycin Upregulates Autophagy by Inhibiting the mTOR-ULK1 Pathway, Resulting in Reduced Podocyte Injury', PLoS ONE. doi: 10.1371/journal.pone.0063799.

Wyss-Coray, T. (2006) 'Inflammation in Alzheimer disease: Driving force, bystander or beneficial response?', Nature Medicine. doi: 10.1038/nm1484.

Xue, Q. et al. (2018) 'Regulation of iNOS on immune cells and its role in diseases', International Journal of Molecular Sciences. doi: 10.3390/ijms19123805.

Yang, D. S. et al. (2011) 'Reversal of autophagy dysfunction in the TgCRND8 mouse model of Alzheimer's disease ameliorates amyloid pathologies and memory deficits', Brain. doi: 10.1093/brain/awq341.

Yang, J. et al. (2014) ‘Monocyte and macrophage differentiation: Circulation inflammatory monocyte as biomarker for inflammatory diseases’, Biomarker Research. doi: 10.1186/2050-7771-2-1.

Yang, J. T. et al. (2018) ‘Sex Differences in Neuropathology and Cognitive Behavior in APP/PS1/tau Triple-Transgenic Mouse Model of Alzheimer’s Disease’, Neuroscience Bulletin. doi: 10.1007/s12264-018-0268-9.

Yu, W. et al. (2012) ‘Macrophage proliferation is regulated through CSF-1 receptor tyrosines 544, 559, and 807’, Journal of Biological Chemistry. doi: 10.1074/jbc.M112.355610.

Zhang, C. et al. (2013) ‘Design and pharmacology of a highly specific dual FMS and KIT kinase inhibitor’, Proceedings of the National Academy of Sciences of the United States of America. doi: 10.1073/pnas.1219457110.

Zhang, D. et al. (2021) ‘Microglial activation contributes to cognitive impairments in rotenone-induced mouse Parkinson’s disease model’, Journal of Neuroinflammation. doi: 10.1186/s12974-020-02065-z.

Zhang, X. J. et al. (2013) ‘Why should autophagic flux be assessed?’, Acta Pharmacologica Sinica. doi: 10.1038/aps.2012.184.

Zhang, Z. J. et al. (2012) ‘Curcumin inhibits LPS-induced CCL2 expression via JNK Pathway in C6 rat astrocytoma cells’, Cellular and Molecular Neurobiology. doi: 10.1007/s10571-012-9816-4.

Zhou, J. et al. (2013) ‘Activation of lysosomal function in the course of autophagy via mTORC1 suppression and autophagosome-lysosome fusion’, Cell Research, 23(4), pp. 508–523. doi: 10.1038/cr.2013.11.

Zhou, Y., Ling, E. A. and Dheen, S. T. (2007) ‘Dexamethasone suppresses monocyte chemoattractant protein-1 production via mitogen activated protein kinase phosphatase-1 dependent inhibition of Jun N-terminal kinase and p38 mitogen-activated protein kinase in activated rat microglia’, Journal of Neurochemistry. doi: 10.1111/j.1471-4159.2007.04535.x.

Zhu, J. et al. (2015) ‘MAPK and NF-κB Pathways Are Involved in Bisphenol A-Induced TNF-α and IL-6 Production in BV2 Microglial Cells’, Inflammation. doi: 10.1007/s10753-014-9971-5.

Zhu, J. H. et al. (2007) ‘Regulation of autophagy by extracellular signal-regulated protein kinases during 1-methyl-4-phenylpyridinium-induced cell death’, American Journal of Pathology. doi: 10.2353/ajpath.2007.060524.

Zöller, T. et al. (2018) ‘Silencing of TGFβ signalling in microglia results in impaired homeostasis’, Nature Communications. doi: 10.1038/s41467-018-06224-y.